

DOCTOR OF PHILOSOPHY

Investigating polymer-peptide conjugates  
and electrospinning for the production of  
advanced materials

Arun Sohdi

2013

Aston University

# **Investigating Polymer-Peptide Conjugates and Electrospinning for the Production of Advanced Materials**

**Arun Andrew Sohdi**

Doctor of Philosophy

**Aston University**

October 2012

© Arun Andrew Sohdi, 2012

Arun Andrew Sohdi asserts his moral right to be identified as the author of this thesis

This copy of this thesis has been supplied on condition that anyone who consults it is understood to recognise that its copyright rests with its author and that no quotation from this thesis and no information derived from it may be published without proper acknowledgement.

Aston University

Investigating Polymer-Peptide Conjugates and Electrospinning for the  
Production of Advanced Materials

Arun Andrew Sohdi

Doctor of Philosophy

2012

This thesis describes the production of advanced materials comprising a wide array of polymer-based building blocks. These materials include bio-hybrid polymer-peptide conjugates, based on phenylalanine and poly(ethylene oxide), and polymers with intrinsic microporosity (PIMs).

Polymer-peptides conjugates were previously synthesised using click chemistry. Due to the inherent disadvantages of the reported synthesis, a new, simpler, inexpensive protocol was sought. Three synthetic methods based on amidation chemistry were investigated for both oligopeptide and polymer-peptide coupling. The resulting conjugates produced were then assessed by various analytical techniques, and the new synthesis was compared with the established protocol. An investigation was also carried out focussing on polymer-peptide coupling via ester chemistry, involving deprotection of the carboxyl terminus of the peptide.

Polymer-peptide conjugates were also assessed for their propensity to self-assemble into thixotropic gels in an array of solvent mixtures. Determination of the rules governing this particular self-assembly (gelation) was required. Initial work suggested that at least four phenylalanine peptide units were necessary for self-assembly, due to favourable hydrogen bond interactions. Quantitative analysis was carried out using three analytical techniques (namely rheology, FTIR, and confocal microscopy) to probe the microstructure of the material and provided further information on the conditions for self-assembly.

Several polymers were electrospun in order to produce nanofibres. These included novel materials such as PIMs and the aforementioned bio-hybrid conjugates. An investigation of the parameters governing successful fibre production was carried out for PIMs, polymer-peptide conjugates, and for nanoparticle cages coupled to a polymer scaffold. SEM analysis was carried out on all material produced during these electrospinning experiments.

***Keywords***

Self-assembly, hydrogel, phenylalanine, poly(ethylene oxide), thixotropic

## **Acknowledgements**

First and foremost, I am indebted to my supervisor, Dr Paul Topham, without whom this project could never have occurred. I thank him for his continued help, patience, guidance, and input throughout all the years of study.

I would also like to thank Dr Dave Adams from the University of Liverpool, for all his expertise and advice in relation to the gelation and rheology studies. I am further grateful to Dr Chris Sammon from Sheffield Hallam University for his expertise regarding ATR-IR spectroscopy and the effect of gelation on hydrogen bond interactions.

I am grateful to Dr Mike Perry for his help and guidance with NMR spectroscopy, and to Professor Brian Tighe for his engaging retreats and his help with language. I further extend thanks to Dr Andy Sutherland who provided organic advice and who owes me many meals.

A big thank you must be made towards Dr Darren Campbell, who aside from being an endless fount of information on a vast array of subjects, was also of invaluable assistance during the writing of our review paper. I express my appreciation to Dr Andrew West from PERA for allowing me to run many, many samples on the SEM there.

Thank you to all members of the Topham group; Nikki, Keith, Harry, Joanna, and Mike for making the years entertaining. I would also like to thank Evita Chundoo and Gwendolen Chimonides for their help, humour, and salad.

Writing a thesis has been an experience and the people who have suffered and supported me most during it, were my friends. There are too many to list here however those who I am especially grateful to are; Luke, Oly, Quinn, Jon, Sophie, Matt, Louisa, Manpreet, Sarah, Amandeep, Stilwell, Jake, Chris and Lewis. Finally, I would like to thank my family for all their unconditional support and love throughout all these years.

## Abbreviations

AA	Amino acid
ATR	Attenuated total reflectance
ATRP	Atom transfer radical polymerisation
BBTO	<i>bis</i> [tri- <i>n</i> -Butyltin(IV)]oxide or tributyltin(IV) oxide
BDDC	1,3- <i>bis</i> (2,2Dimethyl-1,3-dioxolan-4-ylmethyl)carbodiimide
Boc	<i>tert</i> -Butoxycarbonyl
BOP	(Benzotriazol-1-yloxy) <i>tris</i> (dimethylamino)phosphonium hexafluorophosphate
C <sub>2</sub> O <sub>2</sub> Cl <sub>2</sub>	Oxalyl chloride
CrO <sub>3</sub>	Chromium (VI) oxide
CRP	Controlled radical polymerisation
CTA	Chain transfer agent
Da	Daltons
DCC	<i>N,N'</i> -Dicyclohexylcarbodiimide
DCM	Dichloromethane
DHU	Dicyclohexylurea
DIC	<i>Di</i> isopropylcarbodiimide
DIPEA	<i>Di</i> isopropylethylamine
DMAP	4-Dimethylaminopyridine
DMF	<i>N,N</i> -Dimethylformamide
DMSO	Dimethyl sulfoxide
Fmoc	Fluorenylmethoxycarbonyl
FTIR	Fourier transform infra-red spectroscopy
GPC	Gel permeation chromatography
HCl	Hydrochloric acid
HMPA	Hexamethylphosphoramide
HOBt	Hydroxybenzotriazole
HSQC	Heteronuclear single quantum coherence
IBCF	Isobutylchloroformate
LiOH	Lithium hydroxide
MgSO <sub>4</sub>	Magnesium sulfate

mPEO	Monomethoxy-poly(ethylene oxide). Also known as mPEG
NMM	4- <i>N</i> -Methylmorpholine
NMR	Nuclear magnetic resonance spectroscopy
PCl <sub>x</sub>	Phosphorus chlorides
PDI	Polydispersity index (also known as molar mass dispersity)
PEG	Poly(ethylene glycol), also see PEO
PENDANT	Polarisation enhancement nurtured during attached nucleus testing
PEO	Poly(ethylene oxide), also see PEG
Phe	Phenylalanine
PIM	Polymers with intrinsic microporosity
PPC	Polymer-peptide conjugates
PS	Polystyrene
PyBOP	Benzotriazol-1-yl-oxytripyrrolidinophosphonium hexafluorophosphate
RAFT	Reversible addition-fragmentation chain transfer polymerisation
SEM	Scanning electron microscopy
SOCl <sub>2</sub>	Thionyl chloride
SPPS	Solid phase peptide synthesis
TEM	Transmission electron microscopy
TFA	Trifluoroacetic acid
THF	Tetrahydrofuran
THL	Labelling system for nanoparticle cage solutions

## Table of Contents

<b>Abbreviations</b> .....	5
<b>List of tables</b> .....	13
<b>List of figures</b> .....	14
<b>List of schemes</b> .....	20
<b>Chapter 1: Introduction</b> .....	<b>22</b>
<b>1.1: Amino acids</b> .....	<b>23</b>
1.1.1: Phenylalanine .....	27
<b>1.2: Peptide synthesis</b> .....	<b>28</b>
1.2.1: Peptide synthesis in solution .....	30
1.2.2: Peptide synthesis in the solid state .....	31
<b>1.3: Peptide synthesis techniques</b> .....	<b>32</b>
1.3.1: Carbodiimide coupling .....	32
1.3.2: Phosphonium coupling .....	33
1.3.3: Chloroformate coupling .....	35
1.3.4: Other coupling methods .....	36
<b>1.4: Protecting group strategy</b> .....	<b>37</b>
1.4.1: Carboxylic acid group protection .....	37
1.4.2: Amino group protection .....	38
1.4.3: Disadvantages of a protecting group strategy .....	40
<b>1.5: Polymer-peptide conjugates</b> .....	<b>40</b>
<b>1.6: Poly(ethylene oxide) and PEGylation</b> .....	<b>42</b>
1.6.1: Poly(ethylene oxide).....	42
1.6.2: PEGylation .....	43
1.6.3: Drawbacks of poly(ethylene oxide) and its derivatives .....	43
<b>1.7: Polymer-peptide conjugation strategies</b> .....	<b>44</b>
1.7.1: Conjugation Strategies (direct conjugation).....	46
1.7.1.1: <i>Succinimide</i> .....	47
1.7.1.2: <i>Schiff base</i> .....	48
1.7.1.3: <i>Click chemistry</i> .....	48
1.7.1.4: <i>Thiol-maleimide</i> .....	49

1.7.2: Divergent strategies .....	49
1.7.2.1: Peptide growth from polymers .....	49
1.7.2.2: Polymer growth from peptides .....	50
1.7.2.3: Atom transfer radical polymerisation .....	50
1.7.2.4: Reverse addition-fragmentation chain transfer .....	51
<b>1.8: Hydrogels .....</b>	<b>52</b>
1.81: Polymer-peptide conjugate hydrogels .....	52
<b>1.9: Electrospinning .....</b>	<b>53</b>
<b>1.10: Polymer nanofibres .....</b>	<b>54</b>
<b>1.11: Aims .....</b>	<b>56</b>
<b>1.12: References .....</b>	<b>58</b>
<b>Chapter 2: Experimental .....</b>	<b>69</b>
<b>2.1: Materials .....</b>	<b>71</b>
<b>2.2: Peptide Synthesis .....</b>	<b>72</b>
2.2.1: Synthesis of Boc-F <sub>(x+1)</sub> -OEt terminated peptide <b>3</b> using isobutylchloroformate .....	72
2.2.2: Deprotection of Boc-F <sub>(x+1)</sub> -OEt <b>3</b> to produce NH <sub>2</sub> -F <sub>(x+1)</sub> -OEt <b>4</b> .....	72
2.2.3: Synthesis of Fmoc-F <sub>(x+1)</sub> -OEt <b>6</b> using isobutylchloroformate .....	73
2.2.4: Deprotection of Fmoc-F <sub>(x+1)</sub> -OEt <b>6</b> to produce NH <sub>2</sub> -F <sub>(x+1)</sub> -OEt <b>4</b> using piperidine .....	73
2.2.5: Deprotection of Fmoc-F <sub>(x+1)</sub> -OEt <b>6</b> to produce NH <sub>2</sub> -F <sub>(x+1)</sub> -OEt <b>4</b> using diazabicycloundec-7-ene .....	73
2.2.6: Synthesis of N-Protected F <sub>(x+1)</sub> -OEt terminated peptide <b>3</b> or <b>6</b> using <i>N,N'</i> -dicyclohexylcarbodiimide .....	74
<b>2.3: Preparation of carboxylic acid-functionalised monomethoxy-poly(ethylene oxide) <b>8</b> .....</b>	<b>74</b>
<b>2.4: Synthesis of polymer-peptide conjugates .....</b>	<b>75</b>
2.4.1: Synthesis of polymer-peptide conjugate <b>9</b> via isobutylchloroformate coupling .....	75
2.4.2: Synthesis of polymer-peptide conjugate <b>9</b> via <i>N,N'</i> -dicyclohexylcarbodiimide coupling .....	76
2.4.3: Synthesis of polymer-peptide conjugate <b>9</b> via	

benzotriazol-1-yl-oxytripyrrolidinophosphoniumhexafluorophosphate (PyBOP) coupling .....	76
<b>2.5: Deprotection of carboxyl terminus .....</b>	<b>76</b>
2.5.1: Deprotection of the carboxyl terminus of polymer-peptide conjugate <b>9</b> using lithium hydroxide (Method One) to yield conjugate <b>10</b> .....	77
2.5.2: Deprotection of the carboxyl terminus of polymer-peptide conjugate <b>9</b> using lithium hydroxide (Method Two) to yield conjugate <b>10</b> .....	78
2.5.3: Deprotection of the carboxyl terminus of polymer-peptide conjugate <b>9</b> using lithium hydroxide (Method Three) to yield conjugate <b>10</b> .....	78
2.5.4: Deprotection of the carboxyl terminus of polymer-peptide conjugate <b>9</b> using <i>bis</i> -butyl-tin(IV) oxide to yield conjugate <b>10</b> .....	79
<b>2.6: Polymer-peptide synthesis using unmodified monomethoxy poly(ethylene oxide).....</b>	<b>79</b>
2.6.1: Polymer-peptide conjugate <b>11</b> synthesis using unmodified monomethoxy-poly(ethylene oxide) <b>7</b> , via Steglich esterification .....	79
2.6.2: Polymer-peptide conjugate <b>11</b> synthesis using unmodified monomethoxy-poly(ethylene oxide) <b>7</b> via Fischer esterification .....	80
<b>2.7: Gel formation (Self-Assembly) .....</b>	<b>80</b>
2.7.1: Gel formation Method 1 .....	81
2.7.2: Gel formation Method 2.....	81
2.7.3: Gel formation Method 3.....	81
2.7.4: Gel formation Method 4.....	81
<b>2.8: Electrospinning.....</b>	<b>82</b>
<b>2.9: Nuclear magnetic resonance spectroscopy.....</b>	<b>83</b>
<b>2.10: Gel permeation chromatography.....</b>	<b>83</b>
<b>2.11: Fourier transform infrared spectroscopy .....</b>	<b>83</b>
<b>2.12: Scanning electron microscopy.....</b>	<b>84</b>
<b>2.13: Rheology .....</b>	<b>84</b>
<b>2.14: Confocal microscopy .....</b>	<b>84</b>
<b>2.15: High precision ATR-FTIR spectroscopy.....</b>	<b>85</b>
 <b>Chapter 3: Synthesis of Polymer-Peptide Conjugates .....</b>	 <b>86</b>
<b>3.1: Synthesis of phenylalanine peptide sequences.....</b>	<b>87</b>

<b>3.2:</b>	<b>Functionalisation of monomethoxy-poly(ethylene oxide).....</b>	<b>99</b>
<b>3.3:</b>	<b>Polymer-peptide conjugate synthesis .....</b>	<b>108</b>
3.3.1:	Polymer-peptide conjugate coupling methods .....	108
3.3.1.1:	<i>N,N'</i> -Dicyclohexylcarbodiimide-mediated polymer-peptide conjugate synthesis.....	110
3.3.1.2:	<i>IBCF</i> -mediated polymer-peptide conjugate synthesis .....	113
3.3.1.3:	<i>Benzotriazol-1-yl-oxytripyrrolidinophosphonium hexafluorophosphate</i> -mediated polymer-peptide conjugate synthesis .....	114
3.3.1.4:	Summary of polymer-peptide conjugate coupling methods ....	115
3.3.2:	Synthesis of polymer-peptide conjugates using isobutylchloroformate coupling.....	115
3.3.2.1:	Synthesis of <i>mPEO</i> <sub>7</sub> conjugates .....	116
3.3.2.1.1:	<b>Synthesis of <i>mPEO</i><sub>7</sub>-<i>F</i><sub>1</sub>-<i>OE</i>t.....</b>	<b>116</b>
3.3.2.1.2:	<b>Synthesis of <i>mPEO</i><sub>7</sub>-<i>F</i><sub>2</sub>-<i>OE</i>t.....</b>	<b>121</b>
3.3.2.1.3:	<b>Synthesis of <i>mPEO</i><sub>7</sub>-<i>F</i><sub>3</sub>-<i>OE</i>t.....</b>	<b>125</b>
3.3.2.1.4:	<b>Synthesis of <i>mPEO</i><sub>7</sub>-<i>F</i><sub>4</sub>-<i>OE</i>t.....</b>	<b>128</b>
3.3.2.1.5:	<b>Summary of synthesis of <i>mPEO</i><sub>7</sub>-containing conjugates.....</b>	<b>133</b>
3.3.2.2:	Synthesis of <i>mPEO</i> <sub>12</sub> conjugates .....	134
3.3.2.2.1:	<b>Synthesis of <i>mPEO</i><sub>12</sub>-<i>F</i><sub>1</sub>-<i>OE</i>t.....</b>	<b>134</b>
3.3.2.2.2:	<b>Synthesis of <i>mPEO</i><sub>12</sub>-<i>F</i><sub>2</sub>-<i>OE</i>t.....</b>	<b>137</b>
3.3.2.2.3:	<b>Synthesis of <i>mPEO</i><sub>12</sub>-<i>F</i><sub>3</sub>-<i>OE</i>t.....</b>	<b>140</b>
3.3.2.2.4:	<b>Synthesis of <i>mPEO</i><sub>12</sub>-<i>F</i><sub>4</sub>-<i>OE</i>t.....</b>	<b>144</b>
3.3.2.2.5:	<b>Summary of synthesis of <i>mPEO</i><sub>12</sub>-containing conjugates.....</b>	<b>147</b>
3.3.2.3:	Synthesis of <i>mPEO</i> <sub>17</sub> conjugates.....	147
3.3.2.3.1:	<b>Synthesis of <i>mPEO</i><sub>17</sub>-<i>F</i><sub>1</sub>-<i>OE</i>t.....</b>	<b>147</b>
3.3.2.3.2:	<b>Synthesis of <i>mPEO</i><sub>17</sub>-<i>F</i><sub>2</sub>-<i>OE</i>t.....</b>	<b>151</b>
3.3.2.3.3:	<b>Synthesis of <i>mPEO</i><sub>17</sub>-<i>F</i><sub>3</sub>-<i>OE</i>t.....</b>	<b>153</b>
3.3.2.3.4:	<b>Synthesis of <i>mPEO</i><sub>17</sub>-<i>F</i><sub>4</sub>-<i>OE</i>t.....</b>	<b>156</b>
3.3.2.3.5:	<b>Summary of synthesis of <i>mPEO</i><sub>17</sub>-containing conjugates.....</b>	<b>159</b>
<b>3.4:</b>	<b>Alternative route for producing polymer-peptide conjugates ...</b>	<b>160</b>

3.4.1: Proposed synthetic route for alternative production of polymer-peptide conjugates .....	161
3.4.1.1: Deprotection of C-ethyl ester protected amino acids .....	162
3.4.1.2: Production of polymer-peptide conjugates using C-terminal deprotected peptides using Fischer Esterification .....	169
3.4.1.3: Production of polymer-peptide conjugates using C-terminal deprotected peptides using Steglich Esterification .....	172
3.4.1.4: Summary of alternative routes for conjugate production .....	176
<b>3.5: Comparison of methods for production of polymer-peptide conjugates.....</b>	<b>176</b>
<b>3.6: Conclusions .....</b>	<b>182</b>
<b>3.7: References .....</b>	<b>184</b>

## **Chapter 4: Self-assembly behaviour of Bio-Hybrid Materials 186**

<b>4.1: Gelation studies of polymer-peptide conjugates .....</b>	<b>187</b>
4.1.1: Gelation of mPEO <sub>7</sub> -based polymer-peptide conjugates .....	188
4.1.2: Gelation of mPEO <sub>12</sub> -based polymer-peptide conjugates.....	190
4.1.3: Gelation of mPEO <sub>17</sub> -based polymer-peptide conjugates.....	191
4.1.4: Polymer-peptide conjugates gelation trends .....	193
<b>4.2: Quantitative analysis of self-assembled materials .....</b>	<b>197</b>
4.2.1: Rheology of self-assembled materials .....	197
4.2.2: FTIR spectroscopy of self-assembled materials .....	201
4.2.3: Confocal microscopy of self-assembled materials .....	206
<b>4.3: The effect of temperature on self-assembly behaviour.....</b>	<b>210</b>
<b>4.4. Comparison of produced self-assembled materials.....</b>	<b>211</b>
<b>4.5: Conclusions .....</b>	<b>213</b>
<b>4.6: References .....</b>	<b>215</b>

## **Chapter 5: Electrospinning Novel Materials .....217**

<b>5.1: Electrospinning polystyrene.....</b>	<b>218</b>
5.1.1: Electrospinning polystyrene in tetrahydrofuran .....	218
5.1.2: Electrospinning polystyrene from dichloromethane.....	220
<b>5.2: Electrospinning polymers with intrinsic microporosity .....</b>	<b>222</b>

5.2.1: Effect of concentration on fibre formation of electrospun PIM-1 ....	226
5.2.2: Effect of voltage on fibre formation of electrospun PIM-1 .....	230
5.2.3: Effect of tip-to-collector distance on fibre formation of electrospun PIM-1 .....	232
5.2.4: Effect of flow rate on fibre formation of electrospun PIM-1 .....	234
5.2.5: Conclusions on the electrospinning of PIM-1 .....	237
<b>5.3: Electrospinning nanoparticle cages with polymer scaffolds.....</b>	<b>238</b>
5.3.1: Initial attempts of electrospinning nanoparticle cages using polystyrene as a scaffold.....	238
5.3.2: Initial attempts of electrospinning nanoparticle cages using PIM-1 as a scaffold.....	241
<b>5.4: Electrospinning bio-hybrid materials.....</b>	<b>242</b>
5.4.1: Determining the effect of molecular weight on fibre production of poly(ethylene oxide) .....	242
5.4.1.1: <i>Electrospinning poly(ethylene oxide), molecular weight</i> 300,000 Da.....	243
<b>5.4.1.1.1: Effect of solvent composition on electrospinning</b> <b>poly(ethylene oxide)<sub>6820</sub>.....</b>	<b>243</b>
<b>5.4.1.1.2: Effect of voltage on electrospinning poly(ethylene</b> <b>oxide)<sub>6820</sub>.....</b>	<b>245</b>
<b>5.4.1.1.3: Effect of distance on electrospinning poly(ethylene</b> <b>oxide)<sub>6820</sub>.....</b>	<b>246</b>
<b>5.4.1.1.4: Effect of flow rate on electrospinning poly(ethylene</b> <b>oxide)<sub>6820</sub>.....</b>	<b>247</b>
5.4.1.2: <i>Electrospinning poly(ethylene oxide), molecular weight</i> 100,000 Da.....	249
5.4.1.3: <i>Electrospinning poly(ethylene oxide), molecular weight</i> 8,000 Da.....	249
5.4.1.4: <i>Electrospinning poly(ethylene oxide), molecular weight</i> 4,000 Da.....	250
5.4.1.5: <i>The effect of different molecular weight PEO on fibre</i> <i>production.....</i>	250
5.4.2: Electrospinning polymer-peptide conjugates.....	251
<b>5.5: Electrospinning conclusions.....</b>	<b>256</b>

<b>5.6: References .....</b>	<b>257</b>
<b>Chapter 6: Conclusions and Future Work.....</b>	<b>259</b>
<b>6.1: Conclusions .....</b>	<b>260</b>
6.1.1: Innovative synthesis of polymer-peptide conjugates .....	260
6.1.2: Self-assembly behaviour of bio-hybrid materials.....	262
6.1.3: Electrospinning novel materials .....	262
<b>6.2: Future Work.....</b>	<b>264</b>
6.2.1: Future direction of the synthesis of polymer-peptide conjugates ..	264
6.2.2: Future directions of the self-assembly behaviour of bio-hybrid materials .....	264
6.2.3: Future directions of electrospinning novel materials .....	265
<b>Appendices .....</b>	<b>266</b>
<b>Appendix A: Band Assignment of IR Spectra.....</b>	<b>265</b>
<b>Appendix B: Gelation Behaviour of Polymer-Peptide Conjugates .....</b>	<b>284</b>
<b>Appendix C: Rheology of mPEO<sub>17</sub>-F<sub>4</sub>-OEt Gels .....</b>	<b>296</b>
<b>Appendix D : Electrospinning different molecular weight PEO .....</b>	<b>300</b>
<b>Publications .....</b>	<b>309</b>

## List of Tables

- Table 3.1:** Percentage yields of synthesised Boc-F<sub>x</sub>-OEt.
- Table 3.2:** Percentage yields and overall yields for deprotected peptides.
- Table 3.3:** Percentage yields of monomethoxy-poly(ethylene oxide).
- Table 3.4:** Yields obtained for the synthesis of polymer-peptide conjugates using *N,N* dicyclohexylcarbodiimide coupling.
- Table 3.5:** Yields of polymer-peptide conjugates using isobutylchloroformate coupling.
- Table 4.1:** Qualitative observations of gel formation of mPEO<sub>7</sub>-F<sub>4</sub>-OEt. The percentage shows the proportion of organic solvent used in a mixture with water.
- Table 4.2:** Qualitative observation of gel formation of mPEO<sub>12</sub>-F<sub>4</sub>-OEt. The percentage shows the amount of organic solvent used in a mixture with water.
- Table 4.3:** Qualitative observations of gel formation of mPEO<sub>17</sub>-F<sub>4</sub>-OEt. The percentage shows the amount of organic solvent used in a mixture with water.
- Table 4.4:** Dielectric constants of gelation solvents and qualitative solubility observations of the conjugates in the aforementioned solvents.
- Table 4.5:** Hydrogen bonding Hansen parameter ( $\delta H$ ) of gelation solvents.
- Table 5.1:** Qualitative solubility and viscosity observations of PIM-1.
- Table 5.2:** Solubility and viscosity observations of PIM-1 in co-solvent systems.
- Table 5.3:** Proposed optimal system for the production of fibres of PIM-1.
- Table 6.1:** Summary of percentage yields of polymer-peptide conjugates produced using IBCF coupling chemistry.

## List of Figures

- Figure 1.1:** General structure of an amino acid, where the R group varies depending on the specific amino acid.
- Figure 1.2:** Isomers of amino acids: L-amino acid and D-amino acid enantiomers.
- Figure 1.3:** The twenty proteogenic amino acids, classified by side chain property.
- Figure 1.4:** Structure of L-phenylalanine.
- Figure 1.5:** Mixture of products produced when glycine and alanine are directly coupled.
- Figure 1.6:** A cartoon schematic of a polymer-peptide conjugate.
- Figure 1.7:** Structure of poly(ethylene oxide).
- Figure 1.8:** Some of the most common convergent strategies used to synthesise polymer-peptide conjugates.
- Figure 1.9:** Example of applications of nanofibres, adapted from Huang *et al.*
- Figure 2.1:** A typical electrospinning setup.
- Figure 3.1:**  $^1\text{H}$  NMR spectrum of Boc-F<sub>1</sub>-OH.
- Figure 3.2:**  $^1\text{H}$  NMR spectrum of NH<sub>2</sub>-F<sub>1</sub>-OEt.HCl.
- Figure 3.3:**  $^1\text{H}$  NMR spectrum of Boc-F<sub>2</sub>-OEt.
- Figure 3.4:**  $^{13}\text{C}$  NMR spectrum of Boc-F<sub>1</sub>-OH.
- Figure 3.5:**  $^{13}\text{C}$  NMR spectrum of NH<sub>2</sub>-F<sub>1</sub>-OEt.HCl.
- Figure 3.6:**  $^{13}\text{C}$  NMR spectrum of Boc-F<sub>2</sub>-OEt.
- Figure 3.7:** GPC analysis of synthesised products and precursors.
- Figure 3.8:**  $^1\text{H}$  NMR spectrum of NH<sub>2</sub>-F<sub>2</sub>-OEt.TFA.
- Figure 3.9:** Structure of a monofunctional-poly(ethylene oxide), monomethoxy-poly(ethylene oxide) (mPEO<sub>n</sub>).
- Figure 3.10:** Reaction mechanism illustrating the oxidation of mPEO<sub>n</sub> to an aldehyde, and subsequently a carboxylic acid.
- Figure 3.11:** Labelled  $^1\text{H}$  NMR spectrum of mPEO<sub>12</sub>-COOH.
- Figure 3.12:**  $^{13}\text{C}$  PENDANT NMR spectrum of mPEO<sub>12</sub>-COOH.
- Figure 3.13:** GPC trace of mPEO<sub>12</sub> and mPEO<sub>12</sub>-COOH.
- Figure 3.14:** IR spectrum of mPEO<sub>12</sub>-COOH.

**Figure 3.15:** GPC trace of mPEO<sub>7</sub>-F<sub>3</sub>-OEt (produced using DCC coupling) and precursor reagents.

**Figure 3.16:** GPC trace of mPEO<sub>7</sub>-F<sub>4</sub>-OEt (produced using DCC coupling) and precursor reagents.

**Figure 3.17:** <sup>1</sup>H NMR of PyBOP product. The product was expected to be mPEO<sub>7</sub>-F<sub>1</sub>-OEt.

**Figure 3.18:** GPC traces of a polymer-peptide conjugate (mPEO<sub>7</sub>-F<sub>1</sub>-OEt) and the precursor reagents.

**Figure 3.19:** <sup>1</sup>H NMR spectrum of mPEO<sub>7</sub>-F<sub>1</sub>-OEt.

**Figure 3.20:** <sup>13</sup>C PENDANT NMR spectrum of mPEO<sub>7</sub>-F<sub>1</sub>-OEt.

**Figure 3.21:** IR spectrum of NH<sub>2</sub>-F<sub>1</sub>-OEt.

**Figure 3.22:** IR spectrum of mPEO<sub>7</sub>-COOH.

**Figure 3.23:** IR spectrum of mPEO<sub>7</sub>-F<sub>1</sub>-OEt.

**Figure 3.24:** GPC traces showing a polymer-peptide conjugate (mPEO<sub>7</sub>-F<sub>2</sub>-OEt) and the precursor reagents.

**Figure 3.25:** <sup>1</sup>H NMR analysis of mPEO<sub>7</sub>-F<sub>2</sub>-OEt.

**Figure 3.26:** <sup>13</sup>C PENDANT NMR spectrum of mPEO<sub>7</sub>-F<sub>2</sub>-OEt.

**Figure 3.27:** IR spectrum of mPEO<sub>7</sub>-F<sub>2</sub>-OEt.

**Figure 3.28:** GPC traces showing an impure polymer-peptide conjugate (mPEO<sub>7</sub>-F<sub>3</sub>-OEt) and the precursor reagents.

**Figure 3.29:** GPC traces showing a polymer-peptide conjugate (mPEO<sub>7</sub>-F<sub>3</sub>-OEt) and the precursor reagents.

**Figure 3.30:** <sup>1</sup>H NMR spectrum and analysis of mPEO<sub>7</sub>-F<sub>3</sub>-OEt.

**Figure 3.31:** <sup>13</sup>C PENDANT NMR spectrum and analysis of mPEO<sub>7</sub>-F<sub>3</sub>-OEt.

**Figure 3.32:** IR spectrum of mPEO<sub>7</sub>-F<sub>3</sub>-OEt.

**Figure 3.33:** GPC trace showing mPEO<sub>7</sub>-F<sub>4</sub>-OEt and progenitor peaks after initial synthesis.

**Figure 3.34:** GPC trace showing columned mPEO<sub>7</sub>-F<sub>4</sub>-OEt.

**Figure 3.35:** GPC trace showing reprecipitated mPEO<sub>7</sub>-F<sub>4</sub>-OEt and progenitor peaks.

**Figure 3.36:** <sup>1</sup>H NMR spectrum and analysis of mPEO<sub>7</sub>-F<sub>4</sub>-OEt.

**Figure 3.37:** <sup>13</sup>C PENDANT NMR spectrum and analysis of mPEO<sub>7</sub>-F<sub>4</sub>-OEt.

**Figure 3.38:** IR spectrum of mPEO<sub>7</sub>-F<sub>4</sub>-OEt.

**Figure 3.39:** GPC trace showing mPEO<sub>12</sub>-F<sub>1</sub>-OEt and precursor material.

**Figure 3.40:**  $^1\text{H}$  NMR spectrum and analysis of  $\text{mPEO}_{12}\text{-F}_1\text{-OEt}$ .

**Figure 3.41:**  $^{13}\text{C}$  PENDANT NMR spectrum of  $\text{mPEO}_{12}\text{-F}_1\text{-OEt}$ .

**Figure 3.42:** IR spectrum of  $\text{mPEO}_{12}\text{-F}_1\text{-OEt}$ .

**Figure 3.43:** GPC trace showing  $\text{mPEO}_{12}\text{-F}_2\text{-OEt}$  and precursor peaks.

**Figure 3.44:**  $^1\text{H}$  NMR spectrum of  $\text{mPEO}_{12}\text{-F}_2\text{-OEt}$ .

**Figure 3.45:**  $^{13}\text{C}$  PENDANT NMR spectrum of  $\text{mPEO}_{12}\text{-F}_2\text{-OEt}$ .

**Figure 3.46:** IR spectrum of  $\text{mPEO}_{12}\text{-F}_2\text{-OEt}$ .

**Figure 3.47:** GPC traces showing impure  $\text{mPEO}_{12}\text{-F}_3\text{-OEt}$  and precursor peaks.

**Figure 3.48:** GPC traces showing the purified  $\text{mPEO}_{12}\text{-F}_3\text{-OEt}$  and precursor peaks.

**Figure 3.49:**  $^1\text{H}$  NMR spectrum of  $\text{mPEO}_{12}\text{-F}_3\text{-OEt}$ .

**Figure 3.50:**  $^{13}\text{C}$  PENDANT NMR spectrum of  $\text{mPEO}_{12}\text{-F}_3\text{-OEt}$ .

**Figure 3.51:** IR spectrum of  $\text{mPEO}_{12}\text{-F}_3\text{-OEt}$ .

**Figure 3.52:** GPC traces of  $\text{mPEO}_{12}\text{-F}_4\text{-OEt}$  and precursor peaks.

**Figure 3.53:**  $^1\text{H}$  NMR spectrum of  $\text{mPEO}_{12}\text{-F}_4\text{-OEt}$ .

**Figure 3.54:**  $^{13}\text{C}$  NMR spectrum of  $\text{mPEO}_{12}\text{-F}_4\text{-OEt}$ .

**Figure 3.55:** IR spectrum of  $\text{mPEO}_{12}\text{-F}_4\text{-OEt}$ .

**Figure 3.56:** GPC trace of  $\text{mPEO}_{17}\text{-F}_1\text{-OEt}$  and precursor peaks.

**Figure 3.57:**  $^1\text{H}$  NMR spectrum of  $\text{mPEO}_{17}\text{-F}_1\text{-OEt}$ .

**Figure 3.58:**  $^{13}\text{C}$  PENDANT NMR spectrum of  $\text{mPEO}_{17}\text{-F}_1\text{-OEt}$ .

**Figure 3.59:** IR spectrum of  $\text{mPEO}_{17}\text{-F}_1\text{-OEt}$ .

**Figure 3.60:** GPC trace of  $\text{mPEO}_{17}\text{-F}_2\text{-OEt}$  and precursor peaks.

**Figure 3.61:**  $^1\text{H}$  NMR spectrum of  $\text{mPEO}_{17}\text{-F}_2\text{-OEt}$ .

**Figure 3.62:**  $^{13}\text{C}$  PENDANT NMR spectrum of  $\text{mPEO}_{17}\text{-F}_2\text{-OEt}$ .

**Figure 3.63:** IR spectrum  $\text{mPEO}_{17}\text{-F}_2\text{-OEt}$ .

**Figure 3.64:** GPC trace of  $\text{mPEO}_{17}\text{-F}_3\text{-OEt}$  and precursor peaks.

**Figure 3.65:**  $^1\text{H}$  NMR spectrum of  $\text{mPEO}_{17}\text{-F}_3\text{-OEt}$ .

**Figure 3.66:**  $^{13}\text{C}$  PENDANT NMR spectrum of  $\text{mPEO}_{17}\text{-F}_3\text{-OEt}$ .

**Figure 3.67:** IR spectrum of  $\text{mPEO}_{17}\text{-F}_3\text{-OEt}$ .

**Figure 3.68:** GPC trace of  $\text{mPEO}_{17}\text{-F}_4\text{-OEt}$  and precursor peaks.

**Figure 3.69:**  $^1\text{H}$  NMR spectrum of  $\text{mPEO}_{17}\text{-F}_4\text{-OEt}$ .

**Figure 3.70:**  $^{13}\text{C}$  PENDANT NMR spectrum of  $\text{mPEO}_{17}\text{-F}_4\text{-OEt}$ .

**Figure 3.71:** IR spectrum of  $\text{mPEO}_{17}\text{-F}_4\text{-OEt}$ .

- Figure 3.72:**  $^1\text{H}$  NMR spectrum of Boc-F<sub>2</sub>-OEt.
- Figure 3.73:**  $^1\text{H}$  NMR spectrum of Boc-F<sub>2</sub>-COOH after deprotection using LiOH Method One.
- Figure 3.74:**  $^{13}\text{C}$  PENDANT spectrum of Boc-F<sub>2</sub>-COOH after deprotecting using LiOH Method One.
- Figure 3.75:** IR spectrum of Boc-F<sub>2</sub>-COOH after deprotection using LiOH Method One
- Figure 3.76:**  $^1\text{H}$  NMR spectrum of Boc-F<sub>2</sub>-COOH using BBTO deprotection.
- Figure 3.77:**  $^1\text{H}$  NMR spectrum of bis[tri-n-butyltin(IV)]oxide.
- Figure 3.78:**  $^1\text{H}$  NMR of product obtained from Fischer esterification between mPEO<sub>7</sub>-OH and Boc-F<sub>2</sub>-COOH.
- Figure 3.79:**  $^1\text{H}$  NMR of product obtained from Fischer esterification between mPEO<sub>7</sub>-OH and Boc-F<sub>2</sub>-COOH.
- Figure 3.80:**  $^1\text{H}$  NMR of product obtained from Steglich esterification between mPEO<sub>7</sub>-OH and Boc-F<sub>2</sub>-COOH.
- Figure 3.81:**  $^{13}\text{C}$  PENDANT NMR of product obtained from Steglich esterification between mPEO<sub>7</sub>-OH and Boc-F<sub>2</sub>-COOH.
- Figure 3.82:** HSQC NMR spectrum of product obtained from Steglich esterification between mPEO<sub>7</sub>-OH and Boc-F<sub>2</sub>-COOH.
- Figure 3.83:** IR spectrum of product obtained from Steglich esterification between mPEO<sub>7</sub>-OH and Boc-F<sub>2</sub>-COOH.
- Figure 3.84:** GPC trace of product obtained from Steglich esterification between mPEO<sub>7</sub>-OH and Boc-F<sub>2</sub>-COOH.
- Figure 4.1:** Hydrogen bonding of mPEO<sub>n</sub>-F<sub>x</sub>-OEt polymer-peptide conjugates.
- Figure 4.2:** Rheology data for self-assembled mPEO<sub>17</sub>-F<sub>4</sub>-OEt 10 mg/ml in a 20 %v/v solution of DMSO and water.
- Figure 4.3:** Strain sweep data for self-assembled mPEO<sub>17</sub>-F<sub>4</sub>-OEt 10 mg/ml in a 10 %v/v solution of DMSO and water.
- Figure 4.4:** Magnified strain sweep data for self-assembled mPEO<sub>17</sub>-F<sub>4</sub>-OEt 10 mg/ml in a 10 %v/v solution of DMSO and water.
- Figure 4.5:** Frequency sweep data for self-assembled mPEO<sub>17</sub>-F<sub>4</sub>-OEt 10 mg/ml in a 10 %v/v solution of DMSO and water.
- Figure 4.6:** Frequency sweep data for mPEO<sub>7</sub>-F<sub>4</sub>-OEt from the literature.

- Figure 4.7:** FTIR spectrum of mPEO<sub>17</sub>-F<sub>4</sub>-OEt on an ATR crystal in DMSO-water mixture (20 %v/v).
- Figure 4.8:** FTIR spectrum of mPEO<sub>17</sub>-F<sub>4</sub>-OEt on an ATR crystal in DMSO-water mixture (20 %v/v) focusing on the amide I bands.
- Figure 4.9:** FTIR spectrum of mPEO<sub>17</sub>-F<sub>4</sub>-OEt on an ATR crystal in DMSO-water mixture (20 %v/v) focusing on the amide I bands (normalised).
- Figure 4.10:** FTIR spectrum of mPEO<sub>17</sub>-F<sub>4</sub>-OEt on ATR crystal in DMSO-water mixture (20 %v/v) focusing on C-H bonds and carbonyl shifts.
- Figure 4.11:** FTIR spectrum of mPEO<sub>17</sub>-F<sub>4</sub>-OEt on ATR crystal in DMSO-water mixture (20 %v/v) focusing on amide II region.
- Figure 4.12:** Confocal phase-contrast image of self-assembled mPEO<sub>17</sub>-F<sub>4</sub>-OEt.
- Figure 4.13:** Confocal fluorescence image (x100 objective, immersion) of self-assembled mPEO<sub>17</sub>-F<sub>4</sub>-OEt stained with Nile blue.
- Figure 4.14:** Confocal microscopy fluorescence and phase-contrast image (x 10 objective) of mPEO<sub>17</sub>-F<sub>4</sub>-OEt (10 mg) in 20 %v/v DMSO-water solution (2 ml).
- Figure 4.15:** Structure of Nile blue.
- Figure 4.16:** Confocal microscopy fluorescence z stack of mPEO<sub>17</sub>-F<sub>4</sub>-OEt (10 mg) in 20 %v/v DMSO-water solution (2 ml), stained with Nile blue.
- Figure 4.17:** Confocal microscopy image of gels prepared from Fmoc-FF in DMSO (image adapted from original source).
- Figure 4.18:** Structure of polymer-peptide conjugate, mPEO<sub>n</sub>-F<sub>4</sub>-OEt, synthesised using; a) click chemistry, and b) IBCF chemistry.
- Figure 4.19:** Transmission electron microscope image of mPEO<sub>7</sub>-F<sub>4</sub>-OEt showing nanotube structures.
- Figure 5.1:** Structure of polystyrene.
- Figure 5.2:** SEM images of polystyrene electrospun at different concentrations from tetrahydrofuran.
- Figure 5.3:** SEM images of polystyrene electrospun at different concentrations from dichloromethane.

- Figure 5.4:** Structure of a polymer with intrinsic microporosity, PIM-1.
- Figure 5.5:** SEM images of PIM-1 electrospun at different concentrations.
- Figure 5.6:** SEM images of PIM-1 (C3), showing microfibrils.
- Figure 5.7:** SEM images of the non-deposited “wool” from electrospinning PIM 1 (C3), showing fibre production.
- Figure 5.8:** SEM images of PIM-1 (C4), showing microfibrils.
- Figure 5.9:** SEM images of the non-deposited “wool” from electrospinning PIM 1 (C4), showing fibre production.
- Figure 5.10:** SEM images of PIM-1 electrospun at different voltages.
- Figure 5.11:** SEM images of PIM-1 electrospun at different tip-to-collector distances.
- Figure 5.12:** SEM images of the deposited material from electrospinning PIM-1 (E1), showing aggregate deposition.
- Figure 5.13:** SEM images of PIM-1 electrospun at different flow rates.
- Figure 5.14:** SEM images of the material from electrospinning PIM-1 (F2), showing fibres and beading.
- Figure 5.15:** SEM images of the material from electrospinning PIM-1 (F3), showing fibres and beading.
- Figure 5.16:** SEM images of initial attempts of electrospinning nanoparticle cage THL294 with a polystyrene scaffold.
- Figure 5.17:** SEM images of initial attempts of electrospinning nanoparticle cage THL295 with a polystyrene scaffold.
- Figure 5.18:** SEM images of initial attempts of electrospinning nanoparticle cage THL 294 and THL 295 with a PIM-1 scaffold.
- Figure 5.19:** The effect of solvent composition on fibre production of PEO<sub>6820</sub>.
- Figure 5.20:** The effect of voltage on fibre production of PEO<sub>6820</sub>.
- Figure 5.21:** The effect of distance on fibre production of PEO<sub>6820</sub>.
- Figure 5.22:** The effect of flow rate on fibre production of PEO<sub>6820</sub>.
- Figure 5.23:** SEM showing the structures produced when electrospinning different molecular weight PEO using the same spinning parameters.

## List of Schemes

**Scheme 1.1:** Reaction mechanism showing peptide synthesis using *N,N'*-dicyclohexylcarbodiimide (DCC) as a coupling reagent.

**Scheme 1.2:** Reaction mechanism showing peptide synthesis using benzotriazol-1-yl-oxytripyrrolidinophosphonium hexafluorophosphate (PyBOP) as a coupling reagent.

**Scheme 1.3:** Reaction mechanism showing peptide synthesis using isobutylchloroformate (IBCF) as a coupling reagent.

**Scheme 1.4:** Reaction scheme of acyl coupling of amino acids.

**Scheme 1.5:** Reaction scheme showing introduction of *tert*-butyl protecting group to the carboxylic acid end of an amino acid.

**Scheme 1.6:** Reaction scheme showing introduction of *tert*-butoxycarbonyl protecting group to the amine end of an amino acid.

**Scheme 1.7:** Reaction scheme showing introduction of the 9-fluorenylmethoxycarbonyl protecting group to the amine end of an amino acid.

**Scheme 2.1:** General reaction scheme showing overall synthetic routes for the production of polymer-peptide conjugates.

**Scheme 2.2:** Reaction scheme outlining the synthetic route for deprotecting the carboxyl terminus of a polymer-peptide conjugate.

**Scheme 3.1:** Reaction scheme showing synthetic routes utilised for the synthesis of  $\text{NH}_2\text{-F}_{(x+y)\text{-OEt}}$ .

**Scheme 3.2:** Synthetic route for carboxylic acid-terminated monomethoxy-poly(ethylene oxide).

**Scheme 3.3:** General amide bond formation, where it is shown that salt formation is favoured.

**Scheme 3.4:** Racemisation during amide bond formation via oxazolone formation.

**Scheme 3.5:** Cartoon reaction scheme comparing general synthetic routes.

**Scheme 3.6:** Reaction scheme showing synthetic route for deprotecting the carboxyl terminus of a polymer-peptide conjugate.

**Scheme 3.7:** Reaction scheme showing ester cleavage by base hydrolysis (saponification) where AA represents one or more amino acids.

**Scheme 3.8:** Fischer esterification between an acid (deprotected peptide) and an alcohol (polymer).

**Scheme 3.9:** Comparisons of reactions scheme for producing polymer-peptide conjugates; A) Tzokova Click Route and B) IBCF Coupling Route.

# **CHAPTER 1**

## **Introduction**

## 1. Introduction

This thesis contains six distinct chapters, starting with a general introductory chapter, describing the background to the entire project, followed by a chapter describing the experimental methods employed in this work, with the succeeding three chapters comprising results and discussion for each of the disparate work packages (from conjugate synthesis to electrospinning through gelation studies). The final chapter provides an overall conclusion for the thesis and future work to be performed. Each chapter contains its own short, more focussed introduction and references, compiled as a list following the section.

### 1.1. Amino acids

Amino acids are one of the four fundamental biological building blocks (the others being carbohydrates, lipids, and nucleic acids). They play a central role in building the essential proteins and metabolites that are required for life. The function of these molecules ranges from aiding in digestion to synthesising new tissues whilst also being important factors in growth<sup>[1]</sup>. Linking amino acids together in a specific sequence, results in the formation of peptides which can form complex three-dimensional structures. Long-chain peptides (or polypeptides) that fold into these structures are classed as proteins. As is known, the precise structure of the tertiary form of a protein is controlled by the amino acids present and their sequence; the modification of even one can affect the folding. Furthermore, proteins inherit their biological functionality from the precursor amino acids.

The general structure of an amino acid is shown in Figure 1.1. R, the variable group is what infers the particular properties of the amino acid. The structure shown is not strictly accurate, as the acidic proton of the acid (COOH) and the basic protons of the amine group (NH<sub>2</sub>) will interact with each other; the amine group deprotonates the acid group in an intramolecular rearrangement, resulting in the formation of a zwitterion. There is no net charge in amino acid zwitterions as the positive charge from the (protonated) ammonium ion is

balanced out by the negative charge of the (deprotonated) carboxylate ion. Their general carbon skeleton template arises from glycolysis and Krebs cycle intermediates (i.e. from metabolic pathways)<sup>[2]</sup>.

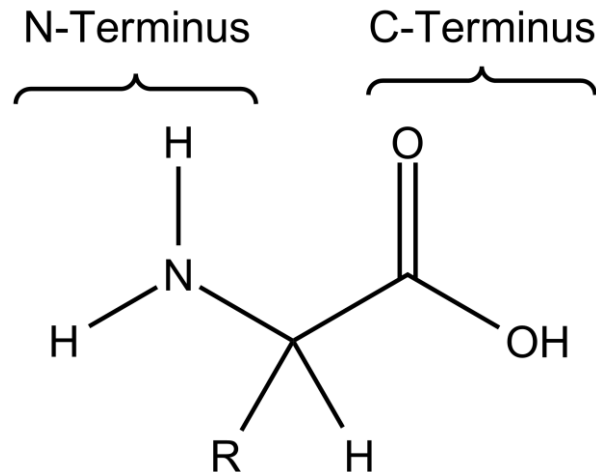


**Figure 1.1:** General structure of an amino acid, where the R group varies depending on the specific amino acid. *N.B. Chirality is not shown in this diagram.*

Amino acids contain at least one asymmetric carbon (with the exception of glycine) and are able to exist as two stereoisomers (enantiomers); an L-configuration and a D-configuration (Figure 1.2)<sup>[3]</sup>. L-amino acids are susceptible to enzyme-catalysed modification and functionalisation. Therefore, in proteins, only the L-isomer is present. It is possible, however, under certain conditions for racemisation to occur, where L-amino acid residues are converted to their respective D forms. This can occur when heat is applied or during pH changes (such as increase in alkalinity). Certain organisms are able to produce D-amino acids biologically<sup>[4]</sup>. Using enzymes, it is possible to convert D-amino acids to DL-mixtures<sup>[5-7]</sup>.

There are twenty “natural” amino acids which are used to produce proteins using a biological process known as translation. In a cell structure (organelle) known as the ribosome, tRNA (transfer RNA) complements and co-ordinates the nucleotide sequence of mRNA (messenger RNA) to produce the corresponding amino acids. The code is deciphered via codons, which are a sequence of three nucleotides that specify which amino acid should be inserted

into the growing peptide chain<sup>[8]</sup>. The genetic code contains a redundancy, known as degeneracy, in which more than one codon may encode an amino acid. However, all codons correspond to one amino acid only.

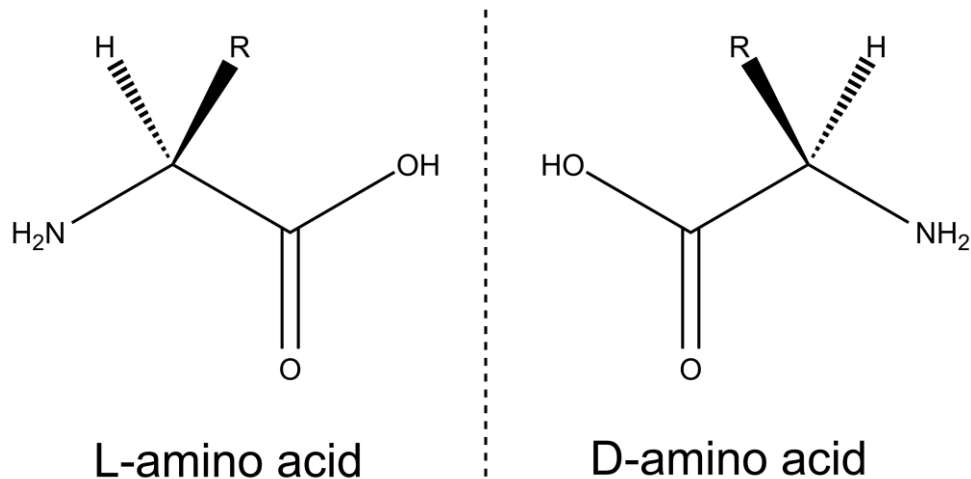


**Figure 1.2:** Isomers of amino acids: L-amino acid and D-amino acid enantiomers.

The twenty amino acids produced in this manner are shown in Figure 1.3, alongside their three letter and single letter abbreviations. They can be further categorised according to the property of their side chain. Of the twenty amino acids, eight have non-polar side chains, and are thus considered hydrophobic amino acids. Amino acids in this group include glycine (which is the only achiral natural amino acid), and phenylalanine (discussed in Section 1.1.1) which contains a benzyl group. The second broad classification group comprises amino acids that have polar side chains, but are uncharged, tending to be hydrophilic. Examples in this category include serine (which contains a hydroxyl group), and cysteine (which contains a thiol group). The third group comprises those amino acids with an acidic, polar side group of which glutamic acid and aspartic acid are members. Finally, the fourth group consists of amino acids with basic polar side groups and includes lysine and arginine (NH<sub>2</sub> side groups). For the latter two groups, the side chains are fully ionised, either protonated or deprotonated, respectively, at physiological pH (7.4).

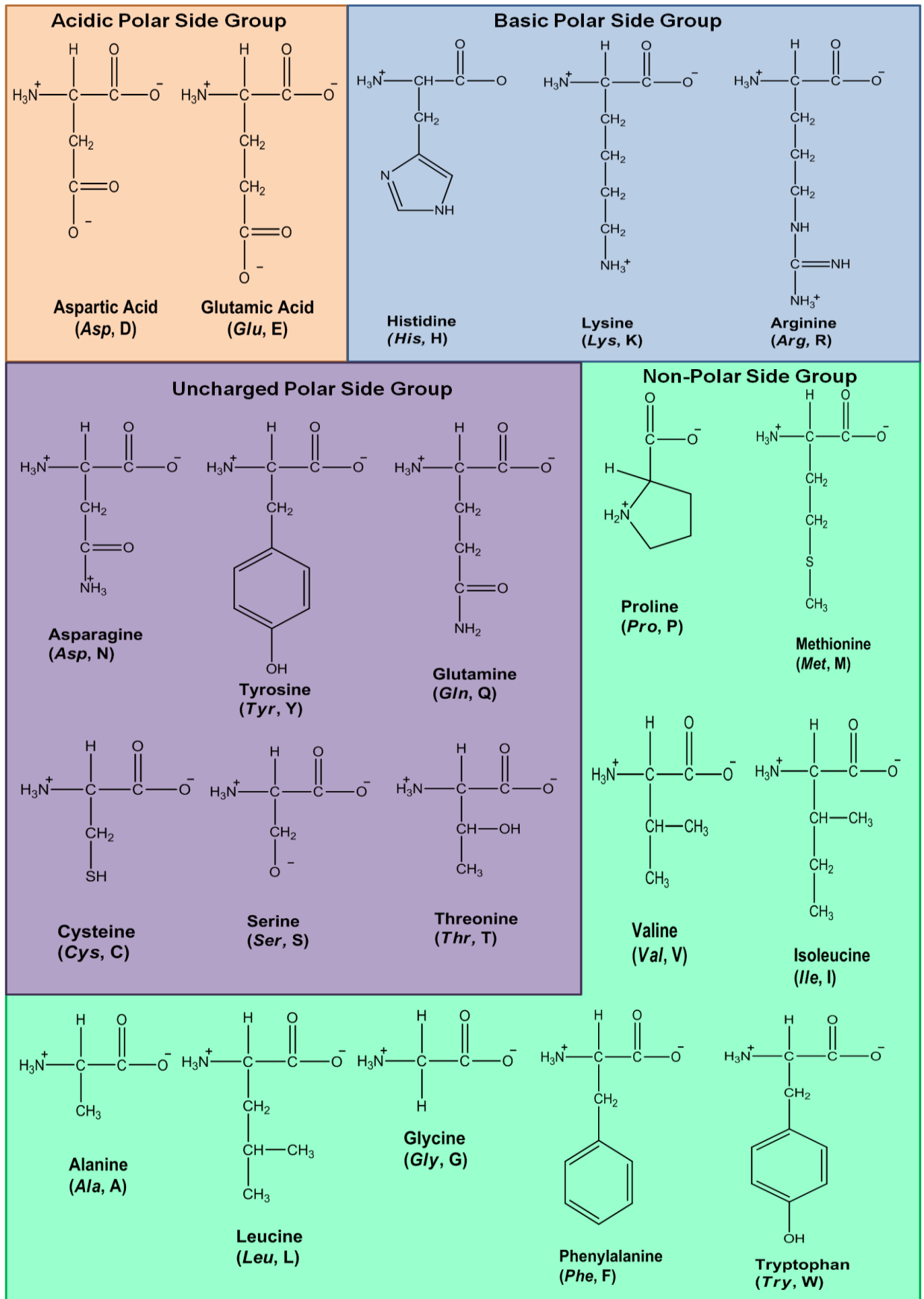


**Figure 1.3:** The twenty proteogenic amino acids, classified by side chain property.

Of the twenty amino acids, nine are considered to be essential amino acids. These amino acids are essential for proper metabolic functioning but cannot be produced by the body. It is imperative that essential amino acids are sourced from the diet, as an insufficient amount of even a single one can seriously impair the body's natural functions, and lead to a degradation in proteins<sup>[9]</sup>. This is further emphasised by the fact that unlike other biological molecules, it is not possible to store excess amino acids for later use. Furthermore, under certain conditions, it is possible that the non-essential amino acids will be unable to be synthesised *de novo* and thus become essential. The essential amino acids in man are: histidine, isoleucine, leucine, lysine, methionine, phenylalanine, threonine, tryptophan and valine<sup>[10]</sup>.

Aside from their biological uses, amino acids have many interesting properties that make them attractive for use in chemistry. It is the ability to introduce beneficial properties (such as enhanced stability, target for labelling, pH-responsive behaviour<sup>[11]</sup>) that make them so desirable for incorporation into other compounds<sup>[12-16]</sup>. Incorporating unnatural functionality into amino acid-derived biomolecules has proven to be a successful strategy in the design of peptides with more desirable properties. The amino acid particularly focussed on in this project was phenylalanine.

### 1.1.1. Phenylalanine

Phenylalanine (Phe, F), shown in Figure 1.4, is a non-polar essential amino acid. In the body, phenylalanine is the precursor to a number of important biological metabolites and hormones (such as dopamine), as well as the amino acid, tyrosine. The hydrophobic character and the phenyl ring structure of the amino acid confer interesting properties that may prove beneficial for use in an assortment of applications. Indeed, the phenyl ring could prove particularly beneficial for self-assembly behaviour. It is known that many compounds and materials take advantage of the effects of non-covalent aromatic<sup>[17]</sup> (known as  $\pi$ - $\pi$  stacking) interactions, such as Kevlar. The use of short chain phenylalanine peptide sequences can result in self-assembly and hydrogel formation occurring<sup>[18,19]</sup>. Formation into a gel allows the hydrophobic nature of

phenylalanine to act as a mask for the properties of a molecule (e.g. hydrophilicity) and further confers some biocompatibility. This presents remarkable opportunities for using phenylalanine as a delivery mechanism for drugs or other soluble or non-soluble substrates<sup>[20]</sup>. However, it has also been shown that after a brief period of time, the self-assembled nanostructure(s) break down. Therefore, whilst the formation of hydrogels is desirable, the stability of such materials is lacking and so, a way to stabilise these materials is required. The most obvious route would be to couple phenylalanine with a stabilising material that does not affect (or minimally affects) overall functionality or biological activity.

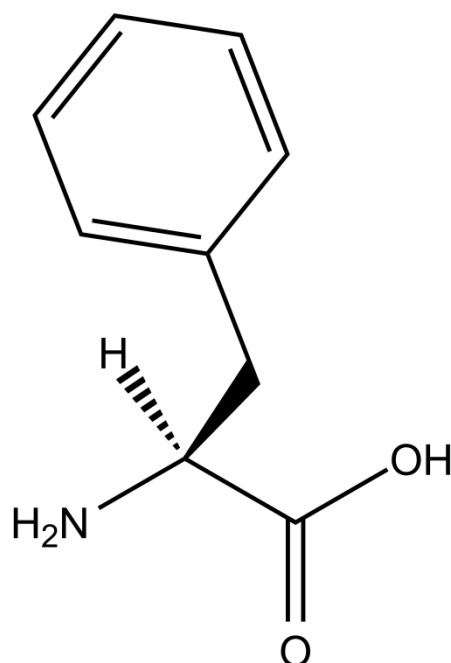


**Figure 1.4:** Structure of L-phenylalanine.

## 1.2. Peptide synthesis

As aforementioned, the building blocks used in the body for peptide coupling are the twenty naturally occurring proteogenic amino acids. It should be noted that there are also synthetic amino acids available for use; however these will not be discussed.

Amide bonds are found in a wide variety of biological compounds. They are especially prevalent in compounds containing peptides, such as proteins or derivatives thereof. These linkages hold amino acid residues together and are often referred to as peptide bonds. Formation of these bonds can take place without modification of the general peptide structure through a simple coupling reaction. One of the most prevalent routes for coupling reactions is complementary group conjugation<sup>[21]</sup>. This approach involves exploitation of the reactivity of the amine (N-terminus) or carboxylic acid group (C-terminus) of the peptide, and the carboxyl group or amine group, respectively, of the second peptide. Further, any side groups with appropriate functionality can be targeted as potential conjugation sites. It should be noted that whilst normally the reacting groups are on the terminus of their respective compounds, this is not always the case, and coupling can take place via groups on side-chains as well<sup>[22, 23]</sup>. The hydroxyl group of the acid is a poor leaving group and would form a salt with the amine if not modified. Therefore, during the reaction, it is typical to use a coupling agent to activate the carboxylic acid functional group, driving the reaction forward. Coupling agents must facilitate the reaction, but also should be easily removable from the final product. The aim of the coupling reaction is to be fast, produce pure products, and occur under mild reaction conditions. To achieve this goal, several coupling methods have been developed<sup>[24]</sup>.

It is imperative to note that there is a need to prevent uncontrolled chain growth between reacting species<sup>[25]</sup>. This would result in a mixture of products (Figure 1.5). To combat this, a protecting group strategy is used. The reacting peptides will have only one functional group accessible; the other is blocked by a protecting group. Once conjugation has been successful, the protecting group is removed allowing further coupling. This type of approach minimises the formation of mixtures. Section 1.4 outlines some of the common techniques used to ensure easy protection/deprotection<sup>[26-28]</sup>.

There are a variety of methods available for creating peptide sequences. Coupling can take place either in solution or on solid supports<sup>[29-31]</sup>. Most experimentalists tend to favour the solid phase approach and a variety of polymer-supported scaffolds are available to facilitate peptide synthesis<sup>[32]</sup>.

Section 1.3 provides examples of coupling methods used to synthesise peptides.

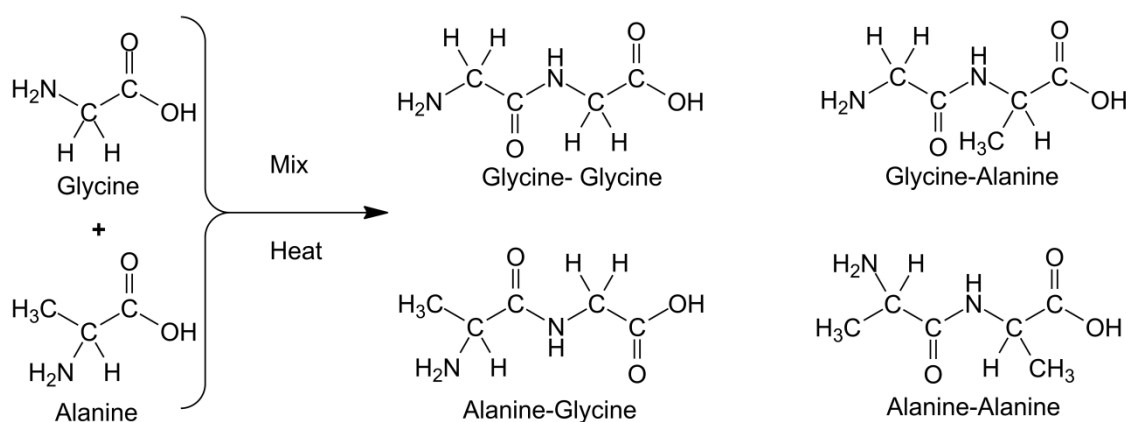


**Figure 1.5:** Mixture of products produced when glycine and alanine are directly coupled. The products produced are bifunctional, and can further couple, to produce trimers, tetramers, and eventually, larger oligomers. This highlights the necessity of a protecting group strategy.

### 1.2.1. Peptide synthesis in solution

Despite some advantages over peptide synthesis in the solid phase, synthesis in the solution state is used less frequently, especially for large peptides, since it is slow, intensive, and can cause problems of racemisation and poor solubility of the synthetic intermediates. However, synthesising using solution phase techniques allows for purification after each repeat unit is added and for precise quantification after each step. As mentioned, solubility issues arise, especially as the peptide length increases. Furthermore, separation from any by-products may prove problematic. It should be noted that the heterogeneous reaction conditions present in solid-phase techniques can also cause several problems, including solvation difficulties<sup>[33]</sup>. Further, the cost of solution phase coupling is cheaper, with reagents being more readily available than corresponding polymer supported reagents, and many more reactions are optimised for solution chemistry. The use of solution phase synthesis also allows for a greater number of protecting group strategies to be used<sup>[34]</sup>.

### 1.2.2. Peptide synthesis in the solid state

In 1963, Merrifield established what is now termed solid phase peptide synthesis (SPPS). He attached an amino acid to an insoluble polymer support, thus immobilising it. From there, it was possible to directly attach subsequent amino acids and thus grow a peptide. Once the chain had been synthesised it could be released from the solid support using an acid<sup>[35]</sup>.

This was innovative as it afforded researchers an effective, reliable route for peptide production. Loss of product was avoided, as it remained anchored to the polymer support, and yields could be further increased by using an excess of reagents. The technique was continuously refined over the succeeding years, and today has become automated.

However, the technique still has caveats that must be addressed. Firstly, the synthesis of long chain peptides remains somewhat problematic. This is due to the decreasing solubility of the growing peptide chain, and its growing incompatibility with the polymer support. Further, the longer the peptide chain length, the more likely it is to encounter incomplete deprotection steps and side-chain conjugation<sup>[34]</sup>. Another major drawback to solid phase techniques are the costs involved. Both the polymer supports, and the protected amino acids can be costly, and in the latter case, this means that consumption to side-chain conjugation (and using sacrificial amino acids) is highly undesirable and should be avoided at all costs. This is also one of the reasons that SPPS is difficult to scale up. Despite these drawbacks, SPPS remains the preferred technique for peptide synthesis.

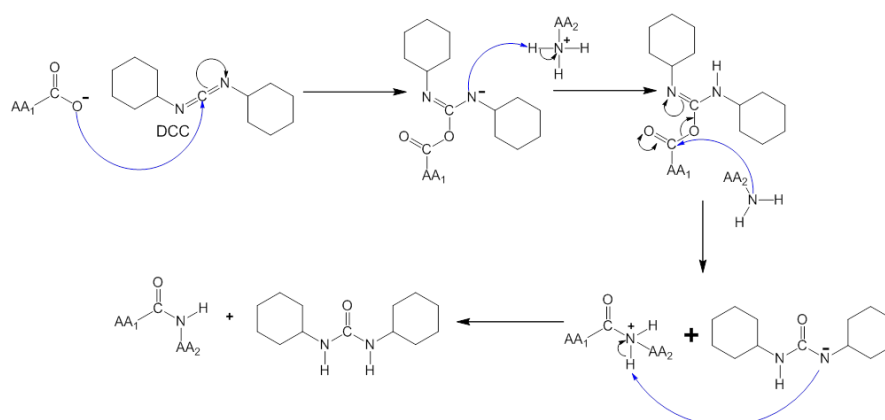
It was decided that a solution phase approach would be taken for peptide synthesis in this project. This was due to the economical and practical benefits outweighing the disadvantages of solution phase approaches. Additionally, it is highly desirable to isolate and analyse each product after each stage of synthesis.

### 1.3. Peptide synthesis techniques

Peptide bond formation should ideally be quick, mild, with minimal (or no) side reactions, and easily removed by-products; these conditions are similar to the criteria for so-called '*click chemistry*'<sup>[36, 37]</sup>. Additives can be added to help increase coupling efficiency and reduce side-reactions. Also, as noted previously, racemisation can occur with amino acids, however certain additives can be used to help suppress such unwanted rearrangements.

#### 1.3.1. Carbodiimide coupling

Dicyclohexylcarbodiimide (DCC) is one of the longest used coupling reagents for peptide synthesis. First published by Sheehan and Hess in 1955<sup>[38]</sup>, it has been used as direct coupling agent ever since. The agent works by activating the carboxylic acid group on the amino acid resulting in the formation of an O-acylisourea intermediate. It is the electron deficient central carbon that is attacked by the carboxylate anion. This intermediate is one of the most reactive acylating groups and reacts with the amine group of a second amino acid forming an amide bond (protected at the C-terminus). The resulting product is the desired peptide, along with dicyclohexylurea (DHU) as a by-product. It is the formation of the markedly stable DHU that drives the reaction. Scheme 1.1 elucidates the mechanism for this reaction.



**Scheme 1.1:** Reaction mechanism showing peptide synthesis using *N,N'*-dicyclohexylcarbodiimide (DCC) as a coupling reagent. AA represents an amino acid.

Conventionally, a small amount (5-10 mg) of 4-dimethylaminopyridine (DMAP) is used to increase the efficiency of the reaction. DHU precipitates in the reaction solution, giving a visual indicator of the reaction progress of the reaction. However, DHU is sparingly soluble and so may not completely precipitate, making purification difficult. It is for this reason that DCC coupling techniques are not favoured for use with SPPS as the DHU precipitate is difficult to separate from the resin.

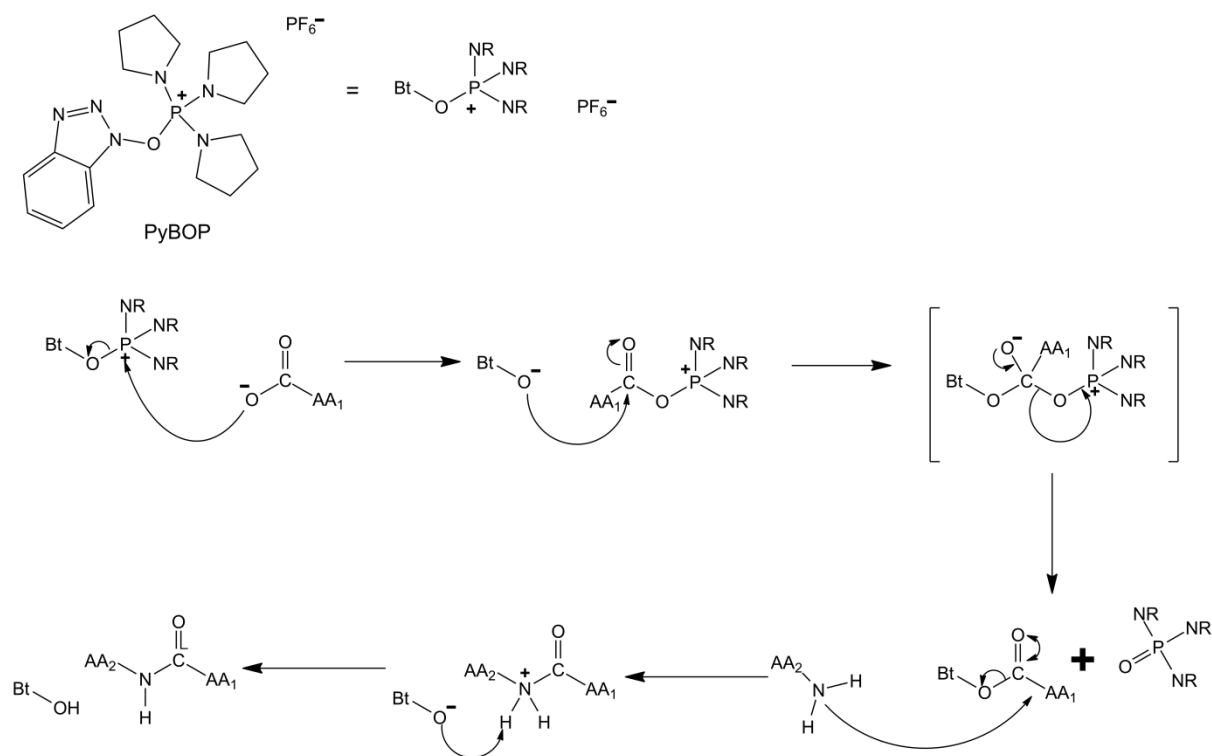
Activation by DCC is highly dependent on the solvent system used. In solvents with low dielectric constants (i.e. relatively low polarity) such as chloroform or dichloromethane, the formation of O-acylisourea is rapid<sup>[39]</sup>. In comparison, reactions in a polar solvent are markedly slower. A reaction in *N,N*-dimethylformamide (DMF), which is a polar aprotic solvent, does not immediately produce this intermediate.

To overcome these problems, diisopropylcarbodiimide (DIC) has been used<sup>[40]</sup>. Whilst the urea by-product of this compound is more soluble, DIC is not soluble in dichloromethane, however it is soluble in a co-solvent system of DMF and DCM (or DMF alone). Recent developments have involved use of 1,3-bis(2,2-dimethyl-1,3-dioxolan-4-ylmethyl)carbodiimide (BDDC) which has been used for coupling in solution phase and minimising racemisation and epimerisation<sup>[40]</sup>.

### 1.3.2. Phosphonium coupling

Whilst carbodiimide coupling is more tailored for solution phase chemistry, coupling using phosphonium salts is the opposite. It was popularised in the early 1970s after extensive work by Castro *et al.*<sup>[41]</sup> One of the earliest and most popular compounds used for direct conjugation from this work was (benzotriazol-1-yloxy)tris(dimethylamino)phosphonium hexafluorophosphate (BOP). BOP allows for *in situ* formation of activated esters such as hydroxybenzotriazolyl esters (HOBt). The reaction is very effective and efficient. However, it has a major disadvantage in that the hexamethylphosphoramide (HMPA) by-product, a phosphoric acid amide derivative, is highly toxic and carcinogenic. Whilst the reagent can be used in small amounts, for large scale

industrial purposes this is not viable, therefore alternate salts were sought. One alternative was benzotriazol-1-yl-oxytripyrrolidinophosphonium hexafluorophosphate (PyBOP) which offers all of the advantages of BOP, with less pernicious by-products (Scheme 1.2).

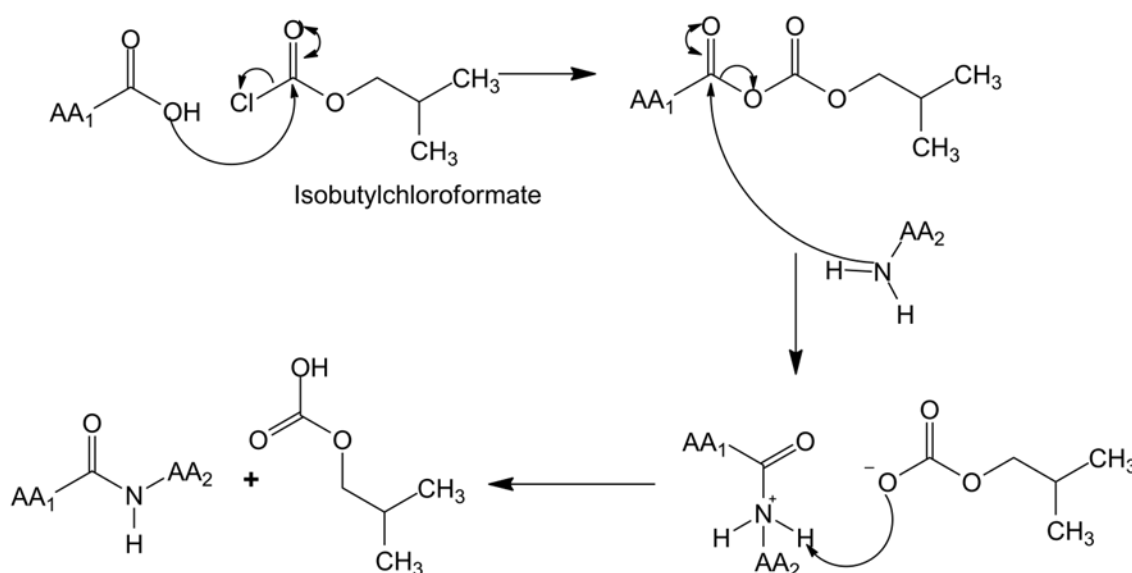


**Scheme 1.2:** Reaction mechanism showing peptide synthesis using benzotriazol-1-yl-oxytripyrrolidinophosphonium hexafluorophosphate (PyBOP) as a coupling reagent. AA represents an amino acid.

The coupling reaction proceeds through the formation of an ester in the presence of a tertiary base, such as Hünig's Base (diisopropylethylamine, DIPEA) or *N*-methylmorpholine (NMM). Tertiary amines generate the carboxylate anion (RCOO<sup>-</sup>) which attacks the phosphorus on the coupling species (BOP/PyBOP). The ester formed is then attacked by the amine of a second amino acid to form the amide bond. Hydrogen bond stabilisation on the intermediate compound helps to form the final product. It has been found that the addition of HOBT accelerates the coupling process.

### 1.3.3. Chloroformate coupling

Chloroformate coupling is a well-known, widely used coupling technique used for peptide synthesis. Use of alkyl chloroformates was first proposed in the early 1950s<sup>[42]</sup>. It became widely used due to its speed, high yielding reactions, and purity of its products. The reaction proceeds first through the formation of a mixed anhydride, where the carboxyl group has been activated. This step conventionally takes place in the presence of a tertiary amine base, such as NMM. It is the mixed anhydride that is able to react with the desired amine<sup>[24, 43]</sup> (Scheme 1.3). However, it is possible for side reactions to occur. One such reaction is another acylation of the amine from the carbonate carbonyl carbon.



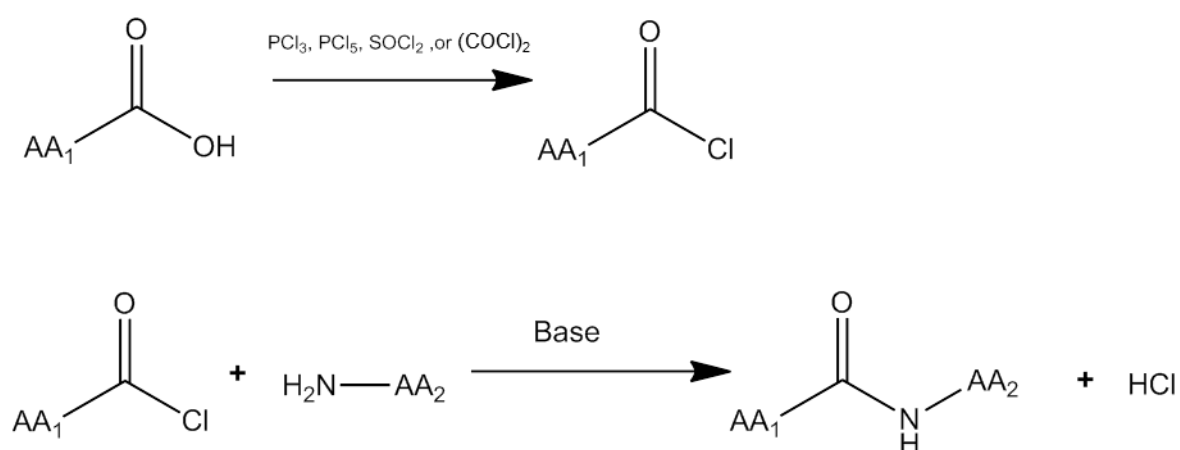
**Scheme 1.3:** Reaction mechanism showing peptide synthesis using isobutylchloroformate (IBCF) as a coupling reagent. AA represents an amino acid.

This can lead to the starting amino acid being liberated at the end of the reaction<sup>[44]</sup>. It is noted that the side-reaction is scale dependant and therefore is not observed at lower concentrations of peptide or coupling reagent. Furthermore, the by-product, a urethane, is easily removable when formed. The bulky *tert*-butyl group in isobutylchloroformate decreases the extent of side-reactions<sup>[45]</sup>, thus making peptide synthesis more reliable<sup>[46]</sup>. Minimisation of by-products, ease of reaction, and simple work-up, render IBCF an attractive

tool for peptide coupling. It is for these reasons that IBCF was chosen for peptide coupling in this project, and also why it was investigated for polymer-peptide coupling for the first time.

#### 1.3.4. Other coupling methods

Acyl chloride coupling is perhaps the easiest and most economical method of forming the amide bond<sup>[47]</sup>. The reaction involves converting the carboxylic acid group of one of the amino acids to an acyl chloride group. This can be achieved using reagents such as oxalyl chloride (COCl)<sub>2</sub>, thionyl chloride SOCl<sub>2</sub>, or phosphorus chlorides, PCl<sub>3</sub> and PCl<sub>5</sub> (Scheme 1.4).



**Scheme 1.4:** Reaction scheme of acyl coupling of amino acids. AA represents an amino acid.

While this method is direct and relatively easy, there are several drawbacks associated with it<sup>[48]</sup>. Firstly, the production of HCl causes problems when using acid-sensitive peptides, such as Boc-protected amino acids. Secondly, the initial carboxylic acid conversion step results in the formation of toxic by-products (the exact nature depending on the reagent used), such as carbon monoxide or sulfur dioxide.

## 1.4. Protecting group strategy

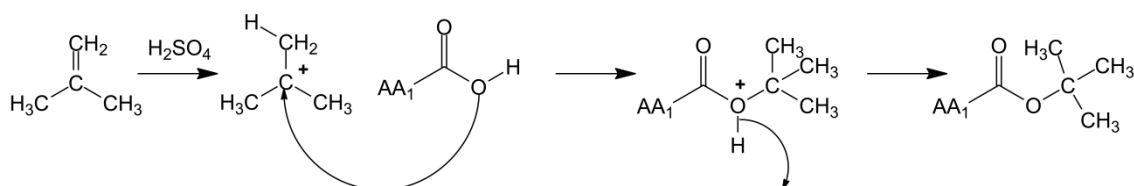
A protecting group strategy is necessary to control or direct a reaction and to prevent product mixtures that can arise when using multifunctional reagents. This approach is also necessary because a functional group in a molecule may interfere with the reaction of another functional group in the same molecule, leading to undesirable products<sup>[49]</sup>. In the case of synthetic polymers, it is possible to incorporate a protecting group during initial synthesis/ polymerisation. For example, monomethoxy-poly(ethylene oxide) is normally synthesised via anionic polymerisation. By occupying one of the hydroxyl groups of PEO, it effectively allows for only one possible modification site; the remaining hydroxyl group. Such a “protection”, whilst useful, is not easily reversed post-synthesis.

Peptides are at least bifunctional and can therefore react with each other or an appropriate substrate in several different ways. Furthermore, each amino acid is able to react with the same species of amino acid (e.g. glycine can react with glycine), due to the reactivity of the end groups. It is very important when synthesising peptides that the sequence of amide bonds is formed in the correct order, and the correct orientation, otherwise the functional effectiveness of the final peptide may be affected. Although there are many different protecting group strategies possible, in practice only a few are actually used. Merrifield defined and developed the first known instance of orthogonal protection, whereby deprotection of multiple protected functional groups takes place sequentially, with each step not affecting any of the other groups in the molecule<sup>[50]</sup>.

### 1.4.1. Carboxylic acid group protection

Carboxylic acid groups are usually protected by converting them into esters, such as methyl esters or benzyl esters. *tert*-Butyl esters are correspondingly more stable than both methyl and benzyl esters due to steric and electronic effects. Consequently, the protected functional group is tolerant to both nucleophilic and basic attack. It should be noted that some susceptibility to

basic attack is required as this is the route used for removal of the protecting group. Protection by esterification is widespread, most likely because esters are readily introduced by simple S<sub>N</sub>2 chemistry, such as using methanol in the presence of an acid (Scheme 1.5). Subsequent removal of the ester protecting group can be performed by treatment with an aqueous base, such as sodium hydroxide or lithium hydroxide.



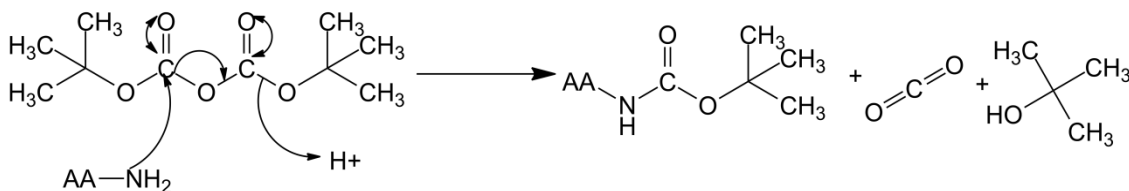
**Scheme 1.5:** Reaction scheme showing introduction of *tert*-butyl protecting group to the carboxylic acid end of an amino acid. AA represents an amino acid.

The *tert*-butyl group can be removed using trifluoroacetic acid (in solid and solution phase) or HCl (solution phase only). It should also be noted that in SPPS, the carboxylic acid is protected by virtue of being linked to the solid support or benzyl ester linker. Further, glutamic acid and aspartic acid which both have two carboxylic acid groups require a slightly different strategy. Selective protection can be carried out by forming an intramolecular anhydride between the internal two carboxylic groups. Other routes for deprotection include the use of zinc chloride which deprotects *tert*-butyl and methyl esters<sup>[27]</sup>.

#### 1.4.2. Amino group protection

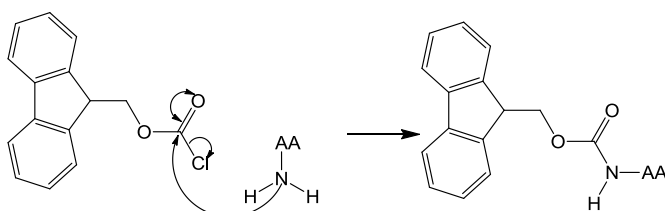
Two main amine protecting group strategies are employed. The first strategy involves conversion to an amide derivative, of which *tert*-butoxycarbonyl (Boc) amide is one of the most widely practised strategies. It is not possible to use Boc-Cl as the resulting reagent is unstable<sup>[51]</sup>. Instead, the anhydride form is used (Boc<sub>2</sub>O). The amine group undergoes a nucleophilic substitution reaction under basic conditions (such as in the presence of bicarbonate) with di-*tert*-butyl carbonate, which results in a bulky acyl group being added to the molecule (Scheme 1.6). Deprotection can take place using a strong acid such

as trifluoroacetic acid (TFA). Although this method is widely used, it does have drawbacks, such as the somewhat harsh deprotection conditions, and the susceptibility of the protecting groups to react with other reagents (e.g. acids).



**Scheme 1.6:** Reaction scheme showing introduction of *tert*-butoxycarbonyl protecting group to the amine end of an amino acid. AA represents an amino acid.

To overcome problems associated with Boc protection, other strategies were developed with milder conditions and shorter reaction times. Fluorenylmethoxycarbonyl chloride (Fmoc-Cl) is considered as an excellent alternative to Boc protection. Fmoc contains a large heterocyclic aromatic system with an acid chloride group. The acid chloride allows for substitution of an ester to form the carbamate which is used for amine protection. Scheme 1.7 illustrates the mechanism of protection using Fmoc. Removal of the Fmoc group is undertaken using a mild base such as piperidine in dimethylformamide. A side product, dibenzofulvene, is formed during deprotection which can easily be removed by filtration. Fmoc protection is the premier technique used in solid phase peptide synthesis (SPPS). Boc protection cannot be used in SPPS due to the acid labile benzyl ester linker, which would be cleaved during deprotection of Boc, whereas the mild basic conditions required for Fmoc deprotection does not affect this linker.



**Scheme 1.7:** Reaction scheme showing introduction of the 9-fluorenylmethoxycarbonyl protecting group to the amine end of an amino acid. AA represents an amino acid.

### 1.4.3. Disadvantages of a protecting group strategy

The use of protection/deprotection chemistry is widespread and considered an essential part of synthetic chemistry, and especially peptide synthesis. However, protection and subsequent deprotection are additional steps in the overall synthetic scheme, and result in a reduction of the final yield. It may also not be possible to stop the reagents involved in the protection/deprotection steps associating with the target compound. For example, TFA is noted to associate with peptides, and can be difficult to remove. Such details should be taken into account when planning synthesis involving protection.

### 1.5. Polymer-peptide conjugates

Many biological entities, e.g. oligonucleotides <sup>[21]</sup>, saccharides <sup>[22]</sup> and lipids <sup>[23]</sup>, have been investigated for conjugation with synthetic polymers, but it is amino acid-containing species as conjugates which have received the majority of attention<sup>[52]</sup>. Polymer-peptide conjugates (PPCs) are hybrid materials which covalently combine peptide sequences with synthetic polymer chains (Figure 1.6). There has been a great deal of interest in the last twenty years or so on the combination of biological and synthetic polymers with a wide range of applications.

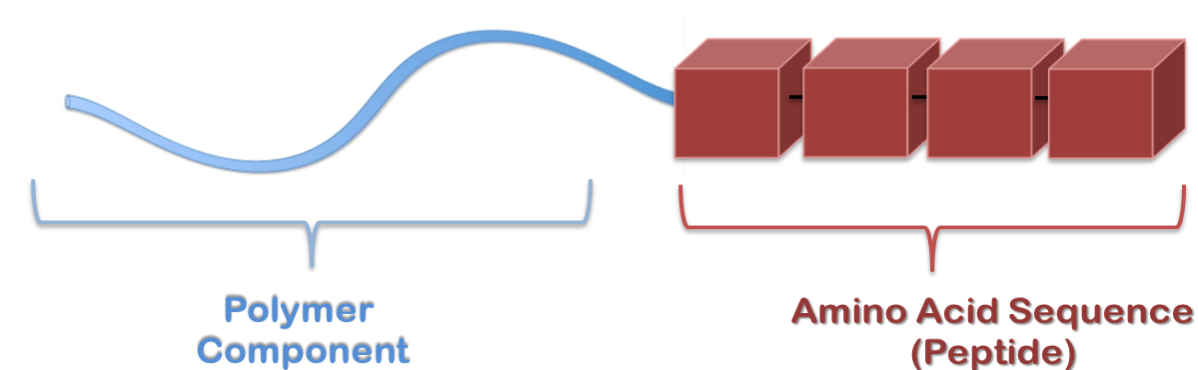


**Figure 1.6:** A cartoon schematic of a polymer-peptide conjugate.

The use of peptides allows for the incorporation of properties such as biocompatibility, bioactivity and self-assembly <sup>[53-56]</sup>, whilst the synthetic polymer component in these materials allows control of physical and chemical

properties, such as solubility, mechanical properties, viscosity and smart behaviour. It has also been shown that the use of synthetic polymers can prolong the lifetimes of materials in the body<sup>[57]</sup>. Supramolecular organisation of asymmetric polymer-peptide molecules offers a gateway to tailor-made materials suitable for a wide range of applications.

There are examples of biological polymer-synthetic polymer conjugates for drug delivery, where the biological entity itself may be the active species, i.e. a drug or pro-drug. The delivery of the peptide via this method is the essence of the Ringsdorf model of drug delivery<sup>[19]</sup>, which can be traced back to a landmark paper in 1975<sup>[58]</sup>. Alternatively, the peptide may be used for therapeutic targeting, for example via biorecognition of the peptide motif <sup>[59, 60]</sup>. It is generally noted that the greater the length of the amino acid chain, the more expensive the cost of synthesis. This is due to the increased number of synthetic and purification steps, and is even more of a concern when considering commercial processes. Therefore control of self-assembly with the lowest number of amino acids is favourable<sup>[61]</sup>.

Jatzekewitz<sup>[62]</sup> published a report in 1954, on what is thought to be the first successful PPC, which sparked a steady interest in the area for the following 30 years. However, in recent years the interest in PPCs has exploded as their potential applications have become realised. This activity was increased further with incredible advances in coupling mechanisms and other synthetic strategies<sup>[63]</sup>. New materials are being produced with greater fidelity, greater purity and novel properties, which leads to an even broader range of potential applications.

One of the most interesting properties of these conjugates is their ability to self-assemble to form complex three dimensional networks. These networks can entangle to form an array of nanostructures <sup>[64]</sup>, which are physically-bound owing to the propensity of the peptide units to aggregate. PPCs have a wide range of applications, such as bio-sensors, artificial enzymes and photonic and nano-electronic devices<sup>[17]</sup>. Notably, PPC hydrogels have been used as scaffolds for tissue engineering and regeneration.

## 1.6. Poly(ethylene oxide) and pegylation

### 1.6.1. Poly(ethylene oxide)

Of all the synthetic polymers available for conjugation to biological entities, perhaps none have received more attention<sup>[52, 65]</sup> than poly(ethylene oxide) [PEO, commonly abbreviated as PEG, originating from poly(ethylene glycol)]. The general structure of the polymer is shown in Figure 1.7. Anionic or cationic polymerisation is the method of synthesis depending on what type of catalyst is used<sup>[66-68]</sup>.

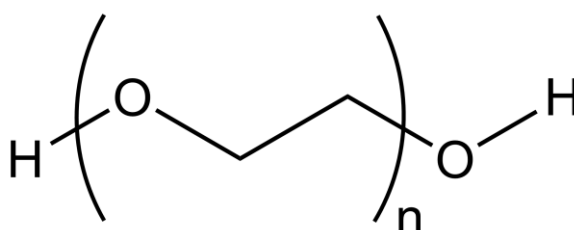


**Figure 1.7:** Structure of poly(ethylene oxide).

Since the early 1970s PEO has been the focus of conjugation efforts with biological molecules, to produce a material with therapeutic action *in vivo*. The reason for the high usage of PEO lies with the properties that it confers to the conjugate material. One such example is its lack of immunogenicity and antigenicity<sup>[69, 70]</sup>. This “invisibility” to the immune system allows PEO-coupled compounds to be transported within the body whilst minimising the chance of an immune response. Other beneficial properties of PEO include general low toxicity, and high degree of solubility in a range of solvents, both aqueous and organic. Many of these conjugate compounds are conveyed into the body in solution, and so addition of PEO results in the hydrodynamic volume also increasing. These properties prolong the lifetime of the conjugated material in the body by either reducing immune attack and by reducing renal clearance. In summary, PEO is non-toxic, non-immunogenic, water soluble, inexpensive, biocompatible, has well known physico-chemical properties<sup>[71]</sup>, and is Federal Drug Agency (FDA) approved for general use<sup>[72]</sup>.

### 1.6.2. PEGylation

The term PEGylation was first used by Abuchowsky in the 1970s whose papers described enzyme modification<sup>[73-75]</sup>. This was highly important as it proved that it was possible to modify enzymes whilst maintaining enzymatic activity. Subsequently, PEGylation expanded exponentially with a wide range of conjugation methods available. It is now possible to modify selected single amino acids using an appropriate PEO or PEO-derivative. Unfortunately, PEGylation of proteins is often accompanied by some loss of biological activity. However, this is compensated for by the prolonged times in the body, as a result of the increased stability, higher hydrodynamic volume and being surrounded by water molecules<sup>[76]</sup>.

PEO itself is a bifunctional polymer, which if involved in a coupling reaction would result in a mixture of products being formed. Accordingly, monomethoxy-poly(ethylene oxide) (mPEO) is used as there is only one active end of the polymer, resulting in a cleaner overall reaction. Furthermore, modification of the unhindered hydroxyl group allows for the synthesis of more reactive monofunctional mPEO adducts, such as mPEO-NH<sub>2</sub>, mPEO-COOH and so forth.

In 1990, PEO-adenosine deaminase (PEG-ADA) was approved by the FDA for therapeutic use.

### 1.6.3. Drawbacks of poly(ethylene oxide) and its derivatives

Whilst the advantages of using PEO and its derivatives have been noted, there are several limitations that should be discussed. Whilst the reduction in renal clearance is advantageous in prolonging the lifetime of the substrate, it is apparent that metabolic clearance decreases as molecular weight increases; PEO will not be able to pass through the Bowman's capsule and thus will not be excreted through urine if it is above a certain weight<sup>[77]</sup>. In this instance, PEO would accumulate in the liver and be removed from the body by biliary excretion<sup>[78]</sup>. During this time the substrate remains in the body and can

lead to adverse effects. This issue of clearance of PEO is problematic as long-term excretion studies have not been carried out<sup>[79]</sup>. The molecular weight threshold at which this occurs has not been fully determined as the hydrodynamic volume of PEO is increased in solution by a large factor. *In vivo*, whilst PEO is generally immune silent, it is still susceptible to enzymatic degradation, and is also still susceptible to degradation by radiation thus affecting overall activity and lifetime. Furthermore, dermal administration of PEO can trigger allergic reactions, for example when used in dentifrice<sup>[80]</sup>.

It should also be noted that the synthetic nature of PEO means that there will be a molecular weight distribution (termed polydispersity, PDI or molar mass dispersity,  $M_w/M_n$ ), in which the polymer is actually made up of many chains of varying length. Synthetic advances allow for the production of PEO with a significantly lower polydispersity than previously available; however the effect can only be minimised not eliminated. Polydispersity in itself is not a disadvantage, however the differing lengths of polymer may have varying biological properties, the most important being immunogenicity and clearance. With higher molecular weight compounds (e.g. proteins, carbohydrates) coupled to PEO, the impact of this issue is reduced as the size of the PEO is less relevant. Conversely, low molecular weight conjugates, such as short-chain peptides, are more dependent on the PEO size characteristic. Also, in mPEO a small amount of diol (i.e. PEO) could also be present, potentially affecting the final conjugation product.

It can be seen that PEO is an extremely useful polymer, with advantageous properties that can be conferred to the desired substrates for prolonged lifetime in the body. PEO can be used to control the self-assembly of materials by affecting the hydrophilic/hydrophobic balance

### **1.7. Polymer-peptide conjugation strategies**

The ability to choose a specific sequence of amino acids, alongside a range of synthetic polymers, allows for the design of various morphologies and materials, such as fibres<sup>[25, 32-34]</sup>, three-dimensional hydrogels<sup>[35, 38, 39]</sup>,

nanosponges<sup>[40, 41]</sup>, microgels/nanogels<sup>[42, 81]</sup>, vesicles<sup>[82]</sup> and micelles<sup>[83]</sup>. Peptide motifs allow self-assembly to occur in a manner in which the structural arrangements are well-defined, and in which the resulting properties are more controllable.

It should be noted, however, that amino acid and monomer selection design rules are not entirely straightforward, as structural analogues often behave very differently and are hugely affected by purity<sup>[30]</sup>. There is also a need to consider the effect of the species which are used in the synthesis of PPCs as these have been shown to affect hydrogel formation. For example, the protecting species fluorenylmethoxycarbonyl (Fmoc) is known to impact upon the formation of hydrogels<sup>[84]</sup>.

There are many methods employed for the synthesis of the precursor peptides (i.e. amino acid coupling strategies) and polymers (i.e. polymerisation techniques) for use in PPCs which are beyond the scope of this thesis and are detailed in the literature. Conjugation strategies fall into two distinct approaches: convergent and divergent. A convergent approach involves both building blocks being synthesised separately and then joined via an additional ligation step. By contrast, a divergent approach entails either the modification of the peptide or polymer block allowing 'growth' of the other component from the first functional unit. Section 1.7.1 details convergent strategies, whilst Section 1.7.2 details divergent strategies. Figure 1.8(a-d) illustrates some of the most common coupling methods used to synthesise PPCs via a convergent approach, whilst Figure 1.8e demonstrates an example of a divergent approach.

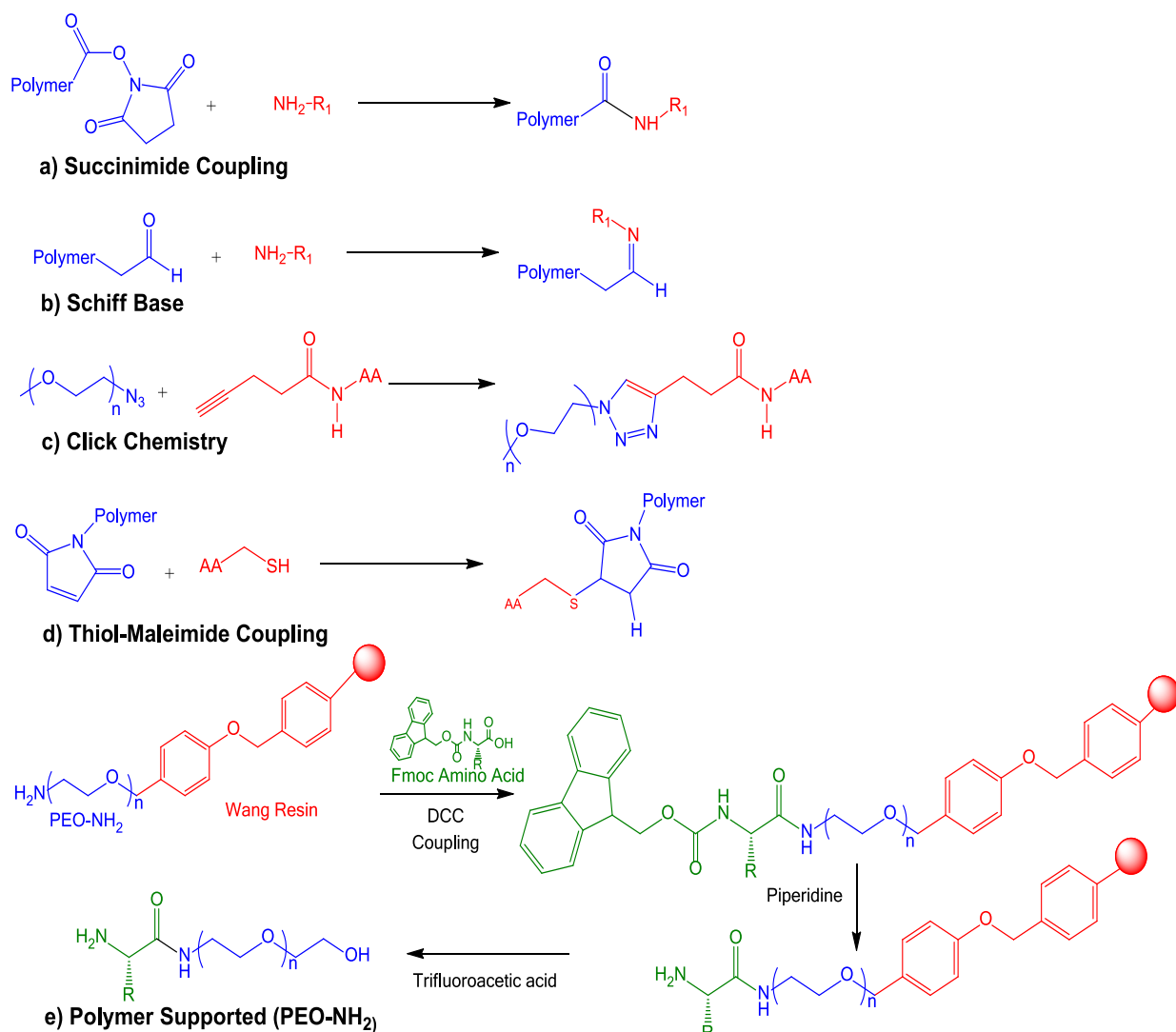


**Figure 1.8:** Some of the most common convergent strategies used to synthesise polymer-peptide conjugates; (a) Succinimide coupling, (b) Schiff base coupling, (c) Azide-alkyne click chemistry, and (d) Thiol-maleimide coupling. (e) An example of a divergent approach synthesising an amino acid sequence from a polymer support.

### 1.7.1. Convergent strategies (direct conjugation)

There are a range of methods available for introducing peptide sequences to synthetic polymers. Coupling can take place either in solution or solid phase. When dealing with peptides, most experimentalists tend to favour the solid phase approach for the peptide synthesis, and then carry out conjugation in either the solid or solution phase. The following section provides examples of

common coupling methods used to link polymers to peptides; (i) succinimide, (ii) Schiff base, (iii) click chemistry, and (iv) thiol-maleimide. Complementary group conjugation is one of most prevalent routes for coupling reactions. This approach involves exploitation of the reactivity of the amine (N-terminus) or carboxylic acid group (C-terminus) of the peptide, and the end group of the synthetic polymer which can be functionalised during, or post, polymer synthesis. Further, any side groups with appropriate functionality can be targeted as potential conjugation sites.

#### 1.7.1.1. *Succinimide*

A good example of complementary group conjugation is demonstrated using *N*-hydroxysuccinimide functional polymers (Figure 1.8a). Succinimidyl esters react readily with amines and are especially useful as they can couple to either the terminal amine group of a peptide, or be directed to an amine side group (in lysine-containing amino acid sequences, for example) by using a protecting group strategy. Polymers can be functionalised with succinimidyl esters, such as succinimidyl carbonates, with relative ease, and many are commercially available, with monomethoxy-poly(ethylene oxide) derivatives being the most commonly used polymers for PPCs<sup>[70]</sup>. Further, it is also possible to modify the peptide to include a succinimidyl moiety, and then directly couple this to an appropriately functionalised polymer<sup>[85]</sup>. Alternatively, benzotriazoles can be used, as they behave in a similar manner. Whilst the succinimidyl esters have wide use, conjugating PEO-succinimidyl succinate introduces a second ester group into the polymer backbone<sup>[69, 86]</sup>. After conjugation to a peptide, this group remains in the final conjugate and is highly susceptible to hydrolysis, which would result in detachment of the PEO and the loss of its beneficial properties. This applies to all conjugates containing readily hydrolysable groups, and must be considered during synthesis and conjugation, depending on their intended application.

### 1.7.1.2. Schiff base

Modifying the polymer end group to an aldehyde affords another potential conjugation route<sup>[63, 87]</sup> (Figure 1.8b). The coupling of the polymer-aldehyde derivative and peptide results in the formation of a Schiff base, which, when treated with a reducing agent (such as sodium cyanoborohydride), produces an amine (or an amide depending on the R group). Roberts reported work describing the partial selectivity of mPEO-propionaldehyde by modifying the pH<sup>[69, 88]</sup>. This resulted in the aldehyde group preferentially reacting with the N-terminal amine, due to the more acidic nature of the  $\alpha$ -amine in comparison with other nucleophilic species.

### 1.7.1.3. Click Chemistry

Click chemistry is used to describe a set of orthogonal reactions amongst which is the widely reported copper-catalysed Huisgen reaction between azides and alkynes (Figure 1.8c)<sup>[89-97]</sup>. Click chemistry is noted for its robustness, insensitivity to a wide variety of functional groups, reliability, and ease of purification. This area of bioconjugation has received a large amount of attention. For example, van Dijk and co-workers<sup>[98]</sup> reported the conjugation between alkyne functionalised-PEO and azide-functionalised alanyl-phenylalanyl-lysyl-(2-azidoethyl)-amide, in which the conjugation took place in the presence of sodium ascorbate and copper (II) sulfate. Tzokova *et al.* reported the synthesis of short chain of PEO-peptide conjugates using click chemistry, but unlike the previous example, the peptide was modified to include the terminal alkyne group<sup>[99]</sup>.

The major disadvantage of this approach is the catalyst system, which most commonly contains copper. This presents a problem for a system required to interact in a biological environment and, as such, materials need to be extensively purified to ensure no toxic contaminants remain. Furthermore, the affinity for amino acids to complex with metals<sup>[100]</sup> means that the conjugation rate is affected and the purification is difficult.

#### 1.7.1.4. *Thiol-maleimide*

Another common coupling strategy that could be considered a “click” reaction exploits the reactivity of the side group in cysteine; the thiol. The vinyl or allyl group(s) in maleimides can react with the thiol group in an addition reaction to form a stable carbon-sulfur-carbon linkage (Figure 1.8d). Cysteine, like lysine, can be engineered into the peptide sequence during synthesis. However, there is the potential problem of forming disulfide bridges, which are generally susceptible to degradation in a biological environment<sup>[101]</sup>. Further, the maleimide moiety can be hydrolysed and undergo ring opening to form maleic acid.

#### 1.7.2. Divergent strategies

It is possible to use a divergent strategy to synthesise PPCs where a sequence is built up from a polymer substrate (Figure 1.8e) or a polymer grown from a peptidic macroinitiator. Consequently, the following section is divided into two: peptide growth from polymers (Section 1.7.2.1), and polymer growth from peptides (Section 1.7.2.2). However, it should be noted that the latter approach is only possible (to date) using radical polymerisation systems due to their tolerance of biological groups, with the two most common controlled radical polymerisation (CRP) techniques being reversible addition-fragmentation chain transfer polymerisation (RAFT)<sup>[102]</sup>, and atom transfer radical polymerisation (ATRP)<sup>[103, 104]</sup>.

##### 1.7.2.1. *Peptide growth from polymers*

There are a group of commercial resins that have PEO preloaded via an acid-labile linker (benzyl ester). The length of the peptide chain, however, heavily determines the solubility of the conjugate and makes isolation difficult<sup>[52]</sup>. For example, Hentschel reported a conjugation involving bound PEO and free amino acids. Here the PEO was part of a Tentagel-PAP resin, and was functionalised with a terminal amine group<sup>[105]</sup>. Protected amino acids were directly conjugated to this group through standard Fmoc and DCC

chemistry<sup>[106]</sup>. The newly formed PPC was then cleaved from the resin using TFA (Figure 1.8e). Using a resin makes isolation and purification easier, however scaling up can be more difficult due to associated costs (as discussed in Section 1.2).

#### 1.7.2.2. *Polymer growth from peptides*

Monomer can be polymerised from a peptidic macroinitiator system, also referred to as a “grafting from” approach. This allows for easier purification as only unreacted reagents will need to be removed, as opposed to the “grafting to” method, in which the unreacted reagents may include the presynthesised polymer, peptide and coupling reagents. CRP provides a useful approach toward the formation of well-defined polymers from peptidic initiators. CRP is commonly used in the synthesis of PPCs, either in the solution or solid phase, with the former favoured due to lack of control in the latter<sup>[107]</sup>. One of the greatest advantages of the CRP techniques arises from the ability to predetermine the functional groups on the chain end of the polymers via selection of appropriate functional reagents (e.g. initiators or chain transfer agents, CTA) or through post-polymerisation modification. Whilst such techniques are commonly exploited to produce functional polymers for conjugation (via the “grafting to” method), this part of the thesis focuses on CRP using peptidic initiators/CTAs only.

#### 1.7.2.3. *Atom transfer radical polymerisation*

Atom transfer radical polymerisation is a controlled free radical polymerisation technique that is mediated by a transition metal catalyst complex. The catalyst complex establishes equilibrium between propagating polymer radicals and dormant chains. Dormant chains are capped with a halogen atom (such as Cl or Br), which is transferred during activation. ATRP has been used in the synthesis of a whole host of designer materials, including polymer brushes<sup>[108-113]</sup>, pH-responsive vesicles<sup>[114, 115]</sup>, hybrid nanoparticles<sup>[116]</sup>, non-fouling gold surfaces and many macromolecules used in biomedical applications<sup>[117]</sup>. Since the discovery of ATRP there has been an evolution of the technique to

overcome some of its initial drawbacks. These newer protocols include AGET<sup>[118]</sup>, ARGET<sup>[119]</sup>, and ICAR<sup>[120]</sup>.

There are numerous examples of peptide-based ATRP initiators in the literature. One particular example by Rettig *et al.*<sup>[107]</sup> focussed on the synthesis of a peptide macroinitiator which was used to prepare peptide-poly(*n*-butyl acrylate). Oligopeptide synthesis was performed using standard SPPS protocols<sup>[106]</sup> with the ATRP initiating group introduced at the terminal amine of the oligopeptide. This was followed by cleavage from the solid support. The oligopeptide macroinitiator initiated the polymerisation of *n*BA in degassed DMSO at 60°C, with a CuBr/CuBr<sub>2</sub>/PMDETA catalyst system. CuBr<sub>2</sub> helped to mediate control of the reaction and PMDETA ensured that the amine groups (which can act as multidentate ligands) of the oligopeptide did not associate with the copper complex. This effect was observed when the authors increased the peptide concentration; a decrease in the overall rate of polymerisation was observed. GPC analysis of the final product revealed a molar mass dispersity of 1.19, highlighting a good level of control. Adams and Young<sup>[121]</sup> used a small family of oligopeptide-based initiators to polymerise 2-(diethylamino)ethyl methacrylate and *tert*-butyl methacrylate. The initiators were prepared from the free N-terminus of a series of short (1 to 4 amino acids) oligo(phenylalanine).

#### 1.7.2.4. *Reversible addition-fragmentation chain transfer*

RAFT polymerisation is a controlled free radical polymerisation in the presence of a CTA, typically based on a dithioester. The CTA, commonly referred to as a RAFT agent, allows the polymer chain to retain a functional end-group post-polymerisation. There are a vast number of examples where a peptide moiety is used as the CTA. Hentschel *et al.*<sup>[122]</sup> reported the synthesis and self-assembly of a PPC via RAFT polymerisation. The peptidic transfer agent (i.e. the CTA) was prepared in a two-step process. Firstly, a resin-bound peptide was modified with a terminal amine group. The oligopeptide was then subsequently reacted with dithiobenzoate to form the CTA. Subsequently, the peptidic CTA was cleaved from the support using TFA in DCM and used to polymerise *n*-butyl acrylate. The final PPC had a molar mass dispersity of 1.29

indicating relatively good control of the polymerisation process. Furthermore, this highlights the tolerance of RAFT with respect to complex, multifunctional peptide structures.

## **1.8. Hydrogels**

Hydrogels are three-dimensional structures comprised of a water phase immobilised by a scaffold<sup>[64]</sup>. Due to their similarity to hydrated body tissues, hydrogels are widely used as biomedical and pharmaceutical materials. The three-dimensional structures of hydrogels are networks of polymer chains which are held together by chemical or physical bonds. Chemically-bonded hydrogels are held in place by irreversible covalent bonds linking the polymer chains together. Physically-bonded hydrogels, on the other hand, are held together by reversible interactions such as molecular entanglements, ionic forces,  $\pi$ - $\pi$  stacking, hydrogen bonding, and van der Waals forces. Self-assembly into such supramolecular constructs occurs under favourable conditions. Formation through non-covalent interactions leads to the spontaneous organisation of molecules into well-defined arrangements<sup>[123]</sup>. Such hydrogels have advantages over chemically-bonded hydrogels for delivery applications. Most notably, physical bonding is reversible, meaning that these hydrogels can potentially be rendered injectable (via a gel-sol-gel transition during injection).

### **1.8.1. Polymer-peptide conjugate hydrogels**

Polymer-peptide conjugate (PPC) hydrogels are physically-bonded networks capable of imbibing large quantities of water. As with proteins, the physical bonding can lead to secondary structure formation, e.g.  $\alpha$ -helices and  $\beta$ -sheets, which can lead to tertiary structure formation. Advantages of using PPC hydrogels for biomaterials include the combination of the best properties of peptides and those of synthetic polymers<sup>[124]</sup>. The peptide component provides increased functional control, well-defined homogeneous hierarchical structures, consistent mechanical properties, and supportive folding/unfolding transitions<sup>[124, 125]</sup>. It is the peptide component that drives the self-assembly in these materials. Synthetic polymers can provide enhanced biocompatibility (e.g.

non-reactivity, low clearance times), enzymatic degradation resistance and adaptability. The combination of peptides and synthetic polymers can provide materials with properties superior to those of the individual components<sup>[124]</sup>. Common methods of self-assembly to give PPC hydrogels include; solvent exchange, direct rehydration, temperature-switch, and salt-triggered processes. Various structures can be obtained depending upon the conditions of assembly, e.g. temperature, solvent, or molar ratio of polymer to peptide.

### **1.9. Electrospinning**

The process of electrospinning has been known since the beginning of the last century, however it only began to receive significant interest in the early 90s when nanotechnology came to the forefront of research<sup>[126]</sup>. Interest in the production of one-dimensional nanostructures has increased dramatically since their first introduction, due to the unique properties that occur at the nanoscale level. This allows for the creation of structures such as carbon nanotubes<sup>[127]</sup>, conductive nanowires, and polymer nanofibres<sup>[128]</sup>. Nanofibres are incredibly useful as their surface area-to-volume ratio is vast.

Electrospinning is a technique which involves the transformation of a conductive fluid into fibrous structures, ranging in diameter sizes from microscale ( $10^{-6}$  m) to the nanoscale ( $10^{-9}$  m). A conductive solution is used, which consists of the required material dissolved in an appropriate solvent or co-solvent system. Electrospinning is an effective approach to construct nanofibres<sup>[129]</sup>. The diameter of such materials can be reduced to as low as a few nanometres, with the aid of electrostatic forces. Typical materials that can be electrospun into nanofibres include polymers, material composites, semiconductors, and ceramics. Polymers are among the most spun materials. It has been found that fibres formed from melts and composites have a larger diameter than those produced from solutions. Fibres are formed in electrospinning when a viscoelastic material is stretched along one axis (uniaxial). As spinning is performed, electrostatic forces are responsible for stretching the solution as it begins to solidify. Simultaneous expulsion of the viscoelastic solution from the aperture will be continuous as long as sufficient

solution is present, thus it can be noted that the process of electrospinning is continuous<sup>[129]</sup>. There are several parameters that control diameter of the fibres including voltage, solution viscosity, concentration, conductivity, tip-to-collector distance, secondary fields, and humidity<sup>[130]</sup>.

The conventional procedure for electrospinning polymers involves the expulsion of a viscous polymer solution from an appropriately narrow aperture, such as a syringe needle forming a droplet. An electric field is applied to the system. The suspended droplet of solution on the tip of the aperture is distorted into a cone shape, through the production of a surface charge. This distorted cone is known as a Taylor cone (first described by Sir Geoffrey Ingram Taylor)<sup>[131]</sup>. As the voltage gradually increases, the surface tension of the droplet is overpowered by the electrostatic repulsion of surface charges, and the solution is expelled from the tip of the Taylor Cone<sup>[132]</sup>.

Electrostatic atomisation then occurs, where the solution leaves the needle and is dispersed into the electric field. Using water as a solvent is somewhat problematic as water has a relatively high electrical conductivity ( $\sigma$ ) and is not easily atomised. Atomisation will only occur when the electrostatic field is strong enough to overcome the surface tension of the solution, causing the droplet to become unstable. The expelled stream travels, via the potential difference of the system, towards the earthed collector, forcing the solvent to evaporate into the atmosphere and undergo uniaxial stretching during which there is a decrease in the diameter of the fibre and an increase in length. This results in the deposition of solid polymer nanofibres on the collector<sup>[132]</sup>.

A typical small scale set-up merely comprises of a syringe, a power supply that can reach high voltages, and a collecting device, which can be as simple as aluminium foil.

### **1.10. Polymer nanofibres**

A polymer nanofibre is defined by industry as any fibre that has a diameter of less than one micron ( $<1000$  nm)<sup>[126]</sup>. Polymer nanofibre morphologies can

either be random, aligned, cross-aligned, sheaths, tubes, yarns, core/shell or tri-layer, all of which are dependent on the injection and collection procedures. Nanofibres are a new class of materials with potential uses in a wide range of applications, such as drug delivery, medical filtration, tissue engineering, and wound management (Figure 1.9). The high surface area to weight ratio is one of the key features that give these materials such advantageous properties over conventional fibres. Due to their small size, hollow nanotubes, which are smaller than erythrocytes, may be able to transport materials (such as drugs) around the body<sup>[133]</sup> or to targeted sites. Encapsulation with nanofibres allows a modicum of control with respect to delivery and release mechanisms. Nanofibres can also be used in wound management, where they can be incorporated into dressing and bandages, which can dissolve into the body once their task is completed. This helps to minimise blood loss and prevent infection.

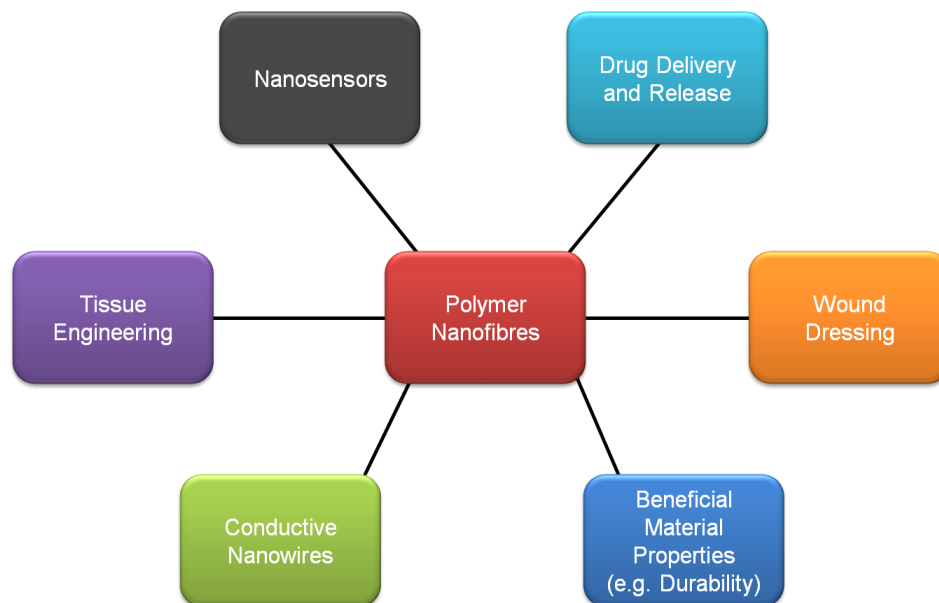


**Figure 1.9:** Example of applications of nanofibres, adapted from Huang *et al.*<sup>[132]</sup>

At present, it is still somewhat expensive to produce nanofibres, in contrast to conventional fibres. This is due to the relatively low production rate and the higher cost of the technology involved (such as the electric field).

### 1.11. Aims

Peptides serve a huge array of biological functions in humans. By coupling them with a synthetic polymer, namely poly(ethylene oxide), the potential for producing novel biocompatible materials with a wide range of potential biological uses is attractive. Such uses include targeted delivery of a non-compatible material, which has great potential in the pharmaceutical fields.

The underlying goal of the project is to produce injectable gels from low concentrations of synthesised biocompatible materials and to create innovative nanofibrous fabrics. Such fibres will have a wide range of potential applications due to their higher surface area, which leads to higher activities and beneficial properties.

To this end, a facile, reliable, and high yielding protocol for the production of polymer-peptide conjugates of monomethoxy-poly(ethylene oxide) and phenylalanine (F) has to be developed. This thesis describes various protection and coupling procedures investigated on a homologous family of peptides (i.e. F<sub>1</sub>, F<sub>2</sub>, F<sub>3</sub>, F<sub>4</sub>, and F<sub>5</sub>) and varying molecular weight polymers (350 Da, 550 Da, and 750 Da). Construction of the conjugates is based around complementary group conjugation in solution, which will allow for industrially/commercially-relevant scale-up.

Once a robust and reliable synthetic strategy had been developed for the creation of these polymer-peptide conjugate biohybrids, the further aim is to assess their propensity to self-assembly at the nanoscale into discrete nano-structures. This involves testing the materials in a range of solvents, and noting how solution concentration and solvent systems affect their behaviour. Directed self-assembly of these materials provides a method in which the product can be used in a biological setting through thixotropic behaviour. Therefore, the design rules for polymer-peptide conjugate self-assembly will be developed.

Finally, the production of nanofibres from these materials will be explored for the first time. Nanofibre fabrics of the novel PPC materials have the potential for use as wound dressings or organic electronics. Electrospinning will be required to produce such fibres, rendering it necessary to spin at different conditions to familiarise with the technique and to optimise the procedure for each parameter. To this extent a range of innovative materials will be spun to provide a good starting foundation before moving on to spin the peptide and conjugate materials.

## 1.12. References

1. Kimball S. R. and Jefferson L. S., Role of Amino Acids in the Translational Control of Protein Synthesis in Mammals, *Seminars in Cell & Developmental Biology*, **2005**, 16(1): p. 21-27.
2. Berg J. M., L T. J., and L S., Biochemistry. 5th Edition ed. **2002**, New York: W H Freeman.
3. Lipmann F., Hotchkiss R. D., and Dubos R. J., The Occurrence Of D-Amino Acids In Gramicidin And Tyrocidine, *J. Biol. Chem.*, **1941**, 141: p. 163-169.
4. Friedman M., Gumbmann M. R., and Masters P. M., Protein-Alkali Reactions: Chemistry, Toxicology, and Nutritional Consequences, *Advances in Experimental Medicine and Biology*, **1984**, 177: p. 367-412.
5. Fotheringham I. G., Kidman G. E., McArthur B. S., Robinson L. E., and Scollar M. P., Aminotransferase-Catalyzed Conversion of D-Amino Acids to L-Amino Acids, *Biotechnology Progress*, **1991**, 7(4): p. 380-381.
6. Warner D. T. and Moe O. A., Amino Acids. II. A New Synthesis of DL-Lysine, *Journal of the American Chemical Society*, **1948**, 70(11): p. 3918-3920.
7. Kino K., Sato M., Yoneyama M., and Kirimura K., Synthesis of DL-Tryptophan by Modified Broad Specificity Amino Acid Racemase From *Pseudomonas putida* IFO 12996, *Applied Microbiology and Biotechnology*, **2007**, 73(6): p. 1299-1305.
8. B A., D B., J L., M R., K R., and P W., Molecular Biology of the Cell. 4th Edition ed. **2002**, New York: Garland Science.
9. Ha E. and Zemel M. B., Functional Properties of Whey, Whey Components, and Essential Amino Acids: Mechanisms Underlying Health Benefits for Active People, *The Journal of Nutritional Biochemistry*, **2003**, 14(5): p. 251-258.
10. Kindt E. and Halvorsen S., The Need of Essential Amino Acids in Children. An Evaluation Based on the Intake of Phenylalanine, Tyrosine, Leucine, Isoleucine, and Valine in Children with Phenylketonuria, Tyrosine Amino Transferase Defect, and Maple Syrup Urine Disease, *The American Journal of Clinical Nutrition*, **1980**, 33(2): p. 279-86.
11. Xie J. and Schultz P. G., A Chemical Toolkit for Proteins - An Expanded Genetic Code, *Nat Rev Mol Cell Biol*, **2006**, 7(10): p. 775-782.
12. Gerfaud T., Chiang Y. L., Kreituss I., Russak J. A., and Bode J. W., Enantioselective, Chromatography-Free Synthesis of  $\beta$ 3-Amino Acids with Natural and Unnatural Side Chains, *Organic Process Research & Development*, **2012**, 16(4): p. 687-696.

13. Chénard S., Barberis C., Otis F., Paquin J. F., Martel J., Banville C., and Voyer N., Synthesis of an Anion-Binding Amino Acid, *Tetrahedron Letters*, **2012**, 53(4): p. 409-411.
14. Margolin A. L., Tai D. F., and Klibanov A. M., Incorporation of D-amino acids into peptides via enzymic condensation in organic solvents, *Journal of the American Chemical Society*, **1987**, 109(25): p. 7885-7887.
15. Kawakami T., Murakami H., and Suga H., Exploration of Incorporation of N<sup>α</sup>-Methylated Amino Acids Into Peptides by Sense-Suppression Method, *Nucleic Acids Symposium Series*, **2007**, 51(1): p. 361-362.
16. Kretlow J. D., Hacker M. C., Klouda L., Ma B. B., and Mikos A. G., Synthesis and characterization of dual stimuli responsive macromers based on poly(N-isopropylacrylamide) and poly(vinylphosphonic acid), *Biomacromolecules*, **2010**, 11(3): p. 797-805.
17. Lutz J. F. and Börner H. G., Modern Trends in Polymer Bioconjugates Design, *Progress in Polymer Science (Oxford)*, **2008**, 33(1): p. 1-39.
18. Hartmann L. and Börner H. G., Precision Polymers: Monodisperse, Monomer-Sequence-Defined Segments to Target Future Demands of Polymers in Medicine, *Advanced Materials*, **2009**, 21(32-33): p. 3425-3431.
19. Elvira C., Gallardo A., San Roman J., and Cifuentes A., Covalent Polymer-drug Conjugates, *Molecules*, **2005**, 10(1): p. 114-125.
20. Braunecker W. A. and Matyjaszewski K., Controlled/Living Radical Polymerization: Features, Developments, and Perspectives, *Progress in Polymer Science (Oxford)*, **2007**, 32(1): p. 93-146.
21. Vaidya A., Agarwal A., Jain A., Agrawal R. K., and Jain S. K., Bioconjugation of Polymers: A Novel Platform for Targeted Drug Delivery, *Current Pharmaceutical Design*, **2011**, 17(11): p. 1108-1125.
22. Pasut G. and Veronese F. M., Polymer-drug conjugation, recent achievements and general strategies, *Progress in Polymer Science (Oxford)*, **2007**, 32(8-9): p. 933-961.
23. Shaji J. and Jain V., Solid Lipid Nanoparticles: A Novel Carrier for Chemotherapy, *International Journal of Pharmacy and Pharmaceutical Sciences*, **2010**, 2(SUPPL. 3): p. 8-17.
24. Han S. Y. and Kim Y. A., Recent Development of Peptide Coupling Reagents in Organic Synthesis, *Tetrahedron*, **2004**, 60(11): p. 2447-2467.
25. Börner H. G., Smarsly B. M., Hentschel J., Rank A., Schubert R., Geng Y., Discher D. E., Hellweg T., and Brandt A., Organization of Self-Assembled Peptide-Polymer Nanofibers in Solution, *Macromolecules*, **2008**, 41(4): p. 1430-1437.

26. Nigama S. C., Mann A., Taddei M., and Wermutha C.-G., Selective Removal of the Tert-Butoxycarbonyl Group from Secondary Amines:  $\text{ZnBr}_2$  as the Deprotecting Reagent, *Synthetic Communications: An International Journal for Rapid Communication of Synthetic Organic Chemistry*, **1989**, 19(18): p. 3139 - 3142.
27. Wu Y. Q., Limburg D. C., Wilkinson D. E., Vaal M. J., and Hamilton G. S., A Mild Deprotection Procedure for *tert*-butyl Esters and *tert*-butyl Ethers Using  $\text{ZnBr}_2$  in Methylene Chloride, *Tetrahedron Letters*, **2000**, 41(16): p. 2847-2849.
28. Xu C. and Kopeček J., Self-Assembling Hydrogels, *Polymer Bulletin*, **2007**, 58: p. 53-63.
29. Bayer E. and Mutter M., Liquid Phase Synthesis of Peptides, *Nature*, **1972**, 237(5357): p. 512-513.
30. Nagarkar R. P. and Schneider J. P., Synthesis and Primary Characterization of Self-Assembled Peptide-Based Hydrogels, *Methods in Molecular Biology*, **2008**, 474(1): p. 61-77.
31. Gravert D. J. and Janda K. D., Organic Synthesis on Soluble Polymer Supports: Liquid-Phase Methodologies, *Chemical Reviews*, **1997**, 97(2): p. 489-510.
32. Kessel S. and Börner H. G., Self-Assembled PEO Peptide Nanotapes as Ink for Plotting Nonwoven Silica Nanocomposites and Mesoporous Silica Fiber Networks, *Macromol. Rapid Commun.*, **2008**, 29(4): p. 316-320
33. Huang L., McMillan R. A., Apkarian R. P., Pourdeyhimi B., Conticello V. P., and Chaikof E. L., Generation of Synthetic Elastin-Mimetic Small Diameter Fibers and Fiber Networks, *Macromolecules*, **2000**, 33(8): p. 2989-2997.
34. Chen X., Ding K., and Ayres N., Investigation into Fiber Formation in *N*-alkyl Urea Peptoid Oligomers and the Synthesis of a Water-soluble PEG/*N*-alkyl Urea Peptoid Oligomer Conjugate, *Polymer Chemistry*, **2011**, 2(11): p. 2635-2642.
35. Yamaguchi N. and Kiick K. L., Polysaccharide-poly(ethylene glycol) Star Copolymer as a Scaffold for the Production of Bioactive Hydrogels, *Biomacromolecules*, **2005**, 6(4): p. 1921-1930.
36. Tornøe C. W., Christensen C., and Meldal M., Peptidotriazoles on Solid Phase: [1,2,3]-Triazoles by Regiospecific Copper(I)-Catalyzed 1,3-Dipolar Cycloadditions of Terminal Alkynes to Azides, *The Journal of Organic Chemistry*, **2002**, 67(9): p. 3057-3064.
37. Meldal M. and Tornøe C. W., Cu-Catalyzed Azide-Alkyne Cycloaddition, *Chemical Reviews*, **2008**, 108(8): p. 2952-3015.

38. Jo Y. S., Gantz F., Hubbell J. A., and Lutolf M. P., Tailoring Hydrogel Degradation and Drug Release via Neighboring Amino Acid-controlled Ester Hydrolysis, *Soft Matter*, **2009**, 5(2): p. 440-446.
39. Yang J., Xu C., Kopecková P., and Kopecek J., Hybrid Hydrogels Self-assembled From HPMA Copolymers Containing Peptide Grafts, *Macromolecular Bioscience*, **2006**, 6(3): p. 201-9.
40. Van der Ende A., Sathiyakumar V., Diaz R., Hallahan D. E., and Harth E., Linear Release Nanoparticle Devices for Advanced Targeted Cancer Therapies with Increased Efficacy, *Polymer Chemistry*, **2010**, 1(1): p. 93-96.
41. Van der Ende A., Croce T., Hamilton K., Sathiyakumar V., and Harth E., Tailored Polyester Nanoparticles: Post-Modification with Dendritic Transporter and Targeting Units via Reductive Amination and Thiol-ene Chemistry, *Soft Matter*, **2009**, 5(7): p. 1417-1425.
42. Oh J. K., Drumright R., Siegwart D. J., and Matyjaszewski K., The Development of Microgels/Nanogels for Drug Delivery Applications, *Prog. Polym. Sci.*, **2008**, 33(4): p. 448-477.
43. Prakasha K. C., Raghavendra G. M., Harisha R., and Gowda D. C., Design, Synthesis and Antimicrobial Screening of Amino Acids Conjugated 2-Amino-4 Arylthiazole Derivatives, *International Journal of Pharmacy and Pharmaceutical Sciences*, **2011**, 3(Suppl 3): p. 120-125.
44. Chaudhary A., Girgis M., Prashad M., Hu B., Har D., Repič O., and Blacklock T. J., Using Mixed Anhydrides from Amino Acids and Isobutyl Chloroformate in N-Acylations: A Case Study on the Elucidation of Mechanism of Urethane Formation and Starting Amino Acid Liberation Using Carbon Dioxide as the Probe, *Tetrahedron Letters*, **2003**, 44(29): p. 5543-5546.
45. Vaughan J. R., Acylalkylcarbonates as Acylating Agents for the Synthesis of Peptides, *Journal of the American Chemical Society*, **1951**, 73(7): p. 3547-3547.
46. Woodward R. B., Sondheimer F., and Taub D., The Total Synthesis of Some Naturally Occurring Steroids, *Journal of the American Chemical Society*, **1951**, 73(7): p. 3547-3548.
47. Zhang L., Wang X. J., Wang J., Grinberg N., Krishnamurthy D. K., and Senanayake C. H., An Improved Method of Amide Synthesis Using Acyl Chlorides, *Tetrahedron Letters*, **2009**, 50(24): p. 2964-2966.
48. Montalbetti C. A. G. N. and Falque V., Amide Bond Formation and Peptide Coupling, *Tetrahedron*, **2005**, 61(46): p. 10827-10852.
49. Schelhaas M. and Waldmann H., Protecting Group Strategies in Organic Synthesis, *Angewandte Chemie International Edition in English*, **1996**, 35(18): p. 2056-2083.

50. Barany G. and Merrifield R. B., A New Amino Protecting Group Removable by Reduction. Chemistry of the Dithiasuccinoyl (Dts) Function, *Journal of the American Chemical Society*, **1977**, 99(22): p. 7363-7365.
51. Isidro-Llobet A., Álvarez M., and Albericio F., Amino Acid-Protecting Groups, *Chemical Reviews*, **2009**, 109(6): p. 2455-2504.
52. Dehn S., Chapman R., Jolliffe K. A., and Perrier S., Synthetic Strategies for the Design of Peptide/Polymer Conjugates, *Polymer Reviews*, **2011**, 51(2): p. 214 - 234.
53. Matson J. B., Zha R. H., and Stupp S. I., Peptide self-assembly for crafting functional biological materials, *Current Opinion in Solid State and Materials Science*, **2011**, 15(6): p. 225-235.
54. Schneider A., Garlick J. A., and Egles C., Self-Assembling Peptide Nanofiber Scaffolds Accelerate Wound Healing, *PLoS ONE*, **2008**, 3(1): p. e1410.
55. Lin H. B., Sun W., Mosher D. F., García-Echeverría C., Schaufelberger K., Lelkes P. I., and Cooper S. L., Synthesis, Surface, and Cell-Adhesion Properties of Polyurethanes Containing Covalently Grafted RGD-Peptides, *Journal of Biomedical Materials Research*, **1994**, 28(3): p. 329-342.
56. Zhu J., Tang C., Kottke-Marchant K., and Marchant R. E., Design and Synthesis of Biomimetic Hydrogel Scaffolds with Controlled Organization of Cyclic RGD Peptides, *Bioconjugate Chemistry*, **2009**, 20(2): p. 333-339.
57. Immordino M. L., Cattel L., and Dosio F., Stealth Liposomes: Review of the Basic Science, Rationale, and Clinical Applications, Existing and Potential, *Int J Nanomedicine*, **2006**, 1(3): p. 297-315.
58. Ringsdorf H., Structure and Properties of Pharmacologically Active Polymers, *J. Polymer Sci. Part C*, **1975**, 51(1): p. 135-53.
59. Kopeček J., Biomaterials and Drug Delivery: Past, Present, and Future, *Molecular Pharmaceutics*, **2010**, 7(4): p. 922-925.
60. Wu K., Liu J., Johnson R. N., Yang J., and Kopeček J., Drug-free macromolecular therapeutics: Induction of apoptosis by coiled-coil mediated crosslinking of antigens on cell surface, *Angew. Chem., Int. Ed.*, **2010**, 49(8): p. 1451-1455.
61. Hentschel J., ten Cate M. G. J., and Börner H. G., Peptide-Guided Organization of Peptide-Polymer Conjugates: Expanding the Approach from Oligo- to Polymers, *Macromolecules*, **2007**, 40(26): p. 9224-9232.

62. Jatzkewitz H., Über den Einbau physiologisch wirksamer Substanzen in ein kolloidales Blutplasma-Ersatzmittel, *Hoppe-Seyler's, Z Physiol. Chem.*, **1954**, 297: p. 149- 156.
63. Le Droumaguet B. and Nicolas J., Recent advances in the design of bioconjugates from controlled/living radical polymerization, *Polym. Chem.*, **2010**, 1(16): p. 563-598.
64. Adams D. J. and Topham P. D., Peptide Conjugate Hydrogelators, *Soft Matter*, **2010**, 6(16): p. 3707-3721.
65. Jain A. and Jain S. K., PEGylation: An Approach for Drug Delivery. A Review, *Critical Reviews in Therapeutic Drug Carrier Systems*, **2008**, 25(5): p. 403-447.
66. Arkhipovich G. N., Dubrovskii S. A., Kazanskii K. S., Ptitsina N. V., and Shupik A. N., Study of Solvation of Alkali Cations with Poly(ethylene oxide), *European Polymer Journal*, **1982**, 18(7): p. 569-576.
67. Worsfold D. J. and Eastham A. M., Cationic Polymerization of Ethylene Oxide. I. Stannic Chloride, *Journal of the American Chemical Society*, **1957**, 79(4): p. 897-899.
68. Worsfold D. J. and Eastham A. M., Cationic Polymerization of Ethylene Oxide. II. Boron Trifluoride, *Journal of the American Chemical Society*, **1957**, 79(4): p. 900-902.
69. Roberts M. J., Bentley M. D., and Harris J. M., Chemistry for Peptide and Protein PEGylation, *Advanced Drug Delivery Reviews*, **2002**, 54(4): p. 459-476.
70. Harris J. M. and Zalipsky S., eds. *Poly(ethylene glycol) - Chemistry and Biological Applications*. ACS Symposium Series. Vol. 680. 1997, American Chemical Society.
71. Lu J. and Shoichet M. S., Self-Assembled Polymeric Nanoparticles of Organocatalytic Copolymerized d,l-Lactide and 2-Methyl 2-Carboxytrimethylene Carbonate, *Macromolecules*, **2010**, 43(11): p. 4943-4953.
72. Shoichet M. S., Polymer scaffolds for biomaterials applications, *Macromolecules*, **2010**, 43(2): p. 581-591.
73. Davis F. F., Abuchowski A., Vanes T., Palczuk N. C., Savoca K. V., Chen R. H. L., and Pyatak P., Soluble, Non-Antigenic Polyethylene Glycol-Bound Enzymes, *Abstracts of Papers of the American Chemical Society*, **1979**(APR): p. 260-260.
74. Savoca K. V., Abuchowski A., Palczuk N. C., Vanes T., and Davis F. F., Immunological and Cytotoxic Effects of Beef-Liver Arginase Modified by Attachment of Polyethylene-Glycol, *Federation Proceedings*, **1979**, 38(3): p. 1179-1179.

75. Savoca K. V., Abuchowski A., Vanes T., Davis F. F., and Palczuk N. C., Preparation of a Non-Immunogenic Arginase by the Covalent Attachment of Polyethylene-Glycol, *Biochimica et Biophysica Acta*, **1979**, 578(1): p. 47-53.
76. Harris J. M. and Chess R. B., Effect of Pegylation on Pharmaceuticals, *Nature Reviews Drug Discovery*, **2003**, 2(3): p. 214-221.
77. Veronese F. M. and Pasut G., PEGylation, successful approach to drug delivery, *Drug Discovery Today*, **2005**, 10(21): p. 1451-1458.
78. Webster R., Didier E., Harris P., Siegel N., Stadler J., Tilbury L., and Smith D., PEGylated Proteins: Evaluation of Their Safety in the Absence of Definitive Metabolism Studies, *Drug Metabolism and Disposition*, **2007**, 35(1): p. 9-16.
79. Knop K., Hoogenboom R., Fischer D., and Schubert U. S., Poly(ethylene glycol) in Drug Delivery: Pros and Cons as Well as Potential Alternatives, *Angewandte Chemie International Edition*, **2010**, 49(36): p. 6288-6308.
80. Ito M., Watanabe D., Kobayashi M., Tamada Y., and Matsumoto Y., Acute Hypersensitivity to Dentifrice, *Contact Dermatitis*, **2006**, 54(4): p. 225-225.
81. Oh J. K., Bencherif S. A., and Matyjaszewski K., Atom Transfer Radical Polymerization in Inverse Miniemulsion: A Versatile Route Toward Preparation and Functionalization of Microgels/Nanogels for Targeted Drug Delivery Applications, *Polymer*, **2009**, 50(19): p. 4407-4423.
82. Ayres L., Hans P., Adams J., Lowik D. W. P. M., and van Hest J. C. M., Peptide-Polymer Vesicles Prepared by Atom Transfer Radical Polymerization, *J Polym Sci Part A: Polym Chem*, **2005**, 43: p. 6355-6366.
83. Cho I., Kim J.-B., and Jung H.-J., Synthesis and characterization of di- and triblock copolymers of poly(ethylene oxide) and poly(DL-valine-co-DL-leucine), *Polymer Bulletin*, **2003**, 44(19): p. 5497-5500.
84. Ryan D. M., Doran T. M., Anderson S. B., and Nilsson B. L., Effect of C-Terminal Modification on the Self-Assembly and Hydrogelation of Fluorinated Fmoc-Phe Derivatives, *Langmuir*, **2011**, 27(7): p. 4029-4039.
85. Vandermeulen G. W. M., Tziatzios C., Duncan R., and Klok H. A., PEG-Based Hybrid Block Copolymers Containing R-Helical Coiled Coil Peptide Sequences: Control of Self-Assembly and Preliminary Biological Evaluation, *Macromolecules* **2005**, 38(3): p. 761-769.
86. Ganesh S. and Jayakumar R., Structural Transitions Involved in a Novel Amyloid-Like  $\beta$ -Sheet Assemblage of Tripeptide Derivatives, *Biopolymers* **2003**, 70(3): p. 336-345.

87. Guvendiren M., Lu H. D., and Burdick J. A., Shear-thinning hydrogels for biomedical applications, *Soft Matter*, **2012**, 8(2): p. 260–272.
88. Börner H. G., Smarsly B. M., Hentschel J., Rank A., Schubert R., Geng Y., Discher D. E., Hellweg T., and Brandt A., Organization of Self-Assembled Peptide-Polymer Nanofibers in Solution, *Macromolecules* **2008**, 41(4): p. 1430-1437.
89. Xu L. Q., Yao F., Fu G. D., and Shen L., Simultaneous "Click Chemistry" and Atom Transfer Radical Emulsion Polymerization and Prepared Well-Defined Cross-Linked Nanoparticles, *Macromolecules*, **2009**, 42(17): p. 6385-6392.
90. Chen R. T., Muir B. W., Such G. K., Postma A., Evans R. A., Pereira S. M., McLean K. M., and Caruso F., Surface "Click" Chemistry on Brominated Plasma Polymer Thin Films, *Langmuir*, **2010**, 26(5): p. 3388-3393.
91. Golas P. L. and Matyjaszewski K., Marrying Click Chemistry with Polymerization: Expanding the Scope of Polymeric Materials, *Chem. Soc. Rev*, **2010**, 39(4): p. 1338-1354.
92. Richter S., Ramenda T., Bergmann R., Kniess T., Steinbach J., Pietzsch J., and Wuest F., Synthesis of neurotensin(8-13)-phosphopeptide heterodimers via click chemistry, *Bioorganic & Medicinal Chemistry Letters*, **2010**, 20(11): p. 3306-3309.
93. Suksiriworapong J., Sripha K., and Junyaprasert V. B., Synthesis and Characterization of Bioactive Molecules Grafted on Poly(epsilon-caprolactone) by "Click" Chemistry, *Polymer*, 51(11): p. 2286-2295.
94. Xu X. Y., Daniel W. L., Wei W., and Mirkin C. A., Colorimetric Cu(2+) Detection Using DNA-Modified Gold-Nanoparticle Aggregates as Probes and Click Chemistry, *Small*, 6(5): p. 623-626.
95. Zhang W. A. and Muller A. H. E., Synthesis of Tadpole-Shaped PUSS-Containing Hybrid Polymers via "Click Chemistry", *Polymer*, **2010**, 51(10): p. 2133-2139.
96. Zhao Z. D., Yuan W. Z., Gu S. Y., Ren T. B., and Ren J., "Click Chemistry" and Its Growing Applications in Biomedical Field, *Progress in Chemistry*, **2002**, 22(2-3): p. 417-426.
97. Ge Z., Zhou Y., Xu J., Liu H., Chen D., and Liu S., High-Efficiency Preparation of Macrocyclic Diblock Copolymers via Selective Click Reaction in Micellar Media, *Journal of the American Chemical Society*, **2009**, 131(5): p. 1628-1629.
98. van Dijk M., van Nostrum C. F., Hennink W. E., Rijkers D. T. S., and Liskamp R. M. J., Synthesis and Characterization of Enzymatically Biodegradable PEG and Peptide-Based Hydrogels *Biomacromolecules*, **2010**, 11(6): p. 1608.

99. Tzokova N., Fernyhough C. M., Topham P. D., Sandon N., Adams D. J., Butler M. F., Armes S. P., and Ryan A. J., Soft Hydrogels from Nanotubes of Poly(ethylene oxide)-Tetraphenylalanine Conjugates Prepared by Click Chemistry, *Langmuir*, **2009**, 25(4): p. 2479-2485.
100. Ishii H., Minegishi M., Lavitpichayawong B., and Mitani T., Synthesis of chitosan-amino acid conjugates and their use in heavy metal uptake, *International Journal of Biological Macromolecules*, **1995**, 17(1): p. 21-23.
101. Pisoni R. L., Acker T. L., Lisowski K. M., Lemons R. M., and Thoene J. G., A cysteine-specific lysosomal transport system provides a major route for the delivery of thiol to human fibroblast lysosomes: possible role in supporting lysosomal proteolysis, *J Cell Biol.* , **1990**, 110(2): p. 327-335.
102. Moad G., Rizzardo E., and Thang S. H., Living Radical Polymerization by the RAFT Process *Aust. J. Chem.*, **2005**, 58(6): p. 379-410.
103. Wang J. S. and Matyjaszewski K., Controlled/"Living" Radical Polymerization. Atom Transfer Radical Polymerization in the Presence of Transition-Metal Complexes, *Journal of the American Chemical Society*, **2002**, 117(20): p. 5614-5615.
104. Kato M., Kamigaito M., Sawamoto M., and Higashimura T., Polymerization of Methyl Methacrylate with the Carbon Tetrachloride/Dichlorotris-(triphenylphosphine) ruthenium(II) / Methylaluminum Bis(2,6-di-tert-butylphenoxide) Initiating System: Possibility of Living Radical Polymerization, *Macromolecules*, **1995**, 28(5): p. 1721-1723.
105. Tzokova N., Fernyhough C. M., Butler M. F., Armes S. P., Ryan A. J., Topham P. D., and Adams D. J., The Effect of PEO Length on the Self-Assembly of Poly(ethylene oxide)-Tetrapeptide Conjugates Prepared by "Click" Chemistry, *Langmuir*, **2009**, 25(18): p. 11082-11089.
106. Merrifield R. B., Solid Phase Peptide Synthesis. I. The Synthesis of a Tetrapeptide, *Journal of the American Chemical Society*, **1963**, 85(14): p. 2149-2154.
107. Rettig H., Krause E., and Börner H. G., Atom Transfer Radical Polymerization with Polypeptide Initiators: A General Approach to Block Copolymers of Sequence-Defined Polypeptides and Synthetic Polymers, *Macromolecular Rapid Communications*, **2004**, 25(13): p. 1251-1256.
108. Edmondson S., Osborne V. L., and Huck W. T. S., Polymer Brushes Via Surface-Initiated Polymerizations, *Chemical Society Reviews*, **2004**, 33(1): p. 14-22.

109. Dunlop I. E., Thomas R. K., Titmus S., Osborne V., Edmondson S., Huck W. T. S., and Klein J., Structure and Collapse of a Surface-Grown Strong Polyelectrolyte Brush on Sapphire, *Langmuir*, **2012**, 28(6): p. 3187-3193.
110. Edmondson S. and Huck W. T. S., Quasi-2D Polymer Objects from Patterned, Crosslinked Polymer Brushes, *Advanced Materials*, **2004**, 16(15): p. 1327-1331.
111. Edmondson S. and Armes S. P., Synthesis of Surface-Initiated Polymer Brushes using Macro-Initiators, *Polymer International*, **2009**, 58(3): p. 307-316.
112. Shivapooja P., Ista L., Canavan H., and Lopez G., ARGET-ATRP Synthesis and Characterization of PNIPAAm Brushes for Quantitative Cell Detachment Studies, *Biointerphases*, **2012**, 7(1): p. 1-9.
113. Coad B. R., Lu Y., Glattauer V., and Meagher L., Substrate-Independent Method for Growing and Modulating the Density of Polymer Brushes from Surfaces by ATRP, *ACS Applied Materials & Interfaces*, **2012**, 4(5): p. 2811-2823.
114. Madsen J., Warren N. J., Armes S. P., and Lewis A. L., Synthesis of Rhodamine 6G-Based Compounds for the ATRP Synthesis of Fluorescently Labeled Biocompatible Polymers, *Biomacromolecules*, **2011**, 12(6): p. 2225-2234.
115. Du J., Tang Y., Lewis A. L., and Armes S. P., pH-Sensitive Vesicles Based on a Biocompatible Zwitterionic Diblock Copolymer, *J. Am. Chem. Soc.*, **2005**, 127 (51): p. 17982-17983.
116. Li J. J., Deng L. D., and Xing J. F., Preparation and characterization of TiO<sub>2</sub>-cationic hybrid nanoparticles as electrophoretic particles, *Applied Surface Science*, **2012**, 258(7): p. DOI: 10.1016/j.apsusc.2011.11.053.
117. Siegwart D. J., Oh J. K., and Matyjaszewski K., ATRP in the design of functional materials for biomedical applications *Progress in Polymer Science*, **2012**, 37(1): p. 18-37.
118. Bencherif S. A., Washburn N. R., and Matyjaszewski K., Synthesis by AGET ATRP of Degradable Nanogel Precursors for In Situ Formation of Nanostructured Hyaluronic Acid Hydrogel, *Biomacromolecules*, **2009**, 10(9): p. 2499-2507.
119. Yungwan Kwak and Krzysztof Matyjaszewski, ARGET ATRP of Methyl Methacrylate in the Presence of Nitrogen-based Ligands as Reducing Agents, *Polymer International*, **2009**, 58(3): p. 242-247.
120. Plichta A., Li W., and Matyjaszewski K., ICAR ATRP of Styrene and Methyl Methacrylate with Ru(Cp\*)Cl(PPh<sub>3</sub>)<sub>2</sub>, *Macromolecules*, **2009**, 42(7): p. 2330-2332.

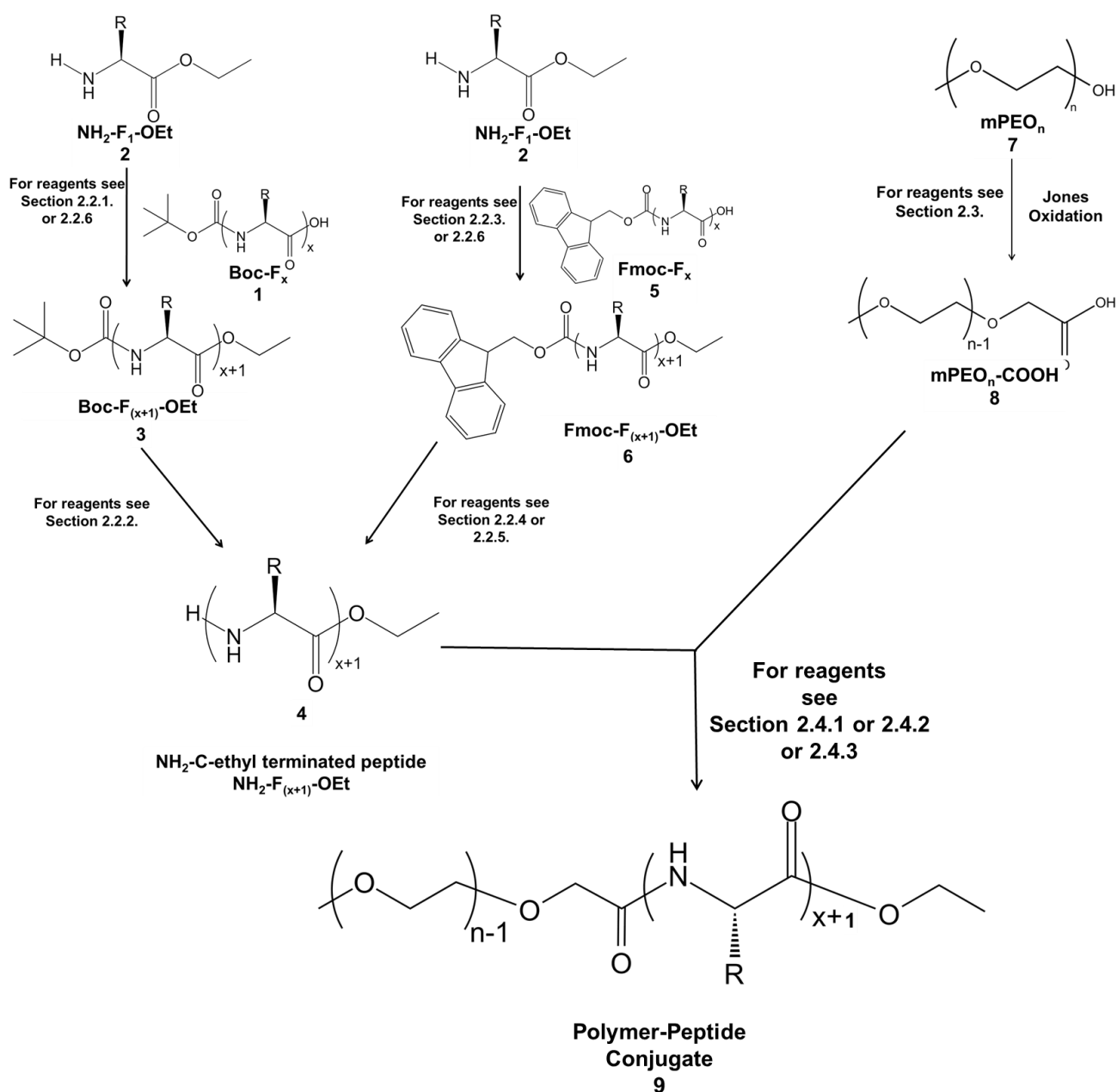
121. Adams D. J. and Young I., Oligopeptide-Based Amide Functional Initiators for ATRP, *Journal of Polymer Science: Part A: Polymer Chemistry*, **2008**, 46(18): p. 6082-6090.
122. Hamley I. W., Ansari I. A., Castelletto V., Nuhn H., Rösler A., and Klok H. A., Solution Self-Assembly of Hybrid Block Copolymers Containing Poly(ethylene glycol) and Amphiphilic  $\beta$ -Strand Peptide Sequences, *Biomacromolecules*, **2005**, 6(3): p. 1310-1315.
123. Carbone A. and Seeman N. C., Molecular Tiling and DNA Self-assembly, in *Aspects of Molecular Computing*, N. Jonoska, G. Paun, and G. Rozenberg, Editors. **2004**, Springer. p. 61-83.
124. Klok H.-A., Peptide/Protein–Synthetic Polymer Conjugates: Quo Vadis, *Macromolecules*, **2009**, 42(21): p. 7990-8000.
125. Van Hest J. C. M., Biosynthetic-Synthetic Polymer Conjugates, *Journal of Macromolecular Science, Part C: Polymer Reviews*, **2007**, 47(1): p. 63-92.
126. Subbiah T., Bhat G. S., Tock R. W., Parameswaran S., and Ramkumar S. S., Electrospinning of nanofibers, *Journal of Applied Polymer Science*, **2005**, 96(2): p. 557-569.
127. Inagaki M., Yang Y., and Kang F. Y., Carbon Nanofibers Prepared via Electrospinning, *Advanced Materials*, **2012**, 24(19): p. 2547-2566.
128. Nataraj S. K., Yang K. S., and Aminabhavi T. M., Polyacrylonitrile-Based Nanofibers—A State-of-the-Art Review, *Progress in Polymer Science*, **2012**, 37(3): p. 487-513.
129. Wee-Eong T., Ryuji I., and Seeram R., Technological Advances in Electrospinning of Nanofibers, *Science and Technology of Advanced Materials*, **2011**, 12(1): p. 013002.
130. Ai Y., Zhen H., Nie J., and Yang D., Aligned Polymer Fibers Produced Via an Additive Electric Field, *Frontiers of Chemistry in China*, **2011**, 6(1): p. 44-47.
131. Geng X., Kwon O. H., and Jang J., Electrospinning of Chitosan Dissolved in Concentrated Acetic Acid Solution, *Biomaterials*, **2005**, 26(27): p. 5427-5432.
132. Huang Z. M., Zhang Y. Z., Kotaki M., and Ramakrishna S., A Review on Polymer Nanofibers by Electrospinning and Their Applications in Nanocomposites, *Composites Science and Technology*, **2003**, 63(15): p. 2223-2253.
133. Ashammakhi N., Wimpenny I., Nikkola L., and Yang Y., Electrospinning: Methods and Development of Biodegradable Nanofibres for Drug Release, *Journal of Biomedical Nanotechnology*, **2009**, 5(1): p. 1-19.

# **CHAPTER 2**

## **Experimental**

## 2. Experimental

Chapter 2 provides an overview of the synthetic steps undertaken in this work and is divided into subsections according to each reaction step shown in Scheme 2.1. A full discussion of each reaction including justification of reagents, is given in Chapter 3, with full characterisation data provided in the appropriate section.



**Scheme 2.1:** General reaction scheme showing overall synthetic routes for the production of polymer-peptide conjugates.

## 2.1 Materials

The reagents used for peptide and/or polymer coupling were isobutylchloroformate (IBCF, 98 %), *N,N'*-dicyclohexylcarbodiimide (DCC), (benzotriazol-1-yloxy)-tripyrrolidinophosphonium hexafluorophosphate (PyBOP, 98 %), 4-methylmorpholine (NMM, 98 %) and 4-dimethylaminopyridine (DMAP), were all purchased from Sigma-Aldrich and used as received.

Reagents used for protection were purchased from a range of sources. Piperidine (99 %) and *bis*-butyl-tin(VI) oxide (BBTO, 96 %) were purchased from Fisher Scientific, whilst lithium hydroxide (LiOH) was obtained from Sigma-Aldrich. Trifluoroacetic acid (TFA, 99 %) and the primary drying agent, anhydrous magnesium sulfate (MgSO<sub>4</sub>, 97 %) were acquired from VWR.

*N*-(*tert*-Butoxycarbonyl)-L-phenylalanine (Boc-F<sub>1</sub>-OH) and L-phenylalanine ethyl ester (NH<sub>2</sub>-F<sub>1</sub>-OEt) were sourced from Fisher Scientific in the highest purity possible (99 %). Fmoc-phenylalanine (Fmoc-F<sub>1</sub>-OH) (98 %) was purchased from Sigma-Aldrich.

Different molecular weight monomethoxy-poly(ethylene oxide) (mPEO<sub>n</sub>), i.e. 350 Da, 550 Da, and 750 Da, were purchased from Sigma-Aldrich, and their molar mass distribution was assessed using gel permeation chromatography (GPC). Polystyrene (PS) and poly(ethylene oxide) (PEO) for electrospinning were sourced from Fisher Scientific in a range of molecular weights (100,000 and 300,000 Da for PEO and 500,000 Da for PS). All other compounds were obtained in the highest purity possible from Fisher Scientific, Sigma-Aldrich, or VWR, as used without further purification unless otherwise stated in the relevant protocols.

All solvents employed, supplied by Fisher Scientific, were laboratory reagent grade and used as received, unless otherwise noted. HPLC grade solvents were used during analysis by RP-HPLC.

## 2.2 Peptide Synthesis

### 2.2.1. Synthesis of Boc-F<sub>(x+1)</sub>-OEt terminated peptide **3** using isobutylchloroformate

Boc-F<sub>x</sub> **1** (10.60 g, 40 mmol) was mixed with NMM (4.4 ml, 40 mmol, 4.04 g) in excess chloroform (at least 100 ml) at 0 °C and was stirred for ten minutes. IBCF (5.2 ml, 40 mmol, 5.46 g) was added dropwise to the reaction mixture. After stirring for a further ten minutes, F<sub>y</sub>-OEt **2** (9.18 g, 40 mmol) was added to the solution, alongside a further addition of NMM (4.4 ml, 40 mmol, 4.04 g). The solution was allowed to warm to room temperature and stirred overnight. Water (3 x 100 ml) was then used to extract any water-soluble reagents, followed by successive washes with hydrochloric acid (3 x 100 ml, 0.2 M), sodium carbonate (3 x 100 ml, 0.2 M), and brine solution (3 x 100 ml). The collected organic (chloroform) layers were subsequently dried over magnesium sulfate, filtered, then concentrated under reduced pressure to yield a white powder **3** (Boc-F<sub>(x+1)</sub>-OEt). This was dried overnight *in vacuo* (when x = 1, 16.71 g, 38 mmol, 96 %).

If further purification was required, the product was dissolved in minimal amounts of acetone and reprecipitated into cold diethyl ether. The precipitate was then filtered and dried *in vacuo*.

### 2.2.2. Deprotection of Boc-F<sub>(x+1)</sub>-OEt **3** to produce NH<sub>2</sub>-F<sub>(x+1)</sub>-OEt **4**

Boc-F<sub>(x+1)</sub>-OEt **3** (16.71 g, 38 mmol) was dissolved in excess chloroform (>100 ml) and stirred at 0°C. To this solution, a small amount of trifluoroacetic acid was slowly added (10 ml, 14.89 g) and the solution left to return to room temperature and stirred overnight. Excess diethyl ether (>400 ml) was added to the solution to precipitate a white solid. The product **4** was collected by filtration and washed thoroughly with diethyl ether (at least 3 x 100 ml), then dried overnight *in vacuo* (when x = 1, 16.80 g, 37 mmol, 97 %).

### 2.2.3. Synthesis of Fmoc-F<sub>(x+1)</sub>-OEt **6** using isobutylchloroformate

*N*-(9-fluorenylmethoxycarbonyl)-L-phenylalanine (Fmoc-F<sub>x</sub>) **5** (15.48 g, 40 mmol) was mixed with NMM (4.4 ml, 40 mmol, 4.04 g) in excess chloroform (at least 100 ml) at 0°C and was stirred for ten minutes. IBCF (5.2 ml, 40 mmol, 5.46 g) was added dropwise to the reaction mixture. After stirring for a further ten minutes, F<sub>y</sub>-OEt **2** was added to the solution, alongside a further addition of NMM (4.4 ml, 40 mmol, 4.04 g). The solution was allowed to return to room temperature and stirred overnight. Water (3 x 100 ml) was then used to extract any water-soluble reagents, followed by successive washes with hydrochloric acid (3 x 100 ml, 0.2 M), sodium carbonate (3 x 100 ml, 0.2 M), and brine solution (3 x 100 ml). The collected organic (chloroform) layers were subsequently dried over magnesium sulfate, filtered, then concentrated under reduced pressure to yield an off-white powder **6** (Fmoc-F<sub>(x+1)</sub>-OEt). This was dried overnight *in vacuo* (when x = 1, 16.80 g, 37 mmol, 75 %).

### 2.2.4. Deprotection of Fmoc-F<sub>(x+1)</sub>-OEt **6** to produce NH<sub>2</sub>-F<sub>(x+1)</sub>-OEt **4** using piperidine

Fmoc-protected phenylalanine **6** was dissolved in excess chloroform (> 100 ml). To this solution piperidine (> 100 ml) was added in excess and the solution was left to stir at room temperature for several hours. The resulting solution was then washed thoroughly with water to remove any unreacted piperidine, leaving only the polymer-peptide conjugate and dibenzofulvene in the organic layer. Dibenzofulvene was removed by washing with 0.2 M sodium carbonate, and the organic layer was dried over magnesium sulfate. Chloroform was then removed under reduced pressure, and the product **4** dried *in vacuo* (see Chapter 3 for information regarding the yield).

### 2.2.5. Deprotection of Fmoc-F<sub>(x+1)</sub>-OEt **6** to produce NH<sub>2</sub>-F<sub>(x+1)</sub>-OEt **4** using diazabicycloundec-7-ene

Fmoc-protected phenylalanine **6** was dissolved in excess chloroform (> 100 ml). To this solution DBU (> 5 ml) was added in excess and the solution was left to

stir at room temperature for several hours. The resulting solution was then washed well with acetonitrile to remove any unreacted DBU. Aqueous and acidic soluble impurities were removed by washing with 0.2 M sodium carbonate, and the organic layers were dried over magnesium sulfate. The chloroform was then removed under reduced pressure, and the product **4** dried *in vacuo* (see Chapter 3 for information regarding the yield).

#### 2.2.6. Synthesis of N-Protected F<sub>(x+1)</sub>-OEt terminated peptide **3** or **6** using *N,N*-dicyclohexylcarbodiimide

Protected peptide was dissolved in dichloromethane and stirred. To this solution a DMAP (5 mg) was added. F<sub>y</sub>-OEt **2** was added at 0°C with NMM. If complete dissolution was not achieved additional NMM was added. The solution was stirred overnight at room temperature. Subsequently, the white precipitate that formed was filtered off and the filtrate was washed with water (3 x 100 ml), hydrochloric acid (3 x 100 ml, 0.2 M), and aqueous potassium carbonate (3 x 100 ml, 0.2 M). The collected dichloromethane layers were subsequently dried over magnesium sulfate, filtered, and then concentrated under reduced pressure. This resulted in a white solid **3** or **6**, which was dried overnight *in vacuo* (when x = 1, yields ranged from 75-90 %).

### 2.3. Preparation of carboxylic acid-functionalised monomethoxy-poly(ethylene oxide) **8**

The following section describes the functionalisation of mPEO<sub>n</sub> with a number average molecular weight ( $M_n$ ) of 350 gmol<sup>-1</sup> as an example. This method is identical for all molecular weights of mPEO<sub>n</sub> used, with subtle differences highlighted where applicable. mPEO<sub>n</sub> **7** (6.3 g, 18 mmol, 1 eq.) was dissolved in acetone (300 ml) and stirred at room temperature. To this solution, 108 ml Jones reagent was added at 0 °C. The Jones reagent consisted of CrO<sub>3</sub> (6.8 g, 67 mmol, 3.8 eq.), sulfuric acid (108 ml, 1.5 M). After stirring for 5-10 minutes, the solution was allowed to return to room temperature. Following further stirring overnight, the solid waste was filtered off, and washed through with acetone; the resulting filtrate was combined with the reaction filtrate.

Acetone was removed under reduced pressure to yield a viscous liquid, to which sodium hydroxide (100 ml, 0.1 M) was added. Propan-2-ol was poured through the solid waste.

Subsequently, the solution was washed with diethyl ether (at least 3 x 100 ml). Sulfuric acid (100 ml, 0.2 M) was added and then the product was extracted with dichloromethane (at least 3 x 200 ml). All of the collected organic layers were combined and dried with magnesium sulfate, filtered, and the dichloromethane removed under reduced pressure. The clear viscous product **8** was dried overnight *in vacuo*. Yields ranged between 60 and 74 %, depending on the molecular weight of the mPEO starting material, which is discussed in detail in Chapter 3.

## 2.4. Synthesis of polymer-peptide conjugates

### 2.4.1. Synthesis of polymer-peptide conjugate **9** via isobutylchloroformate coupling

NMM (1 eq.) was added to mPEO<sub>n</sub>-COOH **8** (1 eq.) in excess chloroform (100 ml) at 0 °C. IBCF (1 eq.) was then added to the reaction mixture and after stirring for 5-10 minutes F<sub>(x+1)</sub>-OEt **4** (0.7 eq.) and NMM (1 eq.) were added to the solution. After stirring overnight at room temperature, the solution was subsequently washed with water (3 x 100 ml), HCl (3 x 100 ml, 0.2 M), Na<sub>2</sub>CO<sub>3</sub> (3 x 100 ml, 0.2 M) and brine (3 x 100 ml). The organic layers were collected and dried over magnesium sulfate. Chloroform was removed under reduced pressure. The final polymer-peptide conjugate **9** was dried overnight *in vacuo*.

Any impurities present after washing, were removed by dissolving in a minimal amount of THF and reprecipitating into excess petroleum ether. Silica gel column chromatography, with a DCM: methanol (20: 1) eluent was also used when necessary.

#### 2.4.2. Synthesis of polymer-peptide conjugate **9** via *N,N'*-dicyclohexylcarbodiimide coupling

mPEO<sub>n</sub>-COOH **8** (1 eq.) was dissolved in dichloromethane (> 20 ml). 5 mg of DMAP was added to the solution and was left stirring in an ice bath. F<sub>(x+1)</sub>-OEt **4** (0.85 eq.) was dissolved in dichloromethane (> 10 ml) and to this solution NMM (1 eq.) was added. This was then added to the mPEO<sub>n</sub>-COOH solution **8**. Excess PEO<sub>n</sub>-COOH was used to ensure complete coupling reaction. Finally, DCC (1.05 eq.) was added to the solution which was left to stir overnight, returning to room temperature. The extent of stirring depends on the length of PEO<sub>n</sub>-COOH chain (see Chapter 3). Any precipitate formed overnight was filtered off and the solution was washed with water (3 x 100 ml), hydrochloric acid (3 x 100 ml, 0.5 M) and potassium carbonate (3 x 100 ml, 0.5 M). The solution was then dried over magnesium sulfate, filtered and DCM was removed under reduced pressure to give the final product polymer-peptide conjugate **9** which was dried overnight *in vacuo*.

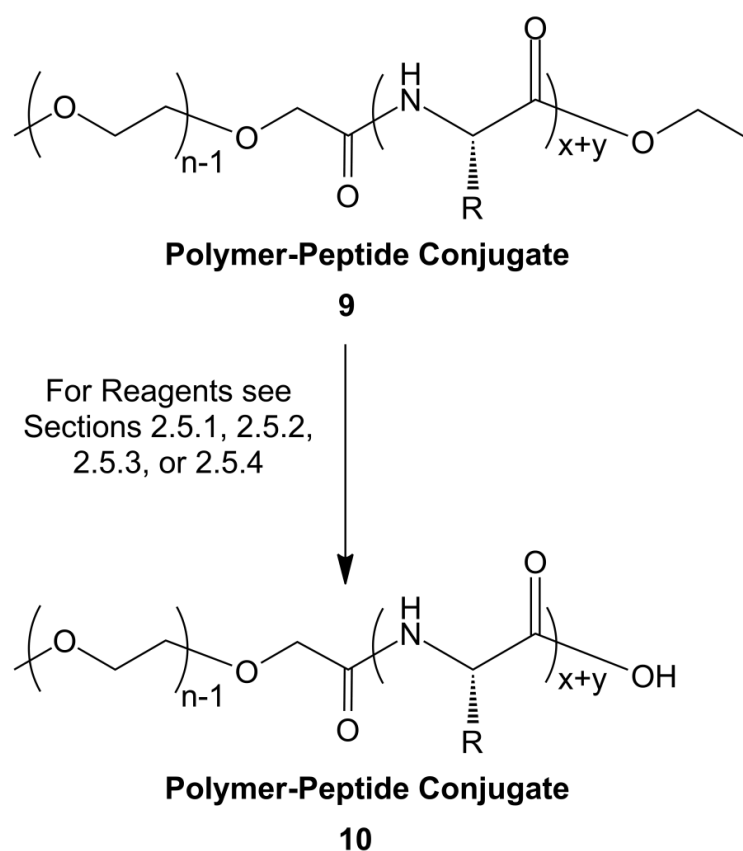
#### 2.4.3. Synthesis of polymer-peptide conjugate **9** via benzotriazol-1-yl-oxytripyrrolidinophosphonium hexafluorophosphate (PyBOP) coupling

F<sub>(x+1)</sub>-OEt **4** (1 eq.) was dissolved in dichloromethane (> 30 ml). mPEO<sub>n</sub>-COOH **8** (1 eq.) was added to the solution and left stirring. To this solution DIPEA (1.35 eq.) was added dropwise. Finally, PyBOP (1 eq.) was added to the reaction mixture which left to the stir for a further thirty minutes. The reaction was expected to turn from cloudy to a clear yellow solution over this duration. After stirring, the reaction mixture was concentrated to dryness *in vacuo*, and 60 ml of diethyl ether was added. Precipitate was filtered and collected, then washed with additional portions of diethyl ether (at least 3 x 20 ml). The product was dried overnight *in vacuo*.

### 2.5. Deprotection of carboxyl terminus

It was not necessary to limit peptidic deprotections to the amine end. Although, it is normally easier to protect and deprotect the amine group(s), the carboxylic

acid group can also be deprotected allowing the resulting material to have end-group functionality (Scheme 2.2). There were four methods used for carboxyl terminus deprotection; three of which use lithium hydroxide (LiOH). Method One (Section 2.5.1) details LiOH deprotection at a moderately low pH, whereas Method Two (Section 2.5.2) takes place at a lower pH and at higher temperature. Finally Method Three (Section 2.5.3) is a faster reaction in which the addition of LiOH is spread over two stages. Section 2.5.4 details deprotections using a different reagent, known as *bis*[tri-*n*-butyltin (IV) oxide] (BBTO).



**Scheme 2.2:** Reaction scheme outlining the synthetic route for deprotecting the carboxyl terminus of a polymer-peptide conjugate.

2.5.1. Deprotection of the carboxyl terminus of polymer-peptide conjugate **9** using lithium hydroxide (Method One) to yield conjugate **10**

LiOH (0.2 g, 8.3 mmol) was added to a solution of dissolved polymer-peptide conjugate **9** (1.3 mmol) in a mixture of THF: water (24 ml: 8 ml). After stirring

overnight, distilled water (100 ml) was added. This was followed by the addition of hydrochloric acid (1.0 M) drop wise until the solution reached pH 3. THF was removed under reduced pressure and the resulting white precipitate was washed well with water (3 x 100 ml) and petroleum ether (3 x 100 ml), and collected by filtration. The final product **10** was dried overnight *in vacuo*.

To note, approximately 0.2 g of LiOH in 25-40 ml of solvent was required to obtain a high enough pH. After deprotection, water was added and if there was formation of precipitate, it was filtered at this stage. HCl was then added. If there was no precipitate formed, then THF was removed under vacuum to recover the product.

#### 2.5.2. Deprotection of the carboxyl terminus of polymer-peptide conjugate **9** using lithium hydroxide (Method Two) to yield conjugate **10**

Polymer-peptide conjugate **9** (1.3 mmol) was dissolved in a solution of THF: water (24 ml: 8 ml). To this solution, lithium hydroxide (0.2 g, 8.3 mmol) was added and left stirring overnight. Distilled water (100 ml) was added to above solution followed by hydrochloric acid (1.0 M) drop wise, until pH 1.2 was reached. The solution was then heated in a water bath at 60 °C for three hours. THF was then removed under reduced pressure. Dialysis of the solution against distilled water was undertaken for up to four days before it was lyophilised.

#### 2.5.3. Deprotection of the carboxyl terminus of polymer-peptide conjugate **9** using lithium hydroxide (Method Three) to yield conjugate **10**

Polymer-peptide conjugate **9** (1.6 mmol) was dissolved in THF: water (100 ml: 100 ml), lithium hydroxide (0.07 g, 10 wt%) was added and the solution stirred at room temperature. Two hours later, additional lithium hydroxide (0.1 g) was added to the mixture. The reaction was then quenched with two units (1 unit is 1.6 mmol) of 200 ml of hydrochloric acid and subsequently extracted with ethyl acetate (EtOAc) (2 x 250 ml) and dried over magnesium

sulfate (MgSO<sub>4</sub>). Ethyl acetate was removed under reduced pressure, and the product **10** dried *in vacuo*.

#### 2.5.4. Deprotection of the carboxyl terminus of polymer-peptide conjugate **9** using *bis*-butyl-tin(IV) oxide to yield conjugate **10**

Polymer-peptide conjugate **9** (0.5 g, 1.14 mmol) was added to a stirred solution of BBTO (1.16 ml, 2.27 mmol) in toluene (10 ml), and the mixture was heated at 80 °C for at least 10 hours. Solvent was subsequently removed under reduced pressure and the resulting product was dissolved in ethyl acetate (10 ml) and extracted with aqueous sodium bicarbonate (3 x 10 ml, 5 %). The organic phase was washed with brine (3 x 10 ml), and dried over MgSO<sub>4</sub>. Product was filtered, concentrated under reduced pressure, and then dried overnight *in vacuo*. Benzene could also have been used as an alternative to toluene. In that instance, the mixture was then heated to 80 °C for at least 13 hours. The others steps of the process are identical to the toluene protocol.

## 2.6. Polymer-peptide synthesis using unmodified monomethoxy-poly(ethylene oxide)

### 2.6.1. Polymer-peptide conjugate **11** synthesis using unmodified monomethoxy-poly(ethylene oxide) **7**, via Steglich esterification

Dichloromethane was distilled prior to use with calcium hydride. DCC was used as a 1.0 M solution in DCM; 0.89 ml of this solution was added. A 100 ml round-bottom flask, equipped with a calcium chloride drying tube, was charged with Boc-F<sub>x</sub> **1** (1 eq.), NMM (1 eq.), dry dichloromethane (40 ml), mPEO<sub>n</sub>-OH **7** (3 eq.), and 5 mg of DMAP. The solution was stirred and cooled to 0 °C while DCC (1 eq.) was added over a five minute period. After a further five minutes stirring at 0 °C, the ice bath was removed and the reaction mixture was further stirred for an additional three hours at room temperature.

A urea derivative was the first precipitate that formed, and was removed by filtration, and the filtrate was washed with hydrochloric acid (2 x 25 ml, 0.2 M)

and saturated sodium bicarbonate solution (2 x 25 ml). Organic dichloromethane layers were collected and combined, then dried over magnesium sulfate, filtered, and concentrated under reduced pressure. The final product, polymer-peptide conjugate **11**, was dried overnight *in vacuo*.

#### 2.6.2. Polymer-peptide conjugate **11** synthesis using unmodified monomethoxy-poly(ethylene oxide) **7** via Fischer esterification

Boc-F<sub>x</sub> **1** (1 eq.) was placed in a 50 ml round-bottom flask, to which three drops of sulfuric acid was added, and swirled until the peptide dissolved. mPEO<sub>n</sub> **7** (1 eq.) and excess toluene (> 30 ml) were added and the flask was again swirled to thoroughly mix the reagents. A boiling stone was added, and the flask fitted with a Dean-Stark water separator and reflux condenser. The flask was heated so that toluene refluxed vigorously. Any water that was formed was collected in the trap. The mixture continued to be heated until no more water separated.

The mixture was allowed to cool to room temperature, and then the solution was diluted with chloroform (10 ml). Subsequently the solution was washed with sodium carbonate solution (3 x 10 ml, 10 %), then with saturated sodium chloride (brine) solution (3 x 10 ml). The organic layers were collected, dried over magnesium sulfate, filtered, and concentrated under reduced pressure to yield the final product, polymer-peptide conjugate **11**, which was dried overnight *in vacuo*.

### 2.7. Gel Formation (Self-Assembly)

Four methods were used to ascertain whether the synthesised product self-assembled on the nanoscale to yield gels. Method 1 (Section 2.7.1) focuses on behaviour in only distilled water, whereas Method 2 (Section 2.7.2) introduces a co-solvent, DMSO. Formation Method 3 (Section 2.7.3) is an extension of Method 2 at elevated temperature. Finally, Method 4 (Section 2.7.4) introduces a greater range of solvent compositions.

### 2.7.1. Gel Formation Method 1

10 mg of the polymer-peptide conjugate **9** was added to a sample vial, to which 1 ml of distilled water was added (i.e. forming a 1 % w/v solution) and the solution was heated until the polymer peptide conjugate dissolved. The resulting solution was then left to stand at room temperature for approximately two hours and the vial was continually observed to note if there had any been gel formation. This was further tested by inverting the vial to see if the product was immobilised.

### 2.7.2. Gel Formation Method 2

10 mg of the polymer-peptide conjugate **9** was dissolved in dimethyl sulfoxide (DMSO) at room temperature (if the solution did not dissolve, more DMSO was added). To this, 1 ml of water was added and the solution was monitored for two hours. If the solution precipitated after the first few minutes, the experiment was deemed to have been unsuccessful, and was then repeated. Should a precipitate have formed after several hours then the process was continued overnight. The vial was observed to verify the presence of gel formation. This was further tested by inverting the vial to see if the product was immobile.

### 2.7.3. Gel Formation Method 3

10 mg of the polymer-peptide conjugate **9** was dissolved in DMSO at room temperature. To this, 1 ml of water was added, and the solution was heated for two hours at 60 °C. The solution was then left overnight at room temperature and the vial was observed to see if there had any been gel formation. This was further tested by inverting the vial to see if the product was immobile.

### 2.7.4. Gel Formation Method 4

Polymer-peptide conjugate **9** was dissolved in an appropriate solvent (DMSO, THF, acetone, ethanol, or DMF) to form a solution (5 % w/v or 10 % w/v). To this solution an appropriate amount of water was added to form a binary solvent

system. The mixtures were left to stand overnight and observed the next day. Mixtures that did not gel, were heated firstly to 37 °C (physiological temperature) and again observed for gel formation, then, on failure, to 60 °C to again note any gel formation.

## 2.8. Electrospinning

A given material was dissolved into solvent (the precise concentration required is dictated by the final viscosity of solution) to form a conductive solution. A needle of appropriate length and diameter was affixed to the end of a syringe which is placed into syringe pump, and controlled flow-rate was programmed (typically 1 ml h<sup>-1</sup>). A high voltage power supply was connected to the needle (acting as the positive electrode), and a grounding wire connected to the metal collecting plate (usually aluminium foil acting as an earth) (Figure 2.1). The pump was switched on allowing the conductive solution to flow through the needle. On the formation of a Taylor cone, high voltage was applied. Spinning usually took place for an hour, and was noted to have occurred successfully when a deposition appeared on the collector.

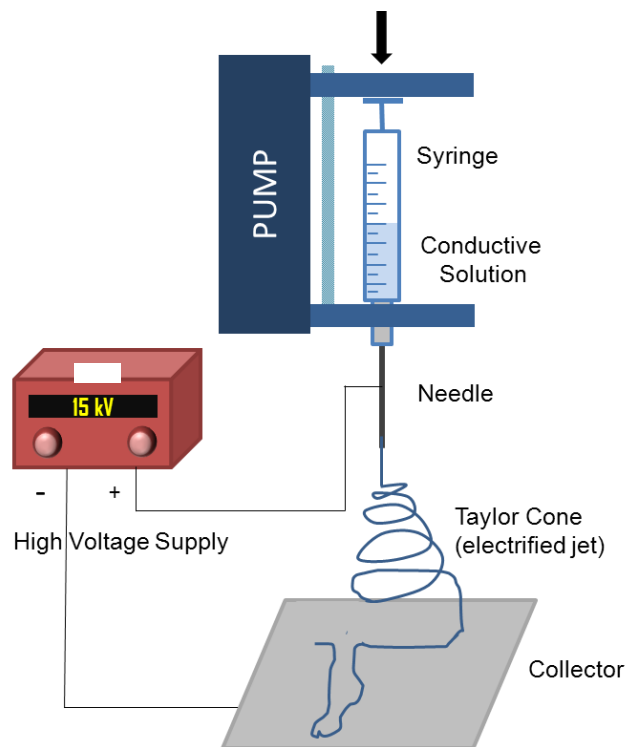


**Figure 2.1:** A typical electrospinning setup.

The entire set up took place in a clear plastic box to ensure maximum safety to the operator, which also contained a vent to allow any vaporised solvent to exit. Experiments were conducted at room temperature and humidity.

## **2.9. Nuclear magnetic resonance spectroscopy**

The compound was dissolved in an appropriate deuterated solvent (10 % w/v), and loaded into a sample tube. Nuclear magnetic resonance (NMR) spectra were recorded on a Bruker Avance at 300 MHz for  $^1\text{H}$  detection, and 75 MHz for  $^{13}\text{C}$  detection. Chemical shifts were recorded in parts per million (ppm) relative to trimethylsilane (TMS). All spectra were recorded at 25 °C in appropriate deuterated solvents.

## **2.10. Gel permeation chromatography**

Gel permeation chromatography (GPC) was carried out on a Varian GPC spectrometer, comprised of three PL gel 5  $\mu\text{m}$  mixed-C columns and a guard column. HPLC grade THF containing triethylamine (TEA) (2 % v/v), and BHT (0.05 % w/v) was used as the eluent at a flow rate of 1.0 ml min<sup>-1</sup>. The column temperature was set to 40 °C. Calibration used either fifteen near-monodisperse PMMA standards ( $M_p = 100 - 100,000$ ), fifteen near-monodisperse PEO standards ( $M_p = 100 - 1,000,000$ ) or ten near-monodisperse polystyrene standards ( $M_p = 100 - 100,000$ ). Samples for analysis were dissolved in the eluent (approximately 5 mg/ml) and injected into the machine. Analysis was performed using Cirrus GPC software supplied.

## **2.11. Fourier transform infra-red spectroscopy**

Fourier transform infra-red (FTIR) spectroscopy was performed using an attenuated total reflectance (ATR) crystal on a ThermoNicolet FTIR spectrometer. Approximately 5 mg of material was placed directly onto the crystal.. Analysis was performed using Omnic V5.1.A supplied.

## **2.12. Scanning Electron Microscopy**

High resolution imaging of polymer morphology was achieved using a Hitachi S-4800 cold Field Emission Scanning Electron Microscope (FE-SEM). The dry samples were prepared on 15 mm Hitachi M4 aluminium stubs using an adhesive high purity carbon tab. Samples were then coated with a 2 nm layer of gold using an Emitech K550X automated sputter coater. The FE-SEM measurement scale bar was calibrated using certified SIRA calibration standards. Imaging was conducted at a working distance of 8 mm and a working voltage of 5 kV using a combination of upper and lower secondary electron detectors.

SEM was also carried using an FEI Phenom Desktop SEM. Samples were affixed to an insert, and placed into the machine under vacuum.

## **2.13. Rheology**

Dynamic rheological experiments were performed using an Anton Paar Physica MCR101 rheometer. The measurements of the shear moduli (storage modulus,  $G'$  and loss modulus,  $G''$ ) were carried out using a cup and vane system. All gels were formed directly in 7 mL Sterilin cups and left overnight (at least 20 hours) at room temperature to gel before the measurements. Frequency scans were performed from  $1 \text{ rad s}^{-1}$  to  $100 \text{ rad s}^{-1}$  under a strain of 0.2 %. The shear moduli (storage modulus,  $G'$  and loss modulus,  $G''$ ) were measured at a frequency of  $10 \text{ rad s}^{-1}$ . The strain amplitude measurements were also performed within the linear viscoelastic region, where the storage modulus ( $G'$ ) and loss modulus ( $G''$ ) are independent of the strain amplitude.

## **2.14. Confocal Microscopy**

High resolution fluorescence microscopy was carried out using a Leica TCS SP5II confocal microscope. Samples were stained with an appropriate dye (usually Nile blue) and placed on a glass slide. A laser was used to excite the

sample (at 44 % of maximum laser power), and fluorescence was measured over appropriate wavelength regions. For magnifications greater than x100 objective, oil was used.

### **2.15. High precision ATR-FTIR spectroscopy**

ATR-FTIR spectra were collected using a Golden Gate single reflection ATR accessory (SpectraTech) with a ThermoNicolet Nexus FTIR spectrometer. The gelation solution was placed into direct contact with the ATR crystal and covered with a cap to prevent water and solvent loss during the scans. Data were collected by averaging over 64 scans at  $2\text{ cm}^{-1}$ . Samples were taken over several days and analysed using Omnic 6.1.A.

# **CHAPTER 3**

## **Synthesis of**

### **Polymer-Peptide Conjugates**

### 3. Synthesis of Polymer-Peptide Conjugates

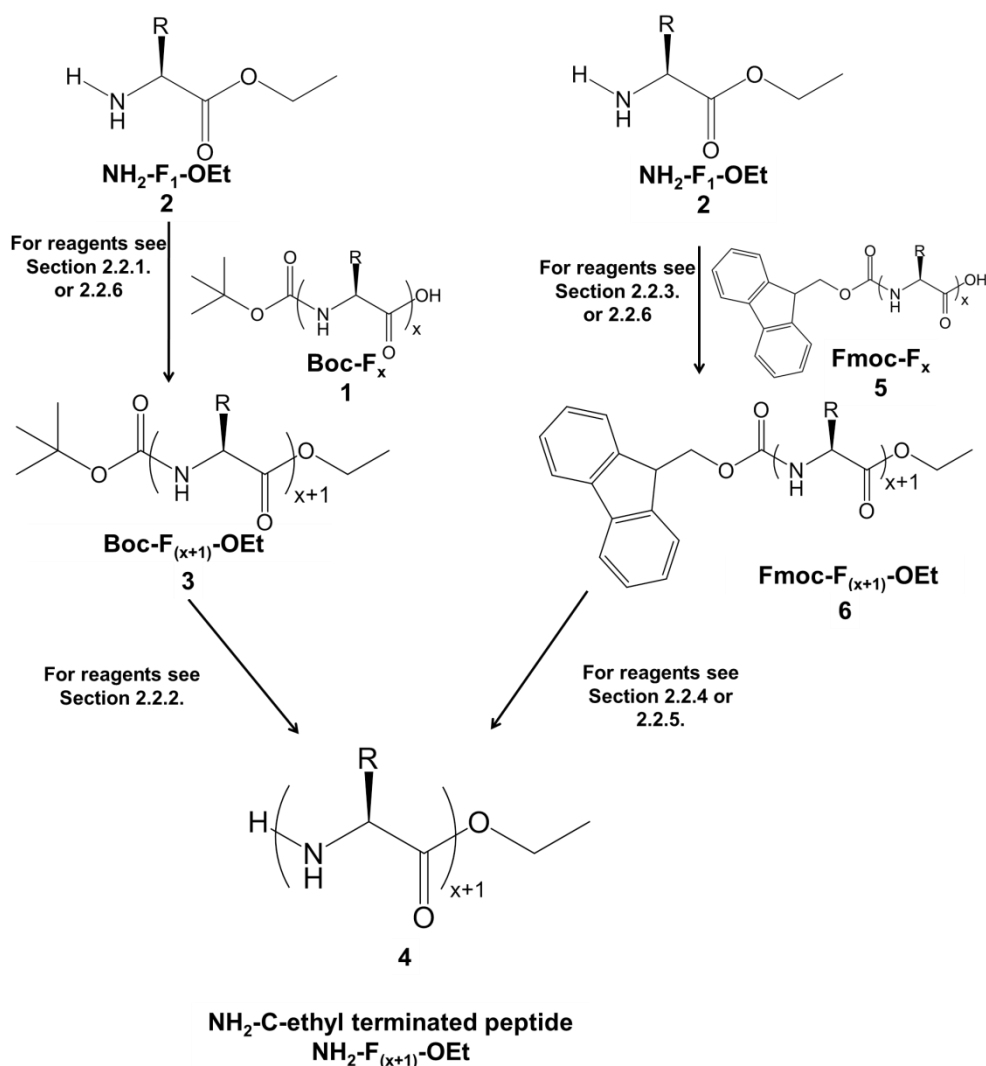
Conjugation between natural peptides and synthetic polymers produces materials that inherit the advantageous properties of both starting materials, such as biocompatibility and enhanced tolerance and functionality. Producing conjugates with a range of functionality allows for the use of such materials in an array of applications, one of the most important being a potential drug delivery device or cell scaffold. This chapter describes the synthetic routes used to produce polymer-peptide conjugates, firstly detailing the preparation of the respective starting reagents (Sections 3.1 and 3.2), and then considering the most effective coupling method (Section 3.3). Section 3.4 describes an alternative method for conjugate fabrication. To put this into a wider context, Section 3.5 briefly draws together all of the discussed points and compares the effectiveness of the chosen coupling method to previously established work in the literature, determining which method is more effective and justifying the need for the new coupling method established in this work. Finally, Section 3.6 concludes the chapter and provides a brief description of the direction for future work.

#### 3.1. Synthesis of phenylalanine peptide sequences

Phenylalanine was the biological amino acid used in this project. The synthesis of phenylalanine oligopeptide sequences was required to be facile, mild, and fast. Scheme 3.1 outlines the general systems considered for the production of oligopeptides of desired length. Generally, an N-protected amino was reacted with a C-protected amino using a coupling reagent. The resulting oligopeptide was then deprotected on the N-terminus to produce the desired mono-functional peptide (C-terminated).

Phenylalanine oligopeptide sequences were prepared in one-step reactions from commercially available *N*-(*tert*-butoxycarbonyl)-L-phenylalanine (Boc-F<sub>1</sub>) and L-phenylalanine ethyl ester hydrochloride (F<sub>1</sub>-OEt) using isobutylchloroformate (IBCF) as a coupling agent. IBCF coupling was chosen

as successful preparation of short-chain phenylalanine oligopeptides has been demonstrated using this reagent in the literature<sup>[1]</sup>. The coupling reaction took place in the presence of 4-methylmorpholine (NMM) and resulted in good yields.



**Scheme 3.1:** Reaction scheme showing synthetic routes utilised for the synthesis of  $\text{NH}_2\text{-F}_{(x+1)\text{-OEt}}$ .

After initial tests, a decision was taken to limit the oligopeptide length to a maximum of six repeat units of phenylalanine to ensure compatibility of the synthesised peptide (and the resulting conjugate) in a wide range of solvents (especially those with a more polar character) and making the process more industrially viable by reducing the amount of material and number of steps required. Consequently, costs are reduced and the impact on the environment

is minimised, in terms of storage, disposal, and large-scale effects. The repeat unit limit was critical in ensuring that the later coupling reactions with the more hydrophilic monomethoxy-poly(ethylene oxide), (mPEO<sub>n</sub>) were viable. Percentage yields for the coupling steps are summarised in Table 3.1. The general trend shows that as the peptide length increases, the yield decreases. This is attributed to the steric effects of the larger peptides, and the decreasing solubility in the reaction solvent.

**Table 3.1:** Percentage yields of synthesised Boc-F<sub>x</sub>-OEt. All of the synthesised compounds were white solids.

Peptide	Peptide Length	Average Yield (%)
Boc-F <sub>2</sub> -OEt	2	81
Boc-F <sub>3</sub> -OEt	3	80
Boc-F <sub>4</sub> -OEt	4	77
Boc-F <sub>5</sub> -OEt	5	69
Boc-F <sub>6</sub> -OEt	6	56

The successful synthesis of the oligopeptides was confirmed by NMR, FTIR, and GPC. Boc-F<sub>2</sub>-OEt has been used as an example of a synthesised oligopeptide. <sup>1</sup>H NMR spectra of the precursor peptides (Boc-F<sub>1</sub>-OH and NH<sub>2</sub>-F<sub>1</sub>-OEt) are shown in Figures 3.1 and 3.2, respectively, and the dipeptide (Boc-F<sub>2</sub>-OEt) in Figure 3.3. Due to the additive nature of the reaction, the synthesised peptide <sup>1</sup>H NMR spectrum is a combination of the NMR spectra of both reagents, but as expected heavily influenced by the groups from Boc-F<sub>1</sub>, since the synthesised peptide is homologous. However, the protons from the amine group (originally from F<sub>y</sub>-OEt) have shifted as they have now become part of the amide bond. The chemical environment in the bond is different and so affects the shielding, and ultimately the position of the proton, shifting it from 8.9 ppm in the F<sub>1</sub>-OEt (amine environment) spectrum to 6.5 ppm in the oligopeptide spectrum (amide environment). Further, the conversion from amine to amide reduces the number of protons from two to one, which is also

reflected in the spectrum. It can be seen that the intensity of the peak has been reduced accordingly in the oligopeptide spectrum.

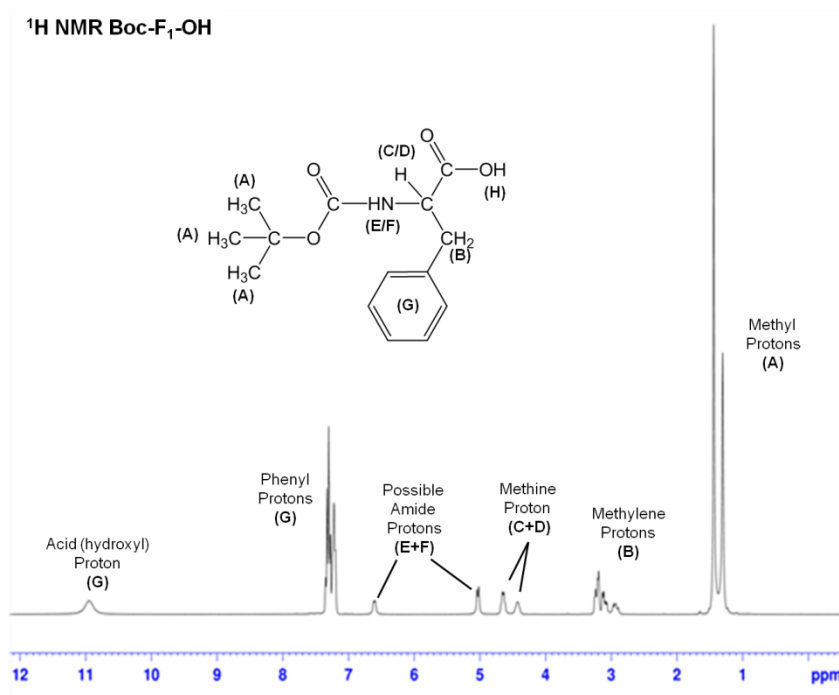


**Figure 3.1:** <sup>1</sup>H NMR spectrum of Boc-F<sub>1</sub>-OH.

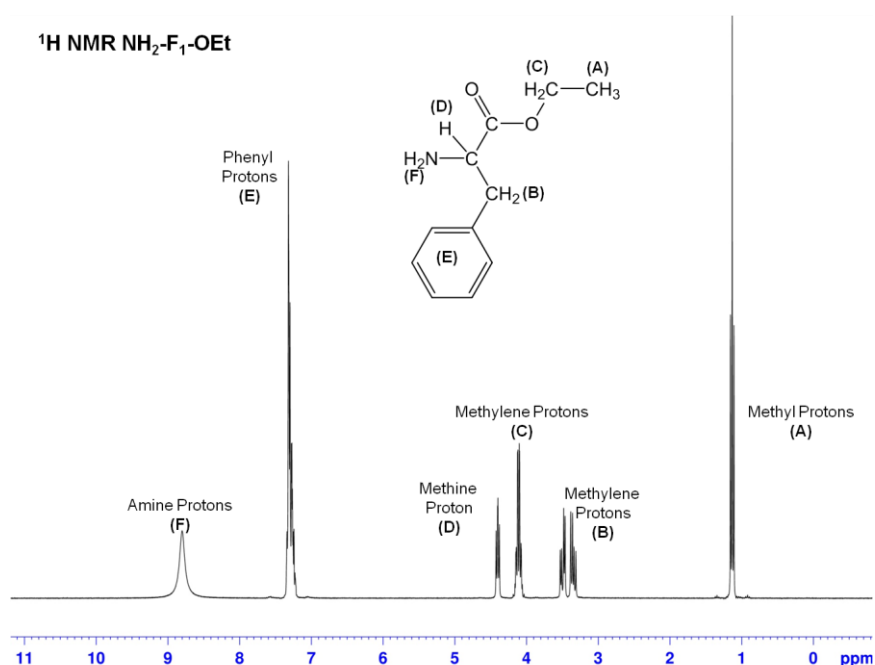


**Figure 3.2:** <sup>1</sup>H NMR spectrum of NH<sub>2</sub>-F<sub>1</sub>-OEt.HCl.

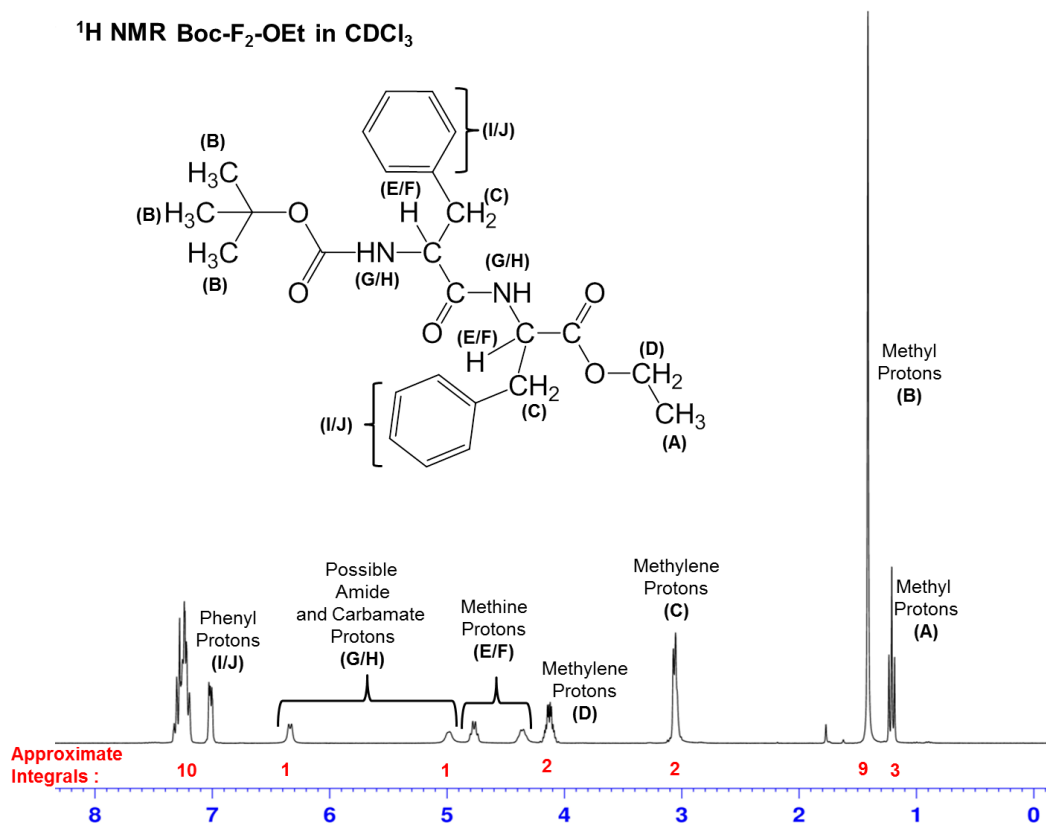


**Figure 3.3:** <sup>1</sup>H NMR spectrum of Boc-F<sub>2</sub>-OEt.

To further confirm the success of the coupling steps, <sup>13</sup>C PENDANT NMR spectra were recorded for all starting materials (Figures 3.4 and 3.5, respectively). Figure 3.6 shows the <sup>13</sup>C NMR spectrum for the product. The appearance of a peak at 171 ppm was observed in all cases, indicative of a carbonyl carbon (amide) and confirms that coupling has taken place. On the spectra, the peak has been negatively phased, therefore indicating that it is either a secondary or quaternary carbon. Due to its high chemical shift it is identified as quaternary carbon (i.e. has no protons attached to it).

GPC analysis revealed that there was an increase in hydrodynamic volume after coupling had taken place (Figure 3.7). The polydispersity index (PDI) remained narrow (1.06). Thus, it can be confirmed that the peptide have successfully coupled. For all of the synthesised peptides, the presence of an additional amide peak (especially in carbon spectra) and GPC analysis (the noted change in hydrodynamic volume) were used to confirm successful conjugation. It is noted that the peaks obtained by GPC are not unimodal. This

is due to the very low molecular weights, which causes the products to have a retention time similar to the stabilisers in the eluent.

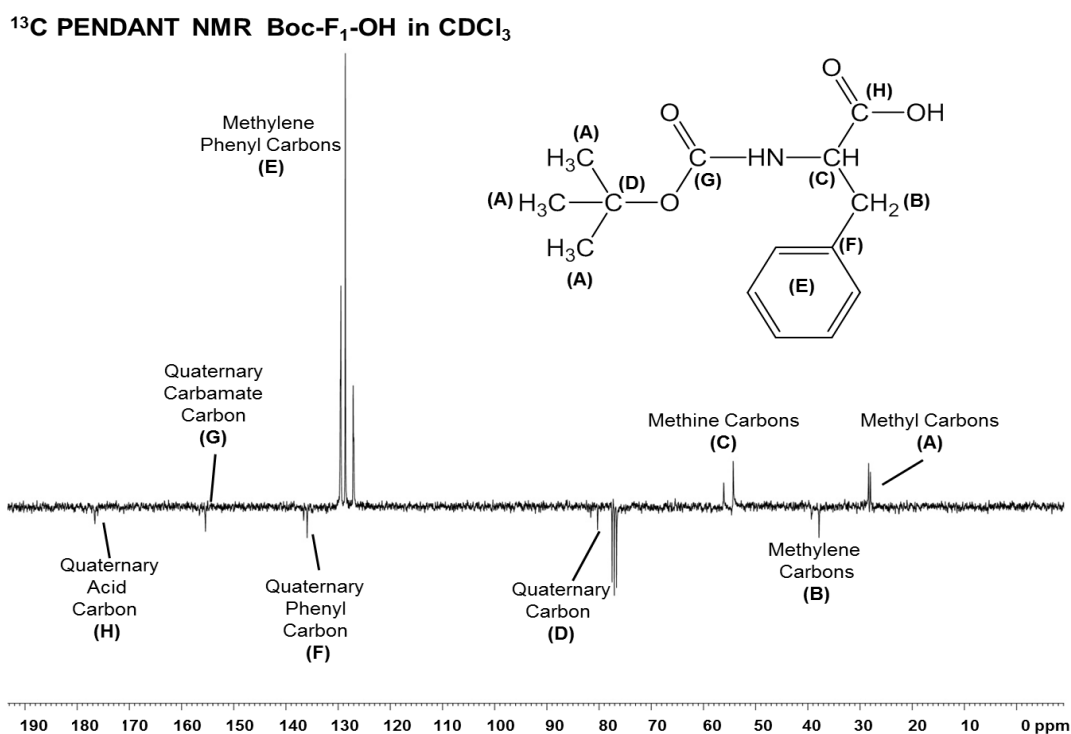


**Figure 3.4:** <sup>13</sup>C PENDANT NMR spectrum of Boc-F<sub>1</sub>-OH.

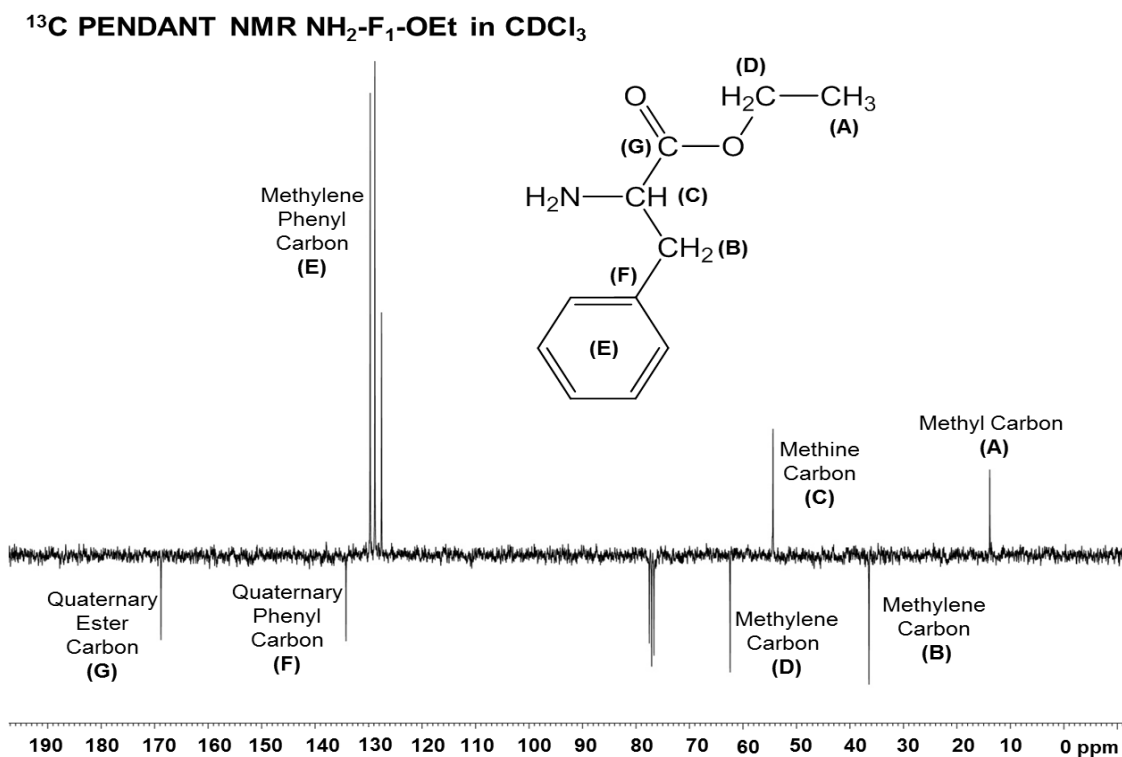


**Figure 3.5:** <sup>13</sup>C PENDANT NMR spectrum of NH<sub>2</sub>-F<sub>1</sub>-OEt.HCl.

**$^{13}\text{C}$  PENDANT NMR Boc-F<sub>2</sub>-OEt in CDCl<sub>3</sub>**

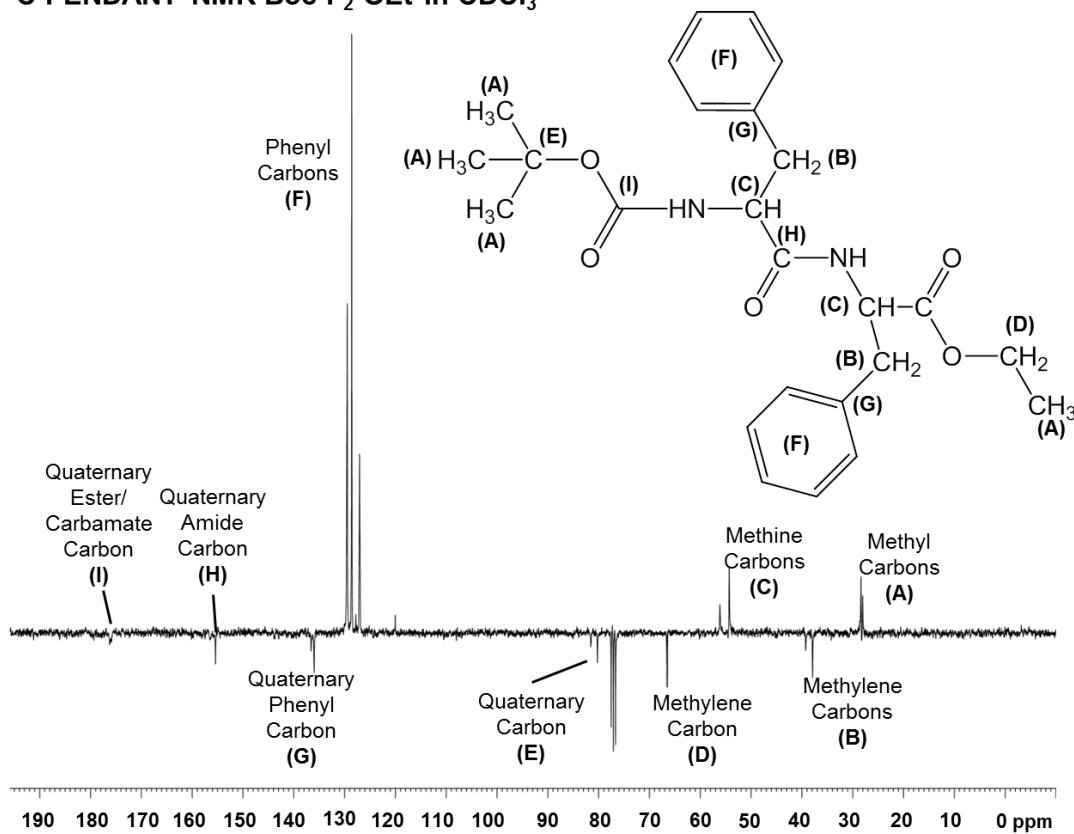


**Figure 3.6:**  $^{13}\text{C}$  NMR spectrum of Boc-F<sub>2</sub>-OEt.

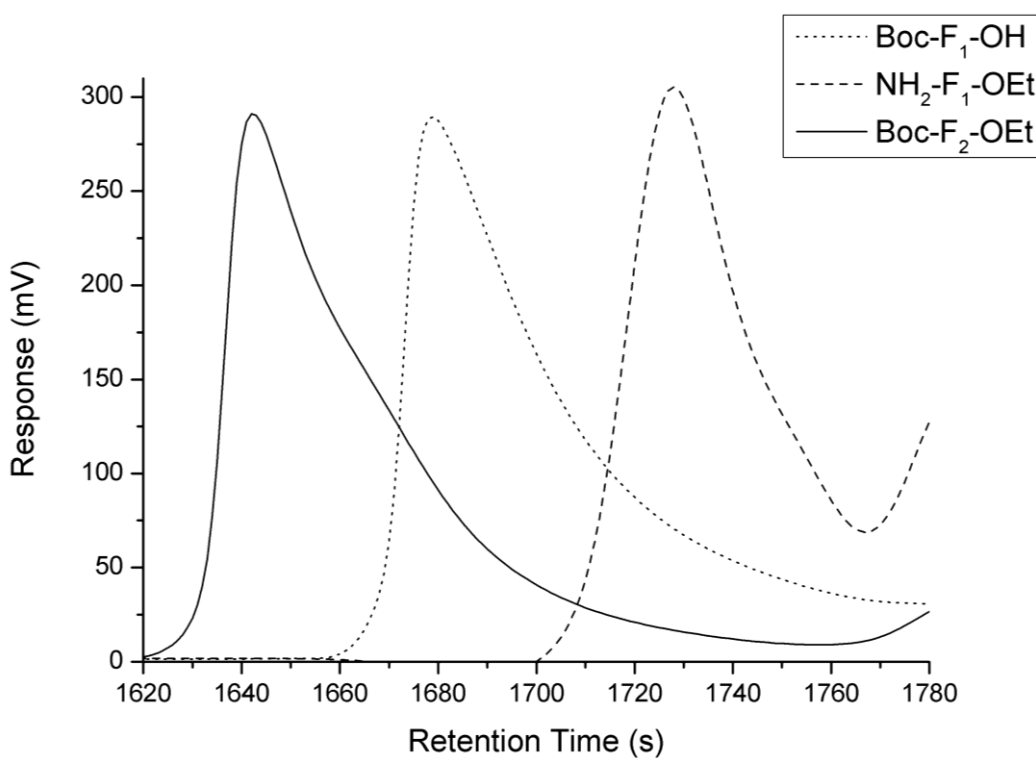


**Figure 3.7:** GPC analysis of Boc-F<sub>2</sub>-OEt, Boc-F<sub>1</sub>-OH and NH<sub>2</sub>-F<sub>1</sub>-OEt.

Removal of the *N-tert*-butoxycarbonyl (Boc) protecting group afforded peptides with increased functionality due to the exposal of the amine group and was necessary for further configuration. Deprotection of the amine group was carried out using excess trifluoroacetic acid (TFA) in chloroform. Although the reaction time was short (3-4 hours), the mixture was left overnight to ensure complete removal. Furthermore, the amount of TFA required increased as the peptide length increased. Table 3.2 summarises the yields for the deprotection step. Synthesis and deprotection of F<sub>6</sub> was also carried out, however work on this material was not continued due to solubility issues encountered during synthesis.

**Table 3.2:** Percentage yield and overall yields for deprotected peptides (where the overall yield depicts synthesis from starting material).

<b>Boc deprotected Peptide</b>	<b>Yield from Boc-F<sub>x</sub>-OEt (%)</b>	<b>Overall Yield (%)</b>
NH <sub>2</sub> -F <sub>1</sub> -OEt	-	
NH <sub>2</sub> -F <sub>2</sub> -OEt	99	79
NH <sub>2</sub> -F <sub>3</sub> -OEt	97	77
NH <sub>2</sub> -F <sub>4</sub> -OEt	97	74
NH <sub>2</sub> -F <sub>5</sub> -OEt	95	69

Complete removal of the Boc groups was confirmed by <sup>1</sup>H NMR, with the disappearance of the *tert*-butyl signals –C(CH<sub>3</sub>)<sub>3</sub> at 1.4 ppm and 1.2 ppm. Two *tert*-butyl peaks are visible as the product is mixture of two isomers, which arise due to the hindered rotation of the C-N bond. <sup>13</sup>C NMR shows the disappearance of the C(CH<sub>3</sub>)<sub>3</sub> signal at 160 ppm, further confirming that deprotection had taken place.

GPC analysis of the compounds revealed that the hydrodynamic volume decreased by only a small amount, as expected. The deprotected peptide produced a narrow unimodal peak with a PDI of 1.06 (NH<sub>2</sub>-F<sub>2</sub>-OEt). It should be noted, however, that TFA associates with the deprotected peptide and may

interfere with results. The only TFA signal detectable by  $^1\text{H}$  NMR would be the  $-\text{OH}$  group which is broad and difficult to detect. Figure 3.8 shows the  $^1\text{H}$  NMR spectrum of  $\text{NH}_2\text{-F}_2\text{-OEt.TFA}$ , and is representative of the oligopeptide chain. Data obtained by NMR analysis is given below for Boc-F<sub>2</sub>-OEt, Boc-F<sub>3</sub>-OEt, Boc-F<sub>4</sub>-OEt,  $\text{NH}_2\text{-F}_2\text{-OEt}$ ,  $\text{NH}_2\text{-F}_3\text{-OEt}$ , and  $\text{NH}_2\text{-F}_4\text{-OEt}$

$^1\text{H}$  NMR  $\text{NH}_2\text{-F}_2\text{-OEt}$  in  $\text{CDCl}_3$

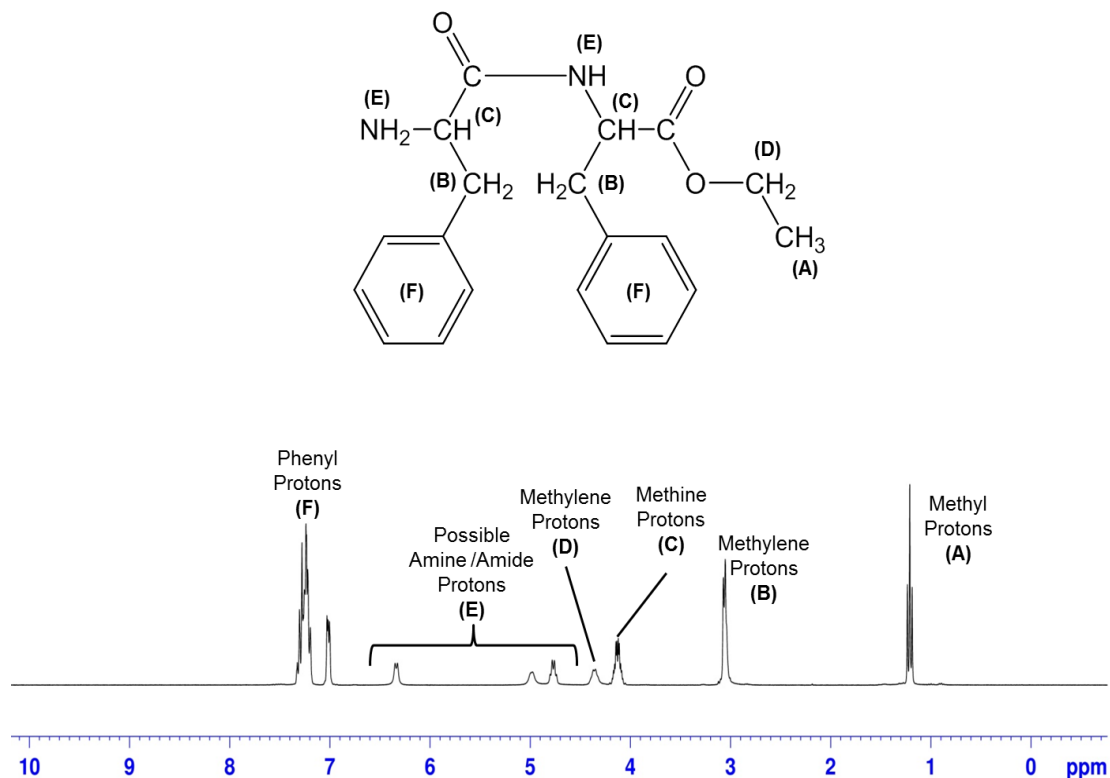


**Figure 3.8:**  $^1\text{H}$  NMR spectrum of  $\text{NH}_2\text{-F}_2\text{-OEt.TFA}$ . (Note: TFA peak not shown on spectrum).

**Boc-F<sub>2</sub>-OEt:**  $^1\text{H}$  NMR ( $\text{CDCl}_3$ ) : 7.26 (8H, Ph, m), 7.00 (2H, Ph, m), 6.31 (1H, NH, bd), 4.94 (1H, NH, bs), 4.75 (1H, CH, m), 4.33 (1H, CH, m), 4.10 (2H,  $\text{CH}_2\text{CH}_3$ , m), 3.04, (4H, 2 x  $\text{CH}_2\text{Ph}$ , m), 1.40 (9H, Boc, s), 1.19 (3H,  $\text{CH}_2\text{CH}_3$ , t,  $^3J_{\text{HH}} = 7.14$  Hz);  $^{13}\text{C}$  NMR (DMSO) 172.29, 171.75, 155.57, 138.53, 137.47, 129.62 (2C), 128.70, 128.44, 127.02, 126.62, 78.46, 60.97, 55.93, 54.04, 37.90, 37.24, 28.58, 14.37 ppm.

**Boc-F<sub>3</sub>-OEt:**  $^1\text{H}$  NMR ( $\text{CDCl}_3$ ) : 7.30 (15H, Ph, m), 6.40 (1H, NH, bd), 6.16 (1H, NH, bs), 4.81 (1H, NH, bs), 4.69 (1H, CH, dt), 4.54 (1H, CH, dt), 4.30 (1H, CH,

m), 4.17 (2H,  $CH_2CH_3$ , m), 2.99 (6H, 3 x  $CH_2Ph$ , m), 1.38 (9H, *Boc*, s), 1.19 (3H,  $CH_2CH_3$ , t,  $^3J_{HH} = 7.14$  Hz) ppm;  $^{13}C$  NMR (DMSO) 171.56, 171.13, 168.36, 137.77, 137.47, 135.14, 130.02, 129.37, 129.24, 128.94, 128.72, 128.60, 127.57, 127.02, 126.90, 61.02, 54.36, 54.15, 53.54, 38.15, 37.45, 37.19, 14.40 ppm.

**Boc-F<sub>4</sub>-OEt:**  $^1H$  NMR ( $CDCl_3$ ): 7.25 (12 H, *Ph*, m), 7.12 (6H, *Ph*, m), 6.98 (2H, *Ph*, bs), 6.49 (2H, 2 x *NH*, bs), 6.30 (1H, *NH*, bd), 4.77 (1H, *NH*, m), 4.72 (1H, *CH*, dt), 4.59 (1H, *CH*, m), 4.49 (1H, *CH*, dt), 4.12 (3H, *CH* and  $CH_2CH_3$ , m), 2.96 (8H, 4 x  $CH_2Ph$ , m), 1.34 (9H, *Boc*, s), 1.20 (3H,  $CH_2CH_3$ , t,  $^3J_{HH} = 7.14$  Hz) ppm;  $^{13}C$  NMR (DMSO) 171.66, 171.60, 171.43, 171.06, 155.46, 138.59, 137.94, 137.92, 137.43, 129.79, 129.60, 129.55, 129.53, 128.72, 128.48, 128.39, 128.28, 127.02, 126.71, 126.62, 126.53, 78.52, 60.96, 56.23, 54.33, 53.13, 53.89, 38.25, 38.11, 37.97, 37.22, 28.56, 14.38 ppm.

**NH<sub>2</sub>-F<sub>2</sub>-OEt:**  $^1H$  NMR ( $CDCl_3$ ): 7.26 (8H, *Ph*, m), 7.00 (2H, *Ph*, m), 6.31 (1H, *NH*, bd), 4.94 (1H, *NH*, bs), 4.75 (1H, *CH*, m), 4.33 (1H, *CH*, m), 4.10 (2H,  $CH_2CH_3$ , m), 3.04 (4H, 2 x  $CH_2Ph$ , m), 1.40 (9H, *Boc*, s), 1.19 (3H,  $CH_2CH_3$ , t,  $^3J_{HH} = 7.19$  Hz);  $^{13}C$  NMR (DMSO) 172.29, 171.75, 155.57, 138.53, 137.47, 129.62 (2C), 128.70, 128.44, 127.02, 126.62, 78.46, 60.97, 55.93, 54.04, 37.90, 37.24, 28.58, 14.37 ppm.

**NH<sub>2</sub>-F<sub>3</sub>-OEt:**  $^1H$  NMR ( $CDCl_3$ ): 7.30 (15H, *Ph*, m), 6.40 (1H, *NH*, bd), 6.16 (1H, *NH*, bs), 4.81 (1H, *NH*, bs), 4.69 (1H, *CH*, dt), 4.54 (1H, *CH*, dt), 4.30 (1H, *CH*, m), 4.17 (2H,  $CH_2CH_3$ , m), 2.99 (6H, 3 x  $CH_2Ph$ , m), 1.38 (9H, *Boc*, s), 1.19 (3H,  $CH_2CH_3$ , t,  $^3J_{HH} = 7.19$  Hz) ppm;  $^{13}C$  NMR (DMSO) 171.56, 171.13, 168.36, 137.77, 137.47, 135.14, 130.02, 129.37, 129.24, 128.94, 128.72, 128.60, 127.57, 127.02, 126.90, 61.02, 54.36, 54.15, 53.54, 38.15, 37.45, 37.19, 14.40 ppm.

**NH<sub>2</sub>-F<sub>4</sub>-OEt:**  $^1H$  NMR ( $CDCl_3$ ): 7.25 (12 H, *Ph*, m), 7.12 (6H, *Ph*, m), 6.98 (2H, *Ph*, bs), 6.49 (2H, 2 x *NH*, bs), 6.30 (1H, *NH*, bd), 4.77 (1H, *NH*, m), 4.72 (1H, *CH*, dt), 4.59 (1H, *CH*, m), 4.49 (1H, *CH*, dt), 4.12 (3H, *CH* and  $CH_2CH_3$ , m), 2.96 (8H, 4 x  $CH_2Ph$ , m), 1.34 (9H, *Boc*, s), 1.20 (3H,  $CH_2CH_3$ , t,  $^3J_{HH} =$

7.19 Hz) ppm;  $^{13}\text{C}$  NMR (DMSO) 171.66, 171.60, 171.43, 171.06, 155.46, 138.59, 137.94, 137.92, 137.43, 129.79, 129.60, 129.55, 129.53, 128.72, 128.48, 128.39, 128.28, 127.02, 126.71, 126.62, 126.53, 78.52, 60.96, 56.23, 54.33, 53.13, 53.89, 38.25, 38.11, 37.97, 37.22, 28.56, 14.38 ppm.

Whilst the synthetic procedure carried out broadly followed the methods outlined in Sections 2.1.1 and 2.2.2, there were a few modifications made to increase purity. It was found that after coupling a faint yellow colour would remain despite repeated washes, which is attributed to unreacted or isomerised IBCF. In order to remove this impurity, the peptide was dissolved in a minimal amount of acetone and reprecipitated into diethyl ether. It was also necessary, especially to ensure complete deprotection of the longer peptides, to lower the mixture of acetone and petroleum to 4 °C, which resulted in additional peptide precipitating. Furthermore, during synthesis, it was necessary to remove the chloroform *in vacuo* for peptides longer than two repeat units (i.e.  $>F_2$ ) before precipitating in diethyl ether to obtain a solid material.

Boc protection was favoured over Fmoc (fluorenylmethoxycarbonyl) protection as it has already been demonstrated in the literature to be compatible with phenylalanine coupling<sup>[1]</sup>. However, an important advantage that Fmoc protection has over Boc protection is its tolerance to a wider range of reaction conditions. The susceptibility of Boc to acidic conditions is discussed later in Section 3.4. It was also noted that Fmoc deprotection is much milder than Boc deprotection and required less time; piperidine in DMF taking approximately 20 to 30 minutes to remove Fmoc, whereas Boc deprotection required several hours to complete. Furthermore, the side product from the Fmoc deprotection reaction becomes visible (as it precipitates out) as the reaction progresses, providing a useful visual indicator.

However, the use of Fmoc also introduced further steps to the synthetic procedure as, unlike Boc deprotection which requires no additional washing after the deprotecting agent is added, any unreacted piperidine (the deprotecting agent) must be removed from the solution by washing. Furthermore, the presence of the by-product, a dibenzofulvene-piperidine

adduct, which is formed during the deprotection, necessitates additional washes to ensure that the product is pure.

Whilst the synthesis of Fmoc-protected peptide was successful, deprotection proved to be more challenging as isolation of the product was difficult and only a limited amount was recovered each time. Fmoc protection is normally used in solid phase peptide synthesis (SPPS), alongside a polymer scaffold (or support) and a linking group, as opposed to synthesis in the solution phase. Indeed, the majority of the literature details peptide synthesis via Fmoc in the solid phase only. SPPS, developed by Merrifield in 1963<sup>[2]</sup>, anchors the peptide onto a solid support, allowing facile modification of functional groups. The advantage of this technique is that the peptide is immobilised in the solid phase whilst reaction by-products and unreacted starting reagents will be washed away in the liquid phase. Subsequently, the solid support can then be removed by treating with a mild acid such as TFA. Purchasing a solid support or linker is typically expensive and therefore not cost effective for scaling up. It is for this reason why SPPS was not the primary strategy for synthesis in this work. However, Fmoc protection/deprotection was potentially a more appropriate route, and therefore this approach was investigated despite its dominance in SPPS only.

This section has focussed on the protection and deprotection of the amine functional group of the peptide. As noted previously, peptides are typically bi-functional, therefore this necessitated the use of a protecting group strategy to ensure that directed coupling was possible. During synthesis, the carboxylic acid group is also protected. However, it is possible to remove its protecting group and further functionalise the peptide post-synthesis. This leads to an interesting situation where bi-functionality of the synthesised oligopeptide is introduced. Another advantage of having the acid group deprotected is that it can react directly with mPEO<sub>n</sub>, without the need to convert the hydroxyl group to a carboxylic acid.

In conclusion, five phenylalanine homologues were synthesised via solution phase peptide synthesis using a Boc protecting group strategy. Overall yields

and purity for the synthesis were high. Four of these peptides (F<sub>1</sub>, F<sub>2</sub>, F<sub>3</sub>, F<sub>4</sub>) were subsequently coupled with mPEO<sub>n</sub>-COOH (see Section 3.2) and their self-assembly behaviour was investigated (Chapter 4).

### 3.2. Functionalisation of monomethoxy-poly(ethylene oxide)

Monomethoxy-poly(ethylene oxide), mPEO<sub>n</sub>, is a monofunctional PEO derivative with a single reactive hydroxyl group (Figure 3.9). Whilst direct conjugation of this group is possible, it is more practical to convert the hydroxyl group into a more reactive functional group. Many examples of this are present in the literature<sup>[3-5]</sup>. In this project, the hydroxyl group was converted to a more reactive carboxylic acid group (Scheme 3.2). There are several protocols for this in the literature. Jones oxidation can be used to convert an alcohol group to an aldehyde, ketone or carboxylic acid<sup>[4, 6]</sup>. The resultant oxidation product is determined by the position of the starting alcohol (i.e. primary, secondary, or tertiary).

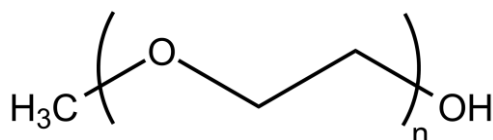
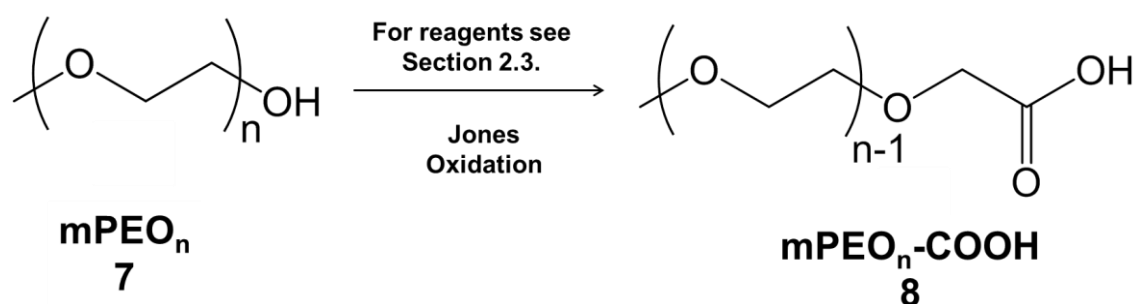


**Figure 3.9:** Structure of a monofunctional-poly(ethylene oxide), monomethoxy-poly(ethylene oxide) (mPEO<sub>n</sub>).



**Scheme 3.2:** Synthetic route for carboxylic acid-terminated monomethoxy-poly(ethylene oxide).

In previous work established elsewhere, modifications were made to the polymer chain end that increased reactivity and introduced a new functional group. However, this group (or a derivative of this functional group) would then be present in the backbone of the final PPC, and may have unexpected (sometimes even adverse) effects on self-assembling behaviour. For example, modifying mPEO-succinate with a succinimidyl group introduces an additional ester group into the polymer backbone, and ultimately the conjugate backbone, resulting in the product being susceptible to hydrolysis. This cleaves the PEO from the peptide resulting in a loss of functionality<sup>[7]</sup>. Furthermore, introduction of activating groups may introduce side products, and may involve long, complex reactions.

One of the desired goals of this overall synthesis is to produce well-defined conjugates in the fewest possible steps. To this end, a PEO derivative with a carboxylic acid group was produced. Owing to the fact that a carboxylic acid can couple directly to an amine forming a stable amide (peptide bond), the amine group of the peptide does not need to be functionalised in any way, and therefore this lowers the number of steps required in the reaction scheme and leads to an increase in overall yields. This is discussed in greater detail in Sections 3.3 and 3.5.

Jones oxidation was carried out as described in Chapter 2.3. This method was carried out on mPEO with three different chain lengths; mPEO<sub>7</sub>, mPEO<sub>12</sub>, mPEO<sub>17</sub>, with molecular weights of approximately 350 Da, 550 Da, and 750 Da, respectively. Amorphous mPEO (less than 2000 Da) was chosen so that the driving force of crystallisation would not interfere with the self-assembling behaviour of the peptidic units. Furthermore, it allows for renal clearance when introduced into the body. Finally, mPEO in this weight range is the most widely available commercially, and therefore the most economical option for this particular biocompatible material.

During synthesis, on addition of the Jones reagent to the reaction mixture (which consists of mPEO<sub>n</sub> dissolved in acetone), an orange-brown solution was formed. This was attributable to the acidified chromium (VI) trioxide (CrO<sub>3</sub>) from

the Jones reagent. As the reaction progressed a deep green colour formed, as the chromium was reduced to chromium (IV) oxide ( $\text{CrO}_2$ ). In actual fact, chromium (VI) oxide was first converted to chromic acid in the presence of aqueous acid ( $\text{H}_2\text{SO}_4$ ).  $\text{mPEO}_n$ , which is a primary alcohol, and chromic acid produce a chromate (VI) ester which then forms (in the presence of water) the corresponding aldehyde,  $\text{mPEO}_n$ -aldehyde (Figure 3.10) and chromium (IV) oxide. The latter cannot take any further part in oxidation reactions.  $\text{mPEO}_n$ -aldehyde is able to be hydrated to form another alcohol. This produces another chromate (VI) ester, finally resulting in the desired carboxylic acid,  $\text{mPEO}_n$ -COOH. The chromium species is reduced to a (IV) oxide, which further disproportionates to chromium (III) oxide ( $\text{Cr}_2\text{O}_3$ ) and  $\text{CrO}_3$ . Propan-2-ol is poured through the filtered solid precipitate to reduce this additional  $\text{CrO}_3$  that forms from the disproportionation, ensuring that the waste is non-toxic.

It is the water, acting as a base, that drives the conversion of the aldehyde to an acid, therefore more hydrophobic substrates would not further convert from an aldehyde (or would convert at a slower rate) due to the inability of the substrate to be hydrated. Formation of an aldehyde derivative from an alcohol may be preferable, and can be achieved when/if anhydrous conditions are used (such as using acetic anhydride). To form a PPC in this instance, it is necessary to produce a Schiff Base through reductive amination (see Figure 1.8).

It was noted that a longer reaction time was required as the  $\text{mPEO}_n$  chain length was increased. The appearance of the green colour was used as an initial visual indicator that conversion had occurred. After purification, NMR, GPC, and IR analyses were used to confirm the production of the acid and to determine purity. Figures 3.11, 3.12, 3.13, and 3.14 show the results from these analyses using  $\text{mPEO}_{12}$  homologues as an exemplar. It was expected that the methylene protons adjacent to the carboxylic acid group ( $\text{CH}_2\text{-COOH}$ ) would form a distinct singlet peak in the  $^1\text{H}$  NMR spectrum, as they moved to a different chemical environment to those in the polymer backbone, and as such, are no longer equivalent. This is confirmed in Figure 3.11 by the singlet peak (Peak C), which has a relative integral of 2, and is downfield due to the

electronegative (deshielding) effect of both the adjacent carbonyl group and oxygen.

The large (and broad) multiplet at 3.55 ppm (Peak B in Figure 3.11) originates from the polymer backbone protons ( $\text{O-CH}_2\text{-CH}_2$ ). A carboxylic acid proton peak is also visible (Peak D) at 9.63 ppm. Interestingly, the carboxylic acid proton is slightly more upfield than expected as, typically, acidic protons are found between 10-12 ppm. It can be argued that this peak is just on the edge of the carboxylic acid chemical shift region, and therefore can be classified as such. However, as it is known that there is a prospect of aldehyde formation, it is possible that this could indicate a degree of impurity. Consequently,  $^{13}\text{C}$  PENDANT NMR spectroscopy and other analytical techniques were used to verify this.

The  $^{13}\text{C}$  PENDANT NMR technique is able to phase the different types of carbons depending on their environment (i.e. primary, secondary, tertiary, and quaternary carbons). Primary and tertiary carbons are phased in an opposite direction to secondary and quaternary carbons. Figure 3.12 shows the spectrum where  $\text{CH}_3$  and  $\text{CH}$  carbons are phased downwards, and the other carbons are phased upwards. At 59 ppm, a downwards phased peak can be observed, indicative of the  $\text{CH}_3$  carbon at the polymer chain end. Peak C, 71 ppm arises from the  $\text{CH}_2$  carbons of the main polymer backbone. Notably, there is a peak at 172 ppm (Peak E), which is phased upwards, and therefore representative of a quaternary carbon; a carbonyl group. The functional groups that appear in that chemical shift range are typically carboxylic acids, and the possibility that the species in an aldehyde is ruled out due to the phase in the spectrum. Therefore, this confirms that complete oxidation has to a carboxylic acid has taken place.

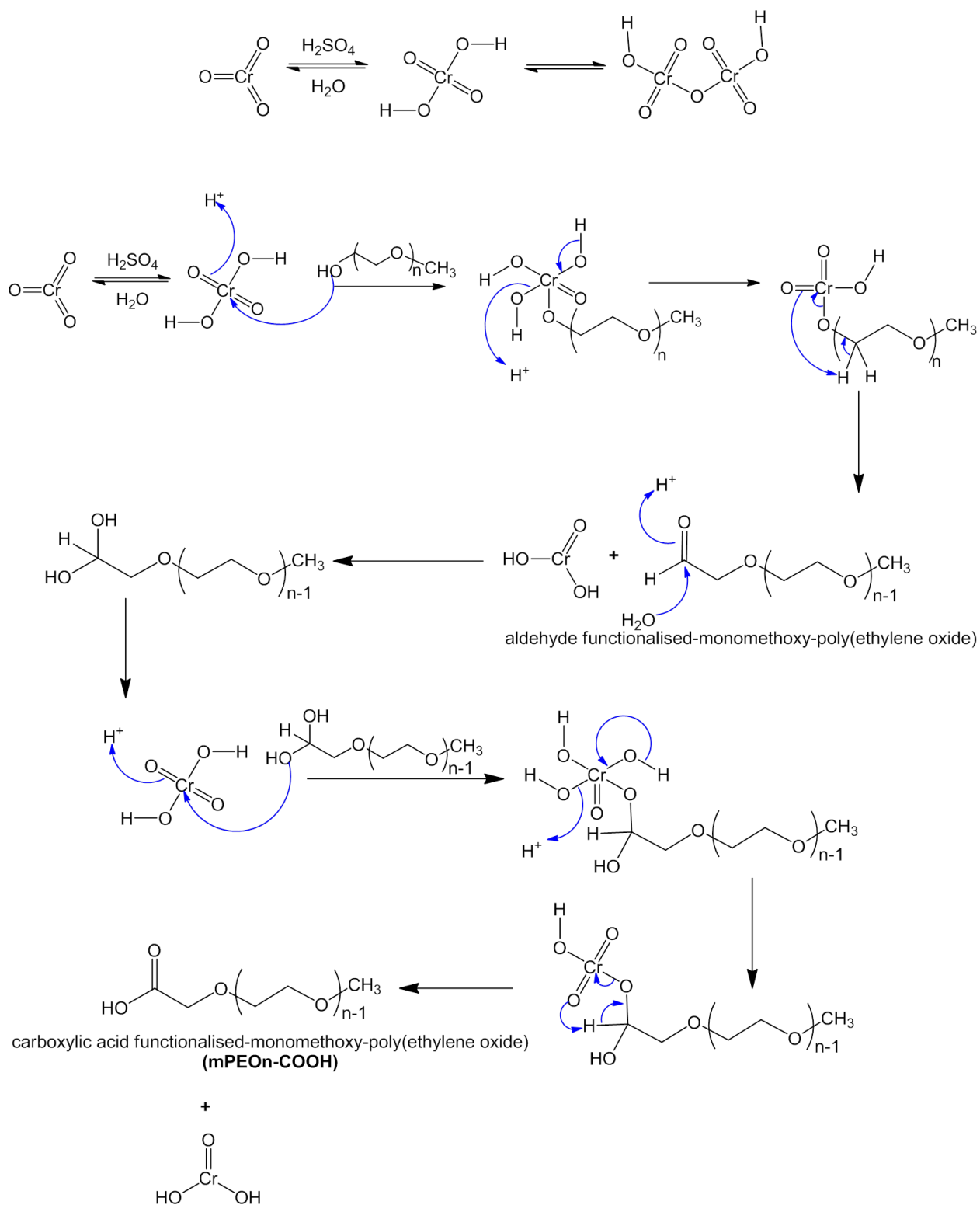


**Figure 3.10:** Reaction mechanism illustrating the oxidation of mPEO<sub>n</sub> to an aldehyde, and subsequently a carboxylic acid<sup>[6]</sup>.

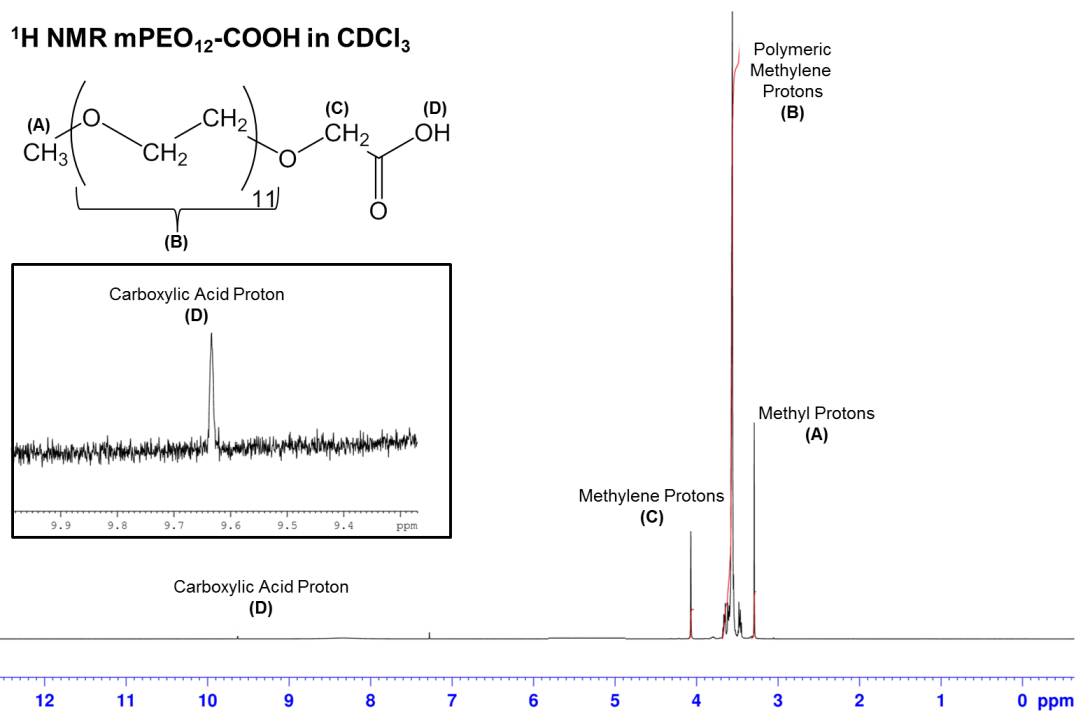


**Figure 3.11:** Labelled  $^1\text{H}$  NMR spectrum of mPEO<sub>12</sub>-COOH.

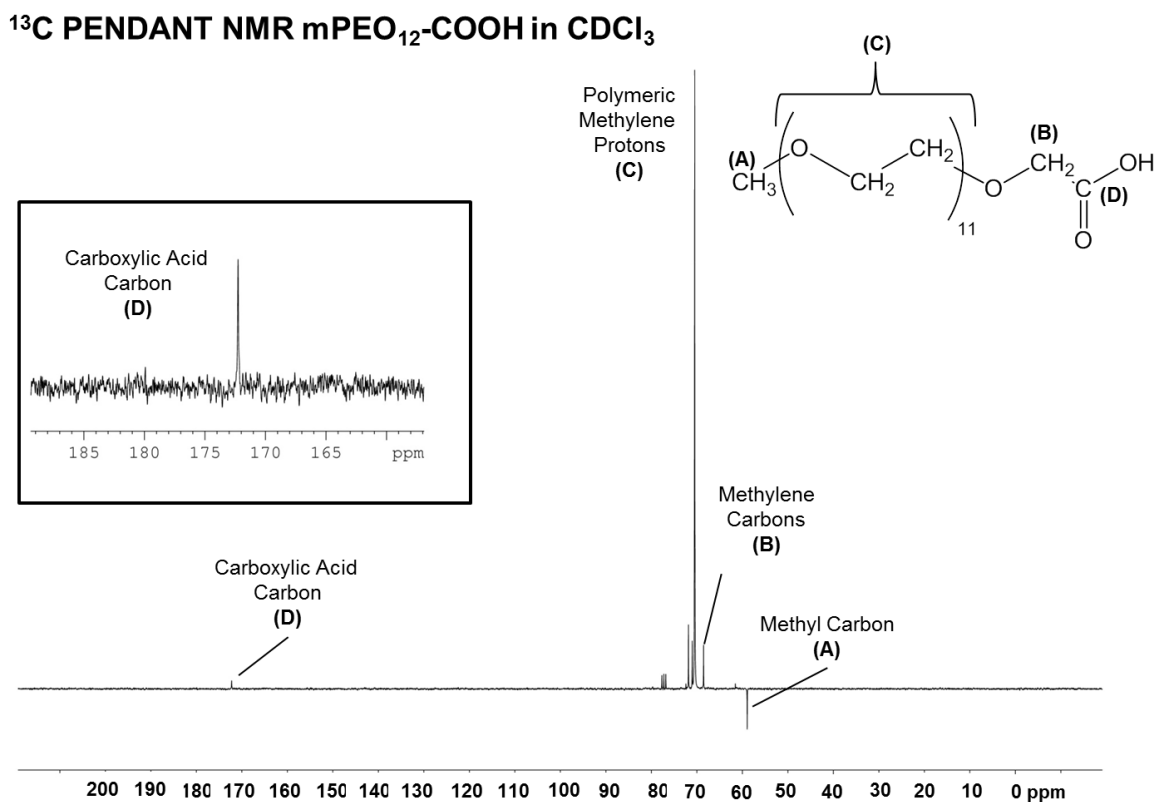


**Figure 3.12:**  $^{13}\text{C}$  PENDANT NMR spectrum of mPEO<sub>12</sub>-COOH, where primary and tertiary carbons are phased downwards and secondary and quaternary carbons are phased upwards.

GPC traces of mPEO<sub>12</sub> are outlined in Figure 3.13. It can be seen that the product displays a moderately narrow peak, at a lower retention time than the progenitor alcohol, indicating, as expected, a small increase in molecular weight. The PDI for the peak is 1.17, and it is noted that the peak for both the product and the parent polymer are unimodal. This is important as it infers that the conversion did not produce any polymer side products or cause degradation of the polymer. Such trends are also observed in the other modified mPEO molecular weights. The small change in molecular weight between the product and the precursor is visible on the GPC trace, however the differences between the two peaks are minimal, as expected.

FTIR analysis showed the presence of a band at 1739 cm<sup>-1</sup>, which is indicative of carbonyl absorption (-C=O) (Band C in Figure 3.14), confirming the presence of the group. Carboxylic acids and their derivatives (such as esters) are typically found at this wavenumber, thus it is not possible to discriminate which functional group is responsible for the peak. As shown by <sup>13</sup>C NMR (Figure 3.12), which confirms the identity of this peak, it is confirmed to originate from the stretching mode of a carboxylic acid group.

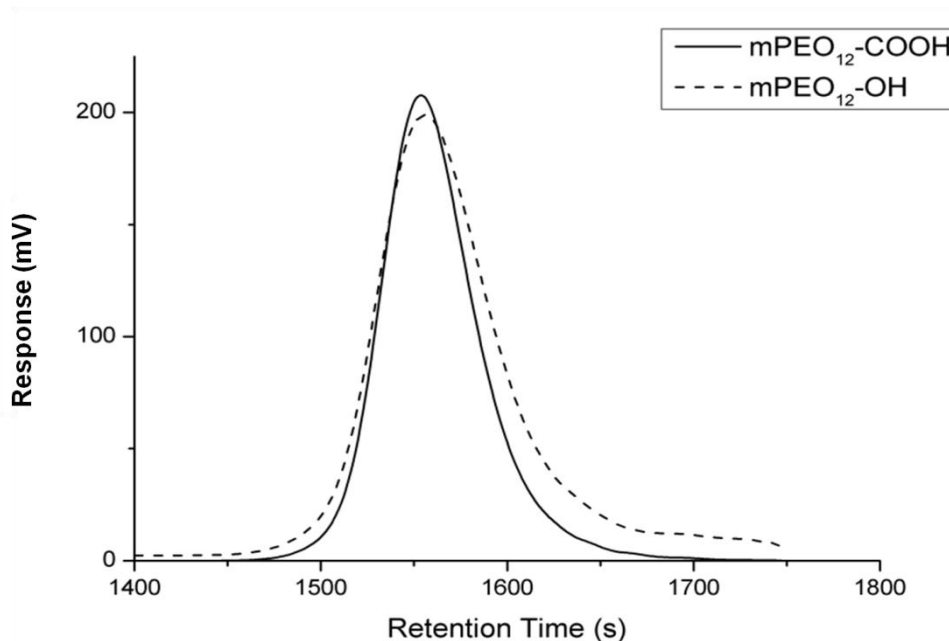


**Figure 3.13:** GPC trace of mPEO<sub>12</sub> and mPEO<sub>12</sub>-COOH.

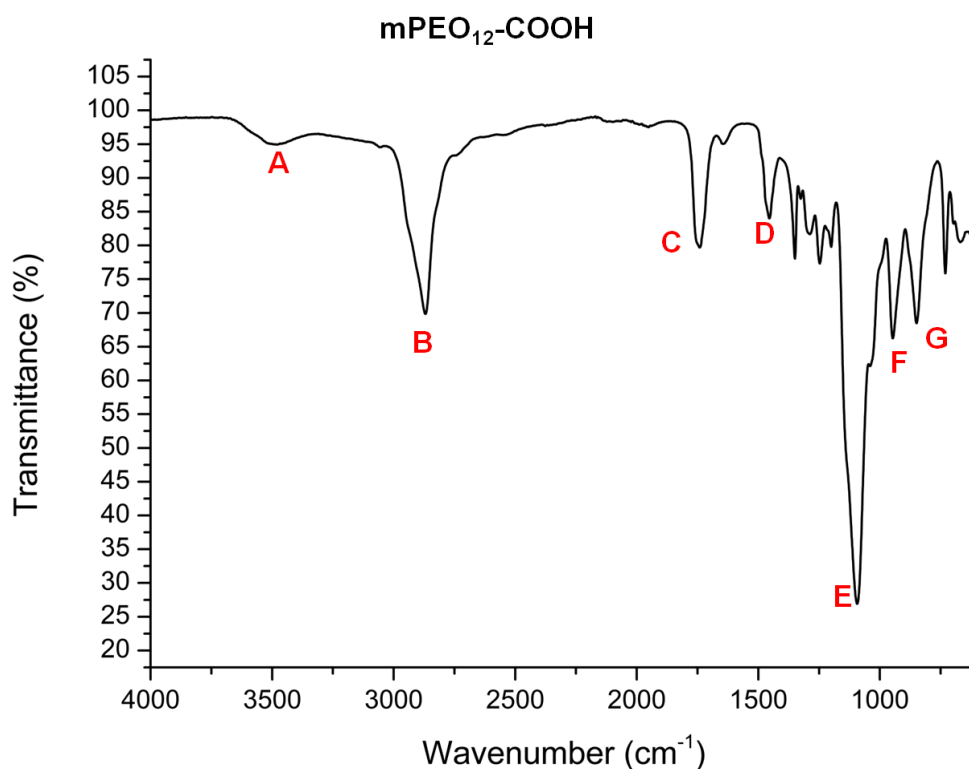


**Figure 3.14:** IR spectrum of mPEO<sub>12</sub>-COOH. For peak assignments see Appendix A.

The combination of NMR, GPC, and FTIR data (Figures 3.11, 3.12, 3.13, and 3.14) confirms that the oxidation product formed is mPEO<sub>12</sub>-COOH.

Yields for the oxidative product are summarised in Table 3.3. Product yields were moderate to high, although it is noted that as chain length increases, there is a slight lowering of the yield. The yields for mPEO<sub>7</sub>-COOH varied from 65% to 89%, which is in agreement with values seen in the literature for Jones-based PEO oxidation<sup>[8]</sup>. This is most likely due to the formation of incomplete oxidation products (aldehyde), which would be subsequently removed during purification, therefore only a proportion of the substrate will have been completely oxidised to an acid (this is true of all the different chain length mPEO). It is also possible that not all of the initial starting material was oxidised at all. As a note of caution, mPEO<sub>n</sub> may contain some chains that are not hydroxyl terminated, although the <sup>1</sup>H NMR spectrum suggests that the material is at least 95% pure.

It has been shown that Jones oxidation is an efficient, reliable way of functionalising monomethoxy-poly(ethylene oxide) with a carboxylic acid group. Whilst simple oxidation is advantageous, the use of chromium (VI) oxide is somewhat problematic due to its inherent health risks. Chromium (VI) oxide is toxic and carcinogenic<sup>[9]</sup>, therefore any residual traces must be thoroughly removed from the reaction mixture after oxidation. This is the reason why propan-2-ol is used during washing. Furthermore, repeated separations were carried out to ensure that the concentration of chromium (VI) oxide was low. It should be noted that chromium (III) oxide, which the (VI) oxide is converted to after complete oxidation, is not carcinogenic and has a low level of toxicity.

**Table 3.3:** Percentage yields of monomethoxy-poly(ethylene oxide).

Polymer	Yield (%)
mPEO <sub>7</sub> -COOH	89
mPEO <sub>12</sub> -COOH	84
mPEO <sub>17</sub> -COOH	78

Additionally, further purification during conjugation with the peptide component will result in further reduction of the level of the toxic oxide present. Although this is a health consideration, the process has advantages over similar oxidative protocols such as dichromate or permanganate oxidation. Dichromate oxidation works in a similar manner to Jones oxidation, however the toxic effects that arise from the (dichromate) oxidation are much more pronounced. Potassium permanganate is highly toxic and also spontaneously combusts on contact with ethylene glycol, of which there may be some residual trace in the polymer starting material.

Alternative synthetic strategies in this area involve converting the alcohol to an even more reactive group than a carboxylic acid, or subsequent conversion of the carboxylic acid to a more reactive group such as an acid chloride. This could be accomplished using PBr<sub>3</sub>, SOCl<sub>2</sub>, or POCl<sub>3</sub>. However, these yield harmful by-products such as HBr or HCl gas. Furthermore, the aforementioned

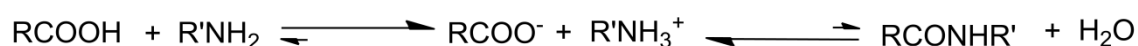
reagents are toxic. Introducing an additional modification step into the process may lower yields, which may not be offset by the increased coupling efficiency in the later stages of the overall PPC synthesis strategy.

### 3.3. Polymer-Peptide Conjugate Synthesis

This section discusses the methods used to produce PPCs reliably, in good yields, and with high purity. A comparison of the coupling methods considered is discussed, with justification for the final method selected. This is followed by analysis of each conjugate synthesised, noting any modifications to the general method, and examining yield, purity, and ease of synthesis.

#### 3.3.1 Polymer-Peptide Conjugate Coupling Methods

The aim of the work reported in Section 3.1 was to produce well-defined monofunctional oligopeptides, with an exposed amine terminus. This was achieved and three oligopeptides were synthesised, thus producing four phenylalanine homologues for use in coupling [i.e. F<sub>1</sub> (used as received), F<sub>2</sub>, F<sub>3</sub>, and F<sub>4</sub>]. Although F<sub>5</sub> was produced in Section 3.1, its incompatibility with the reaction environment prevented it being used for coupling. Section 3.2 details a method for polymer modification via Jones oxidation. The polymer was functionalised with a carboxylic acid group in lieu of a hydroxyl group. Therefore, it is now possible to directly couple these compounds together to form a conjugate through the formation of an amide bond. Such a formation is hindered by the establishment of the acid-base reaction that takes place on mixing an amine [NH<sub>2</sub>-F<sub>(x+y)</sub>-OEt] with a carboxylic acid (mPEO<sub>n</sub>-COOH). The equilibrium for the reaction lies towards salt formation and not synthesis of the final product<sup>[10]</sup> (Scheme 3.3).

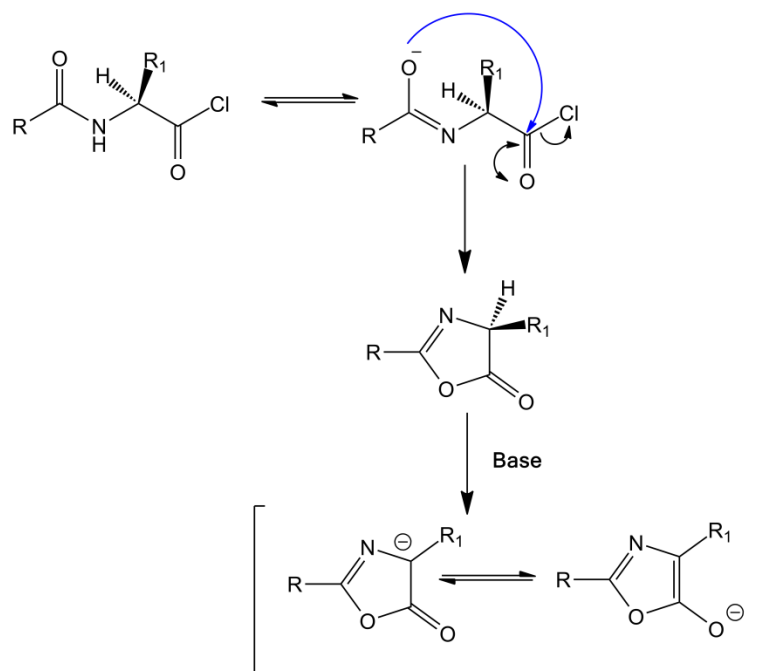


**Scheme 3.3:** General amide bond formation, where it is shown that salt formation is favoured.

In this instance it would be necessary to heat to high temperatures to facilitate coupling, and shift the equilibrium to the right to avoid formation of a salt (i.e.  $\text{RCOO}^- \cdot \text{RNH}_3^+$ ). However, many materials are incompatible with high temperatures, and this is especially true for peptides. High temperature can lead to racemisation (conversion of the peptide into its chiral counterpart, i.e. L-isomer to D-isomer leading to a mixture in the final product) of the peptide resulting in the formation of by-products. To overcome this problem it is necessary to first activate the acid, and then allow aminolysis (splitting the carboxylic acid into two parts on reaction with an amine) to occur. This was achieved by using an activating group in the form of a coupling agent.

Esterification, whilst easier in terms of thermodynamics, was not considered a viable route in this instance, due to the greater number of steps required to deprotect the carboxylic acid terminus of the peptide (Section 3.4). Future work may include this method to produce PPCs which “face” in the opposite direction (see Section 3.6). Pre-coupling modification of the reactive end of either reagent, such as introducing clickable groups (for example azide and alkyne groups, or thiol and maleimide), also has the side-effect of incorporating an additional group which may affect the properties of the final conjugate (discussed in Chapter 4).

Three protocols were chosen for a coupling investigation (Sections 3.3.1.1, 3.3.1.2, and 3.3.1.3, respectively). These were DCC, IBCF, and PyBOP coupling. The reasons for these particular choices were to ensure compatibility with the functional groups, and because it was not necessary to further modify or activate the carboxylic acid as this occurs *in situ* (i.e. they are one-step coupling reactions). This is important as it lowers the numbers of required steps for the overall reaction. Additionally, direct amide bond formation without the presence of a coupling agent can lead to racemisation (Scheme 3.4), which is also a noted problem during conventional peptide synthesis (both in solid and solution phase syntheses).



**Scheme 3.4:** Racemisation during amide bond formation via oxalzone formation<sup>[11]</sup>.

### 3.3.1.1. *N,N'*-Dicyclohexylcarbodiimide-mediated polymer-peptide conjugate synthesis

DCC was considered as a coupling reagent to combine  $m\text{PEO}_n\text{-COOH}$  and homologous phenylalanine oligopeptides. This is one of most commonly used methods for peptide synthesis. Coupling was attempted using a modified peptide conjugation protocol. Yields for DCC coupling between  $m\text{PEO}_n\text{-COOH}$  (where  $n = 7$  and  $12$ ) and phenylalanine oligopeptides are shown in Table 3.4. It can be seen that the general trend for conjugate yield decreases as the peptide length increases; initial yields were moderate but then dropped sharply.

**Table 3.4:** Yields obtained for the synthesis of polymer-peptide conjugates using *N,N'*-dicyclohexylcarbodiimide coupling.

Conjugate	Yield (%)	Conjugate	Yield (%)
$\text{PEO}_7\text{-F}_1\text{-OEt}$	52	$\text{PEO}_{12}\text{-F}_1\text{-OEt}$	33
$\text{PEO}_7\text{-F}_2\text{-OEt}$	45	$\text{PEO}_{12}\text{-F}_2\text{-OEt}$	54
$\text{PEO}_7\text{-F}_3\text{-OEt}$	30	$\text{PEO}_{12}\text{-F}_3\text{-OEt}$	42
$\text{PEO}_7\text{-F}_4\text{-OEt}$	30	$\text{PEO}_{12}\text{-F}_4\text{-OEt}$	61

After purification of the obtained product, GPC analysis was undertaken on the compound. It can be seen in the GPC trace for the exemplar  $F_3$  conjugate (Figure 3.15) that there is a moderate amount of additional material present in the final conjugate. Part of this can be attributed to unreacted starting material, and excess by-product formation (DHU). As aforementioned, some racemisation may have occurred. Indeed, additives (such as HOBt and HOAt) are regularly used to minimise racemisation, however this adds further purification steps, resulting in decreased yields. Additionally, this also adds another potential impurity to the final conjugate. Thus, the yields reported are for material where the purity varies from 50 to 80%.

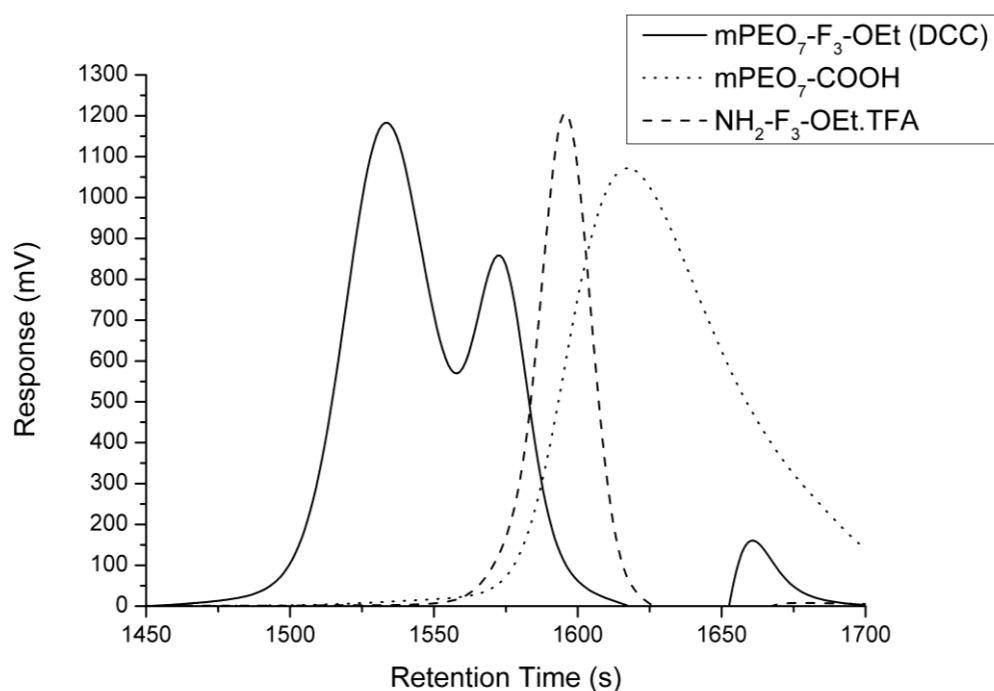


**Figure 3.15:** GPC trace of mPEO<sub>7</sub>-F<sub>3</sub>-OEt (produced using DCC coupling) and precursor reagents.

It was noted that the conjugates were not all white solids; a yellow solid for PEO<sub>7</sub>-F<sub>3</sub>-OEt, and a pale yellow solid for PEO<sub>7</sub>-F<sub>4</sub>-OEt were observed. The desired colour of the conjugates should be white, therefore, despite repeated washes, the conjugate remained impure. Reprecipitation of the product from THF in excess diethyl ether reduced, but did not eliminate, the amount of impurity. The GPC traces in Figure 3.15 show that the impurity peak correlates

to that of the starting peptide ( $F_3$ ). Peptide removal is made somewhat difficult by their propensity to form intermolecular hydrogen bonds, and to the conjugate. Interestingly, reprecipitation of the  $F_4$ -based conjugate generated a product that was reasonably pure (Figure 3.16). The peak is mostly unimodal, and symmetrical, indicating that unwanted materials were not present in the conjugate.

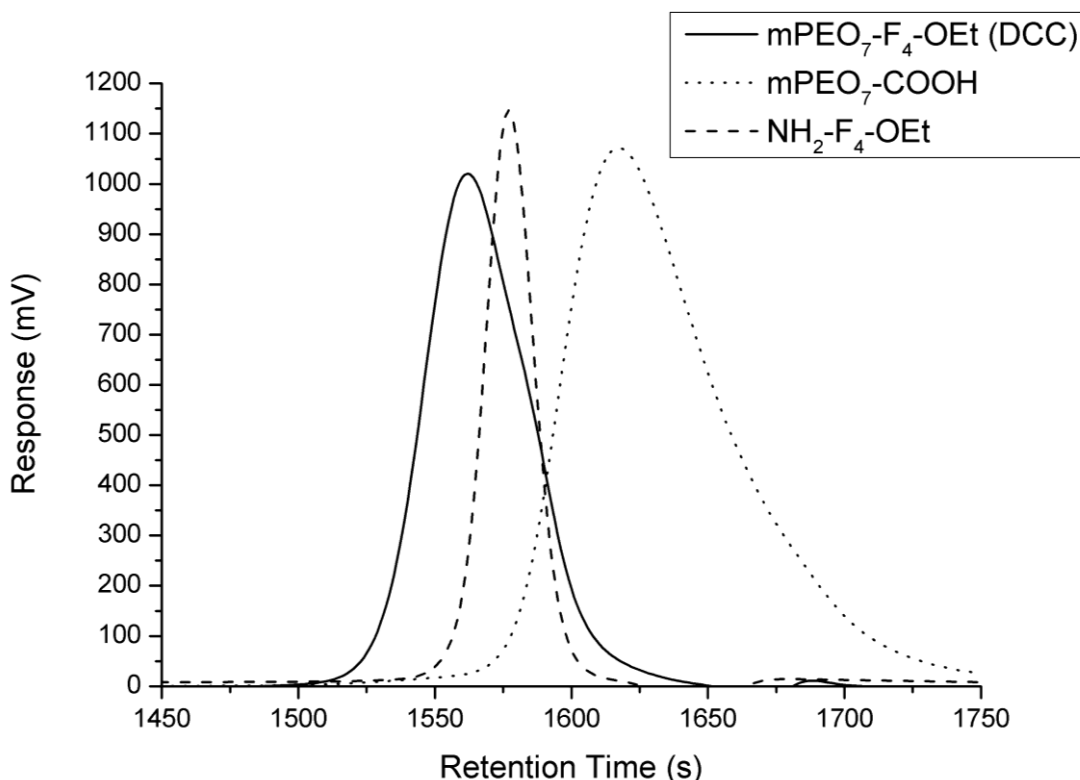


**Figure 3.16:** GPC trace of mPEO<sub>7</sub>-F<sub>4</sub>-OEt (produced using DCC coupling) and precursor reagents.

One of the main by-products of DCC coupling is dicyclohexylurea, which is sparingly soluble in chloroform and thus may not precipitate out completely, making separation from the product difficult. This further accounts for the impurities present, and makes the process undesirable.

In summary, DCC coupling produces conjugates in low-to-moderate yields, with varying purity. The difficulties encountered in removing by-products and unreacted starting materials had an impact on the yield and an additional set of

purification steps. Therefore, the use of DCC to produce polymer-peptide conjugates was not deemed a viable option.

### 3.3.1.2. *Isobutylchloroformate-mediated polymer-peptide conjugate synthesis*

IBCF was used previously as the preferred coupling method to synthesise phenylalanine oligopeptides; therefore it is known to be compatible with at least one of the starting reagents. This is not to say that the other coupling methods are incompatible with the reagent, more so that the compatibility of IBCF with phenylalanine has already been demonstrated and coupling has been successful. The caveat is that the coupling was only successful between identical phenylalanine molecules and not phenylalanine with another species (i.e. a non-amino acid species). Yields for IBCF coupling between  $m\text{PEO}_n\text{-COOH}$  ( $n = 7$  and  $12$ ) and phenylalanine oligopeptides are shown in Table 3.5. With the exception of increasing from  $F_1$  to  $F_2$ , the general trend is the same as DCC coupling; as peptide length increases, yields decrease. However, the yields for the synthesised products were significantly higher than the other coupling methods.

**Table 3.5:** Yields of polymer-peptide conjugates using isobutylchloroformate coupling.

Conjugate	Yield (%)	Conjugate	Yield (%)
PEO <sub>7</sub> -F <sub>1</sub> -OEt	85	PEO <sub>12</sub> -F <sub>1</sub> -OEt	79
PEO <sub>7</sub> -F <sub>2</sub> -OEt	91	PEO <sub>12</sub> -F <sub>2</sub> -OEt	90
PEO <sub>7</sub> -F <sub>3</sub> -OEt	83	PEO <sub>12</sub> -F <sub>3</sub> -OEt	86
PEO <sub>7</sub> -F <sub>4</sub> -OEt	77	PEO <sub>12</sub> -F <sub>4</sub> -OEt	90

Unlike DCC coupling, there is no visible by-product formed to confirm the success of the reaction. The reaction was left to stir overnight to ensure completion. Purification procedures involved simple washings, and then solvent removal under reduced pressure. Occasionally, a product would form with a residual yellow colour, which originates from unreacted IBCF. This was removed by rewashing the product, or reprecipitation into petroleum ether.

Generally, the conjugates produced were either clear liquids (F<sub>1</sub> and F<sub>2</sub>-based) or white solids (F<sub>3</sub> and F<sub>4</sub>-based).

Overall, IBCF coupling produced well-defined conjugates in good yields, with a simple synthesis and easy purification. It was for these reasons that IBCF was investigated further as a coupling technique.

### 3.3.1.3. *Benzotriazol-1-yl-oxytripyrrolidinophosphonium hexafluorophosphate-mediated polymer-peptide conjugate synthesis*

PyBOP coupling is conventionally used for solid-phase peptide synthesis (SPPS)<sup>[2]</sup>, and not often used in solution. However, the mildness of the reaction conditions, high yields, and fast reaction times, make it an attractive protocol for coupling. The reaction was attempted on mPEO<sub>7</sub> and F<sub>1</sub> as an initial test, as they were deemed the easiest to analyse. After the coupling reaction, a white powder formed. This was analysed by <sup>1</sup>H NMR, shown in Figure 3.17. It can be seen that no “hallmark” peaks are visible to indicate that coupling was a success, and that neither of the progenitor species can be easily identified from the spectrum. This indicated that the product synthesised was not a PPC, and therefore coupling was unsuccessful. It can be speculated that the material formed was a mixture of starting reagents and incomplete products.

The reaction did not yield a discernible product. It can be speculated that the reaction failed to work, as it is optimised for peptide-peptide coupling and not polymer-peptide ligation. Furthermore, the attachment of the benzotriazole to the activated carboxylic acid, may encounter difficulties due to steric effects. The procedure was repeated with longer peptide sequences, however the results were the same.

For these reasons, PyBOP coupling was not pursued as a viable coupling technique. However, the technique is worth investigating for use in a solid phase approach, where the polymer can be pre-bound to the resin, and the peptide added sequentially using a protecting group strategy.

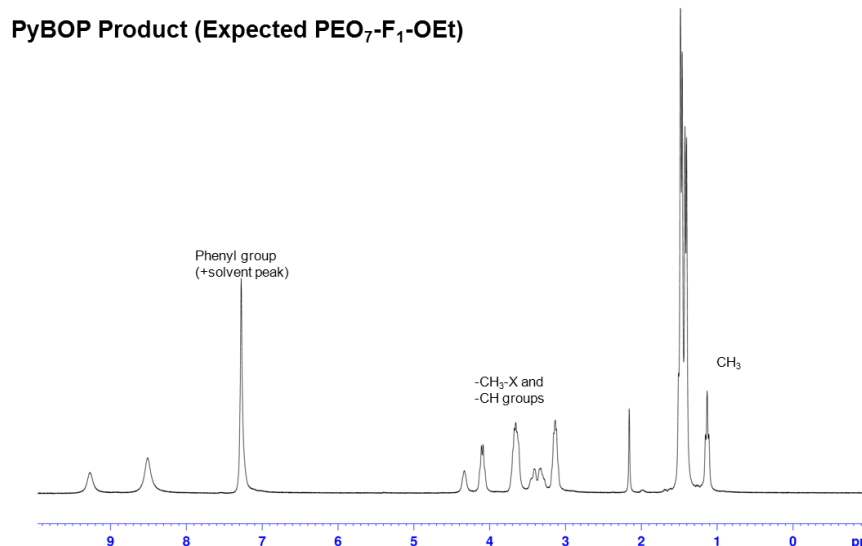


**Figure 3.17:** <sup>1</sup>H NMR of PyBOP product. The product was expected to be mPEO<sub>7</sub>-F<sub>1</sub>-OEt.

#### 3.3.1.4. Summary of polymer-peptide conjugate coupling methods

Three coupling techniques were investigated for the production of polymer-peptide conjugates. The ease of purification is important especially for industrial and commercial viability, and also for the environmental impact of the synthesis. PyBOP coupling did not produce any conjugates, whilst DCC coupling produced conjugates with moderate purity. By contrast, IBCF coupling formed conjugates in high yields, with good purity. Therefore, IBCF coupling was chosen as the preferred method to produce polymer-peptide conjugates.

#### 3.3.2. Synthesis of polymer-peptide conjugates using isobutylchloroformate coupling

A methodical approach was undertaken to produce well-defined polymer-peptide conjugates from phenylalanine and mPEO. The following section is divided by mPEO chain length, and then subdivided by oligopeptide length. Each section discusses the individual aspects of each synthesis and notes where deviation from the standard method was required. NMR, GPC and IR was performed on all conjugates. Note that as the amide peak is concentration dependent, it may not be visible on the <sup>1</sup>H NMR spectrum.

### 3.3.2.1. *Synthesis of mPEO<sub>7</sub> conjugates*

mPEO<sub>7</sub>-based conjugates were the smallest conjugates produced, and provided a template for all successive conjugation reactions.

#### 3.3.2.1.1. *Synthesis of mPEO<sub>7</sub>-F<sub>1</sub>-OEt*

Of all the conjugates, mPEO<sub>7</sub>-F<sub>1</sub>-OEt was the most straightforward to synthesise, as the peptide component did not require synthesis, and could be used as received, with no additional purification required. The conjugate produced is a clear, highly viscous liquid that can have a yellow tinge if certain impurities are present. This provides a good visual indicator of the purity of the product. Interestingly, synthesis of the product resulted in a slight shoulder appearing on the GPC (Figure 3.18), indicative of unreacted peptide, which was removed by further aqueous and acid/base washes. GPC analysis shows a clear increase in the molecular weight of the product compared to the starting material. It can be seen that the final peak is generally unimodal. However, a non-unimodal trace can be produced as it is possible for a small amount of peptide to remain, or because the (low molecular weight) conjugate has a retention time that is similar to the stabilisers present in the eluent.

Although purification was generally facile (consisting primarily of washing the product), dialysis, which is a particularly robust purification technique, could not be used on this conjugate. Dialysis is a highly effective purification technique that separates molecules based on size (linked to molecular weight). The free peptide can be problematic to remove (due to intermolecular hydrogen bonding), therefore making dialysis a practical solution to ensure purity. However in this instance, the molecular weight of the conjugate is not dissimilar enough from that of the peptide to make dialysis a useful purification technique. Other simple purification techniques, such as reprecipitation, also cannot be used. Column chromatography was also considered as a purification technique, however, chromatography is laborious, and difficult to carry out under industrial conditions.

Whilst these limitations are not significant, they highlight a lack of additional simple purification techniques (to be used alongside the washes) available for lower molecular weight (liquid or semi-solid) conjugates. Figures 3.19 and 3.20 show the  $^1\text{H}$  and  $^{13}\text{C}$  PENDANT NMR spectra of the conjugate, respectively, and Figure 3.21 shows the IR spectrum. The peaks on the  $^1\text{H}$  NMR spectrum are well-defined, and the multiplicity clearly visible. On the  $^{13}\text{C}$  spectrum,  $\text{CH}_3$  and  $\text{CH}$  carbons are phased downwards, and  $\text{CH}_2$  and quaternary carbons are phased upwards.

Analysis by  $^1\text{H}$  NMR shows that the integral ratios are close to the expected values. The signal at 1.2 ppm (Peak A), has an integral ratio of 2.7, i.e. 3 protons. This was taken relative to the integral of Peak C (3.37 ppm), which was calibrated to three protons for all conjugates. The integral of the polymer protons was 26, which was slightly higher than the expected amount (24), but is due to the accuracy of the NMR technique at this resolution, and the broadness of the peak(s). The protons represented by peaks C, D, and E all arise from the polymer component. Therefore, they remain constant as the peptide length increases and provide a reference for integration. Peak A should also have a constant integral (three protons), and is also used to provide a reference.

Aromatic protons for  $\text{mPEO}_7\text{-F}_1\text{-OEt}$  should be present at approximately 7.4 ppm, with an integral of 5 protons, represented by two broad multiplet peaks. The broader peak represents ortho- and meta- protons (four protons) whilst the other (more narrow) peak represents the para- proton (one proton). This is shown by Peak H on the  $^1\text{H}$  spectrum (Figure 3.19), which has an integration of 5.3 protons. As before, this is slightly greater than expected, although the solvent peak is present in the same region, thus distorting the result. The integrals for each peak are, **A:** 2.7, **B:** 1.7, **C:** 3, **D:** 26, **E:** 1.6, **F:** 2.1, **G:** 0.9, **H:** 5.3 protons. This shows that the desired product has been synthesised to a high degree of purity. Additionally, Peak J on the  $^{13}\text{C}$  NMR spectrum in Figure 3.20 is representative of an amide carbon, further indication that the coupling was a success.

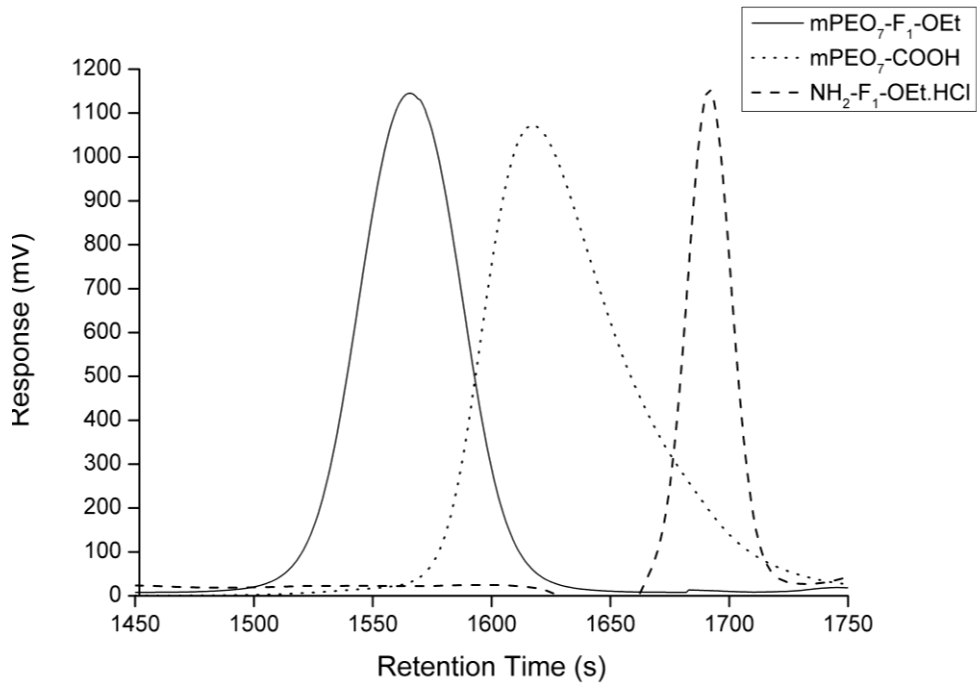


**Figure 3.18:** GPC traces of a polymer-peptide conjugate (mPEO<sub>7</sub>-F<sub>1</sub>-OEt) and the precursor reagents.

**<sup>1</sup>H NMR mPEO<sub>7</sub>-F<sub>1</sub>-OEt in CDCl<sub>3</sub>**

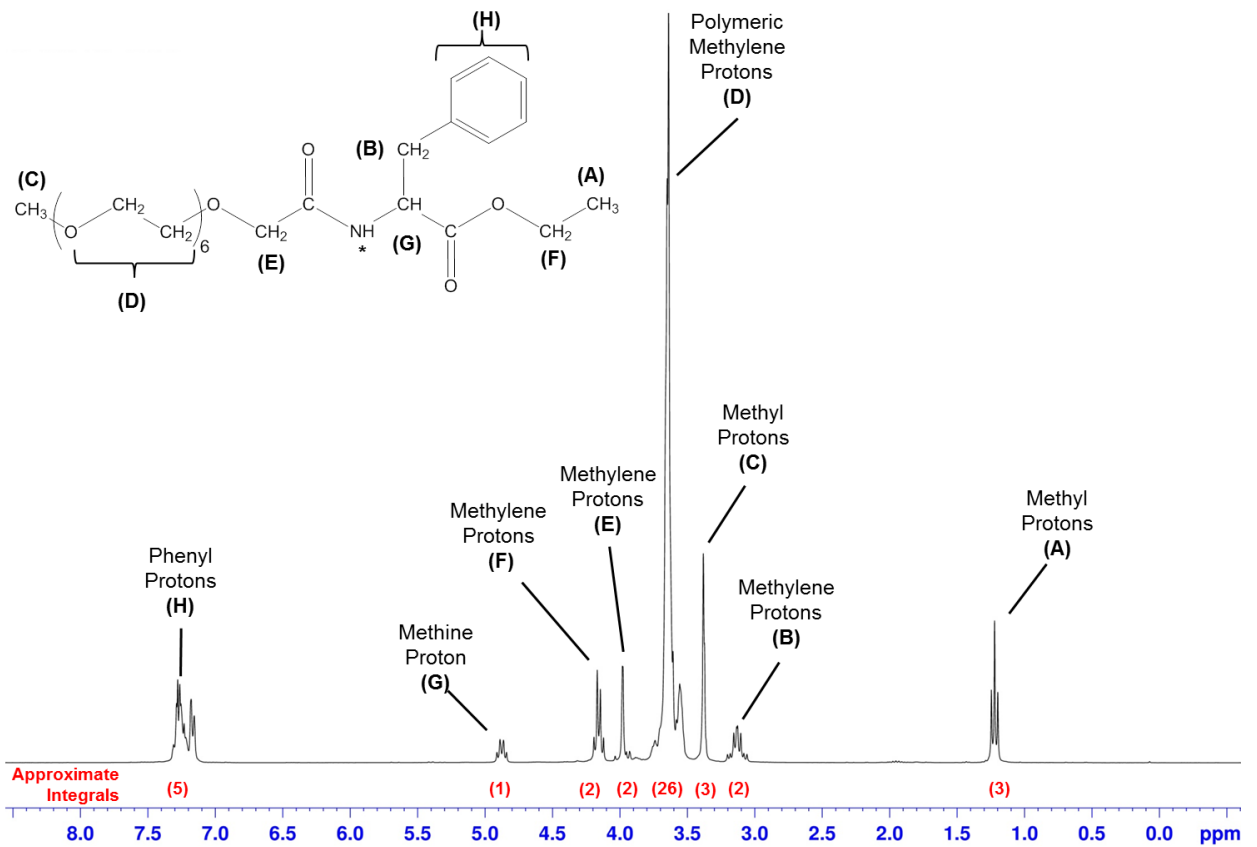


**Figure 3.19:** <sup>1</sup>H NMR spectrum of mPEO<sub>7</sub>-F<sub>1</sub>-OEt.

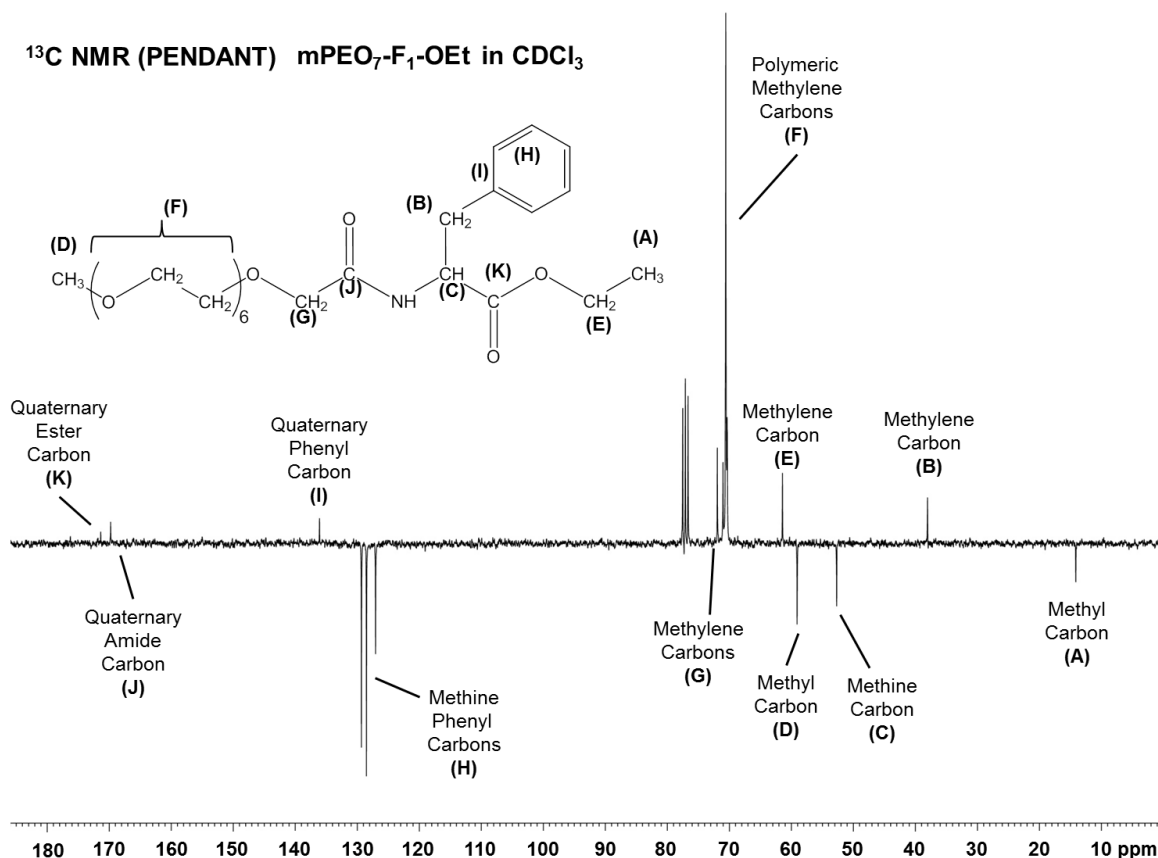


**Figure 3.20:** <sup>13</sup>C PENDANT NMR spectrum of mPEO<sub>7</sub>-F<sub>1</sub>-OEt.

The bands in the IR spectra (Figures 3.21, 3.22, and 3.23) of the conjugate show the presence of a secondary amide bond (R-CONHR') at 1666 and 1637 cm<sup>-1</sup>. These strong peaks are indicative of carbonyl and N-H stretching, respectively, from an amide bond [-C(=O)-N]. Stretching of -C-O ether bonds at 1100 and 1030 cm<sup>-1</sup> confirms the presence of mPEO<sub>7</sub> in the conjugate. Finally, the peaks at 1550 and 746 cm<sup>-1</sup> are aromatic C-H bands, confirming the presence of the phenyl ring and therefore phenylalanine. Alongside the other analytical data this confirms that coupling has been successful. It can be seen that the IR spectrum of the conjugate is a combination of the spectra of the materials used as starting reagents. The most important distinction in the spectra is the amide bands which are only present in the conjugate (1666 cm<sup>-1</sup>, Band E in the conjugate spectra). However, the longer peptides already contain this bond (formed during peptide synthesis), and therefore, in this instance, these signals cannot be used as an absolute confirmation that the coupling was successful.

Overall, the coupling reaction was straightforward and produced a well-defined conjugate. Yields for the reaction were moderate to high, ranging from 55-85 %. The successful synthesis of the conjugate was then used as a template for the manufacturing of the other conjugates in the series.

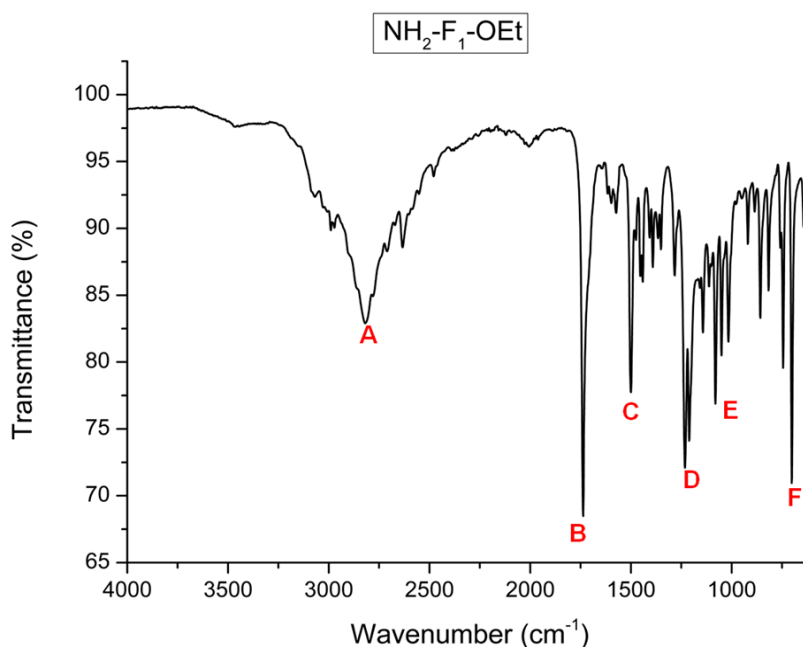


**Figure 3.21:** IR spectrum of  $\text{NH}_2\text{-F}_1\text{-OEt}$ . For peak assignment see Appendix A.

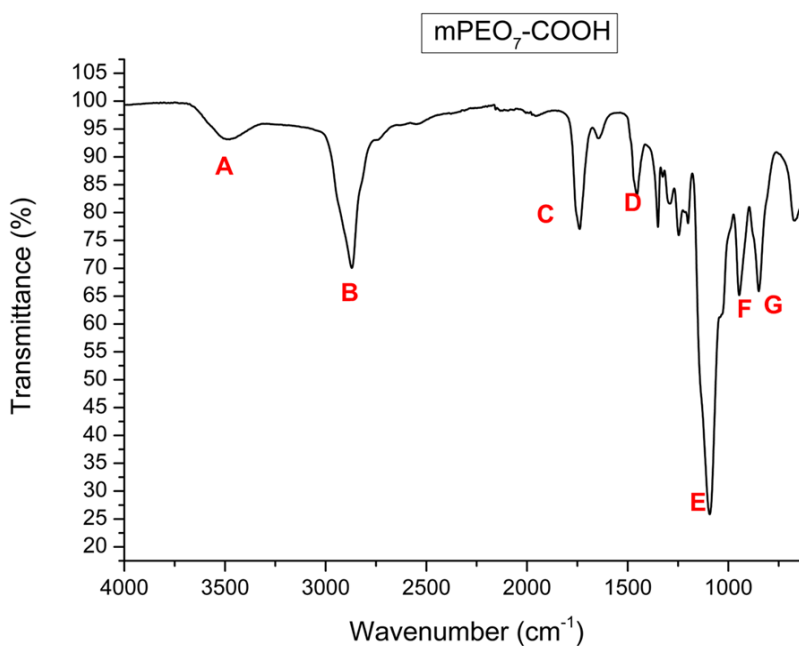


**Figure 3.22:** IR spectrum of  $\text{mPEO}_7\text{-COOH}$ . For peak assignment see Appendix A.

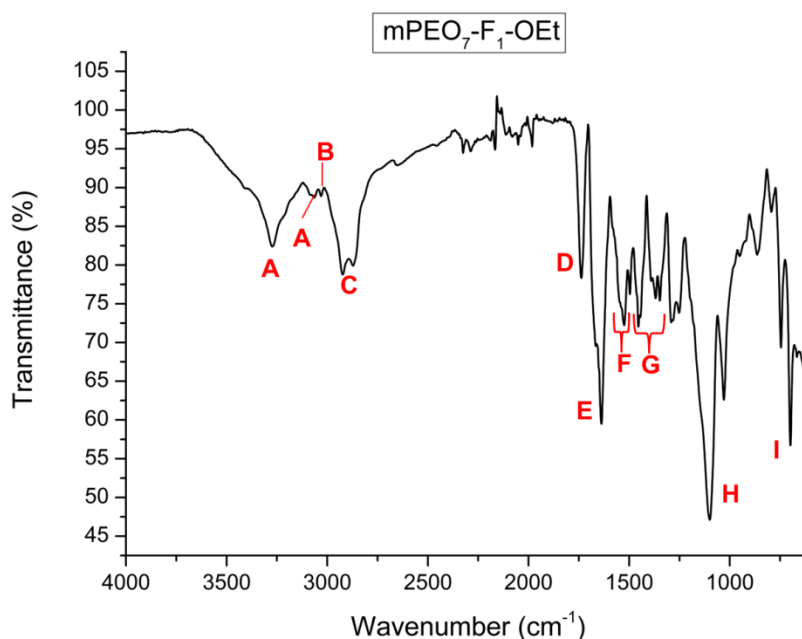


**Figure 3.23:** IR spectrum of mPEO<sub>7</sub>-F<sub>1</sub>-OEt. For peak assignment see Appendix A.

### 3.3.2.1.2. Synthesis of mPEO<sub>7</sub>-F<sub>2</sub>-OEt

The difference in molecular weight between mPEO<sub>7</sub>-F<sub>1</sub>-OEt and mPEO<sub>7</sub>-F<sub>2</sub>-OEt is very small, but it leads to an interesting change in observable physical properties. This is the first conjugate produced using a synthesised oligopeptide (F<sub>2</sub>), and as such the purity of the peptide component (as well as the polymer component) will be reflected in the conjugate. After coupling, the resulting product is initially, similar to mPEO<sub>7</sub>-F<sub>1</sub>-OEt, a clear, highly viscous liquid. However, after standing at room temperature and standard atmospheric pressure, the conjugate formed a clear semi-solid material, with a similar consistency to candle wax, although it still contained some liquid regions. Conjugation followed the protocol described in Chapter 2 with no modifications required. The increased molecular weight of the conjugate with respect to mPEO<sub>7</sub>-F<sub>1</sub>-OEt is obviously associated to the increase of the weight of the peptide.

As noted from GPC analysis (Figure 3.24), there was no free peptide associated with the conjugate. The peak is unimodal, with a slightly broad

character; this is due to the molecular weight distribution of the polymer-component as it is still the dominant factor of the material. As can be seen, the GPC peak for mPEO<sub>7</sub> is somewhat broad, which is reflected in the peak of the conjugate.

The <sup>1</sup>H NMR spectrum (Figure 3.25) shows that the peaks remain generally well-defined, and that multiplicity is still visible. Certain peaks, such as Peak B and Peak G have noticeably multiplet character, as the functional groups they represent (CH<sub>2</sub>-Ph and CH-CO) are part of the peptide backbone, and each amino acid is in a slightly different chemical environment. The integrals again are close to expected. Notably, the integral for the polymer peak is 24 protons. However, due to the increased length of the peptide, the integral for the methine protons (Peak G) is now 2 (which has doubled in comparison to Figure 3.19). The integral of Peak H, representative of the phenyl protons, has also increased compared to mPEO<sub>7</sub>-F<sub>1</sub>-OEt, increasing from approximately five to ten protons. It should be noted that the quaternary ester peak (Peak K) in the <sup>13</sup>C PENDANT NMR spectrum, is more difficult to see, due to the relative increase in intensity of the quaternary carbon amide peak (Peak J) (Figure 3.26) In addition to the increase of the amide peak, the phenyl peaks have also increased in relative intensity. The IR spectrum of mPEO<sub>7</sub>-F<sub>2</sub>-OEt (Figure 3.27) has very similar bands to that of mPEO<sub>7</sub>-F<sub>1</sub>-OEt, therefore confirming that coupling was successful. Of particular interest are certain bands, which are identical to the spectrum of mPEO<sub>7</sub>-F<sub>1</sub>-OEt. These include the band at 1454 cm<sup>-1</sup> (Band G) and the bands representing the (-C-O) ether and ester stretching (1030 and 1100 cm<sup>-1</sup>, Band H). The amide bond peak has also shifted very slightly from 1637 cm<sup>-1</sup> in mPEO<sub>7</sub>-F<sub>1</sub>-OEt to 1642 cm<sup>-1</sup> (Band E) in the mPEO<sub>7</sub>-F<sub>2</sub>-OEt.

Similar to mPEO<sub>7</sub>-F<sub>1</sub>-OEt, this coupling reaction was extremely straightforward and produced a well-defined conjugate. Yields for the reaction were high ranging from 77-91 %.

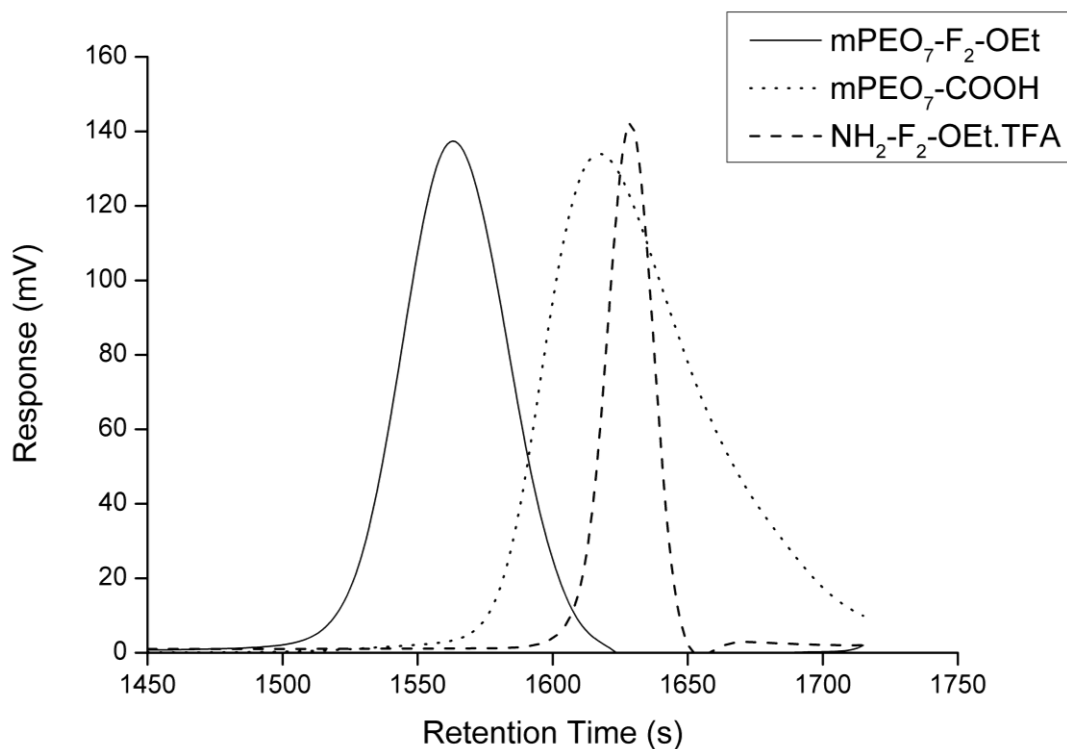


Figure 3.24: GPC traces showing mPEO<sub>7</sub>-F<sub>2</sub>-OEt and the precursor reagents.

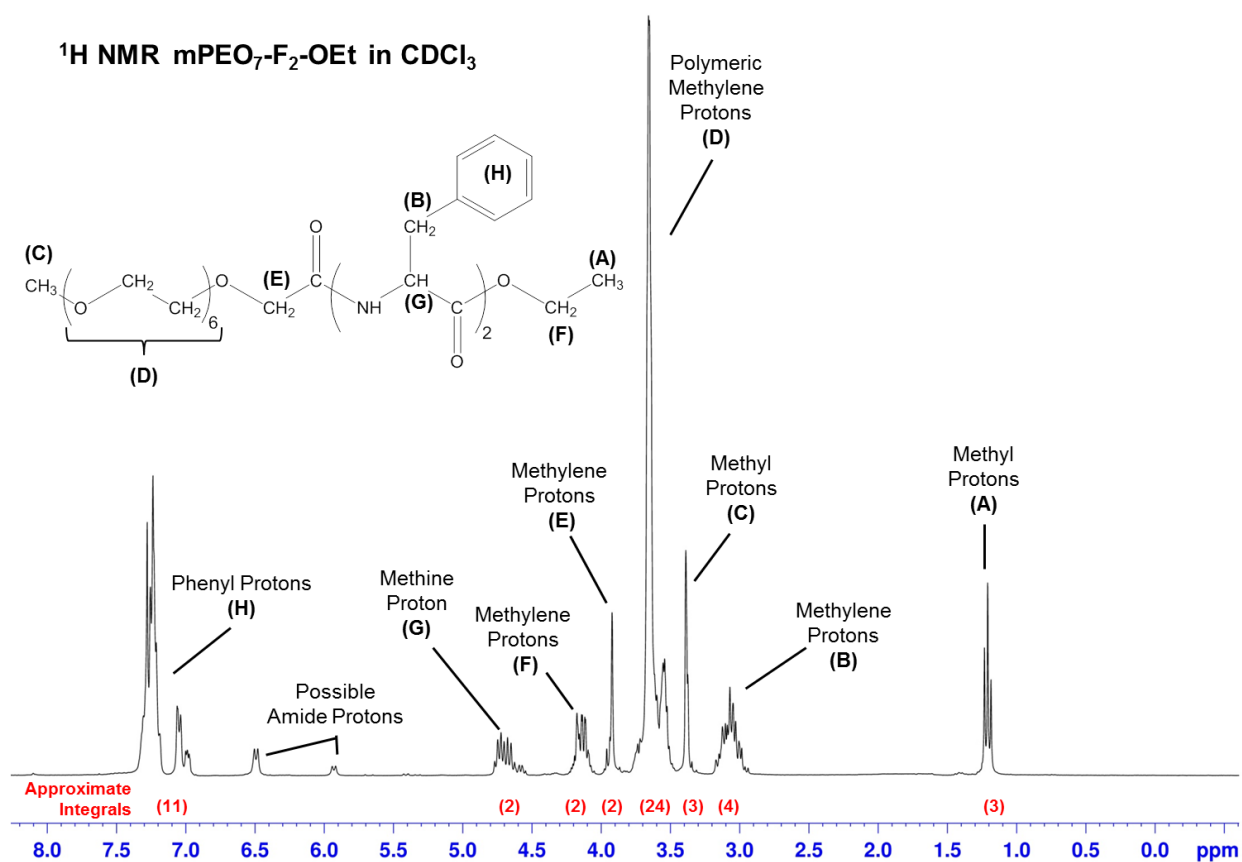
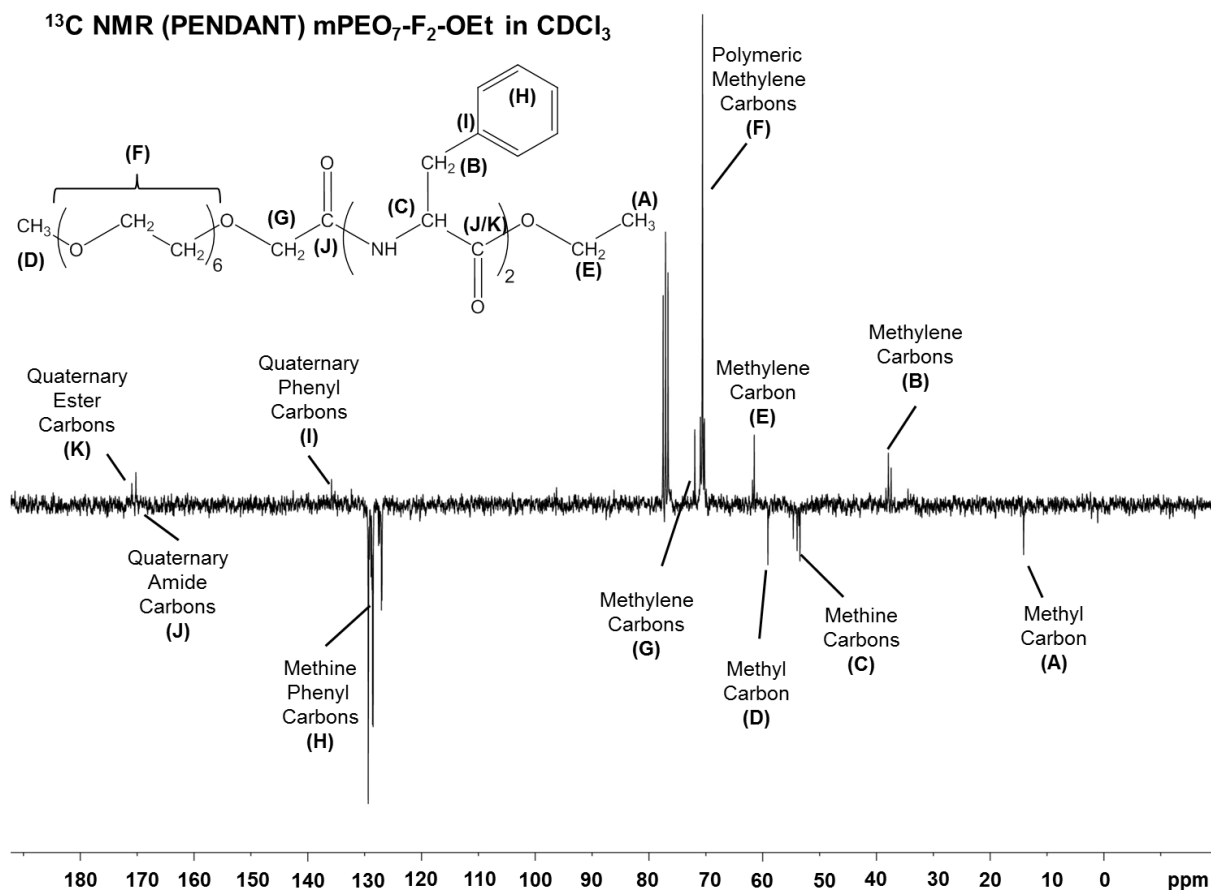
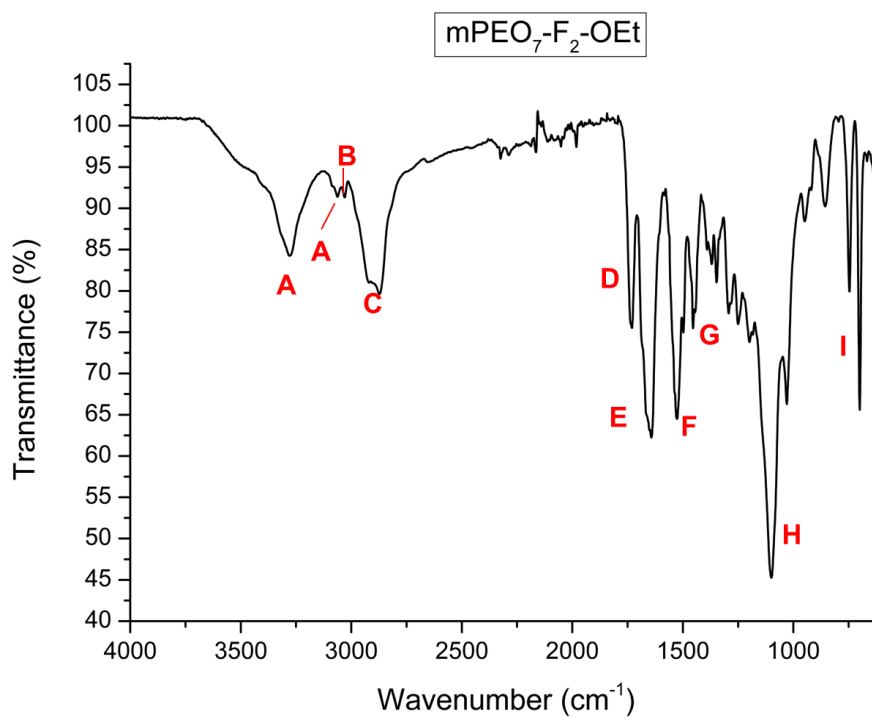


Figure 3.25: <sup>1</sup>H NMR spectrum of mPEO<sub>7</sub>-F<sub>2</sub>-OEt.



**Figure 3.26:**  $^{13}\text{C}$  PENDANT NMR spectrum of mPEO<sub>7</sub>-F<sub>2</sub>-OEt.



**Figure 3.27:** IR spectrum of mPEO<sub>7</sub>-F<sub>2</sub>-OEt. For peak assignment see Appendix A.

### 3.3.2.1.3. Synthesis of mPEO<sub>7</sub>-F<sub>3</sub>-OEt

Of all the synthesised mPEO<sub>7</sub>-derived conjugates, mPEO<sub>7</sub>-F<sub>3</sub>-OEt was perhaps the most difficult to purify, even though the initial synthesis remained straightforward. The increase in molecular weight resulted in the product being a white semi-solid. Conjugation again followed the protocol detailed in Chapter 2, however, additional purification steps were required. After the synthesis and subsequent washes, the product was analysed by GPC to determine purity (Figure 3.28). The GPC trace showed that there was a higher molecular weight bimodal peak, demonstrating that the conjugate was impure. Factoring in the relative positions of the other peaks, it was determined that impurity was mostly linked to free peptide and association of the starting polymer. There was also a residual yellow colour originating from the IBCF reaction.

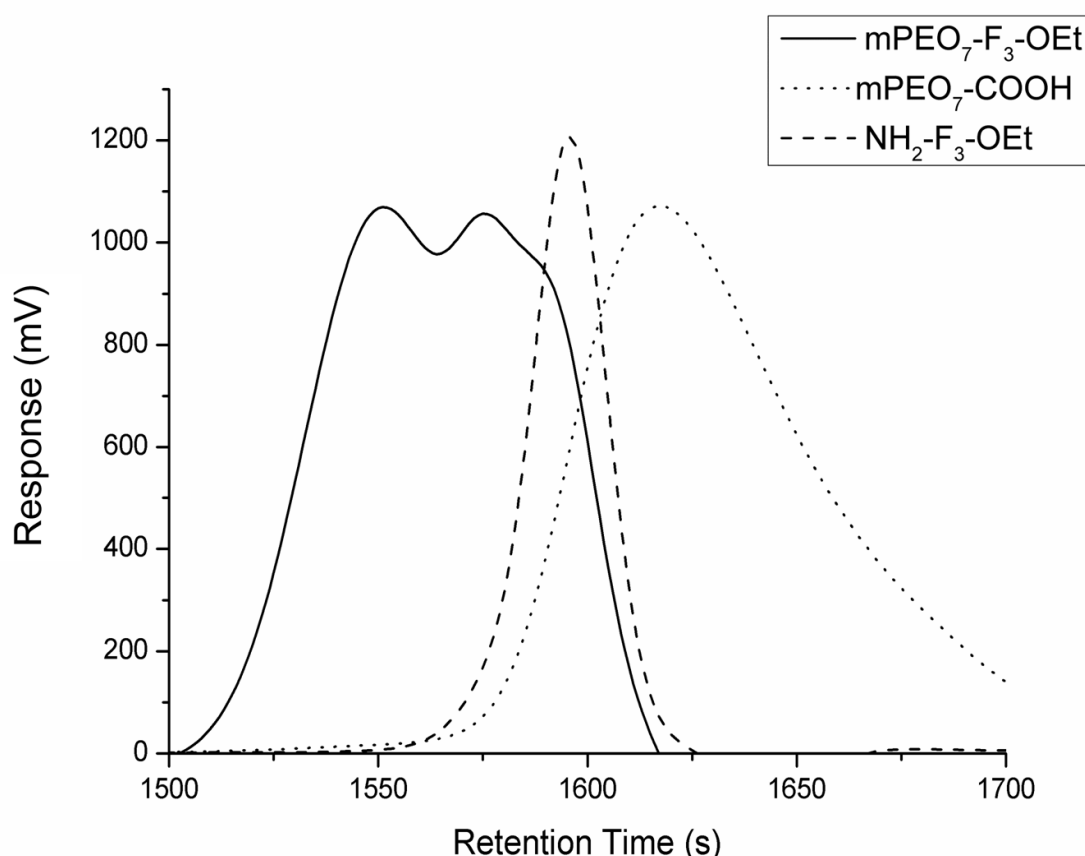


**Figure 3.28:** GPC traces showing an impure polymer-peptide conjugate (mPEO<sub>7</sub>-F<sub>3</sub>-OEt) and the precursor reagents.

The product underwent additional aqueous and acid/base washes to remove the free peptide. Subsequent GPC analysis revealed (Figure 3.29) a narrow peak, alongside a smaller secondary peak. This indicating that the produced material was not pure and likely contained uncoupled mPEO (as the tail visible in the GPC overlaps with the mPEO peak).

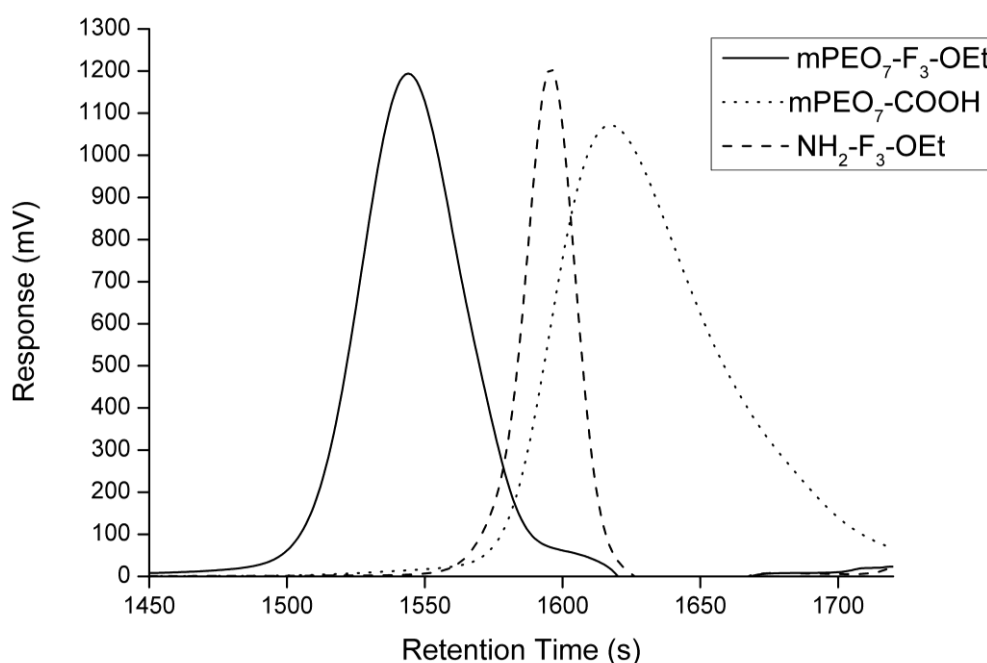


**Figure 3.29:** GPC traces showing a polymer-peptide conjugate (mPEO<sub>7</sub>-F<sub>3</sub>-OEt) and the precursor reagents.

NMR analysis confirmed that the purified product was the desired conjugate. The <sup>1</sup>H NMR spectrum (Figure 3.30) also reveals that many of the peaks that originate from the peptide component are becoming less defined (broader), with multiplicity becoming more difficult to see. However, all of the standard identifiable peaks are present, confirming that the conjugate has been formed to a good degree of purity. In the spectrum, the phenyl proton peaks (Peak H) have become significantly larger in relation to the polymer backbone peak (Peak C), as this is the variable group within peptide. The integral of the phenyl proton peak (Peak H) is measured to be approximately 19 protons (however, as the solvent peak overlaps, this value is an approximation), compared to the integral of the polymer backbone peak (Peak C) which was found to be 24. <sup>13</sup>C NMR further substantiates that coupling has taken place, highlighted by the

increase of amide peaks (Peak J) (Figure 3.31). The IR spectrum is not similar to the spectra of the other conjugates in this series, although the important band for the amide bond present at  $1638\text{ cm}^{-1}$  (Figure 3.32, Band E). Notably, peaks B and C are dissimilar to all other conjugates.

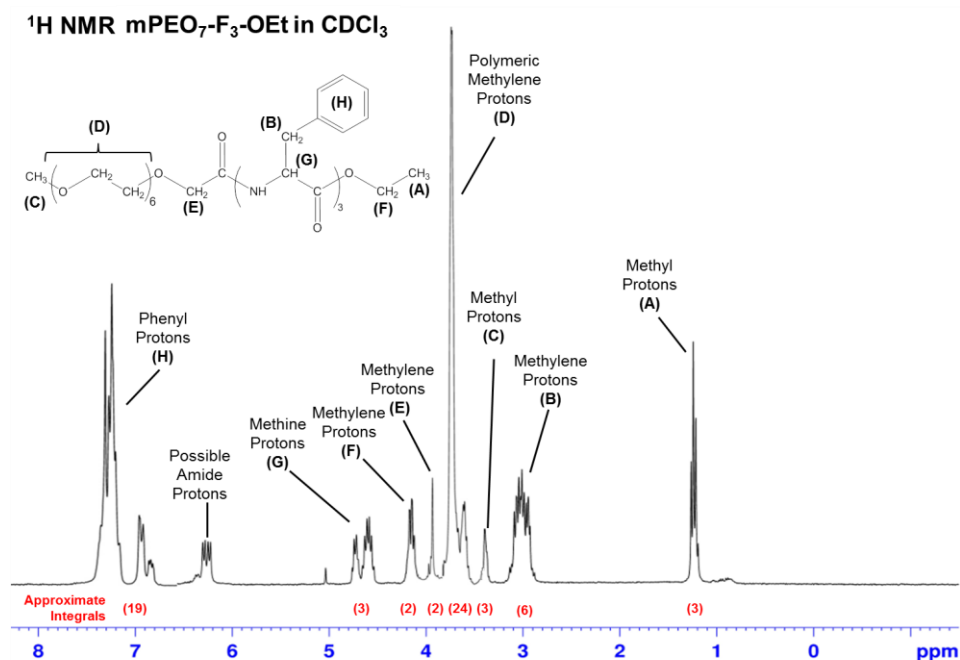


**Figure 3.30:**  $^1\text{H NMR}$  spectrum of  $\text{mPEO}_7\text{-F}_3\text{-OEt}$ .

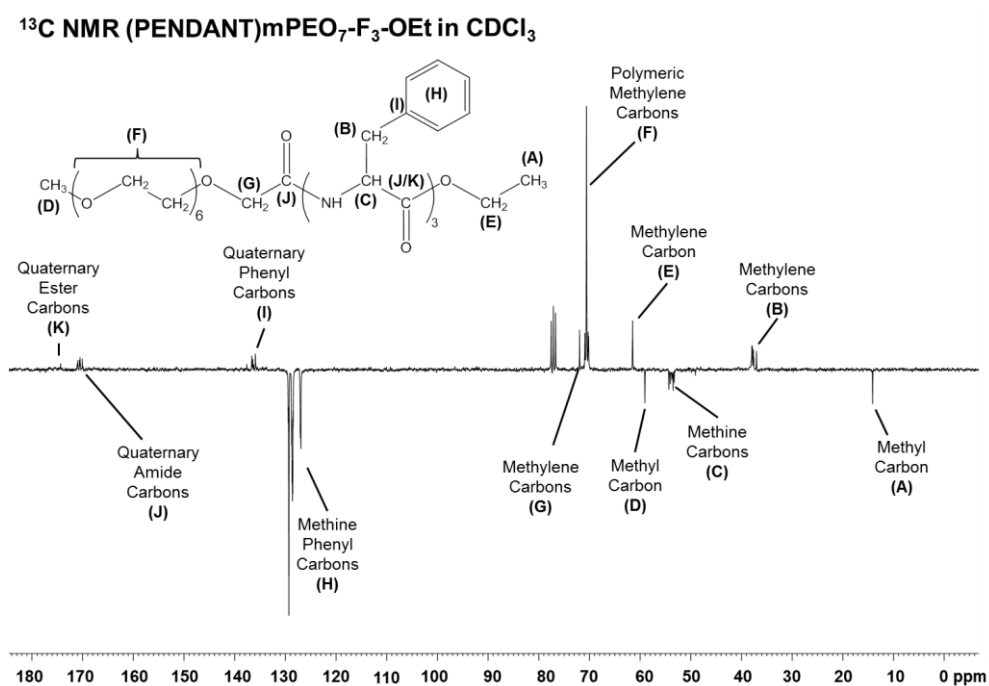


**Figure 3.31:**  $^{13}\text{C PENDANT NMR}$  spectrum of  $\text{mPEO}_7\text{-F}_3\text{-OEt}$ .

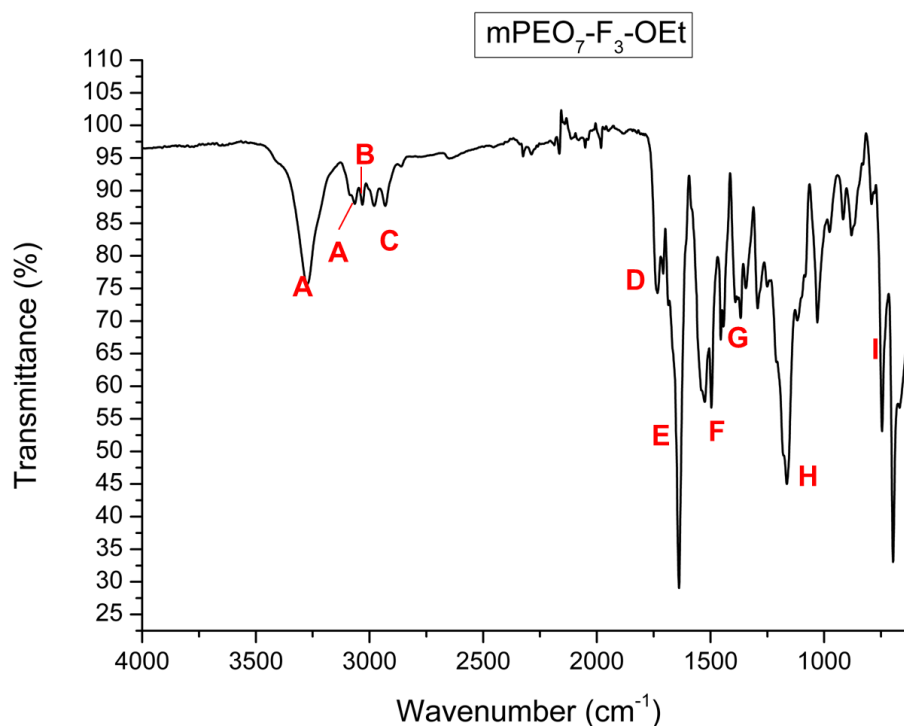


**Figure 3.32:** IR spectrum of  $\text{PEO}_7\text{-F}_3\text{-OEt}$ . For peak assignment see Appendix A.

Despite the difficulties encountered during purification, the reaction produced good yields (~80 %) and a well-defined polymer-peptide conjugate.

#### 3.3.2.1.4. Synthesis of $m\text{PEO}_7\text{-F}_4\text{-OEt}$

The synthesis of  $m\text{PEO}_7\text{-F}_4\text{-OEt}$  was carried out following the protocol outlined in Chapter 2. Initial synthesis was deemed to be successful by visual inspection of the product; a solid that was coloured yellow. This colour indicated an impurity, likely caused by IBCF.

After repeating the purification procedure (i.e. washing), the product retained a yellow hue, albeit in a lighter shade. It was therefore necessary to develop additional purification procedures that would produce a pure product. From the GPC trace (Figure 3.33), it can be seen that the primary impurity was unreacted precursor peptide. The solid nature of the product allowed for the use of reprecipitation to remove both the IBCF impurities and the peptidic impurities.

Additionally, column chromatography was also considered as a viable means of purification. However, both processes add an additional purification step, which allows for increased chances of the loss of the product, impacting the final yield. The yield of the impure conjugate was taken as a means of comparison, and varied between 81 to 92 %, and decreased significantly after the required additional purification. Dialysis was also considered as a potential purification method, however a quicker, more industrially viable purification protocol was required, and so dialysis was not pursued. Nevertheless, this option could be considered if required.

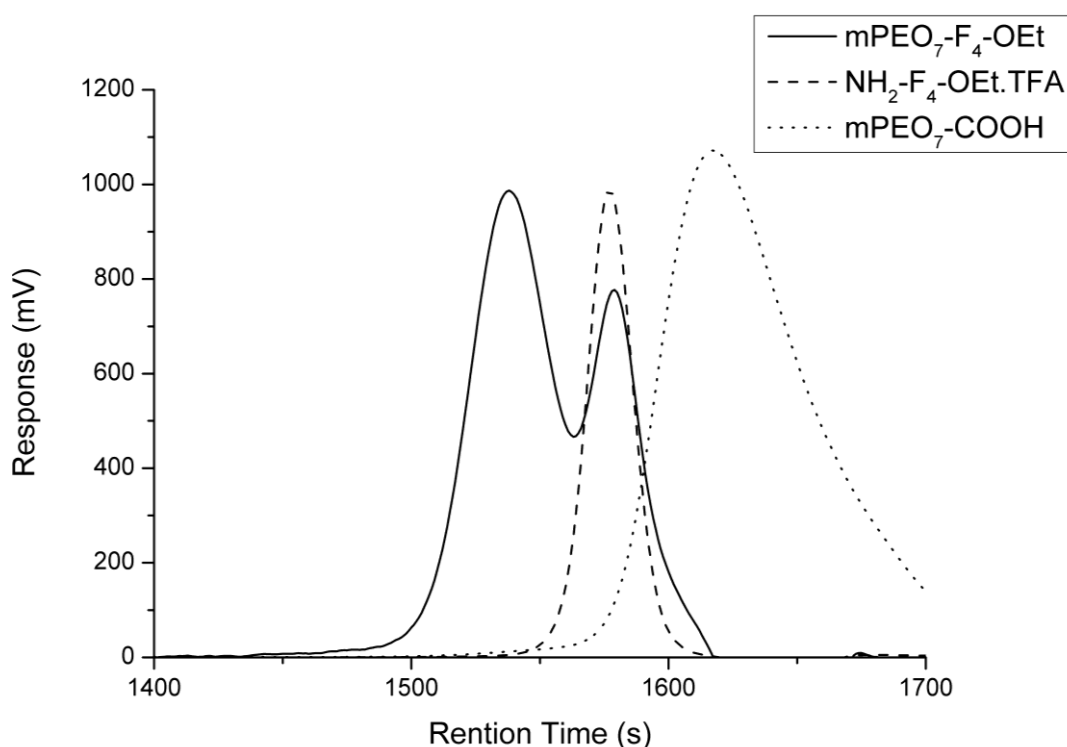


**Figure 3.33:** GPC trace of mPEO<sub>7</sub>-F<sub>4</sub>-OEt and progenitor peaks after initial synthesis.

Column chromatography was performed using an eluent of 20:1 (DCM: MeOH), and the stationary phase used was silica gel. After columning, the purified product was a pale yellow solid. This visual indication implied that at least the majority of IBCF impurity had been removed. GPC analysis was again performed to note assess the purity and species present in the conjugate, which is shown in Figure 3.34.

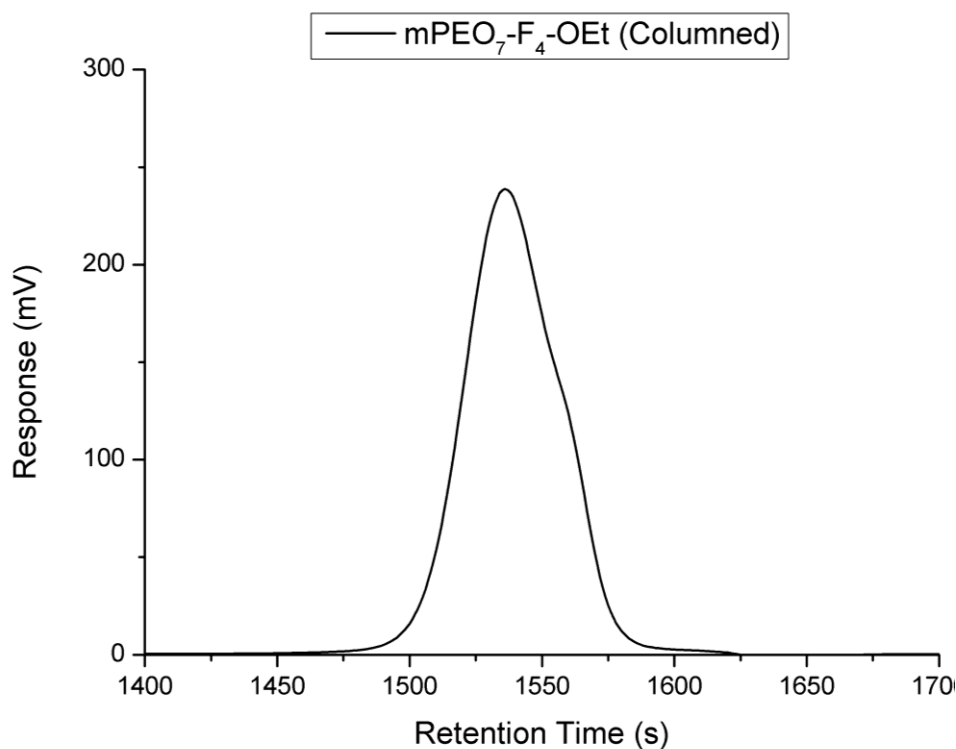


**Figure 3.34:** GPC trace of columned mPEO<sub>7</sub>-F<sub>4</sub>-OEt.

The bimodal character of the conjugate peak in Figure 3.35 has been vastly reduced, though not eliminated (as a shoulder is visible on the trace), inferring that some peptide was still associated with the conjugate. Furthermore, the final yield for the purified conjugate was 41 %. The colour of the product was a pale yellow, indicating that some IBCF impurity remained. This dramatic reduction in the final yield, coupled with the inefficient and only partly effective purification of the product, alongside the long work-up time, renders column chromatography an inefficient method that was not pursued unless absolutely necessary.

A second experiment was carried out using a different purification method. Reprecipitation was undertaken by dissolving the conjugate into a small amount of THF (~20 ml), then slowly adding the solution to excess petroleum ether (~300-400 ml), whilst stirring. The conjugate precipitated as a white solid, which was collected by filtration, washed through with additional petroleum ether, and then dried *in vacuo*. GPC analysis (Figure 3.35) reveals a narrow unimodal peak with no shoulder present, which strongly implies that no unreacted peptide is present, and gives a good indication of overall purity. The yield after

purification was 77 % which is significantly higher than the yield produced after column chromatography, and the overall purification time was quicker. Reprecipitation, with additional washing was determined to be a more effective purification procedure and was used henceforth when viable.

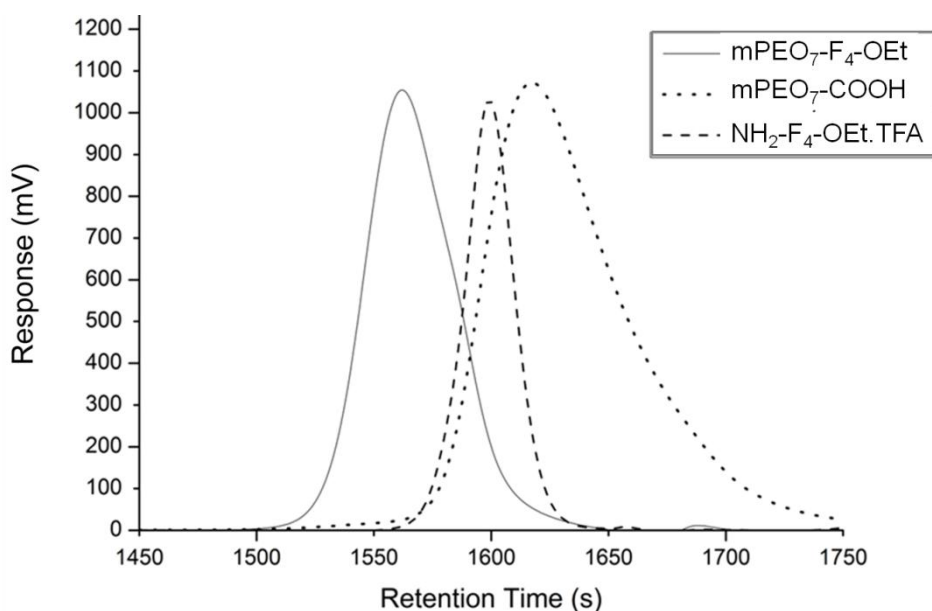


**Figure 3.35:** GPC trace of reprecipitated mPEO<sub>7</sub>-F<sub>4</sub>-OEt and progenitor peaks.

<sup>1</sup>H NMR data is shown in Figure 3.36, where the spectrum clearly illustrates the correspondingly more intense phenyl peaks (integral ratio of 22 protons, Peak H), and the further broadening of the methylene (integral ratio of Peak B is 7.7) and methine peaks (Peak G, which has an integral ratio of 3.3) in the oligopeptide backbone. It is also possible to see amide proton peaks at 7.5 ppm, 8.1 ppm and 8.6 ppm, further confirming that coupling was successful. The <sup>13</sup>C PENDANT NMR spectrum (Figure 3.37) shows four positively phased quaternary carbon peaks representing the amide groups in the molecule (Peak J). It is important to note that the signal from the ester carbon is no longer visible at this resolution, requiring an increased scanning time to detect. IR data is similar to the other conjugates in the series, with the band representing secondary amide bonds noted at 1635 cm<sup>-1</sup> (Figure 3.38). As with the other spectra, the bands have varied by only a small amount (and the relative

intensities have remained consistent, illustrating that the same bonding is present in all the conjugates.

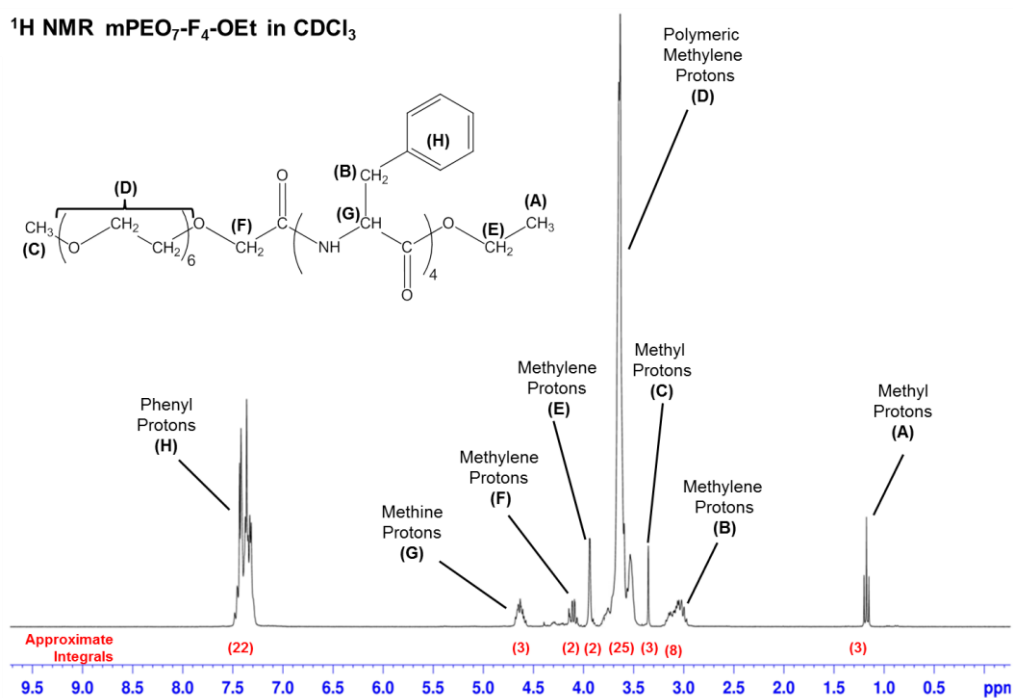


Figure 3.36: <sup>1</sup>H NMR spectrum of mPEO<sub>7</sub>-F<sub>4</sub>-OEt.

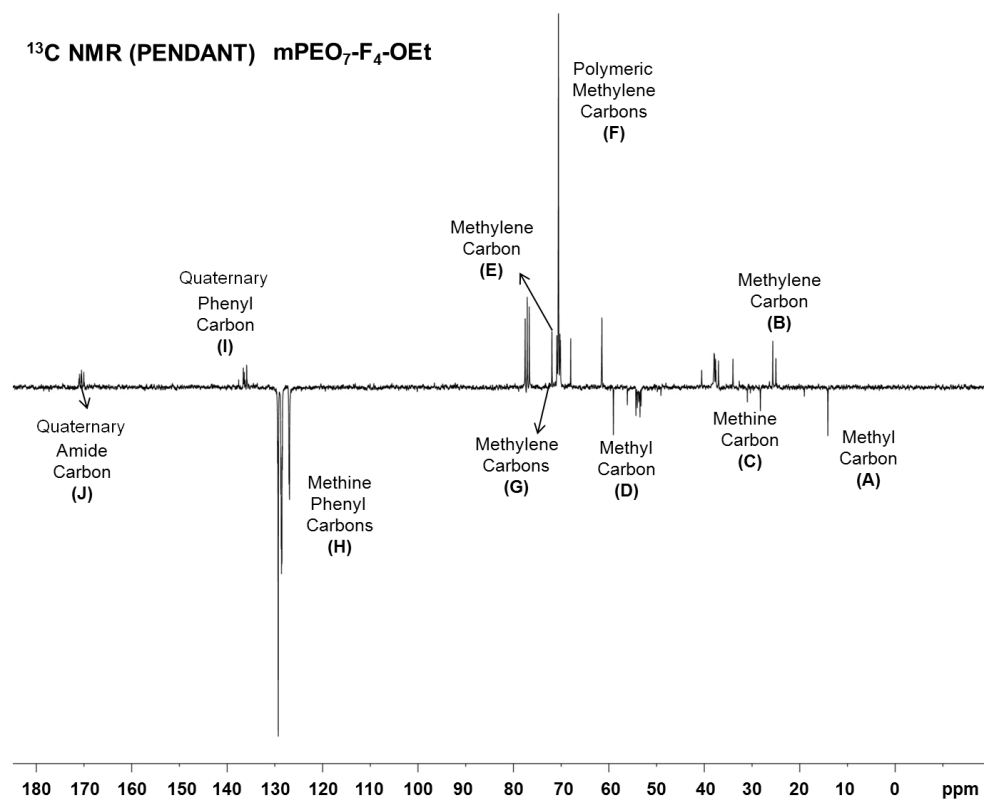
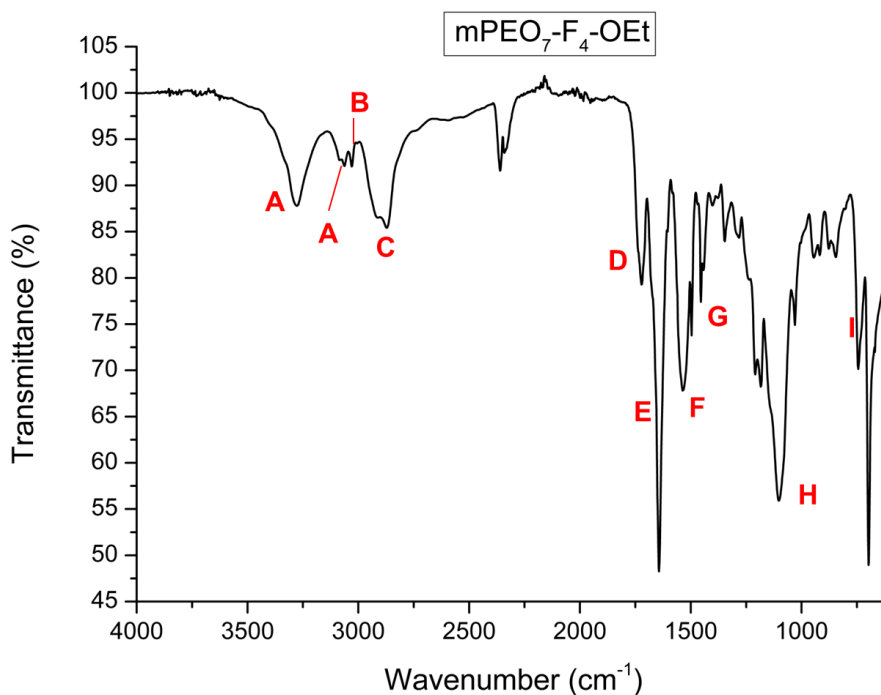


Figure 3.37: <sup>13</sup>C PENDANT NMR spectrum of mPEO<sub>7</sub>-F<sub>4</sub>-OEt.



**Figure 3.38:** IR spectrum of mPEO<sub>7</sub>-F<sub>4</sub>-OEt. For peak assignments see Appendix A.

The synthesis of mPEO<sub>7</sub>-F<sub>4</sub>-OEt was carried out to produce a pure conjugate with high yield (77 %). Initial washing was inefficient so further purification was required with two methods investigated. It was determined that a combination of reprecipitation and re-washing produced the most well-defined conjugate with the best yields.

### **3.3.2.1.5. Summary of synthesis of mPEO<sub>7</sub>-containing conjugates**

Four well-defined conjugates containing mPEO<sub>7</sub>-COOH and phenylalanine oligopeptide homologues were produced using IBCF. Yields for each conjugate were high, but generally showed a decrease as the peptide length increased. This is attributable to compatibility of the peptide in the solvent, which also decreases as peptide length increases alongside the more predictable steric effects.

### 3.3.2.2. *Synthesis of mPEO<sub>12</sub> conjugates*

Synthesis of mPEO<sub>12</sub>-based conjugates is very similar to that of mPEO<sub>7</sub>-based conjugates. To avoid repetition, only analytical information has been included in the following sections for each conjugate, unless any special deviation from the previously established protocols was required.

#### 3.3.2.2.1. *Synthesis of mPEO<sub>12</sub>-F<sub>1</sub>-OEt*

The synthesis of mPEO<sub>12</sub>-F<sub>1</sub>-OEt is similar to the equivalent conjugate synthesis with a smaller polymer component. As before, the peptide component did not require synthesis or additional purification and, therefore, could be used as received. The conjugation product was also generally a clear viscous liquid, however in contrast to mPEO<sub>7</sub>-F<sub>1</sub>-OEt, the conjugate was also observed to have some regions that appeared semi-solid due to its higher molecular weight. A yellow tinge was observed when certain impurities were present (attributed to IBCF), again providing a good visual indicator of product purity. It should be noted that this is only a qualitative measure of purity, and that other methods are used for more quantitative analysis.

A well-defined, narrow unimodal peak was observed on the GPC trace, indicating that no degradation of the product occurred, and that no other precursor species were present in the final product. It should be noted that the GPC of the mPEO<sub>12</sub>-COOH starting reagent overlaps with the conjugate peak on the GPC trace (Figure 3.39). However, the conjugate product peak is symmetrical, suggesting that there is no contamination from free mPEO<sub>12</sub>-COOH (which would produce a low molecular weight shoulder). Addition of NH<sub>2</sub>-F<sub>1</sub>-OEt to the polymer chain leads to a slight increase in molecular weight, which causes the retention time to be shorter by a small amount, reflected in the trace.

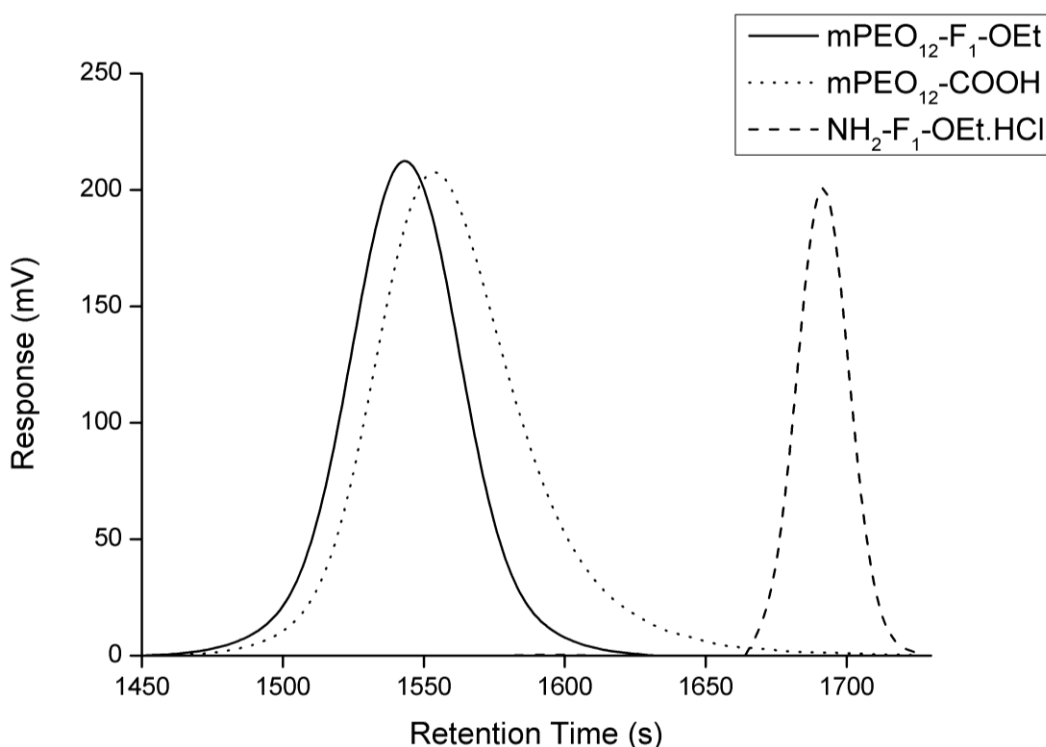


**Figure 3.39:** GPC trace of mPEO<sub>12</sub>-F<sub>1</sub>-OEt and precursor materials.

In contrast to the analogous conjugate from the PEO<sub>7</sub> series, an aqueous and acid/base washing the product were sufficient to produce pure conjugates. Furthermore, the molecular weight of the conjugate is dissimilar enough from the peptide for dialysis to be a viable purification strategy. The <sup>1</sup>H NMR spectrum of the conjugate (Figure 3.40) is very similar to the mPEO<sub>7</sub>-F<sub>1</sub>-OEt spectrum (Figure 3.19), with the peaks occurring at almost identical chemical shifts; the only difference is the intensity of the peaks. This is most visible when comparing the intensity of the phenyl peaks (Peak H) to the polymer backbone peaks (Peak D), where the intensity of the polymer backbone peaks was greater in mPEO<sub>12</sub>-F<sub>1</sub>-OEt. The integral ratio of the phenyl peaks (Peak H) was determined to be 5, and the integral of the polymer backbone peaks was 43 (expected value was 44), a clear increase from the integral of 26 in Figure 3.19. Analysis by <sup>13</sup>C PENDANT NMR (Figure 3.41) produced an identical spectrum, when compared to Figure 3.20, with the exception of the peak intensities, which were reduced with respect to the polymer backbone (Peak F), due to the increase in the number of carbons in the polymer backbone (Figure 3.41). IR spectroscopy showed minor differences between the spectra, most notably a

reduction in the band for secondary amide bond stretching (Band A) at  $3282\text{ cm}^{-1}$  (Figure 3.42).

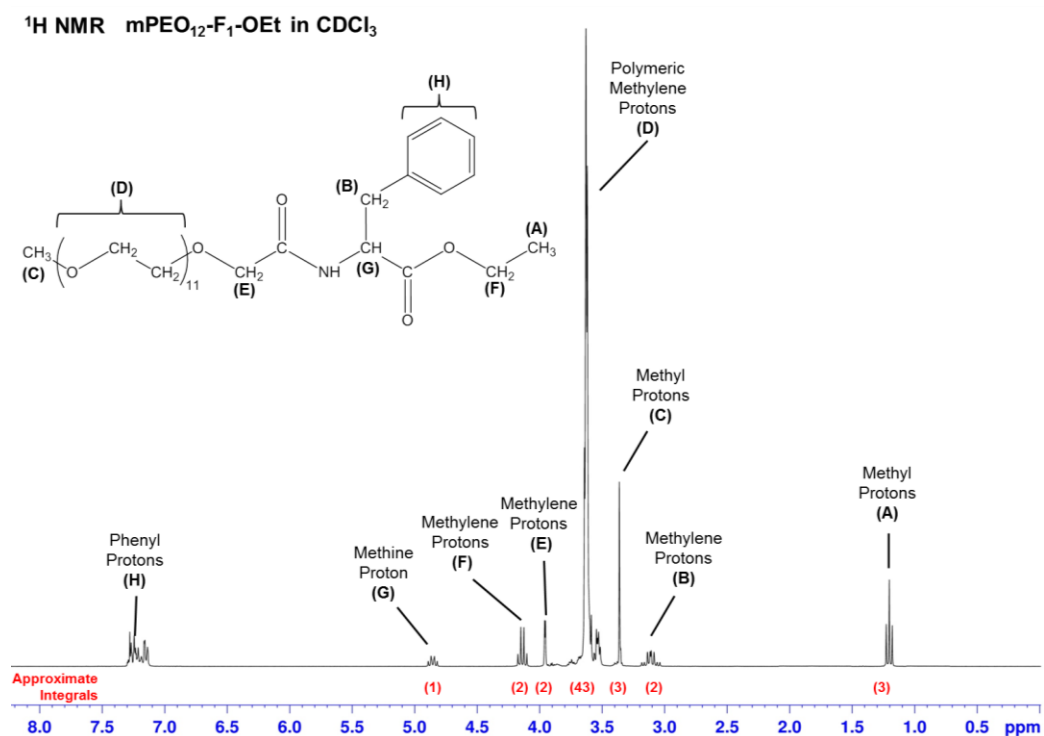


**Figure 3.40:**  $^1\text{H NMR}$  spectrum of mPEO<sub>12</sub>-F<sub>1</sub>-OEt.

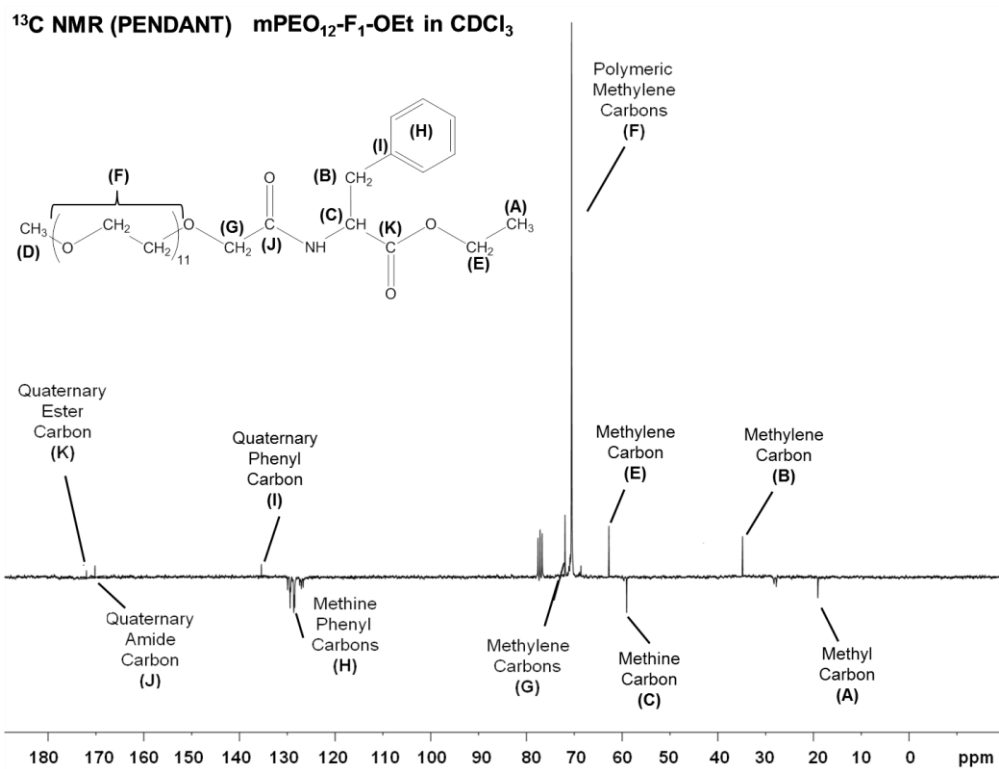


**Figure 3.41:**  $^{13}\text{C}$  PENDANT NMR spectrum of mPEO<sub>12</sub>-F<sub>1</sub>-OEt.

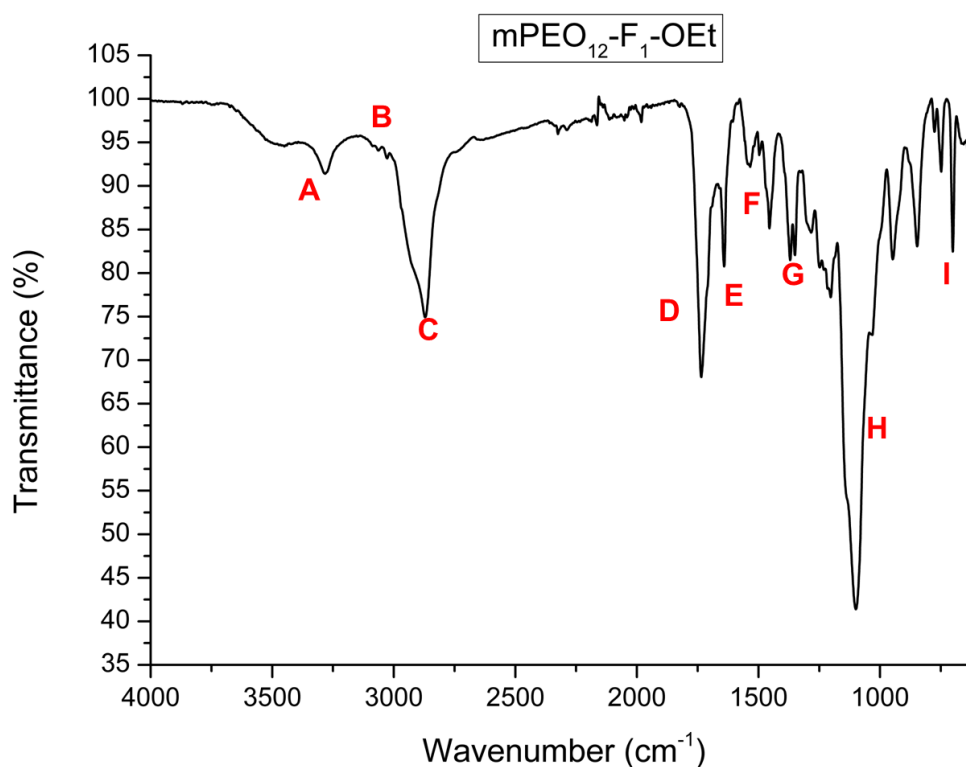


**Figure 3.42:** IR spectrum of mPEO<sub>12</sub>-F<sub>1</sub>-OEt. For peak assignments see Appendix A.

Overall, the coupling reaction was straightforward and produced a well-defined conjugate. Yields for the reaction were moderate to high, ranging from 65 to 79 %. This is slightly lower than the maximum yield obtained for mPEO<sub>7</sub>-F<sub>1</sub>-OEt conjugates using the same peptide.

#### 3.3.2.2.2. *Synthesis of mPEO<sub>12</sub>-F<sub>2</sub>-OEt*

Much like the preceding conjugate, synthesis of mPEO<sub>12</sub>-F<sub>2</sub>-OEt was similar to that of the analogous PEO<sub>7</sub>-based conjugate. However, a noted difference was that the conjugate is a solid (with some regions appearing to be semi-solid) due to the increased molecular weight of the polymer component. There were no modifications to the synthetic protocol as described in Chapter 2. GPC analysis of the conjugate shows a generally unimodal peak (Figure 3.43). NMR analysis of the product shows that the peaks are more defined than mPEO<sub>7</sub>-F<sub>2</sub>-OEt (Figure 3.44), which is clearly emphasised when comparing the

methine protons (Peak G) of the respective spectra. However, the peaks are becoming slightly broader when compared to the spectrum for mPEO<sub>12</sub>-F<sub>1</sub>-OEt, most notably the phenyl peaks. The integral ratios for the conjugate are close to the expected values, with broadness of the peak for the methylene protons adjacent to the phenyl ring (benzyl protons, Peak B) distorting the integral ratio slightly (five protons instead of four). Integration of the different phenyl peaks (Peak H) gave a ratio of ten protons to two, commensurate with the structure of the conjugate. However, this integral is not entirely reliable as the sharp peak visible at 7.3 ppm, which is produced by solvent (CDCl<sub>3</sub>), will distort the integrals. This applies to all of the <sup>1</sup>H NMR spectra where the phenyl ring proton signals overlap the solvent region. Some broadness is also observed by the methylene protons in the ester protecting group (Peak F).

The <sup>13</sup>C PENDANT NMR spectrum shows minor differences compared to mPEO<sub>12</sub>-F<sub>1</sub>-OEt and mPEO<sub>7</sub>-F<sub>2</sub>-OEt, with a notable decrease in the relative intensity of the ester carbon peak, in comparison to the amide peak (Figure 3.45, Peak J). IR analysis shows slight shifting of the bands, with the band for secondary amide bonds (C=O stretching) present at 1641 cm<sup>-1</sup> (Figure 3.46, Band E).

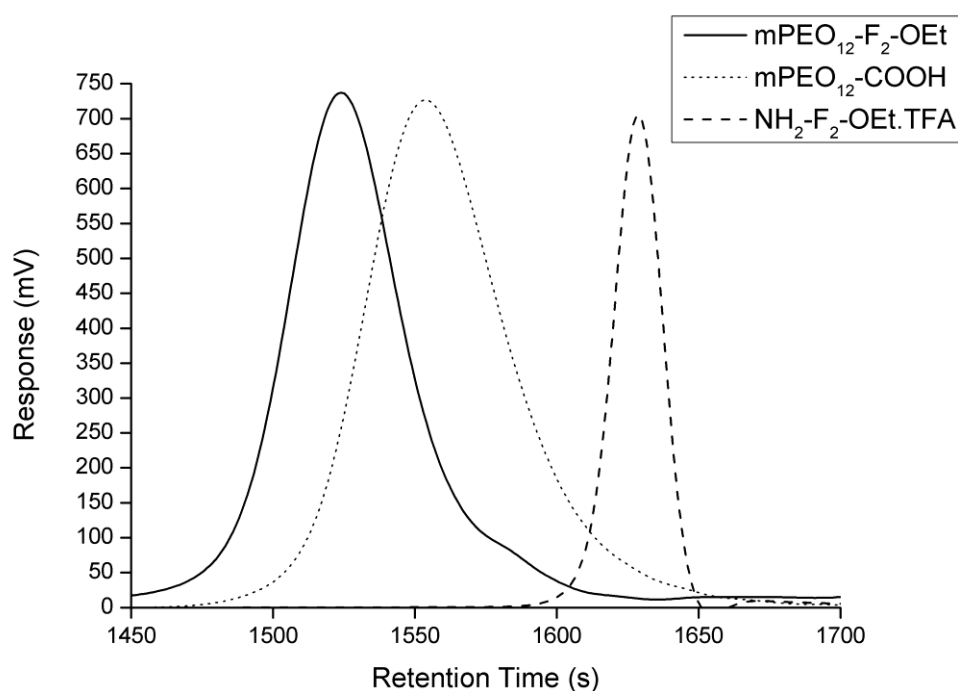


**Figure 3.43:** GPC trace of mPEO<sub>12</sub>-F<sub>2</sub>-OEt and precursor reagents.

<sup>1</sup>H NMR mPEO<sub>12</sub>-F<sub>2</sub>-OEt in CDCl<sub>3</sub>

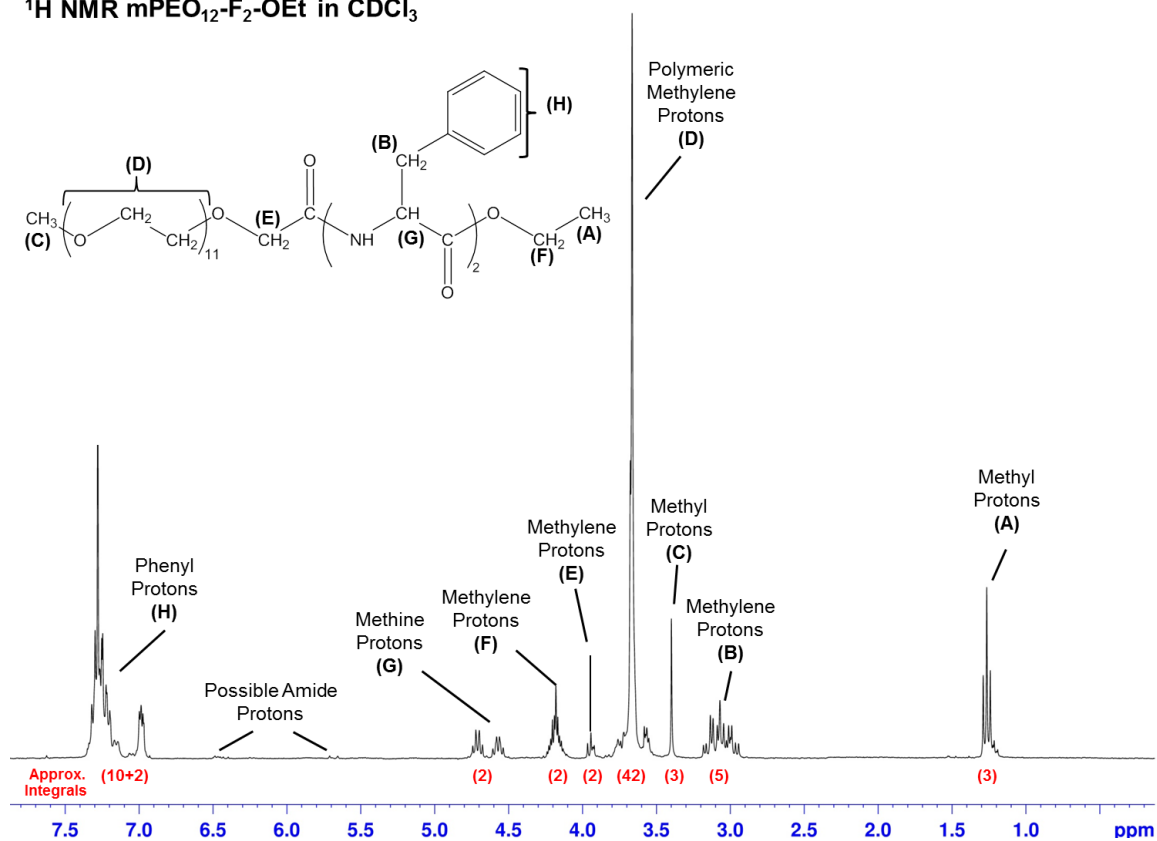


Figure 3.44: <sup>1</sup>H NMR spectrum of mPEO<sub>12</sub>-F<sub>2</sub>-OEt.

<sup>13</sup>C NMR (PENDANT) mPEO<sub>12</sub>-F<sub>2</sub>-OEt in CDCl<sub>3</sub>

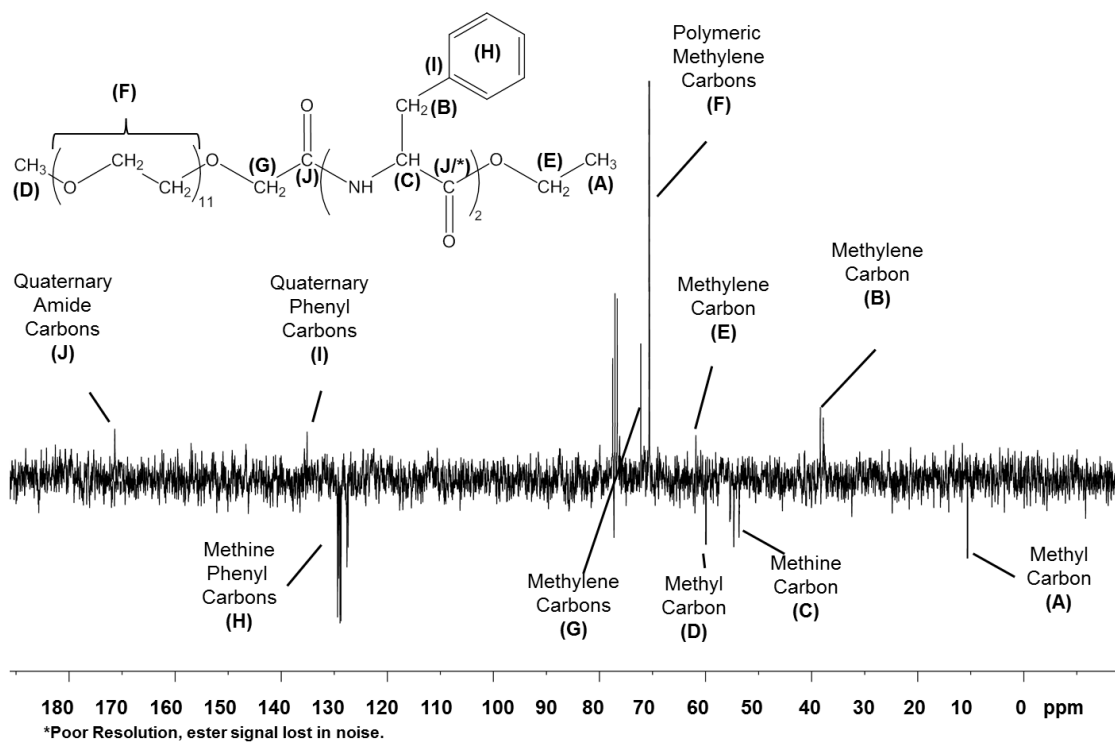
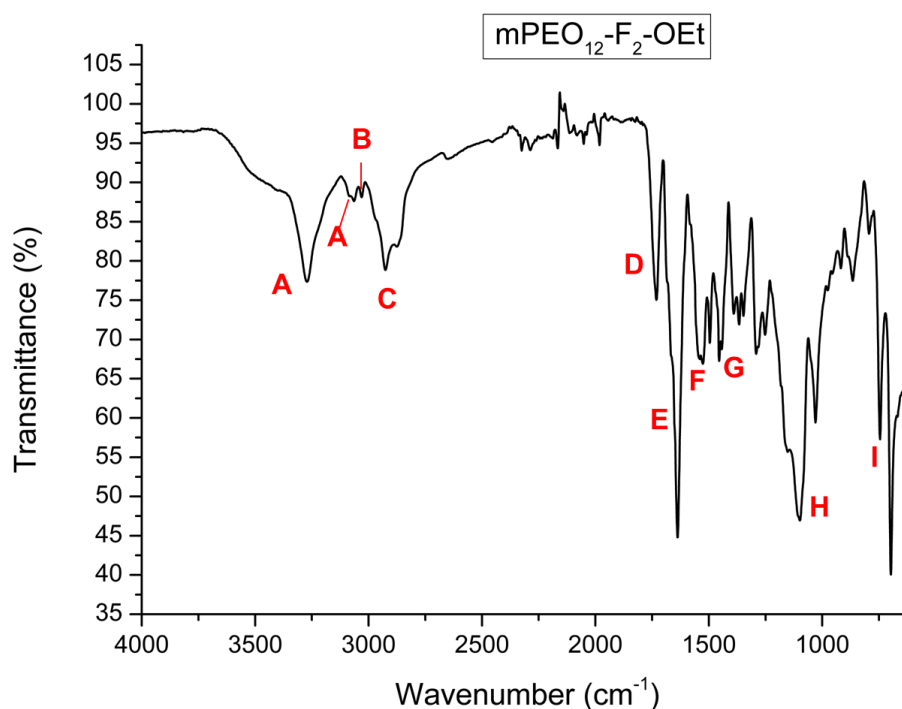


Fig 3.45: <sup>13</sup>C PENDANT NMR spectrum of mPEO<sub>12</sub>-F<sub>2</sub>-OEt



**Figure 3.46:** IR spectrum of mPEO<sub>12</sub>-F<sub>2</sub>-OEt.

Overall, the coupling reaction was again facile and produced a well-defined, pure conjugate. Yields for the reaction were high, ranging from 71 to 90 %. This is slightly lower than the maximum yield obtained for PEO<sub>7</sub>-based conjugates using the same peptide, which is also reflected in the conjugate yield for PEO<sub>12</sub>-F<sub>1</sub>-OEt. Interestingly, the yield for F<sub>2</sub>-based conjugates has been better than F<sub>1</sub>-based conjugates for both polymer chains, suggesting that the short peptide sequence may negatively affect the coupling efficiency, by creating difficulties during the purification process.

### 3.3.2.2.3. Synthesis of mPEO<sub>12</sub>-F<sub>3</sub>-OEt

Synthesis of mPEO<sub>12</sub>-F<sub>3</sub>-OEt followed a similar route to mPEO<sub>7</sub>-F<sub>3</sub>-OEt. The increased molecular weight of the conjugate resulted in the product being a solid with a pale yellow tinge. This is in contrast to the homologous PEO<sub>7</sub>-based conjugate which was a semi-solid. The initial GPC trace (Figure 3.47) shows that the conjugate peak is not unimodal. Elution time of the second peak gives a clear indication that the impurity of the conjugate arises from the precursor

peptide, which has a similar peak character.  $m\text{PEO}_{12}\text{-COOH}$  is easily washed out by repeating the purification procedure detailed in Section 2.3. The precursor peptide is able to associate via hydrogen bonding to the other species in the reaction mixture, such as the conjugate, and thus be eluted alongside them, which explains the lower retention time.

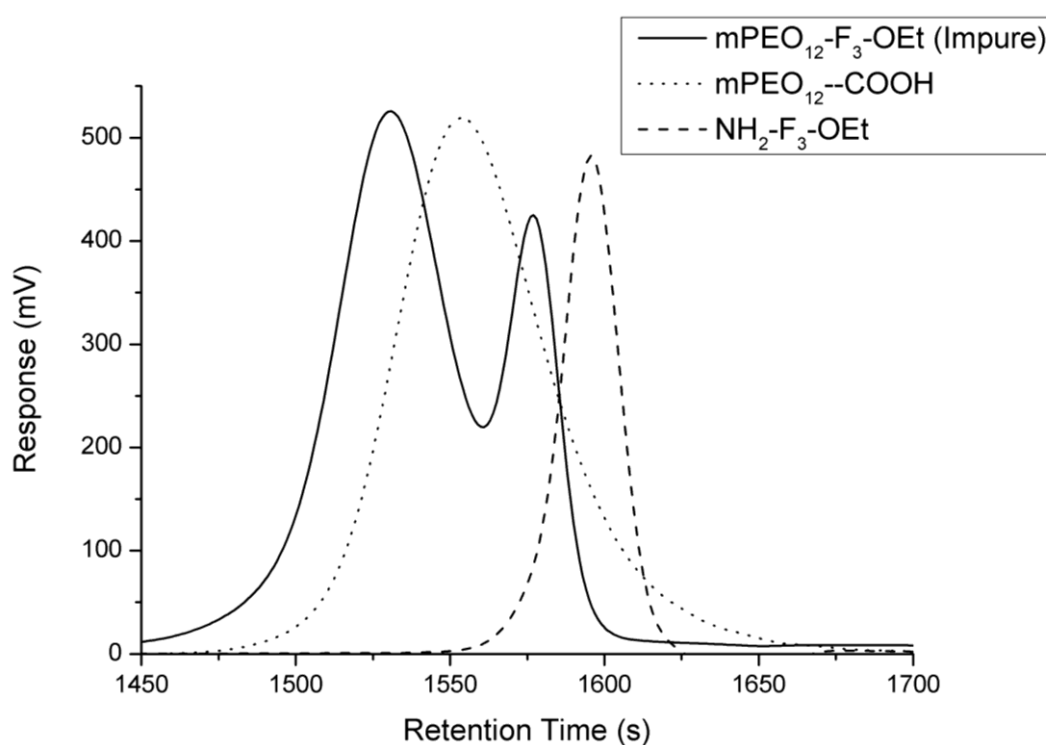


**Figure 3.47:** GPC traces showing impure  $m\text{PEO}_{12}\text{-F}_3\text{-OEt}$  and precursor reagents.

As the conjugate was a solid, reprecipitation, and repeated washes were used to remove the associated peptide. GPC analysis shows that after repurification, a well-defined, narrow unimodal peak is produced (Figure 3.48). The  $^1\text{H}$  NMR spectrum of the purified  $m\text{PEO}_{12}\text{-F}_3\text{-OEt}$  is dominated by the polymeric methylene protons (Peak D), reducing the relative intensities of the other peaks. This is especially noticeable when compared to the  $^1\text{H}$  NMR of  $m\text{PEO}_7\text{-F}_3\text{-OEt}$  (Figure 3.49). Furthermore, it can be seen that the peaks originating from the oligopeptide are much broader and less well-defined, with more multiplets visible, especially the methylene benzylic protons (Peak B). The  $^{13}\text{C}$  PENDANT NMR spectrum shows a further decrease in peak intensities compared to the corresponding  $\text{PEO}_7$ -based conjugate (Figure 3.50). This is due to the relative

increase in intensity of the polymer carbons. IR analysis (Figure 3.51) confirms the presence of a secondary amide bond at  $3270\text{ cm}^{-1}$  and  $1636\text{ cm}^{-1}$  (Band A and E, respectively).

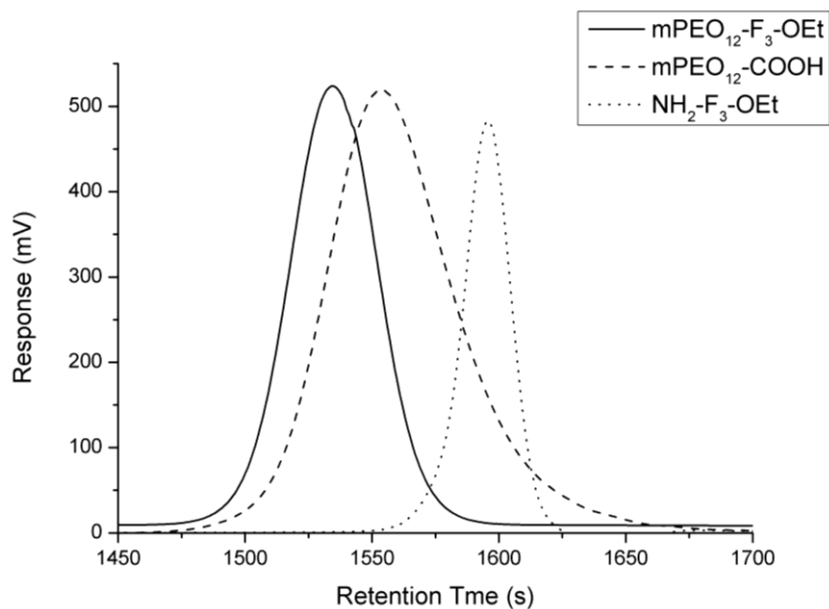


**Figure 3.48:** GPC traces showing the purified  $m\text{PEO}_{12}\text{-F}_3\text{-OEt}$  and precursor reagents.

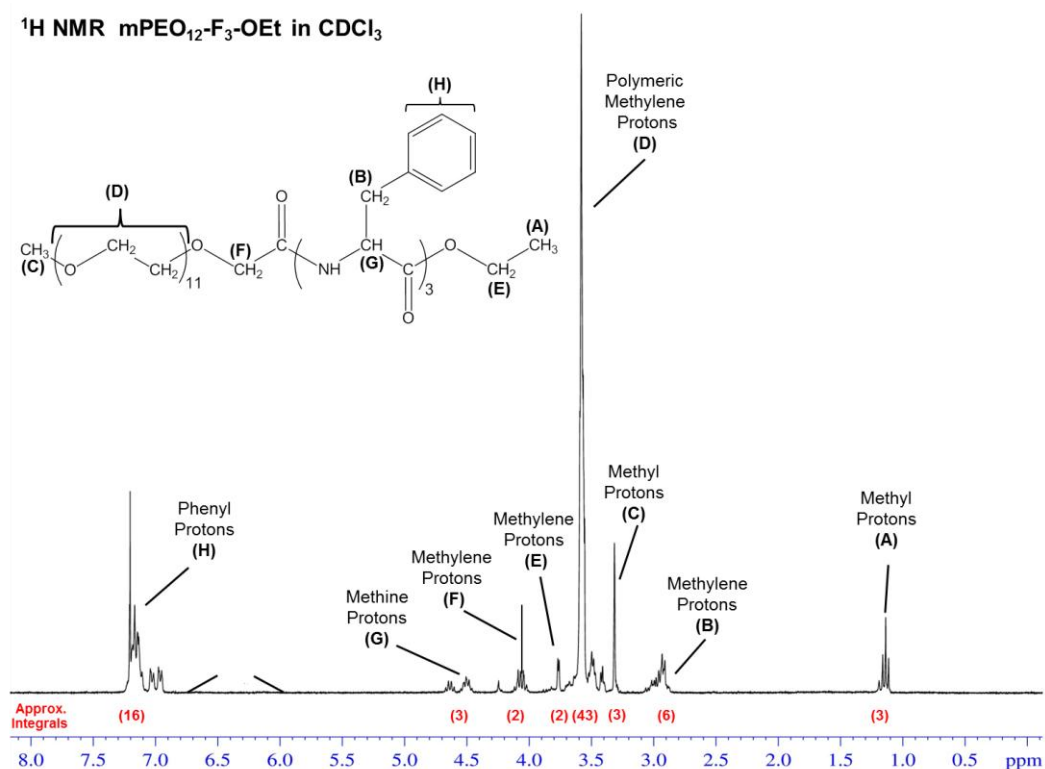


**Figure 3.49:**  $^1\text{H}$  NMR spectrum of  $m\text{PEO}_{12}\text{-F}_3\text{-OEt}$ .

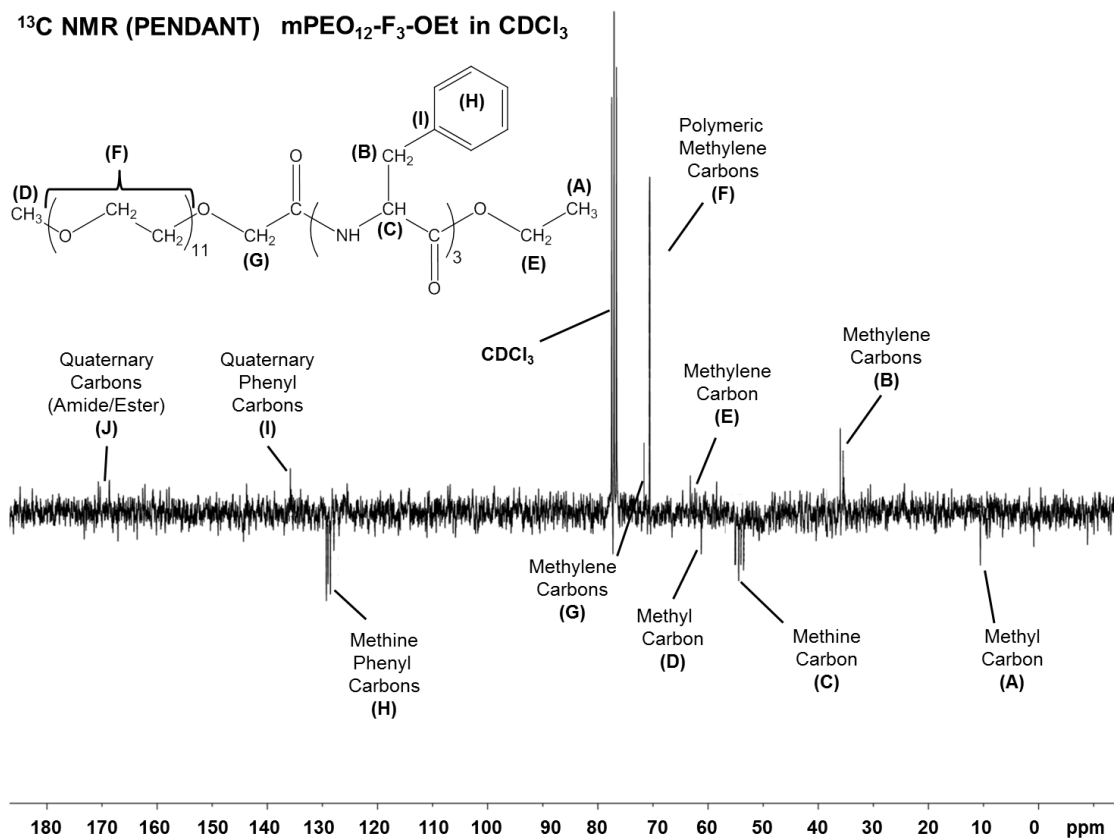


**Figure 3.50:** <sup>13</sup>C PENDANT NMR spectrum of mPEO<sub>12</sub>-F<sub>3</sub>-OEt.

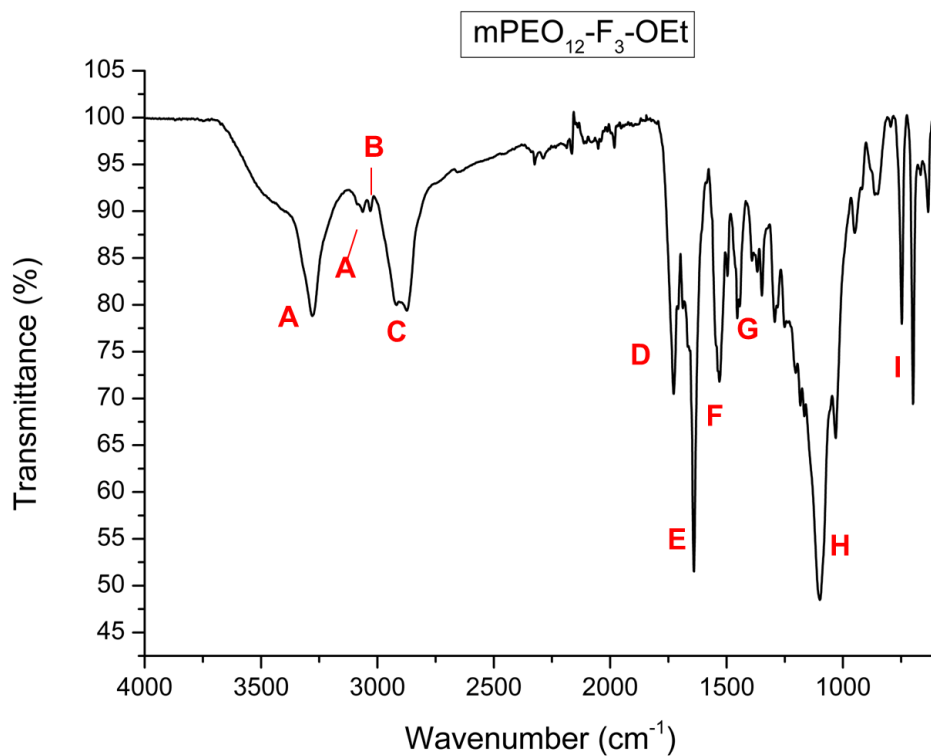


**Figure 3.51:** IR spectrum of mPEO<sub>12</sub>-F<sub>3</sub>-OEt. For peak assignments see Appendix A.

Similar to mPEO<sub>7</sub>-F<sub>3</sub>-OEt, the initial product contained an impurity which required additional purification steps. Additional purification was facile, and resulted in a pure conjugate being produced. Yields were moderate to high ranging from 58 to 72 %. This correlates with the general trend of yield decreasing with increasing peptide length, and also that the yield for conjugates with variable polymer chain length (but identical peptide length) decreases as polymer length increases.

#### **3.3.2.2.4. Synthesis of mPEO<sub>12</sub>-F<sub>4</sub>-OEt**

Synthesis of mPEO<sub>12</sub>-F<sub>4</sub>-OEt was carried out as described in Chapter 2, with no changes to the protocol. Preliminary purification was deemed to be successful by the production of a white solid, which if contaminated with IBCF would have a yellow tint. The increased molecular weight also makes dialysis a viable option, although reprecipitation was still the favoured method to remove impurities. Figure 3.52 shows the GPC trace for the product. It can be seen that the conjugate produced a peak with a prominent shoulder. From the position of the peak, it is speculated that there were potentially trace amounts of free polymer present.

Analysis of the NMR spectra (Figure 3.53 and 3.54) showed that the conjugate produced is consistent with the others in the series; notably the integral ratios are close to the expected values. The peak representing the methylene polymer protons (Peak D) has an integral ratio of 45 (expected value of 44), and the phenyl peak (Peak H) has an integral ratio of 22 (expected value was 20). This is an increase of 4 protons compared to mPEO<sub>12</sub>-F<sub>3</sub>-OEt, although both spectra have the solvent peak overlapping in the same region. The <sup>13</sup>C PENDANT NMR spectrum has a large phenyl carbon peak, lowering the relative intensities of the other peaks, especially the quaternary ester, which is now not visible at the current resolution. Analysis of the IR spectrum confirms the presence of the amide bond at 3270 and 1637 cm<sup>-1</sup> (Figure 3.55). Significantly, in all of the IR spectra for the conjugates produced so far, there has also been a medium intensity peak at 1454 cm<sup>-1</sup>, which is representative of the deformations of -CH<sub>3</sub> and -CH<sub>2</sub> bonds.

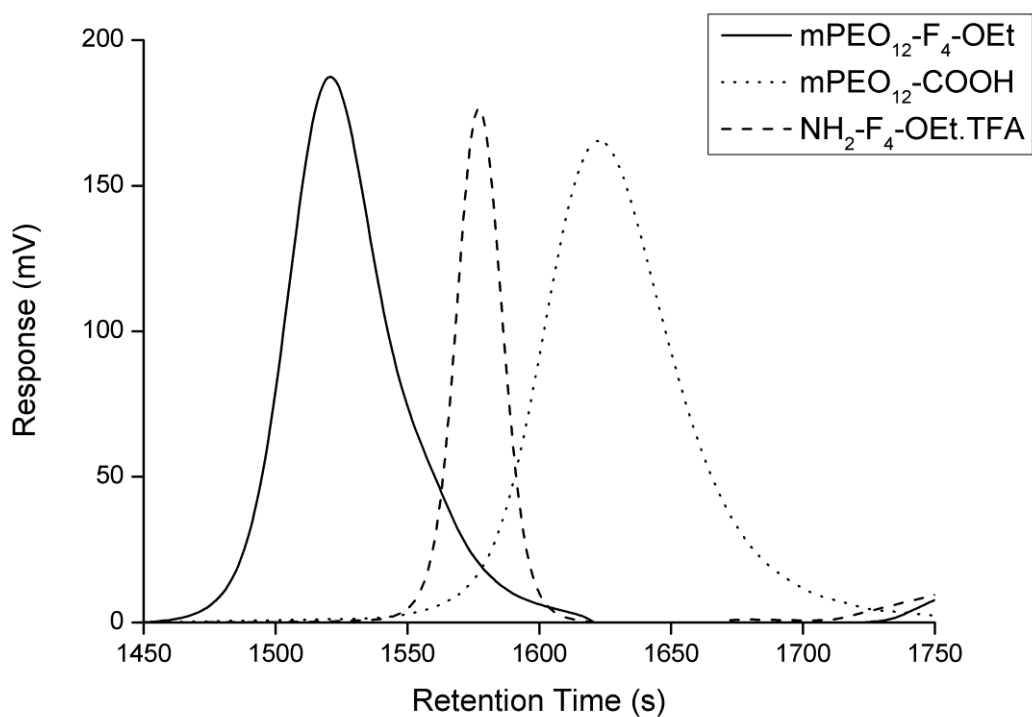


Figure 3.52: GPC traces of mPEO<sub>12</sub>-F<sub>4</sub>-OEt and precursor reagents.

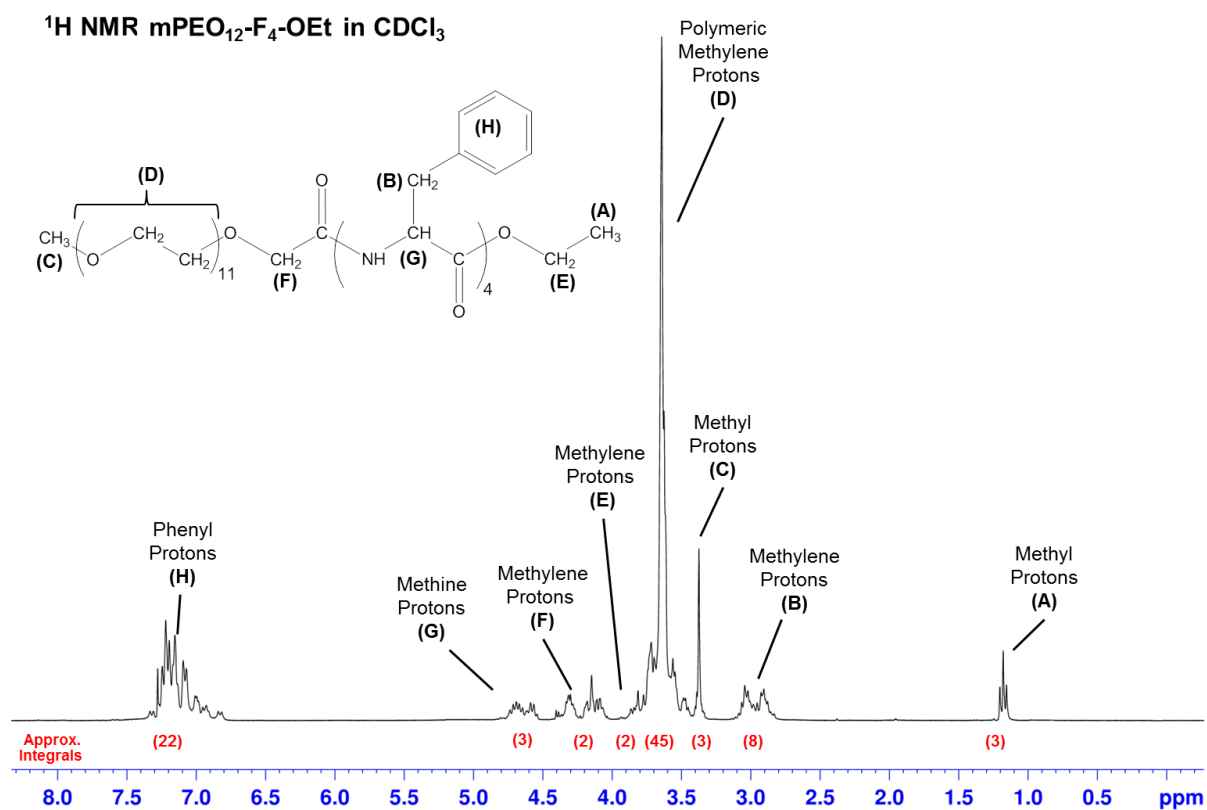
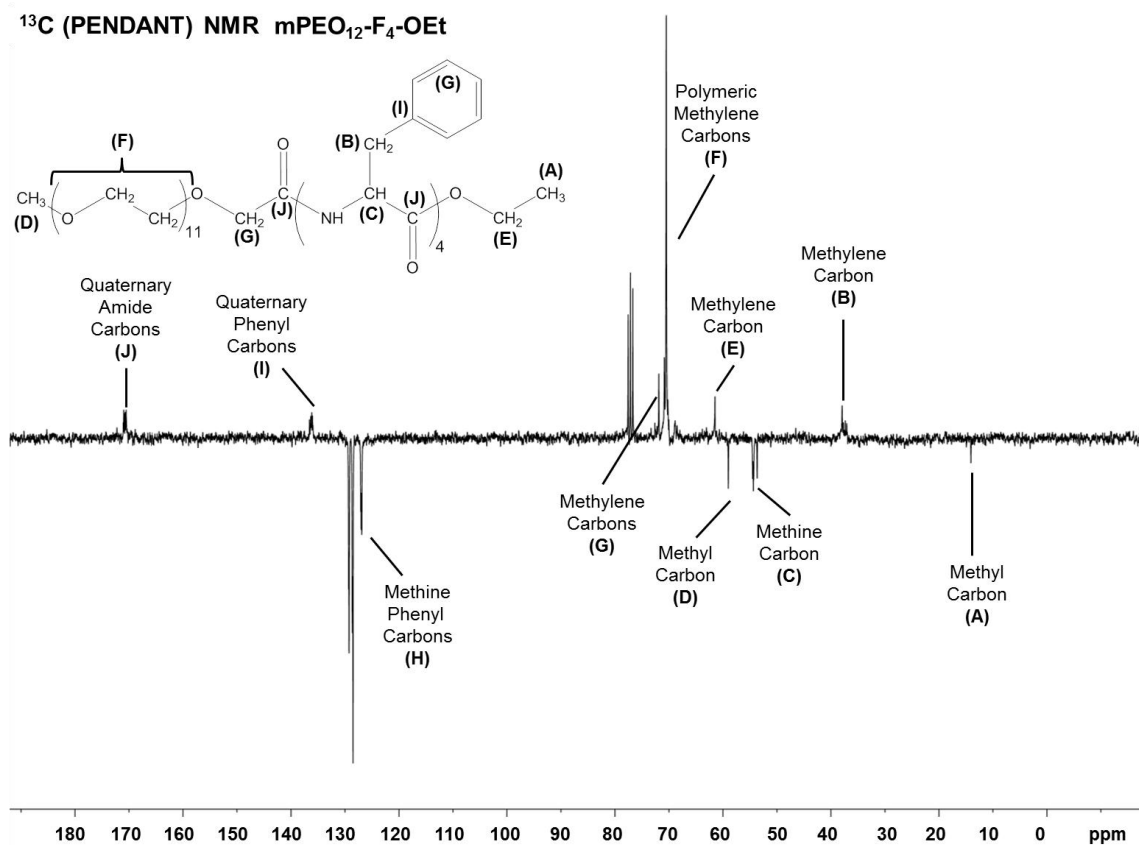
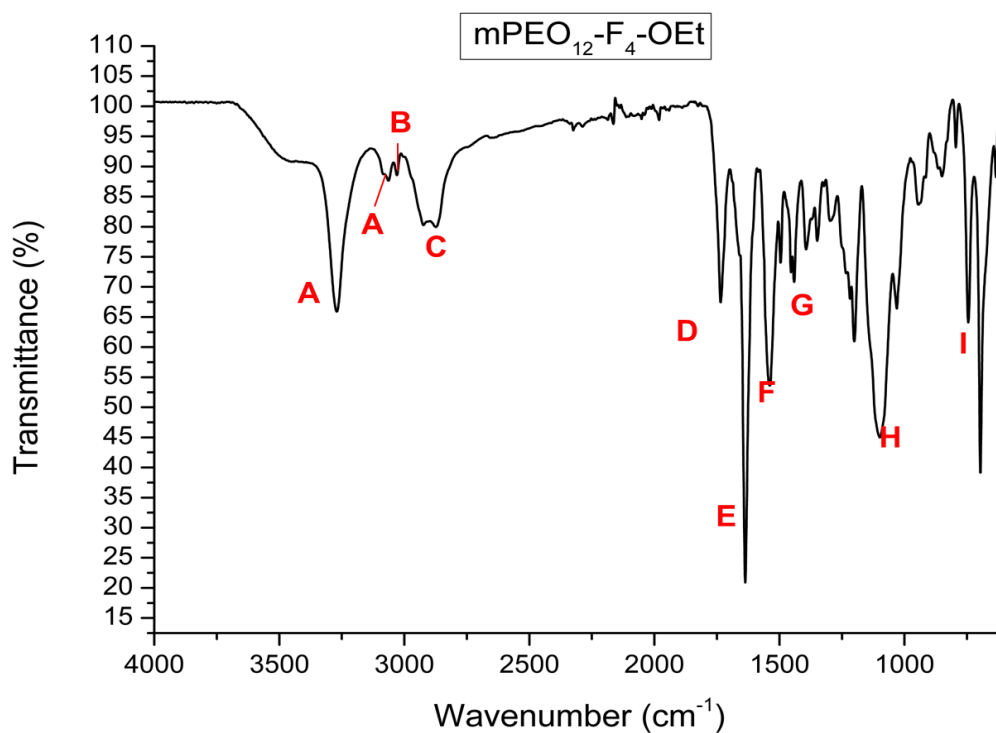


Figure 3.53: <sup>1</sup>H NMR spectrum of mPEO<sub>12</sub>-F<sub>4</sub>-OEt.



**Figure 3.54:**  $^{13}\text{C}$  PENDANT NMR spectrum of mPEO<sub>12</sub>-F<sub>4</sub>-OEt.



**Figure 3.55:** IR spectrum of mPEO<sub>12</sub>-F<sub>4</sub>-OEt. For peak assignments see Appendix A.

The mPEO<sub>12</sub>-F<sub>4</sub>-OEt conjugate was produced with good purity, without the need for additional purification. Yields of the product were moderate to high, ranging from 76 to 90%, which follows the general trend seen so far.

#### **3.3.2.2.5. Summary of synthesis of mPEO<sub>12</sub>-containing conjugates**

Four well-defined conjugates containing mPEO<sub>12</sub> and phenylalanine oligopeptide homologues were produced using IBCF. Yields for each conjugate were high, but generally decreased as the peptide length increased, agreeing with the general trend established for mPEO<sub>7</sub>-based conjugates. Comparative yields between conjugates with the same length peptide also decreased as polymer chain length increased.

#### **3.3.2.3. Synthesis of mPEO<sub>17</sub> conjugates**

Synthesis of mPEO<sub>17</sub>-based conjugates follows the general methodology used for the other conjugates. Notably, below room temperature (at approximately 17 °C) the precursor polymer component solidifies into a white solid. Gentle heating reverted the polymer back into a viscous liquid. This property is consequently inherited by the lower molecular weight conjugates of this series. Analytical information is provided for each conjugate, and any special deviations from the established protocol are noted in the respective section.

##### **3.3.2.3.1. Synthesis of mPEO<sub>17</sub>-F<sub>1</sub>-OEt**

Synthesis of mPEO<sub>17</sub>-F<sub>1</sub>-OEt was similar to that of the other lower molecular weight F<sub>1</sub>-based conjugates. The resulting conjugate was a clear, waxy solid, which if IBCF impurities were present would have a yellow tint. Purification was facile, requiring a repeat wash to ensure removal of any by-products. Analysis by GPC reveals no degradation or additional products, showing a unimodal peak, with a partially broad character (Figure 3.56) due to the polymer component. The symmetrical character of the peak indicates that there are no (or negligible amounts of) impurities present in the conjugate. <sup>1</sup>H NMR analysis (Figure 3.57) shows well-defined peaks, with multiplicity clearly visible and

decreased peak intensities relative to the increased polymer backbone proton peak. The integral of the polymeric peak (Peak D) is 60 protons, which is lower than the 64 protons expected. This likely arises due to the accuracy of the technique (~95 %), and the increasingly broad nature of the polymeric peak. Integration of the phenyl peaks (Peak H) was 5, thus confirming that a species with a monosubstituted phenyl constituent is present in the product (i.e.  $\text{NH}_2\text{-F}_1\text{-OEt}$ ). The  $^{13}\text{C}$  NMR spectrum is similar to other  $\text{F}_1$ -based conjugates, with increased intensity for the carbons in the polymer backbone (Peak F), making the quaternary amide (Peak I) and especially the ester carbon peaks impractical to see at 171 and 174 ppm, respectively (Figure 3.58). Therefore, it is necessary to use the IR spectrum to confirm the presence of the presence of the amide bond.

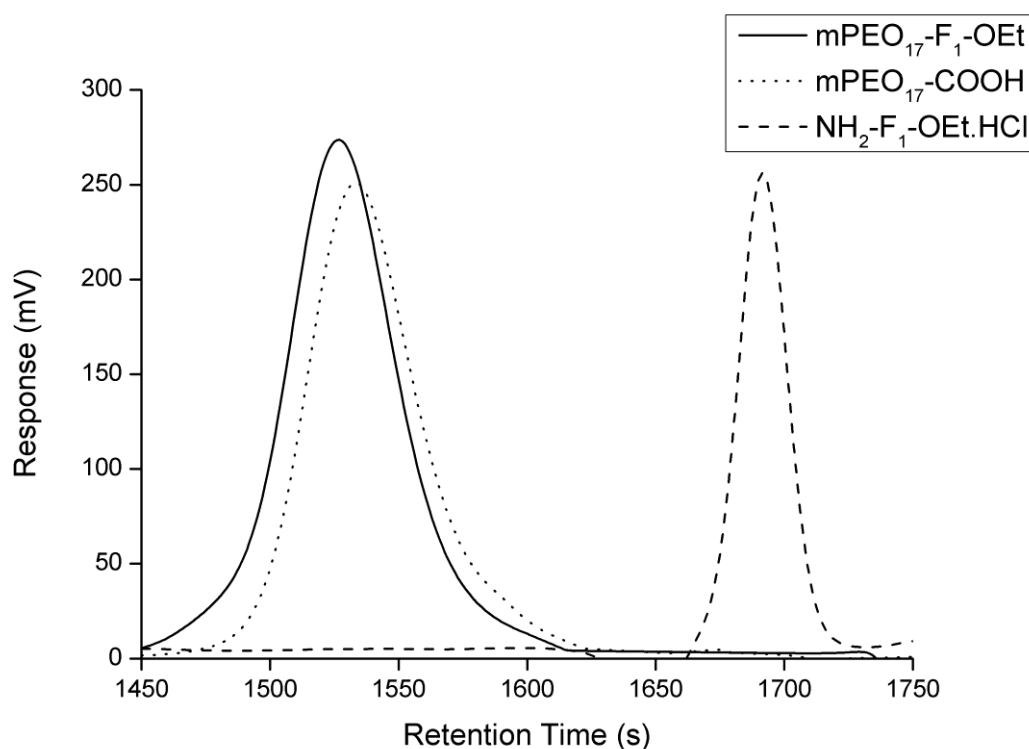


**Figure 3.56:** GPC trace of mPEO<sub>17</sub>-F<sub>1</sub>-OEt and precursor reagents.

The IR spectrum is similar to the other conjugate spectra, with a medium intensity peak at  $1454\text{ cm}^{-1}$  (Figure 3.59, Band G). There is a weak, broad band at  $3320\text{ cm}^{-1}$  (Band A), that is caused by the N-H stretch of a secondary amide bond. Stretching of the carbonyl group ( $\text{C}=\text{O}$ ) of this secondary amide bond

results in a medium intensity peak at  $1664\text{ cm}^{-1}$  (Band E), thus confirming the presence of a secondary amide bond. As the precursor peptide ( $\text{NH}_2\text{-F}_1\text{-OEt}$ ) does not contain a secondary amide bond, the origin of Band E can only be from successful coupling between the peptide and the polymer. Therefore, in addition to the other analytical data obtained, it can be seen that the synthesis of a pure conjugate was successful. Yields for the reaction were moderate, ranging from 54-73 %, which is slightly lower in comparison to the other  $\text{F}_1$ -based conjugates.

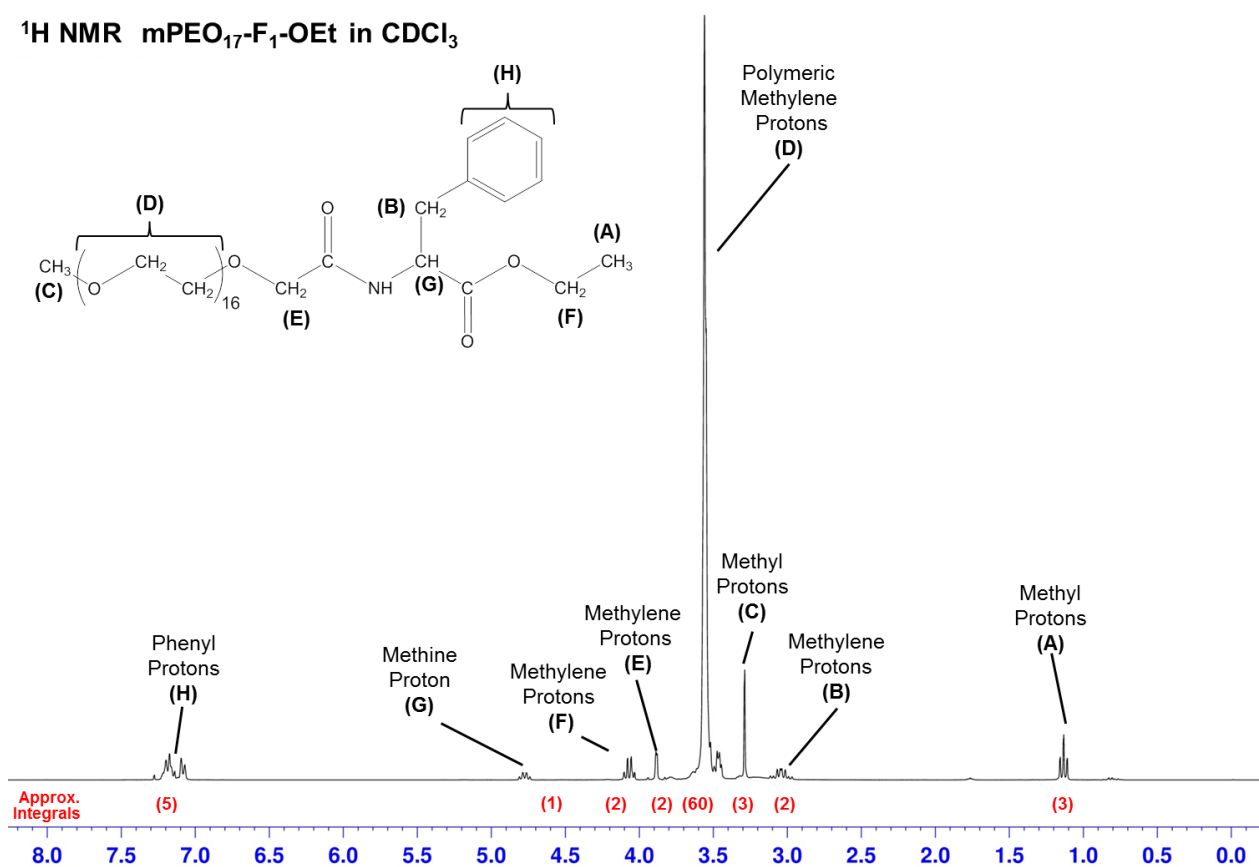


**Figure 3.57:**  $^1\text{H NMR}$  spectrum of mPEO<sub>17</sub>-F<sub>1</sub>-OEt.

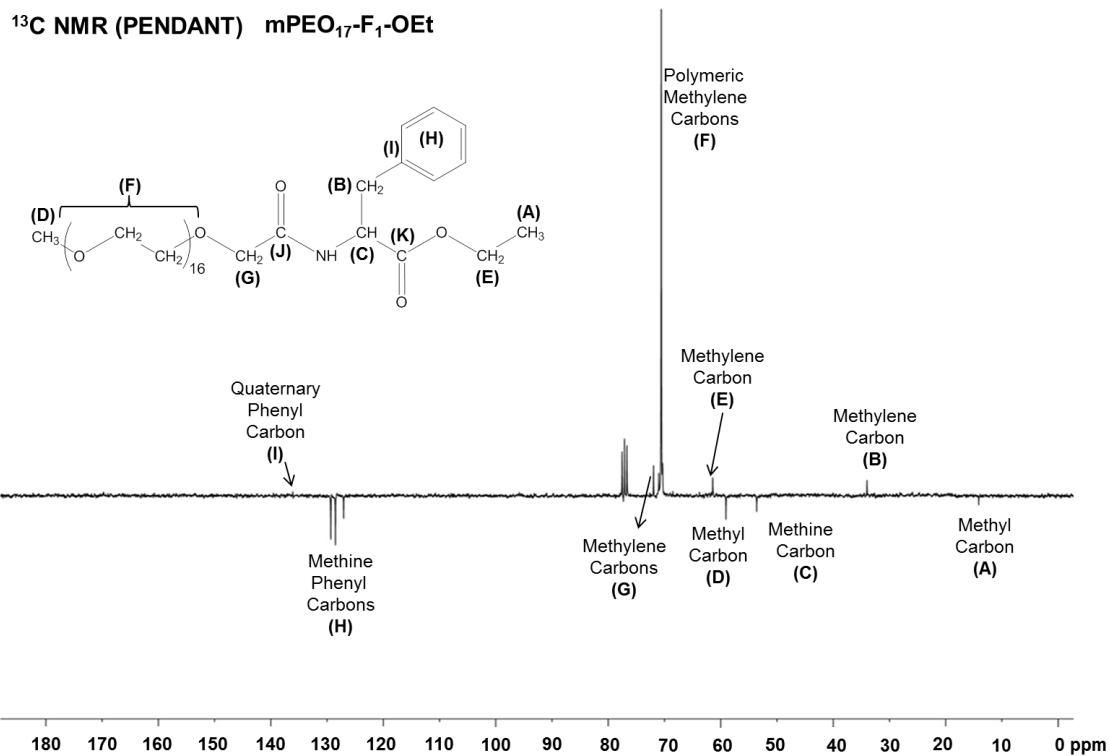


**Figure 3.58:** <sup>13</sup>C PENDANT NMR spectrum of mPEO<sub>17</sub>-F<sub>1</sub>-OEt.

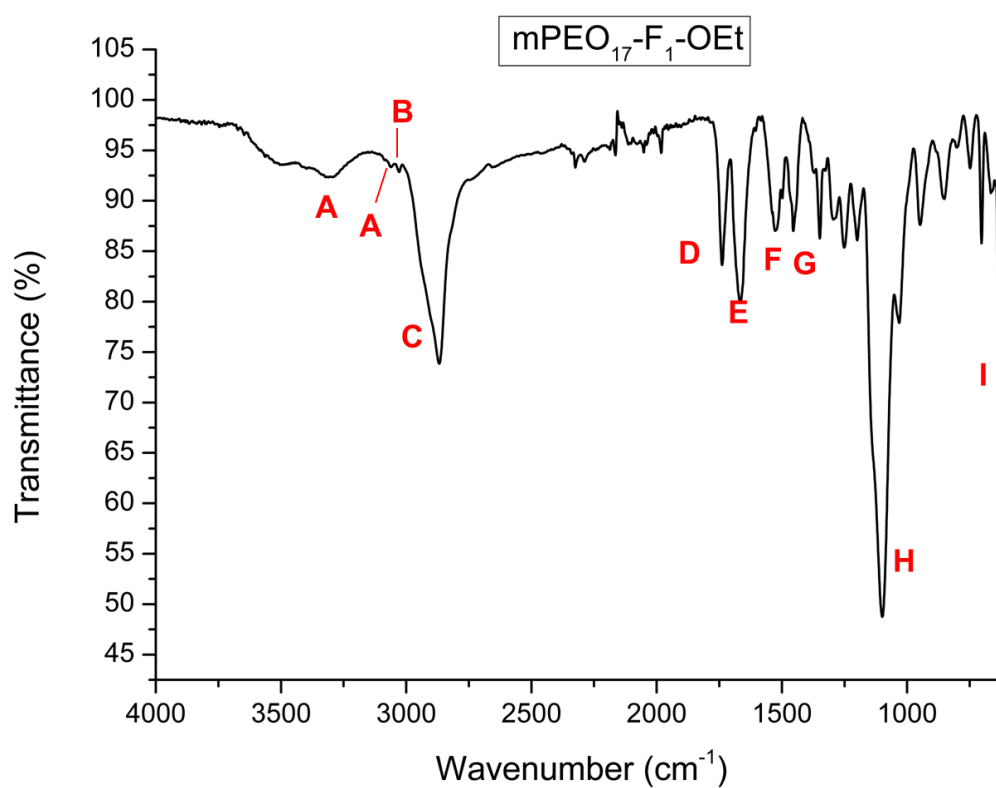


**Figure 3.59:** IR spectrum of mPEO<sub>17</sub>-F<sub>1</sub>-OEt. For peak assignments see Appendix A.

### 3.3.2.3.2. Synthesis of mPEO<sub>17</sub>-F<sub>2</sub>-OEt

Synthesis of mPEO<sub>17</sub>-F<sub>2</sub>-OEt was carried out according to the protocol outlined in Chapter 2. The conjugate produced was, like the preceding conjugate, a waxy solid. Initial GPC analysis (Figure 3.60) showed a symmetrical unimodal peak, which is slightly broader than the preceding conjugate and also conjugates with the same peptide length, but lower polymer size. No additional purification steps were required. The <sup>1</sup>H NMR spectrum (Figures 3.61) shows an increase in the relative intensity of the phenyl proton peaks (Peak H), with the integral rising from 5 protons to 10 protons, indicating that two monosubstituted phenyl rings are present in the conjugate (as expected). <sup>13</sup>C PENDANT NMR spectrum (Figure 3.62) is comparable to mPEO<sub>7</sub> and mPEO<sub>12</sub>-based conjugates. Of note, the methylene carbon (Peak B) shows multiple peaks, representing the different chemical environments. The IR spectrum shows minute differences in contrast to the other spectra of conjugates of comparable size (Figure 3.59). As aforementioned, a peak at 1454 cm<sup>-1</sup> is present, and peaks arising from an amide bond are also visible (Bands A and E).

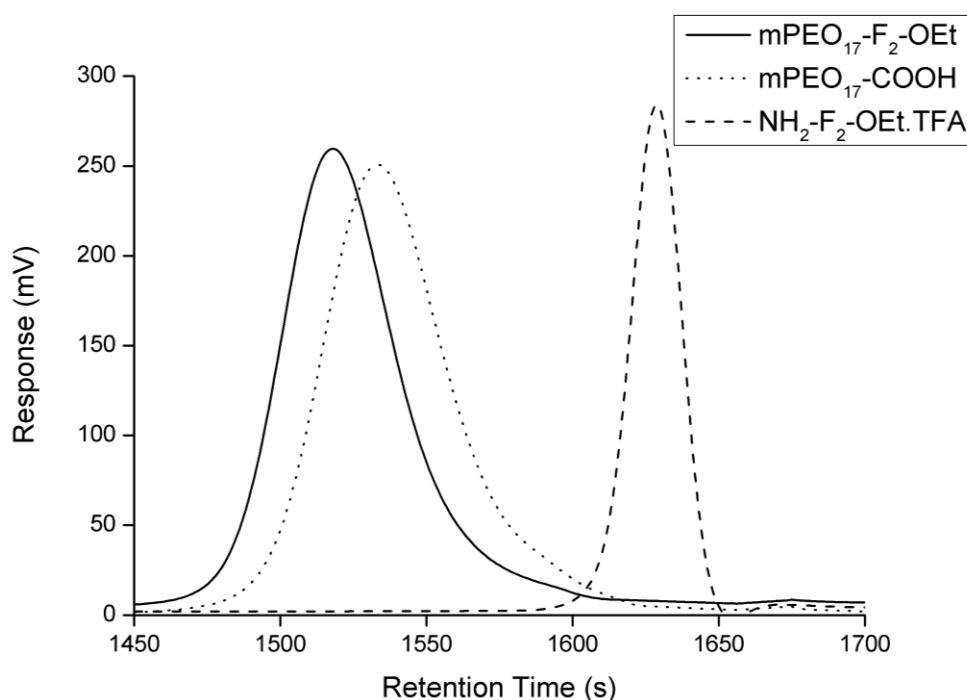


**Figure 3.60:** GPC trace of mPEO<sub>17</sub>-F<sub>2</sub>-OEt and precursor reagents.

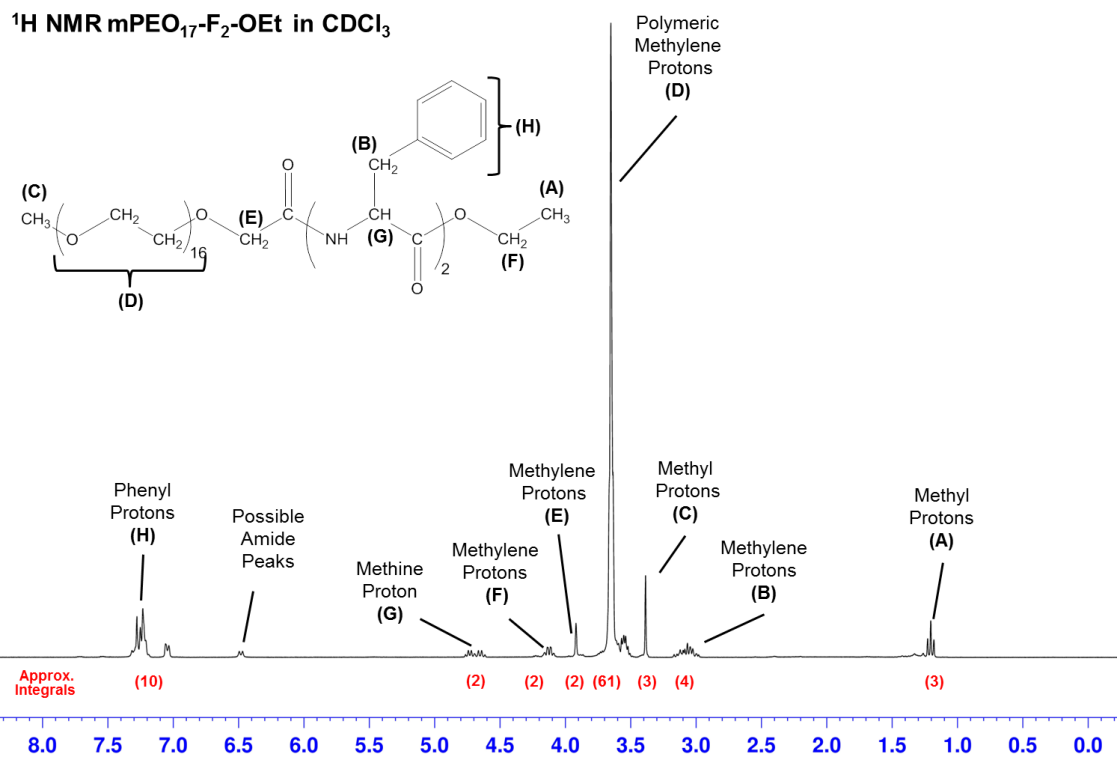


**Figure 3.61:** <sup>1</sup>H NMR spectrum of mPEO<sub>17</sub>-F<sub>2</sub>-OEt.

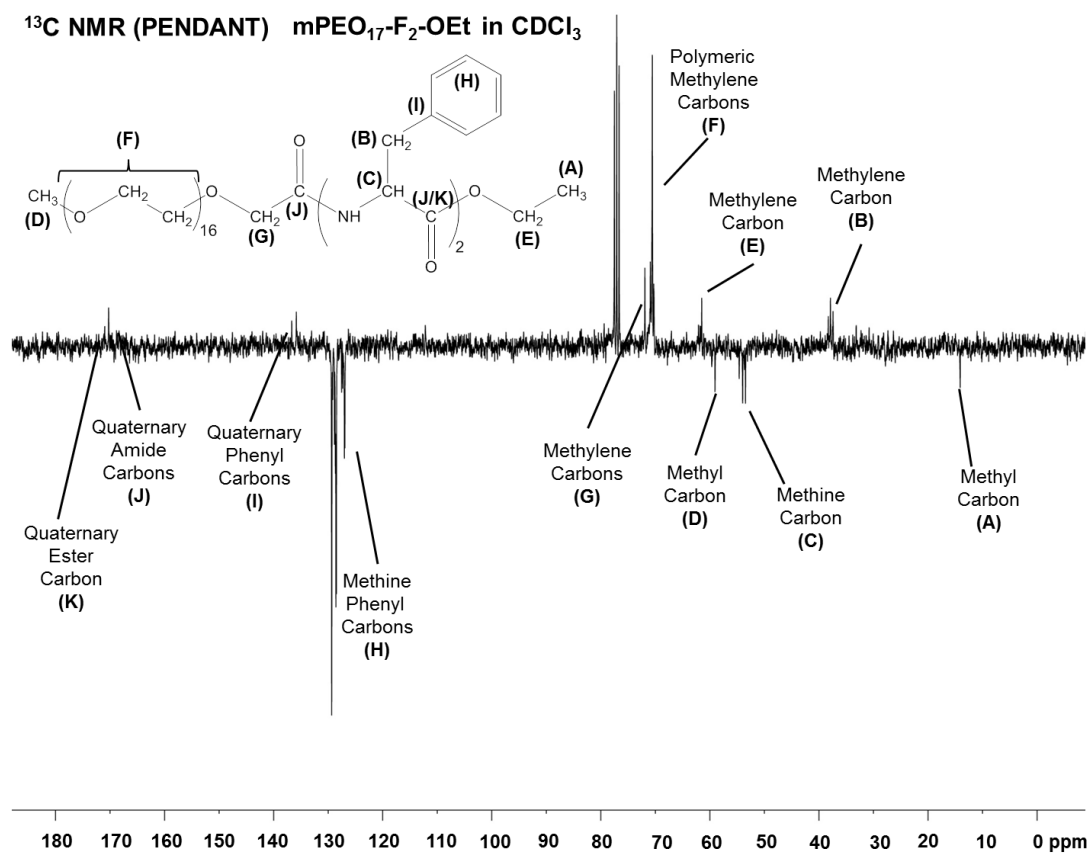


**Figure 3.62:** <sup>13</sup>C PENDANT NMR spectrum of mPEO<sub>17</sub>-F<sub>2</sub>-OEt.

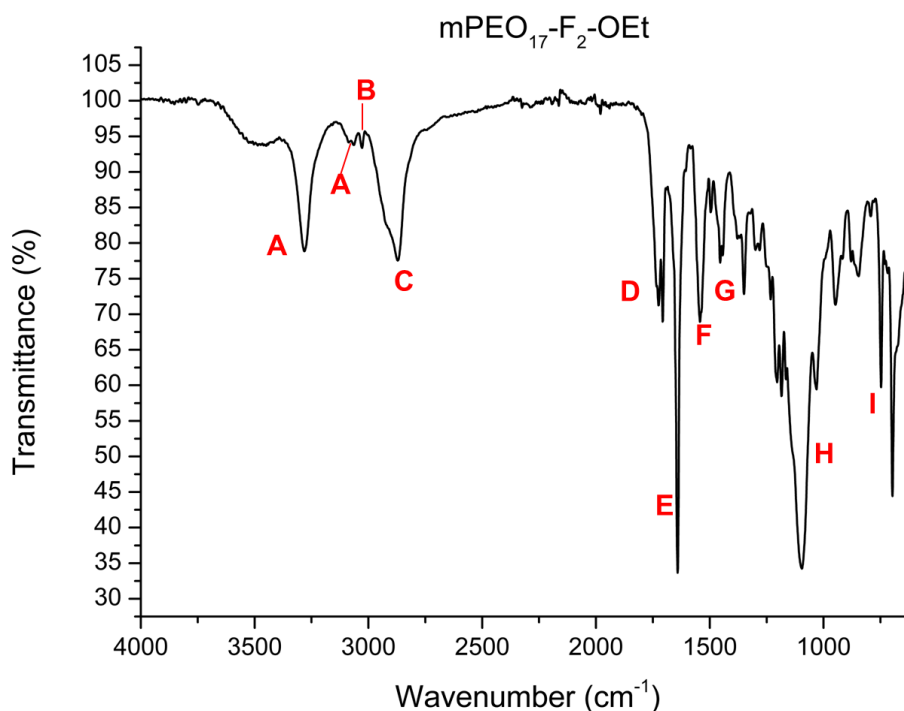


**Figure 3.63:** IR spectrum of mPEO<sub>17</sub>-F<sub>2</sub>-OEt. For peak assignments see Appendix A.

Overall, mPEO<sub>17</sub>-F<sub>2</sub>-OEt was synthesised to a high degree of purity, with moderate yields (ranging from 45 to 70 %), which is lower than mPEO<sub>7</sub>-F<sub>2</sub>-OEt and mPEO<sub>12</sub>-F<sub>2</sub>-OEt (91 and 90 %, respectively). This is attributable to the increasing incompatibility between the (larger) polymer and peptide components. Further increases to the peptide or polymer size (length) may result in further reductions of the yield.

### 3.3.2.3.3. *Synthesis of mPEO<sub>17</sub>-F<sub>3</sub>-OEt*

Like previous examples of F<sub>3</sub>-based conjugates, the synthesis of mPEO<sub>17</sub>-F<sub>3</sub>-OEt was not as straightforward forward as the other conjugates. The synthesis results in the production of a white solid. However, despite repeated washes and several recrystallisation attempts, the GPC trace shows a peak that is much broader than previously encountered, with a more prominent shoulder visible (Figure 3.64). This suggested that the product was contaminated with free polymer. Integration of the peaks in the <sup>1</sup>H NMR spectrum (Figure 3.65) shows that the polymer methylene peak represents

about 63 protons. However, the integral for the phenyl peaks was 12 protons, which is lower than expected. This was most likely due to polymer impurity in the sample, which is also reflected in the GPC peaks trace.

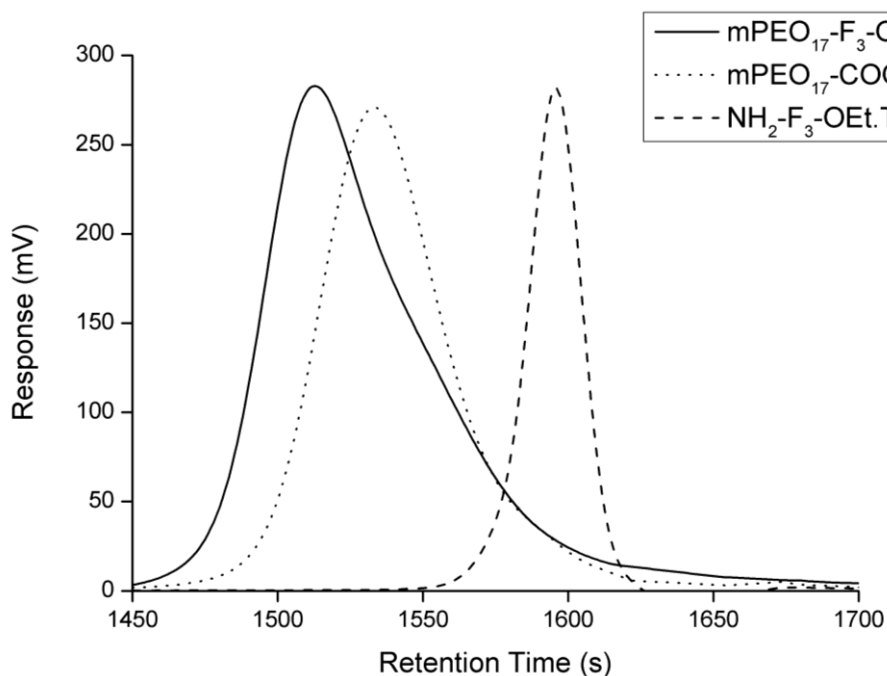


Figure 3.64: GPC trace of mPEO<sub>17</sub>-F<sub>3</sub>-OEt and precursor reagents.

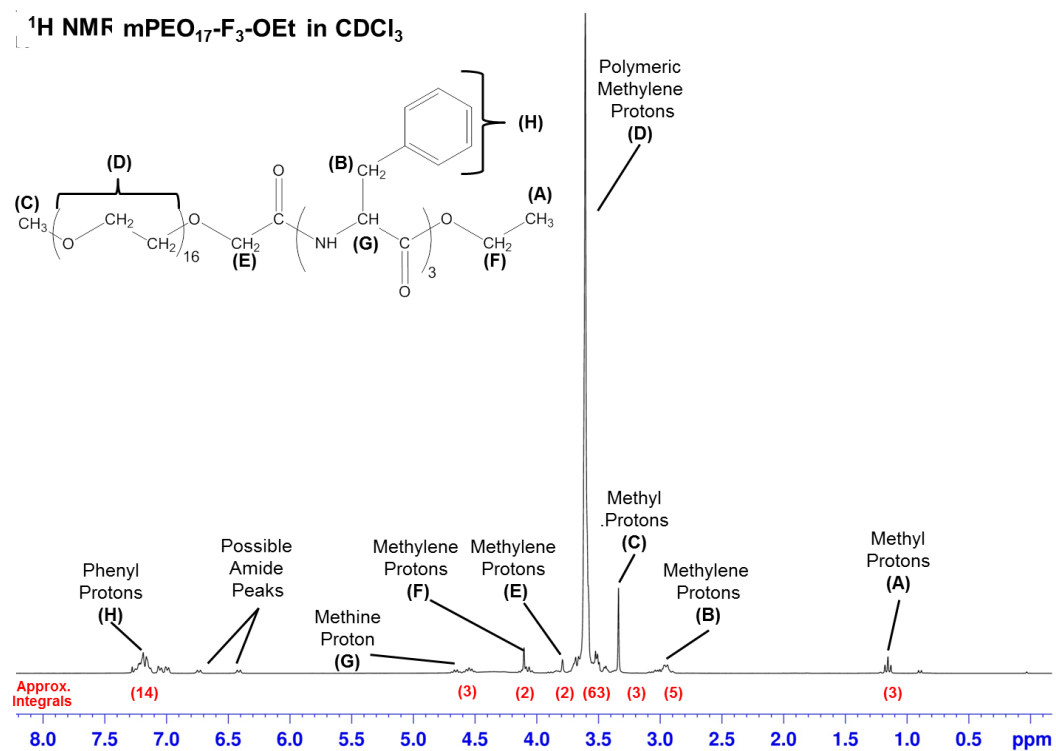
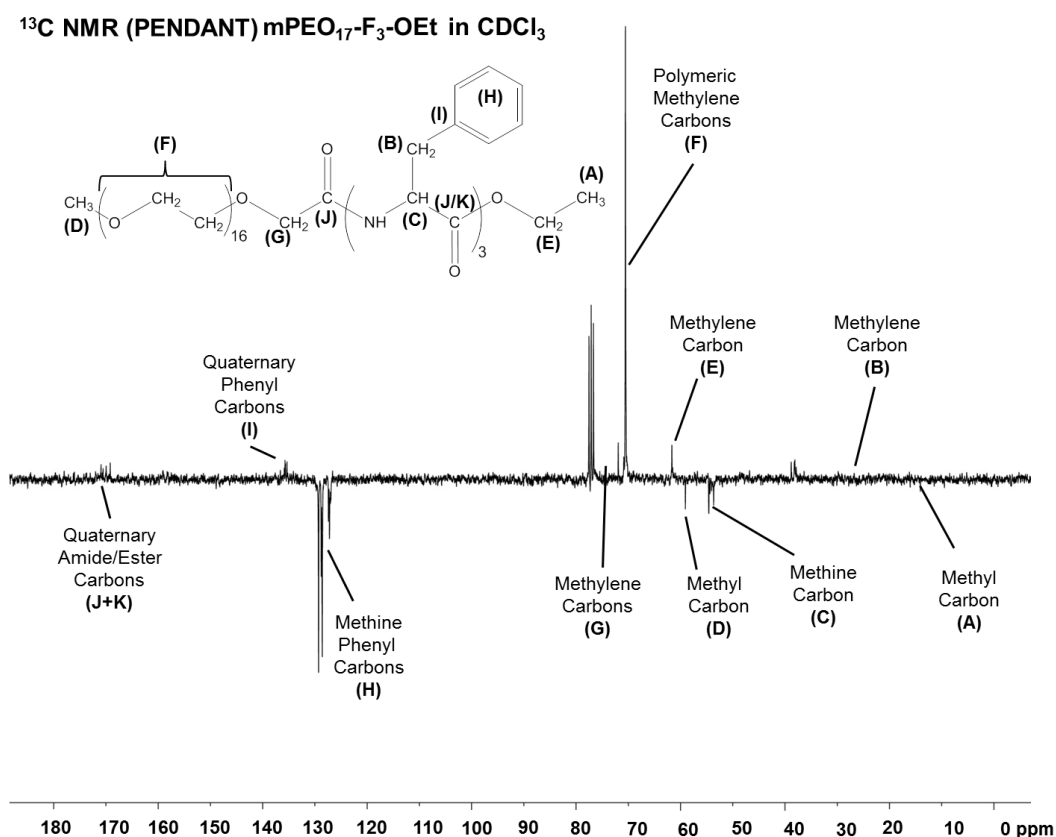


Figure 3.65: <sup>1</sup>H NMR spectrum of mPEO<sub>17</sub>-F<sub>3</sub>-OEt.

Analysis of the  $^{13}\text{C}$  PENDANT NMR spectrum (Figure 3.66) shows that the relative intensity of the phenyl and polymer carbon peaks (Peaks F and H, respectively) makes detection of the other peaks, such as the methyl carbon (and especially the quaternary carbon signals), difficult. Nevertheless, it can be seen that the amide carbon peak (Peak J) is present at 171 ppm and has multiple signals showing the differing environments that the amide carbon encounters (i.e. peptide-peptide bond and polymer-peptide bond). The ester peak cannot be seen at this resolution.



**Figure 3.66:**  $^{13}\text{C}$  PENDANT NMR spectrum of mPEO<sub>17</sub>-F<sub>3</sub>-OEt.

The IR spectrum is similar to the other conjugates analysed (Figure 3.62). Stretching of the N-H group of an amide bond appears at  $3278\text{ cm}^{-1}$ , and carbonyl stretching of an amide bond forms a peak at  $1637\text{ cm}^{-1}$ . The C-H deformation peak is again present at  $1454\text{ cm}^{-1}$ . Remarkably, the amide peak at  $1637\text{ cm}^{-1}$  has been slightly split into two signals suggesting a minimal difference in the amide bonds (peptide-peptide and polymer-peptide amide bonds).

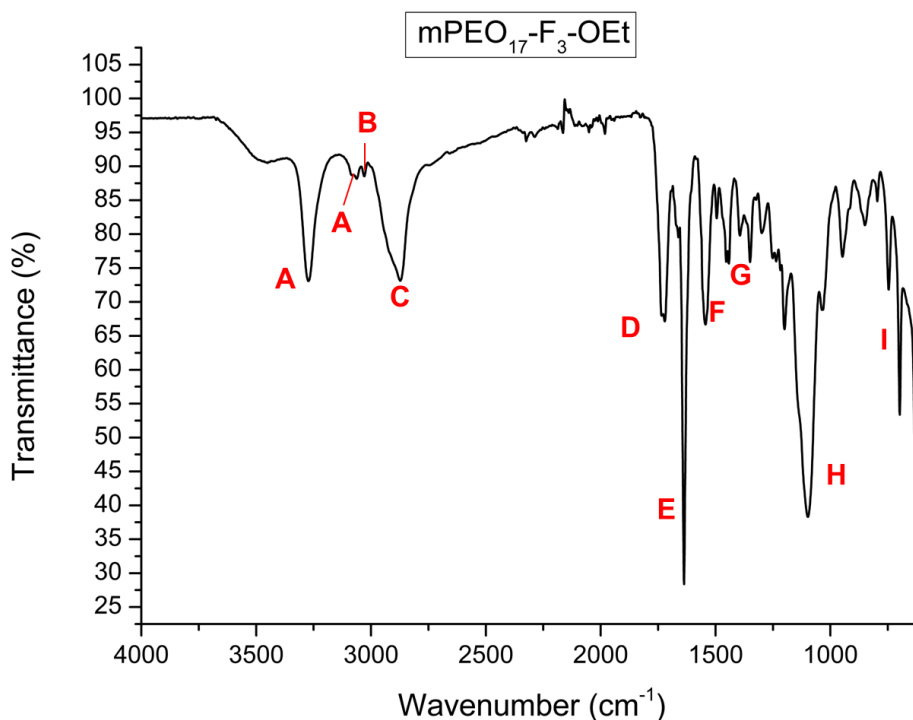


**Figure 3.67:** IR spectrum of mPEO<sub>17</sub>-F<sub>3</sub>-OEt. For peak assignments see Appendix A.

Synthesis of mPEO<sub>17</sub>-F<sub>3</sub>-OEt encountered some difficulty during purification. Analysis of the material revealed a broader GPC peak despite repeated purification. NMR and IR analysis confirmed that despite the broadness of the peak, the manufactured conjugate was pure. However, as expected, the yield for the reaction again decreased compared to the preceding PEO<sub>17</sub>-conjugate, ranging from 41 – 67 %.

#### **3.3.2.3.4. Synthesis of mPEO<sub>17</sub>-F<sub>4</sub>-OEt**

The final conjugate produced in the PEO<sub>17</sub> series was PEO<sub>17</sub>-F<sub>4</sub>-OEt. Synthesis was carried out as described in Chapter 2 with no modifications to the protocol or any additional purification required. The final conjugate produced was a white solid. Unlike previous PEO<sub>17</sub>-based conjugates, the product remained solid at elevated temperatures. Purification only involved repeated washes and reprecipitation when necessary.

In contrast to the GPC trace of PEO<sub>17</sub>-F<sub>3</sub>-OEt (Figure 3.64), it can be seen that the GPC trace for the reaction product is unimodal, and narrower, indicating no association of the starting materials, and no degradation (or additional products) as a result of the synthesis (Figure 3.68). <sup>1</sup>H NMR analysis shows an increase in the intensity of the polymer peak (integral of 66), but a relative decrease in the integral of the phenyl protons (18 protons instead of the expected 20) (Figure 3.69). The other integrals match the expected values. It can be seen that the peaks are now very broad, with multiplicity impossible to determine. Notably, on the <sup>13</sup>C PENDANT NMR spectrum (Figure 3.70), it can be seen that there are now multiple phased peaks, especially prevalent for the methylene carbon peak at 37 ppm (Peak B) and the methine carbon peak at 53 ppm (Peak C), which shows the difference in the chemical environment of these carbons. Both NMR spectra are dominated by the polymer peak, to the detriment of the resolution of the other signals.

The IR spectrum of mPEO<sub>17</sub>-F<sub>4</sub>-OEt (Figure 3.71), is typical of a conjugate spectrum, with the -CH deformation band present at 1454 cm<sup>-1</sup> and the critical amide bands visible at 3278 cm<sup>-1</sup> (N-H stretching) and 1637 cm<sup>-1</sup>.

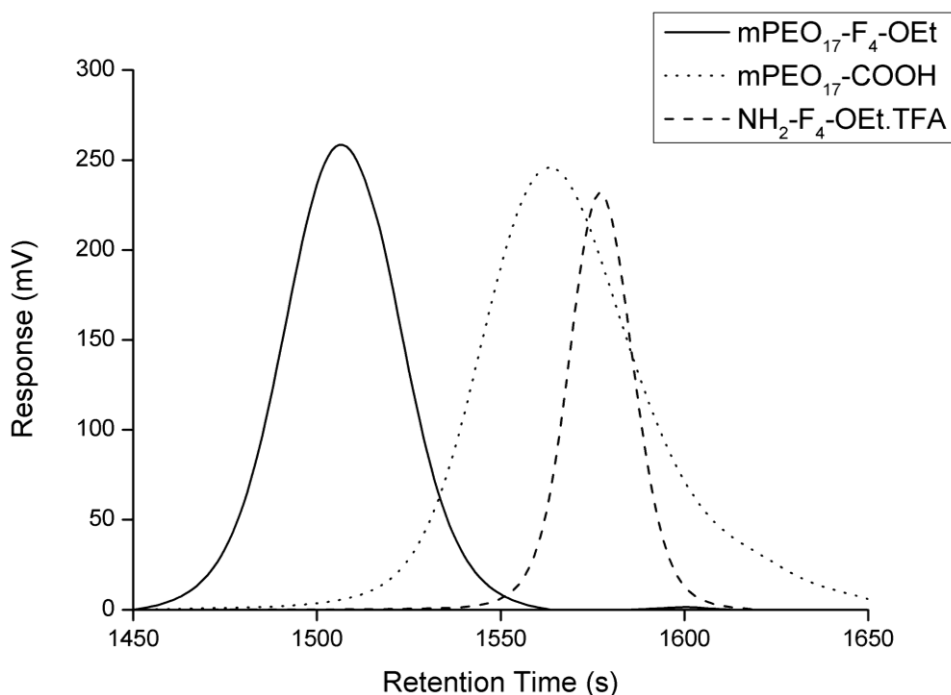


**Figure 3.68:** GPC trace of mPEO<sub>17</sub>-F<sub>4</sub>-OEt and precursor reagents.

$^1\text{H}$  NMR mPEO<sub>17</sub>-F<sub>4</sub>-OEt in CDCl<sub>3</sub>

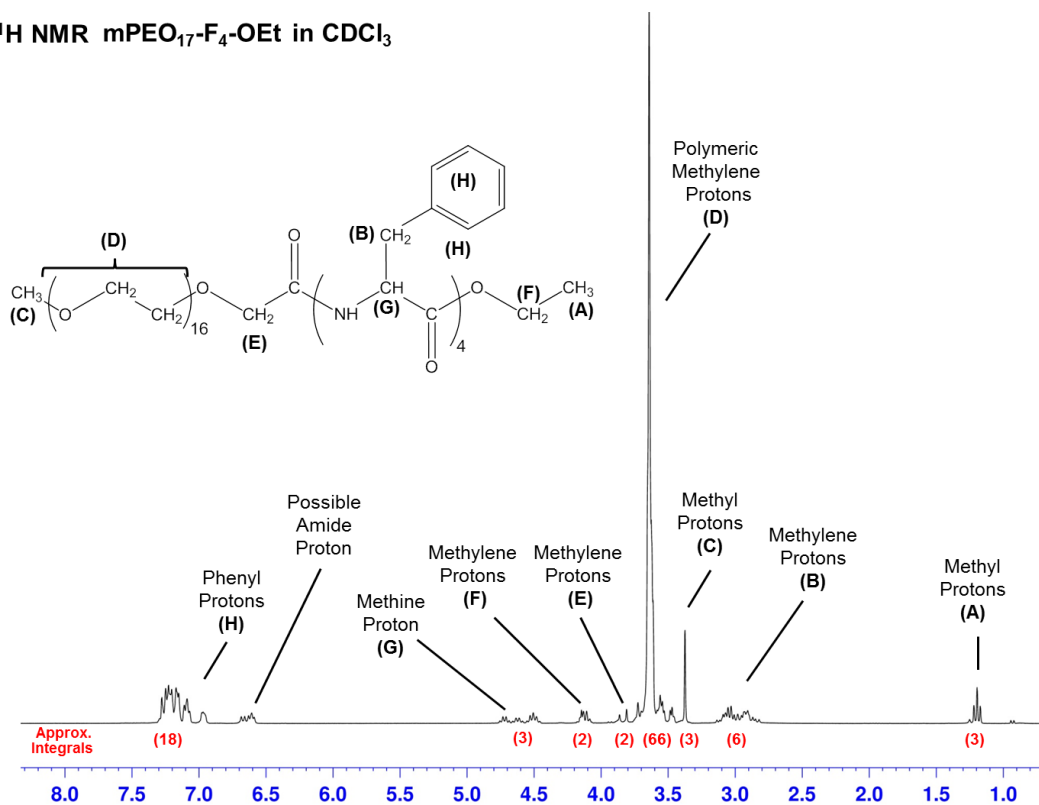


Figure 3.69:  $^1\text{H}$  NMR spectrum of mPEO<sub>17</sub>-F<sub>4</sub>-OEt.

$^{13}\text{C}$  NMR (PENDANT) mPEO<sub>17</sub>-F<sub>4</sub>-OEt

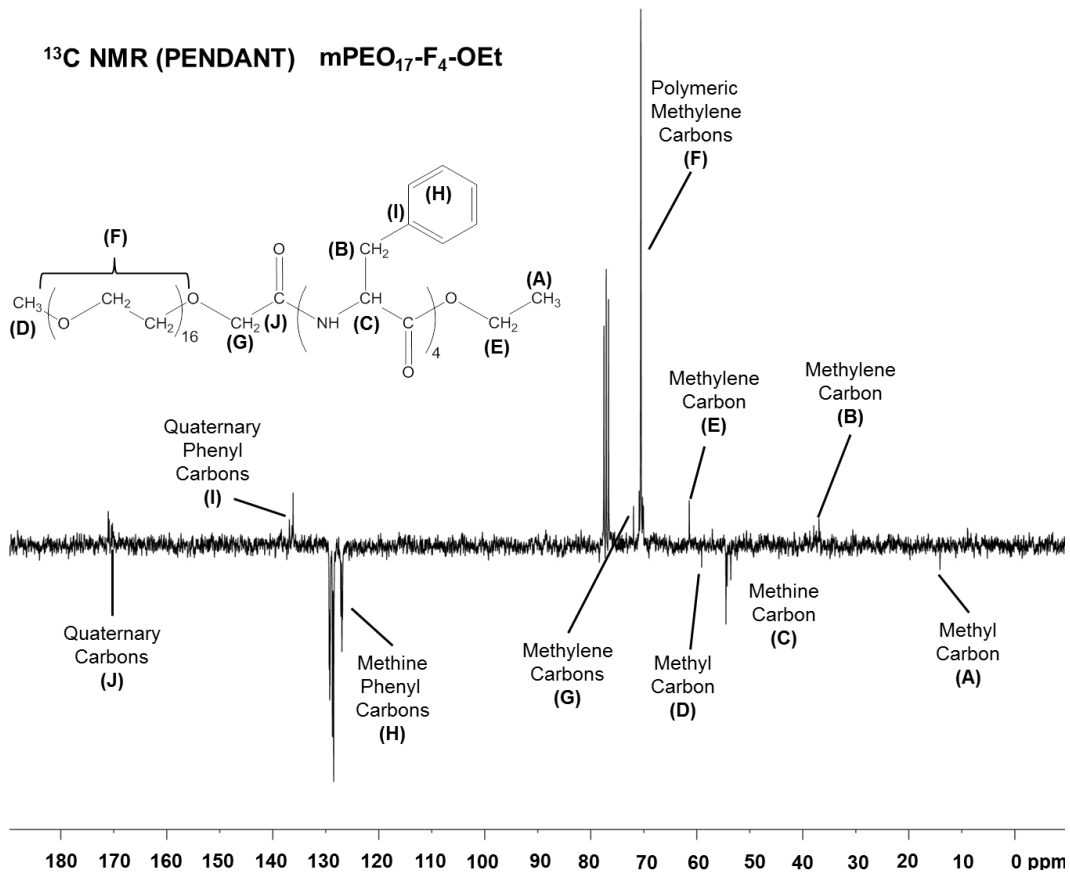
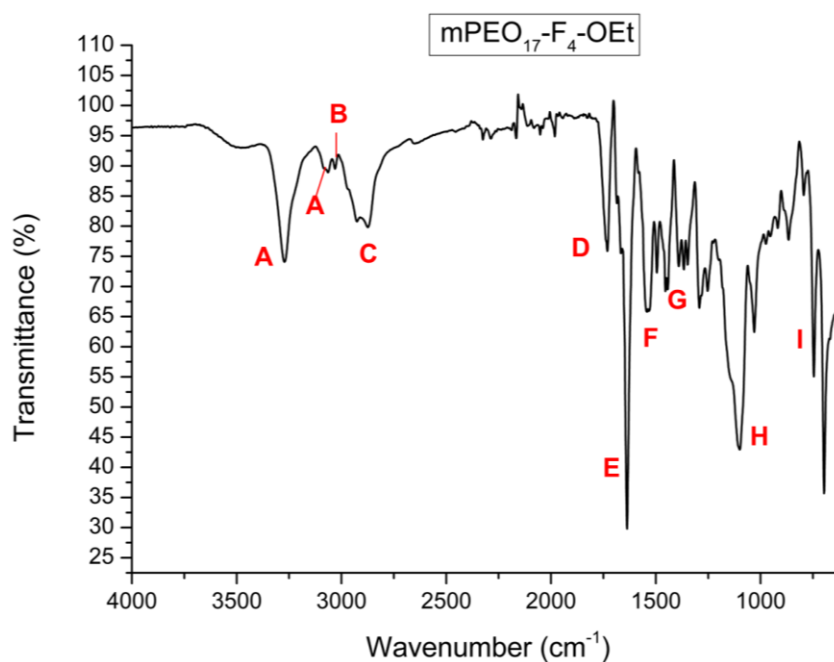


Figure 3.70:  $^{13}\text{C}$  PENDANT NMR spectrum of mPEO<sub>17</sub>-F<sub>4</sub>-OEt.



**Figure 3.71:** IR spectrum of mPEO<sub>17</sub>-F<sub>4</sub>-OEt. For peak assignments see Appendix A.

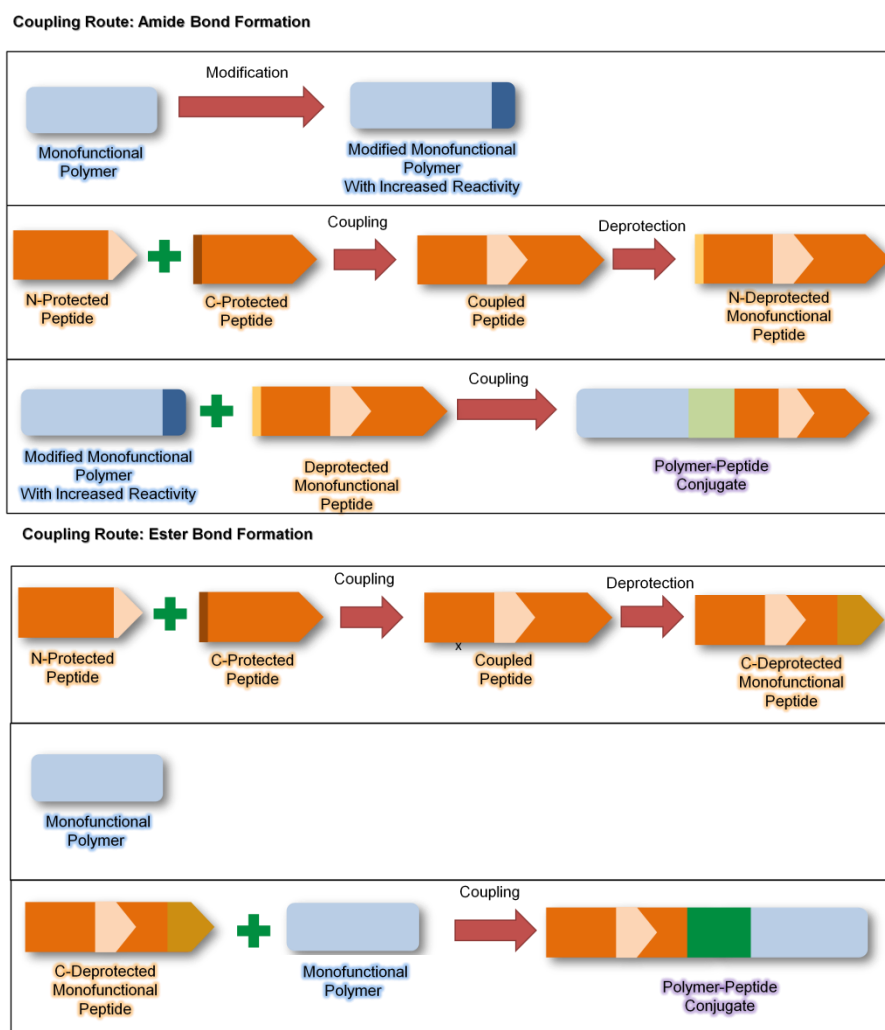
Synthesis of mPEO<sub>17</sub>-F<sub>4</sub>-OEt produced pure products with relative ease. In contrast to mPEO<sub>17</sub>-F<sub>3</sub>-OEt, the GPC trace was narrower without the need for extensive purification. Further analysis confirmed the purity of the synthesised conjugate. The yield for the reaction decreased compared to the preceding PEO<sub>17</sub>-conjugate, ranging from 37 to 50 %. This is also a reduction when comparing the product to conjugates with a smaller polymer component (i.e. PEO<sub>7</sub>- and PEO<sub>12</sub>- based conjugates).

### **3.3.2.3.5. Summary of the synthesis of mPEO<sub>17</sub>-containing conjugates**

Four well-defined conjugates containing mPEO<sub>17</sub>-COOH and phenylalanine oligopeptide homologues were produced using IBCF. Yields for each conjugate were moderate, and showed a further decrease as the peptide length increased, attributable to compatibility of both the peptide and polymer component, together with the more predictable steric effects (due to the longer polymer chain). Furthermore, whilst purification was generally facile, purification problems were encountered with the F<sub>3</sub>-based conjugate.

### 3.4. Alternative route for producing polymer-peptide conjugates

Sections 3.2 and 3.3 show how modifying monomethoxy-poly(ethylene oxide) with an appropriate (activated) functional group, a carboxylic acid, enabled direct conjugation to a peptide via the formation of an amide bond. A notable concern regarding the reaction is the use of chromium to oxidise the PEO-alcohol to an acid. Whilst rigorous and repeated washings were used to ensure complete elimination of the chromium, which is filtered off in the initial washing stages after polymer modification, it would be more beneficial not to use the toxic material at all. Accordingly, an alternative method was investigated in an attempt to overcome this problem (Scheme 3.5). Section 3.4 details the initial attempts of this method and compares it to the coupling efficiency described in Section 3.3.

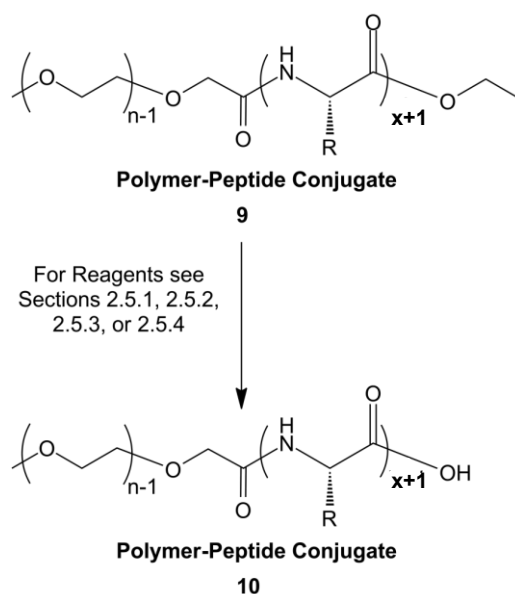


**Scheme 3.5:** Cartoon reaction scheme comparing general synthetic routes.

### 3.4.1. Proposed synthetic route for alternative production of polymer-peptide conjugates

The bi-functionality of peptides is one of their greatest strengths, but can also be viewed as a fundamental disadvantage. It is necessary to prevent the formation of mixed products and side reactions, which would ultimately lower the final yields and purities of a synthetic material. Therefore, protection strategies are routinely used to prevent side-reactions and to direct the synthesis. Section 3.1 details a protection/deprotection approach that targeted the amine terminus of the peptide. However, throughout all of the reaction stages the peptide was also protected on the carboxylic acid terminus as an ethyl ester.

Removal of the carboxylic terminus protecting group and exposing a group which can couple directly to mPEO<sub>n</sub>-OH, avoided the need for modification (and for chromium). Furthermore, this method could potentially be expanded for use on conjugates produced via the method outline in Section 3.3 (Scheme 3.6), to produce triblock copolymer-like structures.



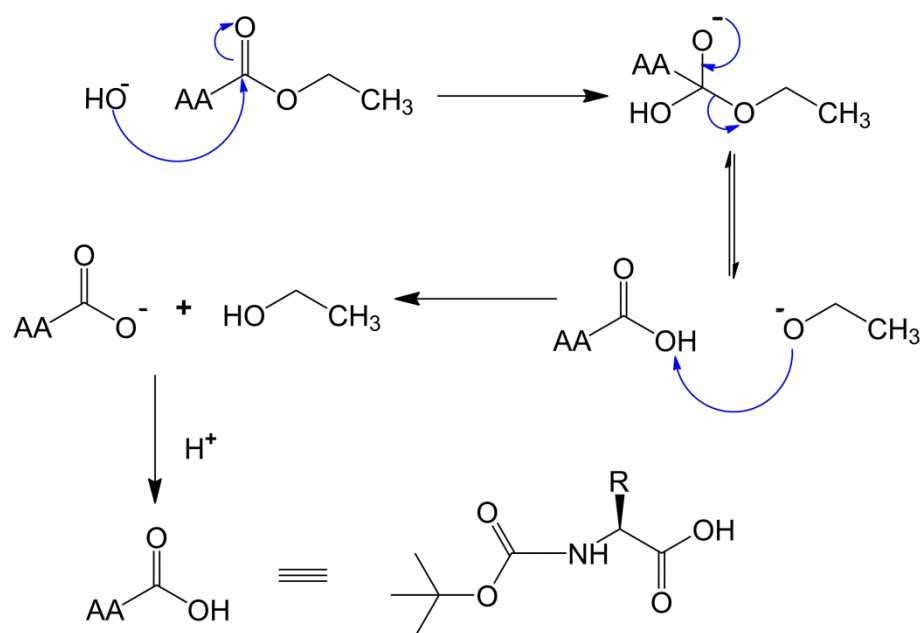
**Scheme 3.6:** Reaction scheme showing synthetic route for deprotecting the carboxyl terminus of a polymer-peptide conjugate.

#### 3.4.1.1. Deprotection of C-ethyl ester protected amino acids

The deprotection of C-ethyl ester-protected oligophenylalanine ( $F_x$ -OEt, where  $x > 1$ ) was undertaken. To ensure that the resulting peptide was monofunctional, Boc protection on the amine group remained. Several methods were considered for the deprotection of the ethyl ester. Four methods are described here, three of which are based around the use of lithium hydroxide (LiOH).

Deprotection involves converting an ester into a carboxylic acid (i.e. ester hydrolysis). This can be achieved either by using an acid or a base. Acid hydrolysis results in the formation of an acid and an alcohol. For example, acid hydrolysis of ethyl propanoate yields the formation of ethanol and propanoic acid. However, these reactions are reversible and the products formed may be difficult to separate. Indeed, whilst distillation can be used to separate the products, exposing peptides to high temperatures will potentially result in the formation of isomers, thus affecting the final yields. Acid hydrolysis would also lead to deprotection of the N-terminus. Conversely, base hydrolysis is generally a one-way process, which produces an alcohol and a salt, which is dependent on the base used (in this case a lithium salt would be formed). This allows for easier separation and the salt can then be converted to the corresponding carboxylic acid with excess dilute acid<sup>[5]</sup>. Base hydrolysis of esters is known as saponification (Scheme 3.7).

Initial deprotection was carried out using Method One as described in Section 2.5.1. The deprotected peptide was only sparingly soluble in the solvent system, thus was easily collected by filtration and then treated with dilute acid. This method was carried out on three peptides; Boc- $F_2$ -OEt, Boc- $F_3$ -OEt, and Boc- $F_4$ -OEt. These peptides were chosen as their synthesis was reliable, high yielding, and compatible with the solvent system (specifically an organic, chloroform-based solvent).



**Scheme 3.7:** Reaction scheme showing ester cleavage by base hydrolysis

(saponification) where AA represents one or more amino acids.

Figure 3.72 shows the  $^1\text{H}$  NMR spectrum of Boc-F<sub>2</sub>-OEt, and Figures 3.73 and 3.74 show the  $^1\text{H}$  and  $^{13}\text{C}$  PENDANT NMR spectra of the product after deprotection, respectively. It can clearly be seen that the peaks labelled **A** and **D** in Figure 3.72 are significantly reduced in the Boc-F<sub>2</sub>-COOH spectrum (Figure 3.73). These peaks are associated with the methyl protons (Peak A) and methylene protons (Peak D) of the ethyl ester protecting group. The functional group marked by the asterisk in Figure 3.73 is the remnant methyl end of the protecting group, and the integral of this group is 0.03 (relative to the Boc protons with an integral of nine in Figure 3.72 and 3.73), giving an approximate deprotection efficiency of 97%.  $^{13}\text{C}$  NMR spectrum shows the loss of the methyl signal, which was distinguishable at 27 ppm. IR analysis (Figure 3.75) reveals a broad band at  $3045\text{ cm}^{-1}$ , which is indicative of O-H stretching of a carboxylic acid group, and a sharp band at  $1730\text{ cm}^{-1}$ , which is indicative of carbonyl stretching of a carboxylic acid group.

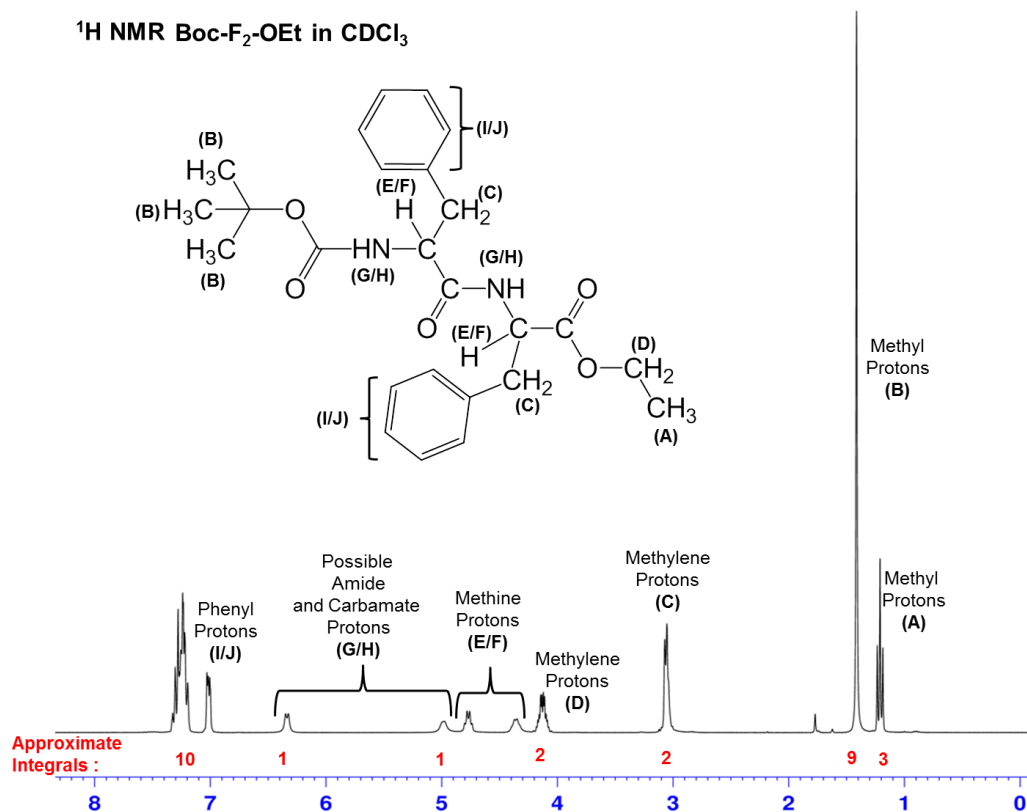


**Figure 3.72:** <sup>1</sup>H NMR spectrum of Boc-F<sub>2</sub>-OEt.

Although it can be seen that deprotection was carried out successfully and efficiently, the yields of the reactions varied greatly, ranging from 23% for Boc-F<sub>2</sub>-OEt, to 45% for Boc-F<sub>3</sub>-OEt, and 55% for Boc-F<sub>4</sub>-OEt. Such low and varied yields do not make the reaction reliable for the production of oligopeptides or for large scale processes.

Method One was not deemed a practical route for peptide production, however the ease of the reaction was favoured. Therefore, the effects of modifying this method of deprotection were investigated. Method Two (Section 2.5.2) was considered and initially tested. However, the process involved heating the peptide solution to high temperatures, which was undesirable. Consequently, Method Two was not carried forward.

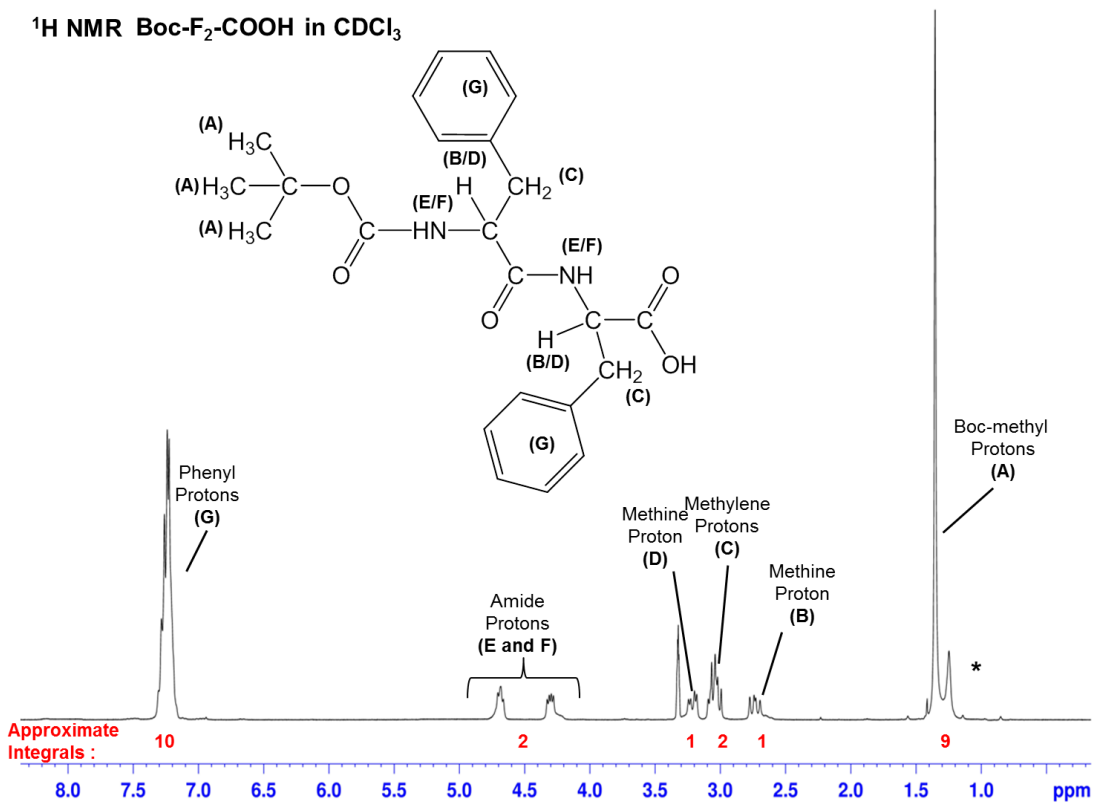


**Figure 3.73:** <sup>1</sup>H NMR spectrum of Boc-F<sub>2</sub>-COOH after deprotection using LiOH Method One.

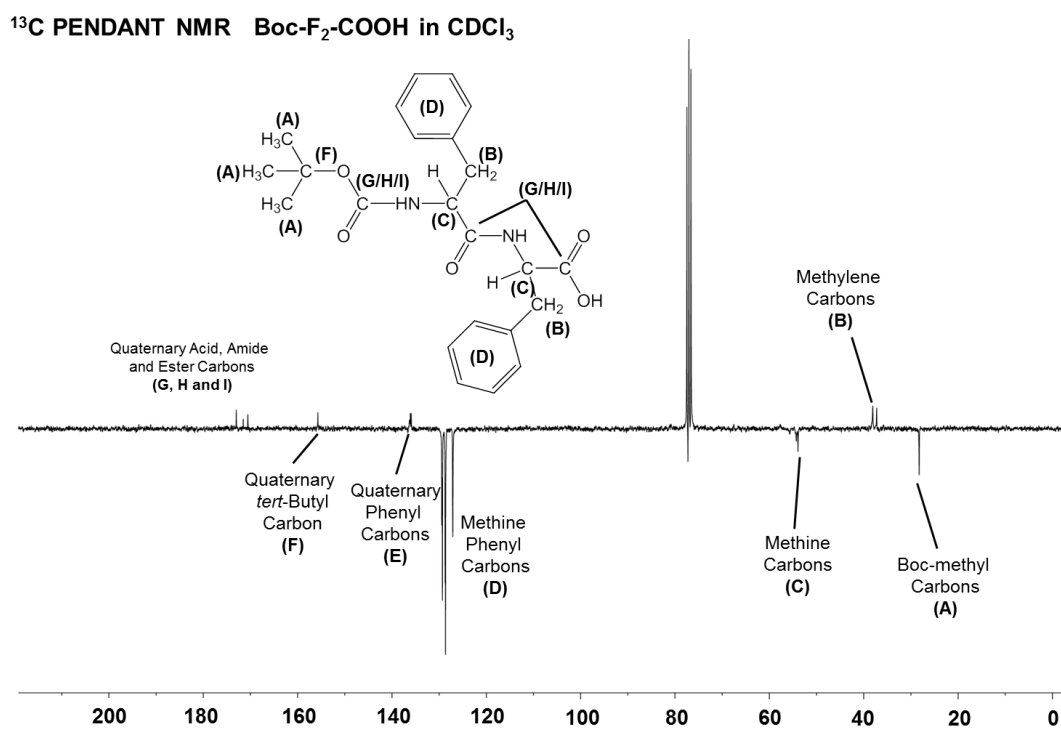


**Figure 3.74:** <sup>13</sup>C PENDANT spectrum of Boc-F<sub>2</sub>-COOH after deprotecting using LiOH Method One.

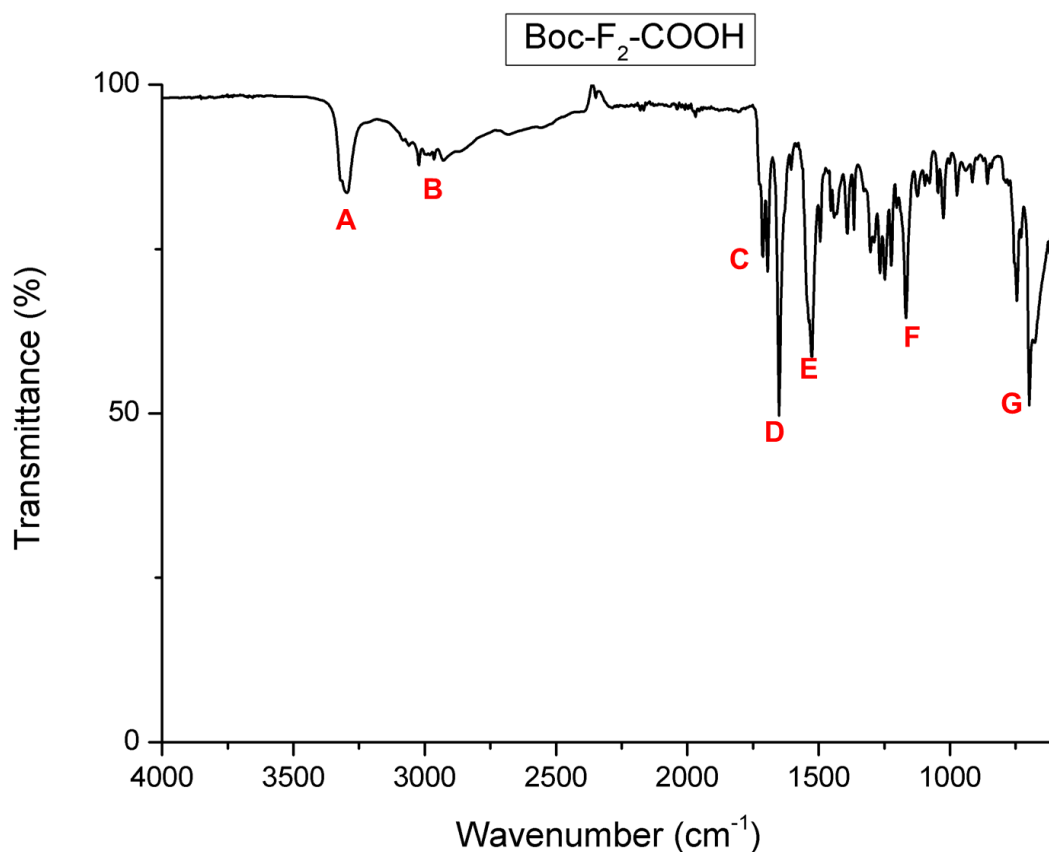


**Figure 3.75:** IR spectrum of Boc-F<sub>2</sub>-COOH after deprotection using LiOH Method One. For peak assignments see Appendix A.

Unlike the previous two methods, which were one-step processes, “Method Three” (Section 2.5.3) was a two-step process. However, the additional step was offset by the shorter reaction time compared to overnight reactions for Methods One and Two. The reaction could be completed in a few hours. A small amount of LiOH was initially added to establish the pH required. Additional LiOH was added later, to further increase the pH, followed by the addition of dilute acid. Purification consisted of extraction with ethyl acetate. Whilst the reaction time was shorter, yields were decreased, ranging from 18 to 35 % for all peptides.

Although, LiOH is generally effective for deprotection, the yields were not feasible for production of peptides and therefore this deprotection method was not considered a replacement for peptide production via Boc deprotection.

A final method for deprotection was investigated. *Bis*(tributyltin)oxide (BBTO) has been utilised previously for the deprotection of a range of esters<sup>[12, 13]</sup>. The deprotection herein was carried out as described in Section 2.5.4, using toluene as a solvent. This method was initially carried out on Boc-F<sub>2</sub>-OEt, which was chosen as it was easy to reliably reproduce the synthesis deprotection. Figure 3.76 shows the <sup>1</sup>H NMR spectrum of the product after the reaction had taken place.

On the spectrum (Figure 3.76) it can be seen that there are multitude of peaks upfield, between 0.9 and 1.7 ppm. They have integrals in ascending order of chemical shift of 18, 12, 20, and 11. It is known that the Boc protons should form a singlet peak with an integral of 9 within this region. However, none of the peaks show this character, although it is possible that the multiplet peaks are overlapping the signal. Figure 3.77 shows the <sup>1</sup>H NMR spectrum of the deprotecting agent BBTO. It can be seen that there are four peaks on the spectrum with integrals of 18 (Peak A), 10 (Peak B), 12 (Peak C), and 12 (Peak D). If this spectrum is compared to the spectrum of the deprotected product (Figure 3.76), the upfield peaks between 0.9 and 1.7 ppm correspond to the signals from BBTO, and indeed the integral ratios are not dissimilar. Of note, the third peak at 1.4 ppm has a much higher integral ratio than expected (20 instead of 12). As aforementioned, the singlet signal for the Boc protons is not visible on this spectrum, therefore coupled with the higher integral, it is assumed that this peak is the combination of the two signals.

Due to the broad nature of the BBTO peaks, the disappearance of the CH<sub>3</sub> signal from the protecting ethyl ester is difficult to note. In contrast, the reduction of the CH<sub>2</sub> ethyl ester peak at 4.1 ppm, labelled with an asterisk in Figure 3.76 (changing from an integral of 2 to 0.6), indicates that deprotection was successful. Comparison of the integral of the precursor and the product gives a deprotection efficiency of approximately 70 %. In contrast to this high efficiency, the yield for the reaction was poor; approximately 6 %. Furthermore, as can be seen from the <sup>1</sup>H NMR spectrum, the product is contaminated with the deprotecting reagent, despite purification. Further intensive purification, such as dialysis or column chromatography would be laborious, protracted, and

would present additional opportunities for yield reduction. Changing the reaction solvent from toluene to benzene yielded the same results. It is pertinent to note that during deprotection, elevated temperatures are required (up to 80 °C), which can affect the peptide and lead to a mixture of products. For these reasons, BBTO was not considered a viable route for the manufacture of C-terminal deprotected peptides.

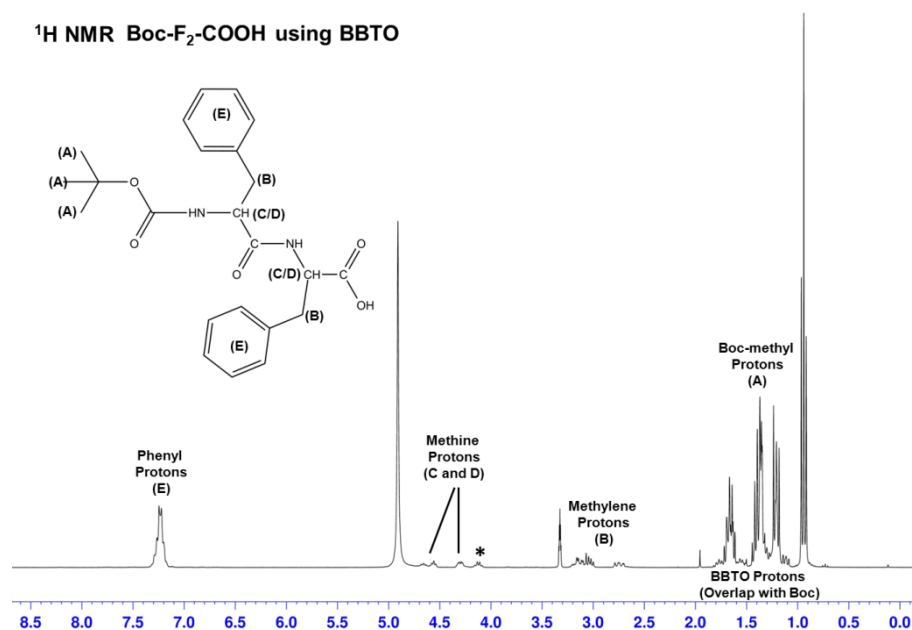


**Figure 3.76:** <sup>1</sup>H NMR spectrum of Boc-F<sub>2</sub>-COOH using BBTO deprotection.

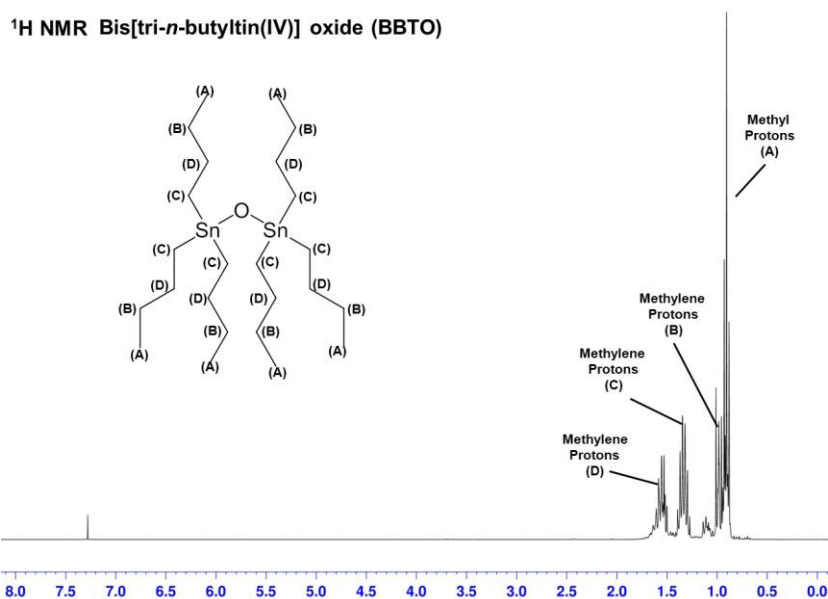


**Figure 3.77:** <sup>1</sup>H NMR spectrum of bis[tri-*n*-butyltin(IV)]oxide.

In summary, four different methods were used to deprotect the peptide component at the carboxylic acid terminus; three based on lithium hydroxide, and one based on BBTO. Lithium hydroxide was efficient, quick, and generally mild, though yields were moderate at best. By contrast, deprotection using BBTO was a long process requiring high temperatures, and was low yielding. Whilst lithium hydroxide is a superior deprotection technique compared to BBTO, in practical terms deprotection of the amine group (using trifluoroacetic acid to remove the Boc group) is milder, more facile, and higher yielding. Therefore, amine deprotection is the favoured method for producing functional peptides.

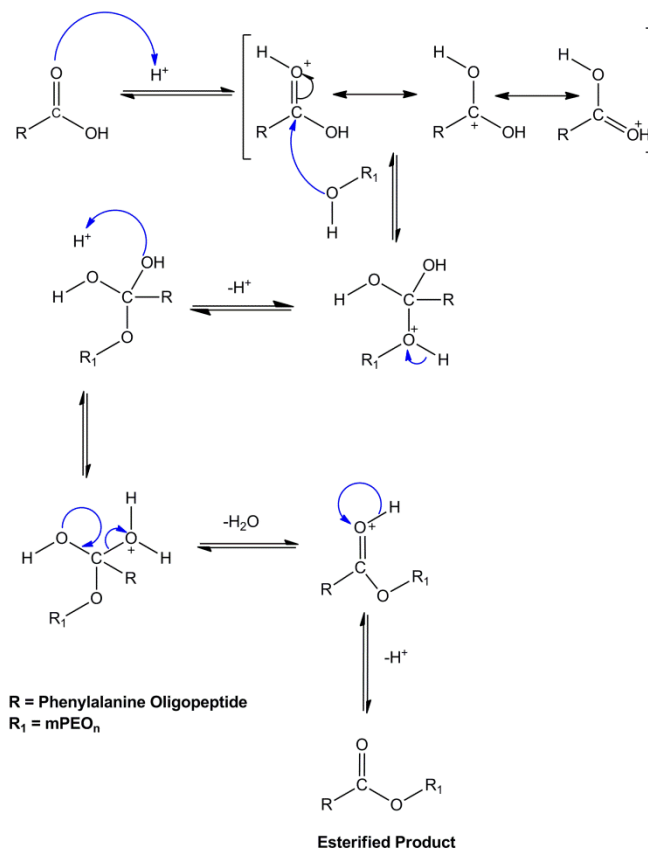
#### 3.4.1.2. *Production of polymer-peptide conjugates using C-terminal deprotected peptides using Fischer Esterification*

Using peptides with a reactive carboxylic acid terminus allows for the potential production of polymer-peptide conjugates without the need for polymer modification. This can be achieved using esterification. Two methods of esterification were considered, Fischer esterification and Steglich esterification.

Fischer esterification introduces the carboxylic acid and alcohol in the presence of a strong acid, resulting in the formation of the ester and water as products. The reaction is reversible and therefore affected by the position of the equilibrium. By removing the water, thus exploiting Le Chatelier's principle, the product yields can be increased. However, this therefore requires that the reaction be undertaken in an environment in which exposure to water is minimised (such as through anhydrous solvents, dried glassware, sealed systems). This introduces additional costs and enhanced environment impact. Scheme 3.8 shows the reaction mechanism for this esterification.

An experiment was undertaken using the protocols as described in Chapter 2. Boc-F<sub>2</sub>-COOH (deprotected using LiOH) was coupled with mPEO<sub>7</sub>-OH using sulfuric acid. To ensure that water was removed from the reaction, a Dean-Stark separator was used to collect the water produced, thus shifting the equilibrium towards ester formation. After refluxing overnight at 80 °C, the

product was then purified by washing. Already, the process was noted to have unfavourable conditions for peptides; high temperatures can lead to racemisation.



**Scheme 3.8:** Fischer esterification between an acid (deprotected peptide) and an alcohol (polymer).

The  $^1\text{H}$  NMR spectrum of the product of the esterification reaction (Figure 3.78) showed a peak corresponding to the  $\text{CH}_2$  polymer backbone at 3.7 ppm, which had an integral of 26 (expected value was 28). Further, at 3.4 ppm was a peak resulting from the methyl protons on the polymer component of the molecule, which has been used as the reference point for the integrals (integral of three). These peaks confirmed that the product contains  $\text{mPEO}_7$ . However, there were no identifying signals for the peptide component. Notably, the phenyl peaks at 7.26 ppm were not present, nor are the Boc peaks at 1.1 ppm. This was further supported by the  $^{13}\text{C}$  PENDANT NMR spectrum (Figure 3.79), which showed three species present; the polymer backbone carbons at 69 ppm (positively phased), the methyl carbon at 60 ppm, and a further  $\text{CH}_2$  group at 62 ppm. This



The Boc group is removed from the peptide using TFA. It is speculated that during the esterification, sulfuric acid (which is a strong acid) interacted with the peptide and cleaved the Boc group. The free peptide units could then interact with each other (forming long hydrophobic oligopeptides) that would be removed by extraction. Using a weaker acid that would not interfere with the protecting group would be offset by the increased reaction time. However, replacing the Boc group with a more tolerant protecting group, for example Fmoc, may overcome this problem. This provides a good avenue for future work, as well as a reaction that does not require elevated temperatures. In summary, Fischer esterification was not considered a viable route for the production of polymer-peptide conjugates, due to the sensitivity of the protecting group to the acidic conditions necessary.

#### *3.4.1.3. Production of polymer-peptide conjugates using C-terminal deprotected peptides using Steglich Esterification*

An alternative method to Fischer esterification, Steglich esterification, was considered for the manufacture of conjugates. Steglich esterification uses a previously discarded coupling method; DCC coupling. In this protocol, DCC activates the carboxylic acid allowing the addition of the alcohol. The reaction was carried out as described in the protocol in Chapter 2. Unlike Fischer esterification, the reaction takes place at low temperatures (0 °C) initially and is then allowed to proceed at room temperature. <sup>1</sup>H and <sup>13</sup>C NMR analysis (Figures 3.80 and 3.81) showed several identifiable peaks, alongside possible contamination (such as the peak complex at 1.2 ppm). It can be seen that the backbone peak from the polymer is visible at 3.7 ppm with an integral of 22 (expected 28). This was much more downfield than the expected error arising from the accuracy of NMR, and is due to the different chemical environment of the protons next to the ester bond (Peak D), which when combined have an integral ratio of approximately 4. This is confirmed by the heteronuclear single quantum coherence (HSQC) spectrum (Figure 3.82). Notably, the peak at 1.3 ppm is representative of the Boc protons (which has an integral of 8.5) that were conspicuously absent from the spectrum of the Fischer esterification

product. Furthermore, the peak at 7.2 ppm is indicative of the phenyl protons, which has an integral of 9.4 (expected value of 10).

The  $^{13}\text{C}$  PENDANT NMR spectrum (Figure 3.81) also shows hallmark peaks, especially the polymer carbons at 72 ppm, the phenyl carbons at 130 ppm, and the Boc carbons at 28 ppm. Notably, the presence of the ester carbonyl carbon is visible, at relatively low intensity (Peak J) at 175 ppm, adjacent to the amide carbons (Peak I). Further, the methylene carbons adjacent to the polymer-peptide ester bond are visible (Peaks E). IR analysis shows that the product is similar to conjugates produced using IBCF coupling chemistry (Figure 3.83). Notably however, the bands at 1728 and 1660  $\text{cm}^{-1}$  (Bands D and E, respectively) are almost equal in intensity and are representative of carbonyl bond stretching in the ester and the amide groups. Analysis by GPC (Figure 3.84) shows a narrow peak with a slight bimodal character, arising from a small amount of impurity present associated with the final conjugate (notably, the main peak is symmetrical).

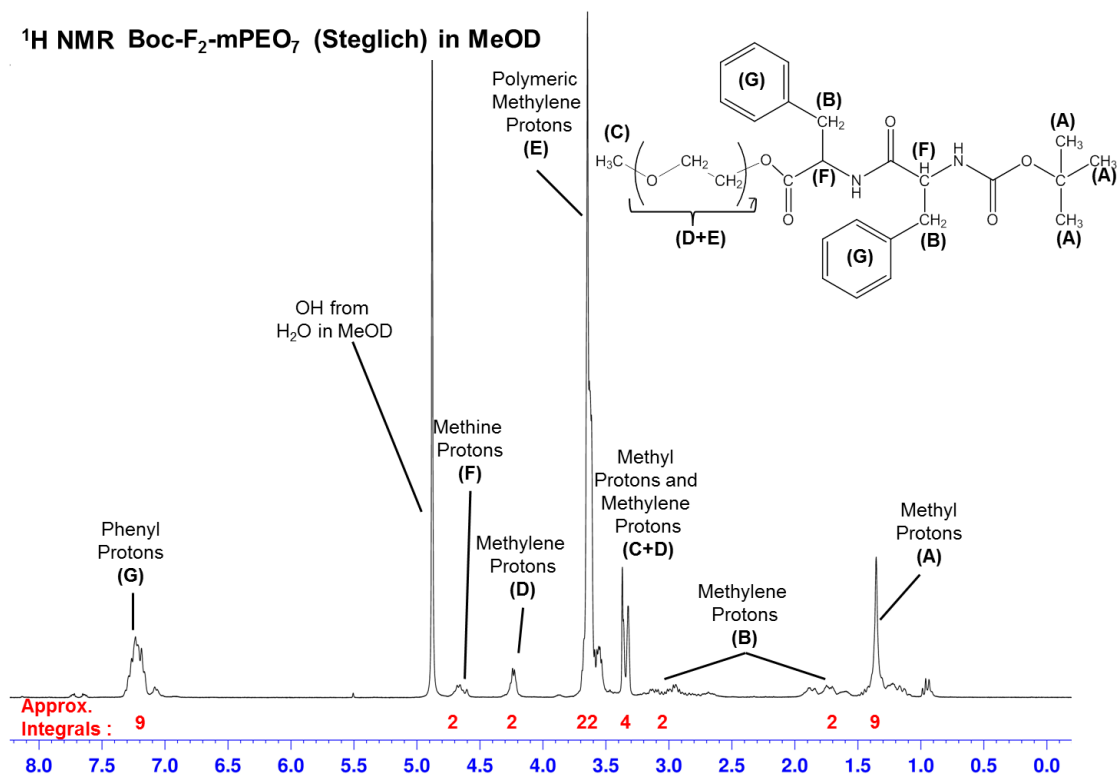


**Figure 3.80:**  $^1\text{H}$  NMR of product obtained from Steglich esterification between mPEO<sub>7</sub>-OH and Boc-F<sub>2</sub>-COOH.

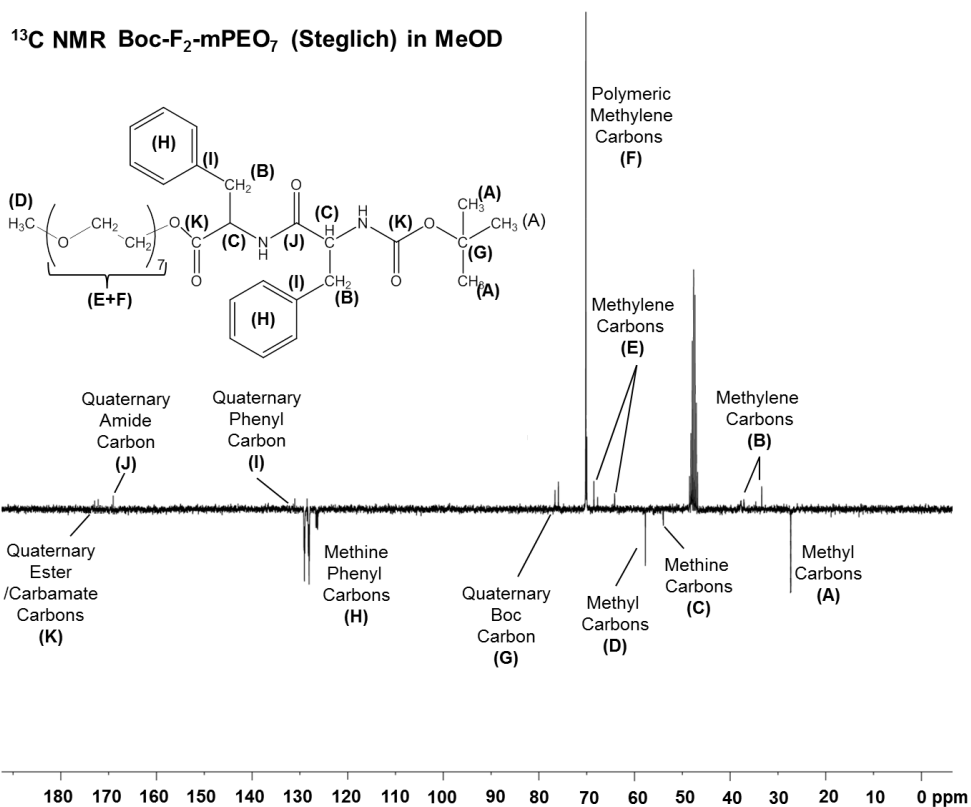


**Figure 3.81:** <sup>13</sup>C PENDANT NMR spectrum of product obtained from Steglich esterification between mPEO<sub>7</sub>-OH and Boc-F<sub>2</sub>-COOH.

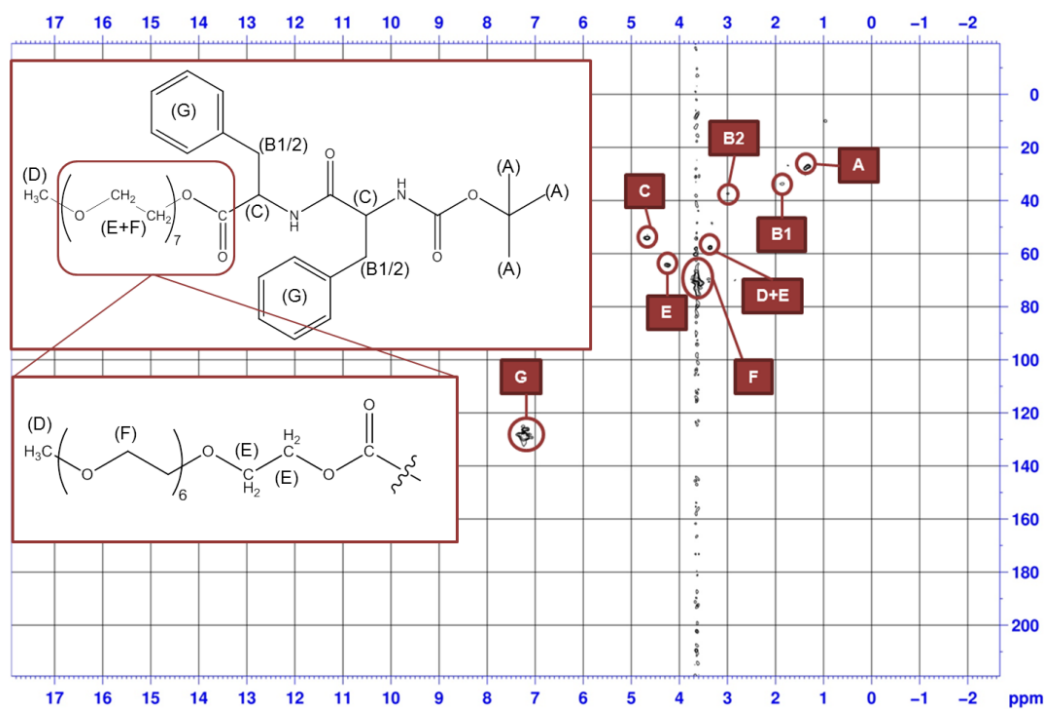


**Figure 3.82:** HSQC NMR spectrum of product obtained from Steglich esterification between mPEO<sub>7</sub>-OH and Boc-F<sub>2</sub>-COOH. Only cross-peaks have been labelled.

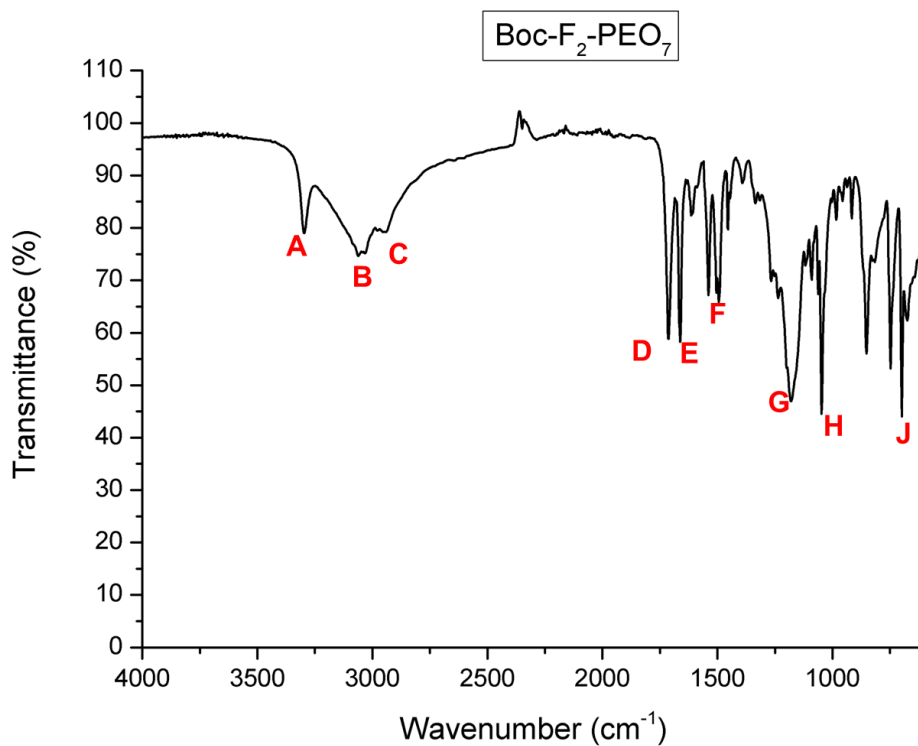


**Figure 3.83:** IR spectrum of product obtained from Steglich esterification between mPEO<sub>7</sub>-OH and Boc-F<sub>2</sub>-COOH. For peak assignments see Appendix A.

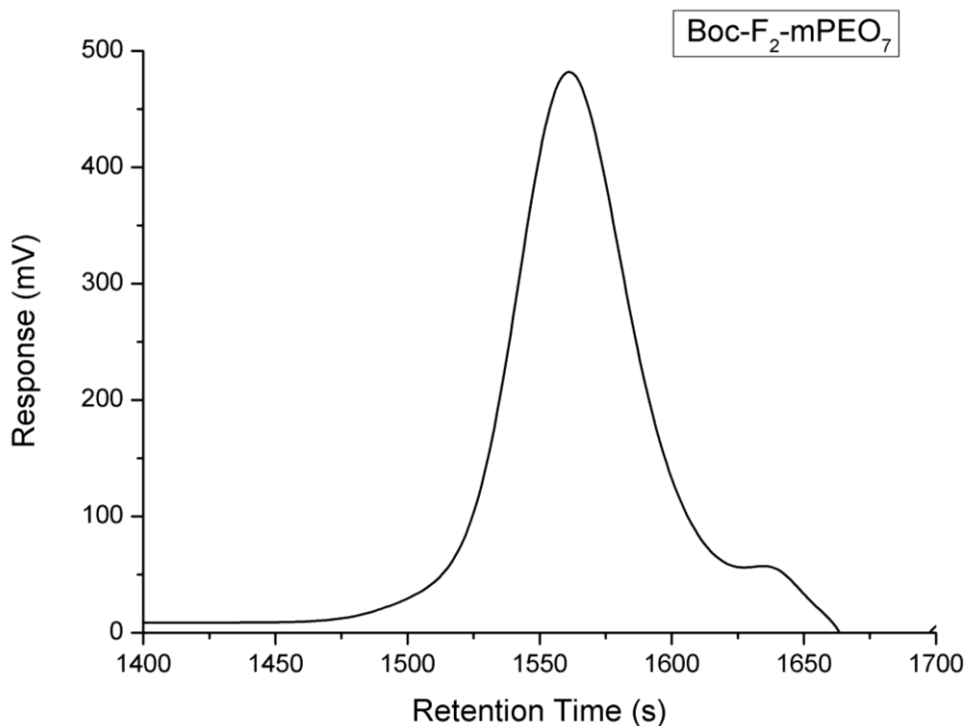


**Figure 3.84:** GPC trace of product obtained from Steglich esterification between mPEO<sub>7</sub>-OH and Boc-F<sub>2</sub>-COOH.

The yield for the reaction was moderate, with a maximum yield of 60 % obtained. In comparison to the yield for the equivalent conjugate produced by amidation via IBCF coupling, 91 %, this is substantially lower. Yields for the F<sub>3</sub>- and F<sub>4</sub>-based conjugates were similar; 52 and 49 %, respectively. The primary advantage of this technique was avoiding chromium use and conjugation without modification to the polymer component, resulting in shorter reaction times.

Although the production of conjugates in a short reaction time is desirable, the trade-off for yield and purity is not viable, and therefore this technique was not continued.

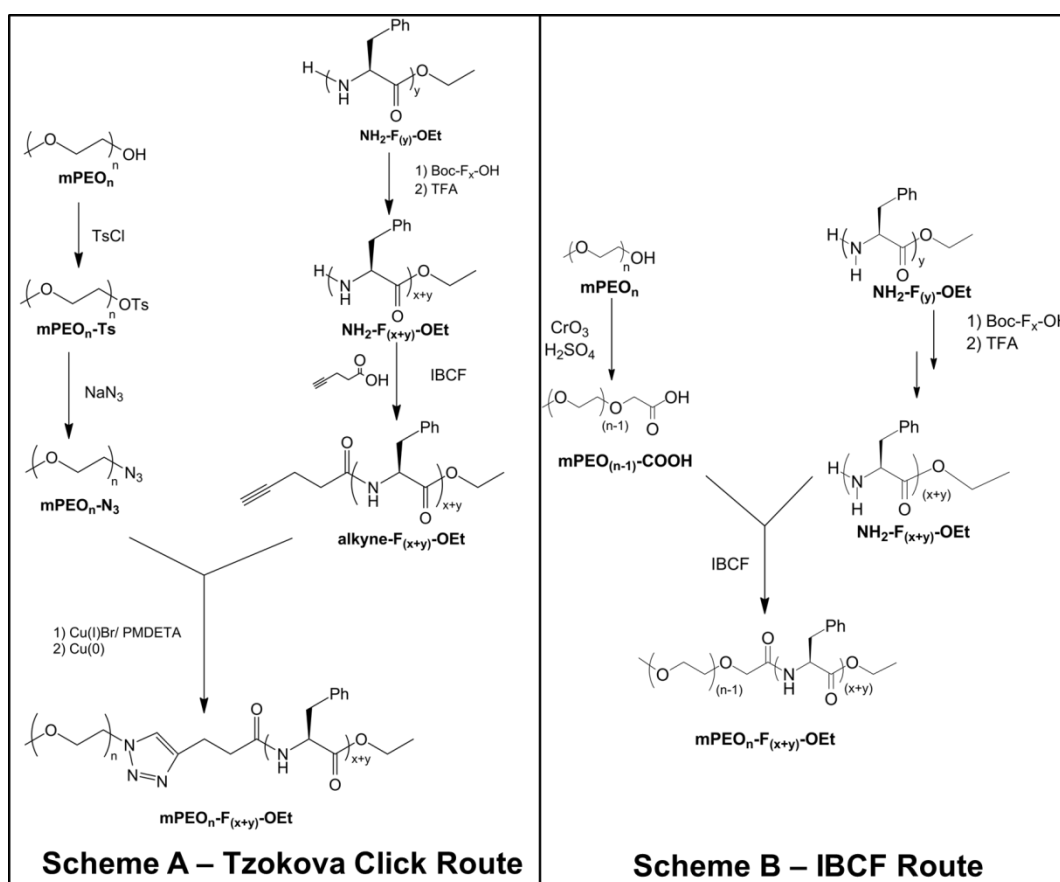
#### *3.4.1.4. Summary of alternative routes for conjugate production*

Deprotection of the C-terminus of Boc-F<sub>2</sub>-OEt via LiOH exposed a reactive carboxylic acid group that could be utilised for esterification with the polymer component. This potentially allowed for coupling without the need for the chromium or polymer modification, thus shortening the reaction times. Fischer esterification was used initially, however the Boc protecting group was incompatible with the reaction conditions required, thus no conjugate was produced. An alternative method, Steglich esterification was then undertaken. Esterification was successful producing a well-defined conjugate. However, the technique was not as high yielding as IBCF amide-bond formation, and so was not considered a viable as primary method to produce conjugates. However, future work undertaken in this area should focus on optimisation of the esterification protocol attempting to further increase the yield and purity.

### **3.5. Comparison of methods for production of polymer-peptide conjugates**

Previously, in the literature, a synthetic route was described where polymer-peptide conjugates were fabricated using click chemistry<sup>[14]</sup>. In this method the polymer was initially functionalised with a tosyl group, which is an excellent leaving group. This was subsequently reacted with sodium azide to

produce a PEO-azide. The peptide component was produced in the same manner as described in Section 3.1, via IBCF chemistry. After synthesis, 4-pentynoic acid was coupled to the N-terminus, thus introducing an alkyne group into the product. Finally, the peptide and polymer were coupled together using copper catalysed azide-alkyne cycloaddition, a form of “click chemistry”. Scheme 3.9 shows the previously described method **(A)** and the new method developed in this project **(B)**.



**Scheme 3.9:** Comparisons of reactions scheme for producing polymer-peptide conjugates; A) Tzokova Click Route <sup>[13]</sup> and B) IBCF Coupling Route.

Henceforth, the two methods will be referred to as **A** and **B** as shown on Scheme 3.9. Initial observations show that Scheme A has a greater number of steps than Scheme B. This is due to the need to overcome the poor leaving character of the hydroxyl group, which arises because of the strength of the C-OH bond. Unlike Scheme B, the coupling in Scheme A requires specific functional groups to process; an azide and an alkyne. Introduction of the azide

group to mPEO takes place via an S<sub>N</sub>2 reaction therefore prior conversion to the larger (and excellent leaving group) tosylate is critical. Introduction of the tosylate group is somewhat demanding, requiring a nitrogen atmosphere and dried solvents to prevent side reactions. Introduction of the tosylate group took place overnight, therefore increasing the reaction time of the scheme. Purification of the product was carried out using column chromatography. Insertion of the azide group was also an overnight reaction, requiring high temperature reflux.

In contrast, the preparation of mPEO for coupling in Scheme B was a one-step process. The alcohol was converted to an acid group by Jones oxidation, and purification involved filtration and washes. Yields for the final prepared mPEO, i.e. the compound used directly in the coupling reaction, were moderate. In Scheme A, reported yields were 69% for mPEO<sub>7</sub>. Conversely, the yield for Scheme B for mPEO<sub>7</sub> was 89%. Coupled with the shorter reaction time, this shows that Scheme B has more favourable synthetic conditions than A. However, the use of chromium is a disadvantage, as discussed in Section 3.2. An approximate cost-analysis of starting materials only shows that producing a functionalised polymer using Scheme A was 50% more expensive than using Scheme B. This was a crude calculation from the cost of all the materials used in modification, from Sigma-Aldrich and was found to be approximately £100 and £66, respectively.

Peptide synthesis in both schemes is the same. However, in Scheme A, an additional step was required to include an alkyne group necessary for the cycloaddition onto the polymer. This was achieved using 4-pentynoic acid, which formed an amide bond, thus introducing the alkyne group on to the peptide. The reaction conditions for this additional step were generally mild but included an overnight step, thus prolonging the overall reaction time. Purification via repeated washings was facile and the yield of alkyne functionalised peptide produced was reported to be high (95%). However, it is important to note that this is 95% of the synthesised peptide (which was F<sub>4</sub>). Therefore, the highest possible final yield of the peptide in Scheme A (assuming that the maximum yields were achieved as reported earlier<sup>[15]</sup>) was

71%. In comparison, the maximum possible yield for the peptide component (prior to coupling) is slightly higher at 75%, and again the reaction time is shorter.

In Scheme A, the coupling reaction shown is a copper-catalysed click reaction, which results in the formation of a 1,4-triazole ring however the reaction conditions are somewhat stringent. The peptide-alkyne and the polymer-azide were dissolved in dry THF under nitrogen. It was imperative that oxygen was removed from the system to prevent oxidation of the copper catalyst. Copper (I) bromide (CuBr) and a ligand (such as PMDETA) were dissolved in dry solvent and added to reaction mixture. After stirring for 24 hours, copper [Cu(0)] was added and the mixture stirred for an additional 24 hours. Purification of the product involves quenching with methanol, followed by silica gel column chromatography. This coupling reaction is a long process, taking at least three days. Furthermore, the purification is laborious and must be carried out rigorously to ensure the complete removal of all by-products and spent reactants. It is imperative copper is completely eliminated from the product, especially if the material is designed for use in biological systems, as it is toxic even at very low concentrations ( $1 \text{ mg m}^{-3}$  [16]). The yield for the coupling step was high (73%) and purity was also reported as high.

The coupling step in Scheme B has been described in Section 3.3. However, in comparison to Scheme A, the reaction conditions are significantly milder. The reaction vessel does not require purging, and whilst dry solvents are preferable, they are not critical. Furthermore, the reaction time is significantly shorter, with the coupling being a one-step overnight reaction. Purification was also simpler, utilising washing to remove unreacted starting material, and reprecipitation to remove the coupling reagent (in certain cases). More rigorous purification methods were rarely used; column chromatography was used in one instance and only as a final resort for one of the conjugates.

However, both reaction schemes show the use of a biologically toxic metal. Scheme A shows the use of copper in the coupling step (both a copper salt and copper metal), and Scheme B shows the use chromium (VI) oxide, which is

converted after the reaction to chromium (III) oxide. The use of a toxic metal is highly disadvantageous as rigorous purification must be undertaken to ensure removal, otherwise the product cannot be used in any biological systems. In Scheme A, the use of the copper in the final coupling step is problematic as only the purification steps of the conjugate will ensure the removal of the copper. Furthermore the peptide chelated to the copper rendering separation of the compounds difficult. Scheme B uses a metal to oxidise the polymer, which takes place in the initial stages of the overall process. The chromium precipitates out of the reaction mixture and can be filtered off with ease. Furthermore, the additional washes required in the purification of mPEO will help to remove any residual chromium traces. Additionally, the purification after the coupling step involves several repeated washes, which again can remove any chromium traces present in the system. Thus, whilst the use of the chromium is unavoidable, there are a greater number of opportunities for its removal through the reaction scheme.

The yield for the coupling step for Scheme B for mPEO<sub>7</sub>-F<sub>4</sub>-OEt was approximately 67% and purity was high. This yield is lower than that of the click chemistry coupling reaction (73%), however only by a marginal amount. Table 3.5.1 summarises the reaction schemes. Calculating the overall yields for the reaction shows that Scheme A produces a lower yield (~36%) than Scheme B (~46%). The reaction times for each Scheme also varied. Scheme A took a minimum of approximately ten days to complete; six days to produce the peptides, alongside tosylate functionalisation, and then a further day for azide/alkyne functionalisation. Two days are then required for the click coupling reaction, plus an additional day for purification. To ensure complete removal of starting materials and copper, dialysis was used, extending the overall reaction time by a significant amount (from several days to weeks). Furthermore, dialysis is not viable for industrial processes. Conversely, Scheme B is shorter, although it again requires six days for peptide production, alongside which polymer modification can take place. After this, IBCF coupling takes place over a further day, thus bringing the minimum approximate reaction time to seven days.

In conclusion, it has been shown that in comparison to the previously established solution phase method of producing PEO-phenylalanine conjugate via click chemistry, the method developed using IBCF as a coupling reagent was shorter, facile, and better yielding. Furthermore, the shortcoming of using a toxic metal in the reaction process has been minimised during polymer production, as opposed to during conjugate production, thus reducing the possibility for toxicity of the final product, and allowing for a greater range of potential uses.

**Table 3.6:** A summary of the two reactions used to produce polymer-peptide conjugates.

<b>Reaction Stage</b>	<b>Reaction Scheme A</b>	<b>Reaction Scheme B</b>
Polymer Preparation	Two-step reaction Moderate reaction conditions (N <sub>2</sub> , high T) Moderate yield No harmful by-products Purification requires column chromatography	One-step reaction Mild reaction conditions (0 °C) High yield Chromium by-product (toxic) Purification carried out by washing
Peptide Preparation	Generally the same as B High yield High purity Additional modification step	Generally the same as A High yield High purity
Coupling Reaction	Click chemistry High yield Difficult purification Two-step process Stringent reaction conditions (N <sub>2</sub> ) Copper catalyst (toxic)	IBCF coupling Moderate yield Facile purification One-Step process Mild reaction conditions

### 3.6. Conclusions

A new synthetic protocol has been developed to produce well-defined polymer-peptide conjugates based on mPEO and phenylalanine, with high purity and in high yields. IBCF coupling was used to conjugate the separate amino acids together to form the oligopeptide, and to couple the peptide component with the polymer component via the formation of an amide bond. Other coupling protocols were also investigated (DCC and PyBOP), however none were found to be as effective. The chosen peptide protection strategy was based on Boc protection, although Fmoc protection was also considered. Five oligopeptides were produced via this chemistry. Three different chain length mPEO polymers (7, 12, and 17) were modified by Jones oxidation, converting the terminal hydroxyl group to a more reactive carboxylic acid group. Conjugation between the modified polymer component and the oligopeptides used IBCF chemistry. Purification was generally facile, though as noted previously, F<sub>3</sub>-based conjugates encountered some purification difficulties, which were overcome primarily using reprecipitation and re-washing. The resulting products were produced in good yields, up to 91 %, and were synthesised to a high degree of purity, as confirmed by the GPC traces, IR, and NMR spectra.

A second method for producing polymer-peptide conjugates was investigated. This method involved deprotection of the ester protecting group on the C-terminus of the amino acid (in contrast to Boc deprotection on the N-terminus). Exposure of the reactive carboxylic acid group allowed for coupling to potentially proceed through direct esterification between the terminal hydroxyl group of the polymer and the deprotected carboxylic acid. LiOH deprotection was found to be the most efficient deprotecting method, although the yields were moderate. Alternative deprotection methods (including BBTO) were less effective and lower yielding than LiOH. Esterification was undertaken using Fischer and Steglich protocols, however only Steglich esterification resulted in the production of conjugates, albeit at lower yields compared to IBCF coupling of the same material.

Initial esterification attempts have proved promising and have laid the foundation for future work. Such work includes optimisation of the esterification conditions to improve yields and reduce reaction times. Production of these “backwards” facing conjugates also allows for the facile manufacturing of a “tri-block” material, which can be easily introduced at the N-terminus of the peptide (easily generated deprotection by using TFA). The original IBCF protocol can be further investigated for longer chain length mPEO and larger peptide sizes. It may be necessary to change from a solution-phase based reaction system to a solid-phase system, though issues surrounding expense and compatibility remain.

### 3.7. References

1. Adams D. J. and Young I., Oligopeptide-Based Amide Functional Initiators for ATRP, *Journal of Polymer Science: Part A: Polymer Chemistry*, **2008**, 46(18): p. 6082-6090.
2. Merrifield R. B., Solid Phase Peptide Synthesis. I. The Synthesis of a Tetrapeptide, *Journal of the American Chemical Society*, **1963**, 85(14): p. 2149-2154.
3. Mitsunobu O. and Yamada M., Preparation of Esters of Carboxylic and Phosphoric Acid via Quaternary Phosphonium Salts, *Bulletin of the Chemical Society of Japan*, **1967**, 40(10): p. 2380-2382.
4. Bowden K., Heilbron I. M., Jones E. R. H., and Weedon B. C. L., 13. Researches on acetylenic compounds. Part I. The Preparation of Acetylenic Ketones by Oxidation of Acetylenic Carbinols and Glycols, *Journal of the Chemical Society (Resumed)*, **1946**: p. 39-45.
5. McMurry J., Organic Chemistry, in *Organic Chemistry*. **2004**, Thomson Learning: London. p. 605-614.
6. Tojo G. and Fernández M., Oxidation of Alcohols to Aldehydes and Ketones. Basic Reactions in Organic Synthesis, ed. G. Tojo. **2006**: Birkhäuser.
7. Roberts M. J., Bentley M. D., and Harris J. M., Chemistry for peptide and protein PEGylation, *Advanced Drug Delivery Reviews*, **2002**, 54(4): p. 459-476.
8. Lele B. S. and Kulkarni M. G., Single step room temperature oxidation of poly(ethylene glycol) to poly(oxyethylene)-dicarboxylic acid, *Journal of Applied Polymer Science*, **1998**, 70(5): p. 883-890.
9. United States Department of Labor, Chromium (VI) (Hexavalent Chromium), **2006** [cited May 2012, 2012].
10. Montalbetti C. A. G. N. and Falque V., Amide Bond Formation and Peptide Coupling, *Tetrahedron*, **2005**, 61(46): p. 10827-10852.
11. Doonan S., Peptides and Proteins. **2002**, London: Royal Society of Chemistry.
12. Pérez M. G. and Maier M. S., Mild deprotection of steroid esters by Bis(tributyltin)oxide, *Tetrahedron Letters*, **1995**, 36(19): p. 3311-3314.
13. L. E. Furlan R., G. Mata E., and A. Mascaretti O., Efficient, non-acidolytic method for the selective cleavage of N-Boc amino acid and peptide phenacyl esters linked to a polystyrene resin, *Journal of the Chemical Society, Perkin Transactions 1*, **1998**(2): p. 355-358.

14. Tzokova, Fernyhough C. M., Topham P. D., Sandon N., Adams D. J., Butler M. F., Armes S. P., and Ryan A. J., Soft Hydrogels from Nanotubes of Poly(ethylene oxide)-Tetraphenylalanine Conjugates Prepared by Click Chemistry, *Langmuir*, **2009**, 25(4): p. 2479-2485.
15. Adams D. J. and Young I., Oligopeptide-based amide functional initiators for ATRP, *Journal of Polymer Science Part A: Polymer Chemistry*, **2008**, 46(18): p. 6082-6090.
16. Jatzkewitz H., Über den Einbau physiologisch wirksamer Substanzen in ein kolloidales Blutplasma-Ersatzmittel, *Hoppe-Seyler's, Z Physiol. Chem.*, **1954**, 297: p. 149- 156.

# **CHAPTER 4**

## **Self-Assembly of Bio-Hybrid Materials**

## 4. Self-Assembly of Bio-Hybrid Materials

A gel is semi-solid mass of lyophilic sol (dispersion of a solid in a liquid), in which all of the dispersion medium (i.e. the solvent) has penetrated the sol particles<sup>[1]</sup>. The characterisation of the gel is dependent on the formulation of the dispersion medium. If the solvent is water, then the gel is classed as a hydrogel. Conversely, if the solvent is organic, then the gel is classed as an organogel<sup>[2]</sup>. In this chapter, the work carried out focuses on mixed hydro/organogels, consisting of the gelator material and the solvent. The three-dimensional structure of a gel is a network of chains which are held together by chemical or physical bonds. Chemically-bonded hydrogels are held in place by irreversible covalent bonds linking the polymer chains together. Physically-bonded hydrogels, on the other hand, are held together by reversible interactions such as molecular entanglements, ionic forces,  $\pi$ - $\pi$  stacking, hydrogen bonding, and van der Waals forces<sup>[3]</sup>. These reversible physical interactions are advantageous in applications such as drug delivery as it allows for the creation of injectable material via thixotropic behaviour of the gel (i.e. increasing shear force decreases viscosity, which then recovers upon the removal of the force). As the material is dissolved in an appropriate solvent, at specific concentrations, it experiences chemical or physical interactions that potentially lead to entangled three-dimensional networks. These networks consist of long, fibre-like structures, which can entangle and immobilise the dispersion medium<sup>[4]</sup>. This chapter describes efforts to form gels using mPEO-derived polymer-peptide conjugates. The chapter is divided into two sections; firstly qualitatively detailing macroscopic observations when attempting to gel the material (initial screening process for the gels), including any general trends, and secondly, analysis of the microstructure of formed gels.

### 4.1. Gelation studies of polymer-peptide conjugates

In Chapter 3, the reliable production of twelve polymer-peptide conjugates based on monomethoxy-poly(ethylene oxide) and phenylalanine was discussed. The following sections detail gelation studies of these materials, and

are organised by mPEO length. Five solvents were chosen for the co-solvent system with water; dimethyl sulfoxide (DMSO), tetrahydrofuran (THF), acetone, ethanol, and dimethylformamide (DMF). Initial experiments with just water (as described in Chapter 2) were not successful, therefore necessitating the use of a binary solvent system. The volume of solvent in each system was constant (2 ml), and gelator material was used at two different concentrations (5 mg/ml and 10 mg/ml). Finally, the solvent composition was varied. Conjugate material was added to the organic solvent, and fully dissolved. An appropriate amount of water was added to the mixture, and left the resulting mixture to stand at room temperature overnight.

#### 4.1.1. Gelation of mPEO<sub>7</sub>-based polymer-peptide conjugates

Four mPEO<sub>7</sub>-based conjugates were synthesised with varying phenylalanine oligopeptide length (F<sub>1</sub> through to F<sub>4</sub>). No gel formation was observed initially at either concentration, however the viscosity of the F<sub>4</sub>-containing solution had qualitatively increased. Gel formation occurred after a further day standing at room temperature. Table 4.1 shows that some gels formed in this series (F<sub>4</sub>-based); in 40 %v/v DMSO and THF (5 mg/ml). Increasing the concentration of the gelator (10 mg/ml) resulted in an additional gel forming very weakly in 20 %v/v DMSO. Elevating the temperature of the solutions to 60 °C and then allowing them to return to temperature resulted in further gels being produced. This is likely due to the temperature dependence of molecular interactions, including hydrogen bonding, which can lead to phase separation<sup>[5]</sup>.

Notably, at the lower critical solution temperature (i.e. the temperature below which all components in a mixture are miscible), hydrogen bonding becomes unfavourable between the polymer and solvent, thus the macromolecule can dehydrate into a more hydrophobic structure<sup>[5]</sup>. This was carried out at both concentrations of gelator (5 and 10 mg/ml). The additional gels formed in 20 %v/v DMSO and THF. Those gels were very weak, and underwent a gel-to-sol transition, thus collapsing the gel with minimal agitation (handling the vial triggered the transition). Such gels are not listed in Table 4.1 because they were not stable. This was in contrast to the gels formed in 40 %v/v solutions

which were able to free stand. Appendix B contains tabulated observations detailing the results of gel formation for all conjugates in this series.

Gel formation using mPEO<sub>7</sub>-based conjugates was limited, with only mPEO<sub>7</sub>-F<sub>4</sub> showing any gel character. This suggests that there are few entanglements occurring at these concentrations, and that increasing the concentration may aid gel formation, as this alters the position in the phase diagram. Furthermore, there was insufficient hydrogen bonding taking place when the smaller conjugates (i.e. <F<sub>4</sub>) were used as discussed further in Section 4.1.4.

**Table 4.1:** Qualitative observations of gel formation of mPEO<sub>7</sub>-F<sub>4</sub>-OEt. The percentage shows the proportion of organic solvent in the mixture with water.

mPEO <sub>7</sub> -F <sub>4</sub> -OEt	Gels at Room Temperature				Gels at 60 °C			
Solvents	5 %	10 %	20 %	40 %	5 %	10 %	20 %	40 %
DMSO	x	x	x	y	x	x	y (very weak)	y
THF	x	x	x	y	x	x	y (very weak)	y
Acetone	x	x	x	x	x	x	x	x
Ethanol	x	x	x	x	x	x	x	x
DMF	x	x	x	x	x	x	x	x
5 mg/ml								
mPEO <sub>7</sub> -F <sub>4</sub> -OEt	Gels at Room Temperature				Gels at 60 °C			
Solvents	5 %	10 %	20 %	40 %	5 %	10 %	20 %	40 %
DMSO	x	x	y	y	x	x	y (very weak)	y
THF	x	x	x	y	x	x	y (very weak)	y
Acetone	x	x	x	x	x	x	x	x
Ethanol	x	x	x	x	x	x	x	x
DMF	x	x	x	x	x	x	x	x
10 mg/ml								

*N.B. x represents no gel forming (or an unstable gel), and y represents a stable gel forming.*

#### 4.1.2. Gelation of mPEO<sub>12</sub>-based polymer-peptide conjugates

Lengthening the polymer chain from mPEO<sub>7</sub> to mPEO<sub>12</sub>, and therefore increasing the molecular weight whilst rendering the conjugate more hydrophilic, affected the gel formation of the aforementioned conjugates. As with mPEO<sub>7</sub>-based conjugates, gel formation was only observed when four phenylalanine units were incorporated into the conjugate (Table 4.2). However, the solvent systems in which gelation occurred were different to the previous efforts. At room temperature, no gel formed in any solvent composition when the concentration of the gelator was 5 mg/ml. However, in 40 %v/v DMSO, the solution was qualitatively observed to have increased viscosity, with regions appearing semi-solid. This indicated that some self-assembly was taking place (and is denoted as “partial”, **p**, in Table 4.2). Increasing the concentration to 10 mg/ml resulted in gel formation, but again not in the same solvent systems previously observed for mPEO<sub>7</sub>-F<sub>4</sub>. Gelation occurred in 10 and 20 %v/v acetone, with “partial” gels forming in 40 %v/v DMSO and 5 %v/v THF. Appendix B contains tabulated observations detailing the results of gel formation for all conjugates in this series.

Increasing the temperature of the gel mixture to 60 °C and then allowing the samples to cool to room temperature resulted in further gelation. The “partial” gels from 40 %v/v DMSO (5 and 10 mg/ml) formed more complete gels after heating, although the gel was observed to be weak when made from 5 mg/ml of material. Notably, gelation occurred in 10 and 20 %v/v acetone from 5 mg/ml of gelator material, but also formed at all mixtures (except DMF) when using 10 mg/ml. Furthermore, at high gelator concentrations, self-assembly was observed at all compositions with THF. Conspicuously, no gel formed from DMF at any solvent composition, instead aggregates were noted to form in the reaction vial.

mPEO<sub>12</sub>-based conjugates assembled into gels in more solvent compositions than mPEO<sub>7</sub>-based conjugates. This is likely attributable to the longer polymer chain, which allows for more entanglements. As with the previous experiment, only F<sub>4</sub> conjugates showed any gel behaviour. Based on the trends seen so far,

it was expected that mPEO<sub>17</sub>-F<sub>4</sub>-OEt would also produce gel material, and from a greater range of solvent compositions than mPEO<sub>7</sub>-F<sub>4</sub>-OEt and mPEO<sub>12</sub>-F<sub>4</sub>-OEt.

**Table 4.2:** Qualitative observation of gel formation of mPEO<sub>12</sub>-F<sub>4</sub>-OEt. The percentage shows the amount of organic solvent used in a mixture with water.

mPEO <sub>12</sub> -F <sub>4</sub> -OEt	Gels at Room Temperature				Gels at 60 °C			
Solvents	5 %	10 %	20 %	40 %	5 %	10 %	20 %	40 %
DMSO	x	x	x	p	x	x	x	y (weak)
THF	x	x	x	x	x	x	x	y
Acetone	x	x	x	x	x	y (weak)	y (weak)	x
Ethanol	x	x	x	x	x	x	x	x
DMF	x	x	x	x	x	x	x	x
5 mg/ml								
mPEO <sub>12</sub> -F <sub>4</sub> -OEt	Gels at Room Temperature				Gels at 60 °C			
Solvents	5 %	10 %	20 %	40 %	5 %	10 %	20 %	40 %
DMSO	x	x	x	p	x	x	x	y
THF	p	x	x	x	Y	y	y	y
Acetone	x	y	y	x	p	y	y	y
Ethanol	x	x	x	x	x	x	x	y
DMF	x	x	x	x	x	x	x	x
10 mg/ml								

*N.B. x represents no gel forming (or an unstable gel), y represents a stable gel forming, and p denotes "partial" self-assembly behaviour.*

#### 4.1.3. Gelation of mPEO<sub>17</sub>-based polymer-peptide conjugates

mPEO<sub>17</sub>-based conjugates contained the longest polymer chain of all the conjugates tested for gelation. This, in turn, made the conjugate more hydrophilic which affected the behaviour of the conjugate in the solvent. As with all of the conjugates tested before, only the F<sub>4</sub> conjugate (mPEO<sub>17</sub>-F<sub>4</sub>-OEt)

formed gels. All other conjugates either remained as a solution, or precipitated from the solvent. As predicted, more gels were formed across the parameters studied. At room temperature, gelation took place in 10 and 20 %v/v DMSO (5 and 10 mg/ml). Further, at a higher (10 mg/ml) gelator concentration, gels were also formed in 40 %v/v THF and acetone. On heating the gel mixtures, further gels were formed, with all compositions of DMSO resulting in gels, as well as the majority of acetone and THF. No gels were formed in ethanol or DMF (Table 4.3). Self-assembly of mPEO<sub>17</sub>-F<sub>4</sub>-OEt was more prevalent than the previous experiments with shorter mPEO chains. It is likely that the longer polymer chain (and the increased hydrophilic character) led to increased entanglements, and more advantageous solvent interactions, thus forming a wider range of gels.

**Table 4.3:** Qualitative observations of gel formation of mPEO<sub>17</sub>-F<sub>4</sub>-OEt. The percentage shows the amount of organic solvent used in a mixture with water.

mPEO <sub>17</sub> -F <sub>4</sub> -OEt	Gels at Room Temperature				Gels at 60 °C			
Solvents	5 %	10 %	20 %	40 %	5 %	10 %	20 %	40 %
DMSO	p	y	y	x	y	y	y	y
THF	x	x	x	x	x	x	y	y
Acetone	x	p	p	x	x	y	y	y
Ethanol	x	x	x	x	x	x	x	x
DMF	x	x	x	x	x	x	x	x
5 mg/ml								
mPEO <sub>17</sub> -F <sub>4</sub> -OEt	Gels at Room Temperature				Gels at 60 °C			
Solvents	5 %	10 %	20 %	40 %	5 %	10 %	20 %	40 %
DMSO	p	y	y	y	y	y	y	y
THF	x	x	p	y	y	y	y	y
Acetone	x	x	x	y	p	y	y	y
Ethanol	x	x	x	x	x	x	x	x
DMF	x	x	x	x	x	x	x	x
10 mg/ml								

*N.B. x represents no gel forming (or an unstable gel), y represents a stable gel forming, and p denotes "partial" self-assembly behaviour.*

#### 4.1.4. Polymer-peptide conjugates gelation trends

From a macroscopic point of view, the most obvious trend derived from the gelation results of polymer-peptide conjugates is that four phenylalanine peptide units are required to form a gel. No other conjugate combination (i.e. F<sub>1</sub>, F<sub>2</sub>, or F<sub>3</sub>) resulted in the formation of gel.

Arguably, there are several factors that may be responsible for F<sub>4</sub>-conjugated self-assembly, the most important is that intermolecular hydrogen bonding arising from interactions between the amide, carbonyl, and ester groups help to stabilise three-dimensional structures that form. As expected, when the number of phenylalanine units increases, the number of hydrogen bonding groups also increases, thus providing stability for networked structures. Indeed, work reported by Hamley<sup>[6]</sup> indicates that the  $\beta$ -sheet structure is formed only when four phenylalanine peptide units are used in the conjugate. Using less than four peptide units did not result in  $\beta$ -sheet or fibril formation, likely due to the insufficient rigidity of the molecules, due to the vastly reduced amount of hydrogen bonding when compared to F<sub>4</sub>. The ratio between hydrophilic groups (such as the mPEO polymer backbone) and lipophilic groups (such as the phenyl rings of the peptide) are also noted as being important for self-assembly.

Figure 4.1 shows the hydrogen bonding that can potentially occur in each of the conjugates. In F<sub>1</sub>-based conjugates, there is only one pair of linkages per molecule, and these linkages only occur on one side of the molecule. Increasing the peptide length to two (F<sub>2</sub>) also increases the number of pairs of hydrogen bond linkages per molecule to two. However, as shown in Figure 4.1, there is only one linkage possible per side of each molecule. The situation was slightly different when increasing the peptide length to three units (F<sub>3</sub>). In that instance, there would be three pairs of hydrogen bond linkages, arranged with two pairs on one side of the molecule, and one pair on the other side. Finally, when the peptide consists of four phenylalanine units (F<sub>4</sub>), there are four pairs of hydrogen bond linkages per molecule, arranged evenly with two per side per molecule.

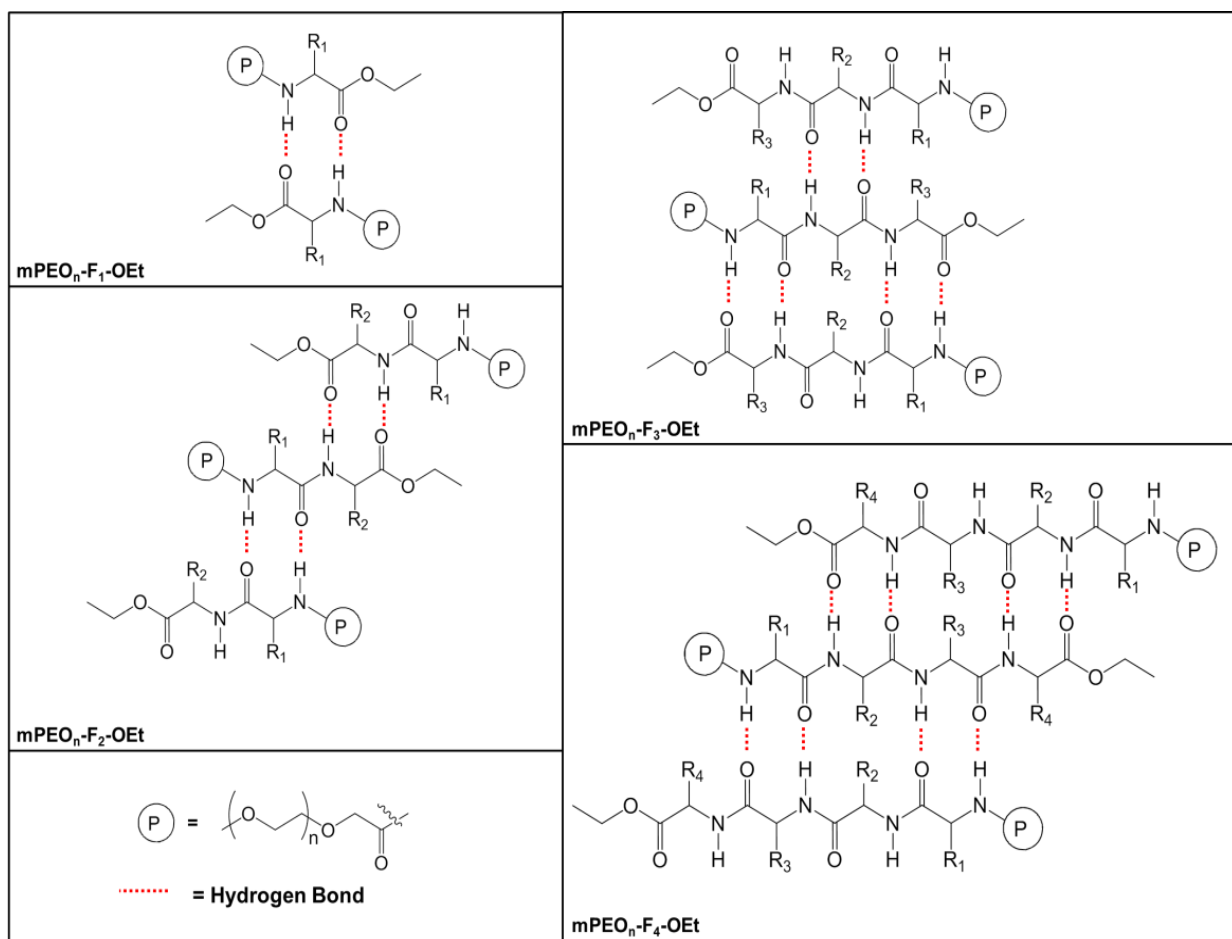


**Figure 4.1:** Hydrogen bonding of mPEO<sub>n</sub>-F<sub>x</sub>-OEt polymer-peptide conjugates.

Correlating the number and position of hydrogen bond pairs to gelation reveals that at least two pairs of hydrogen bond linkages are required on each side of the molecule for successful gelation. If the system has only one pair (on either side) the material will not gel. Speculatively, a very small amount of energy (for example  $E$  joules) is required to overcome the stabilisation effect of the hydrogen bonding and disrupt one linkage pair, hence why F<sub>1</sub>- and F<sub>2</sub>-based conjugates did not form gels. Although F<sub>3</sub>-based conjugates have three pairs of linkages, the orientation (two on one side and one on the other) of these linkages means that the structure can be disrupted on the side with one pair of linkages with a small amount of energy ( $E$  joules). However, in the case of F<sub>4</sub>-based conjugates, applying  $E$  joules of energy will only disrupt one linkage pair on a given molecule. However, as the second linkage pair will remain bonded (as  $2E$  joules would be needed to disrupt it), the overall structure remains stabilised, albeit obviously weakened. Furthermore, due to the second

pair of linkages allowing the chains to maintain their orientation (and keeping them bonded), the disrupted hydrogen bonds have the opportunity to reform over a time period.

Another consideration is that systematically increasing the number of phenylalanine units correspondingly increases the number of phenyl groups (rings) in the final conjugate. This in turn augments the potential amount of intermolecular  $\pi$ - $\pi$  stacking, thus turning it into an additional stabiliser, aiding entanglement by acting as a physical cross-link<sup>[7]</sup>. Furthermore, this stacking provides an excellent hydrophobic domain which can accommodate hydrophobic molecules (such as hydrophobic therapeutic agents), an important consideration for the future use of such biomaterials.

The solvent used for gelation also had an effect on self-assembly. This is clearly seen by the lack of gelation in DMF and ethanol (generally) even when using F<sub>4</sub>-based materials. Table 4.4 lists the solvents used alongside the dielectric constant of the solvents (which gives a rough indication of polarity) and qualitative observations of the solubility of the conjugate in the solvent.

**Table 4.4:** Dielectric constants of gelation solvents and qualitative solubility observations of the conjugates in the aforementioned solvents.

Solvent	Dielectric Constant	Dissolution Speed
<b>Tetrahydrofuran</b> <sup>[8]</sup>	8	Quick
<b>Acetone</b> <sup>[9]</sup>	21	Moderate
<b>Ethanol</b> <sup>[9]</sup>	25	Slow
<b>Dimethylformamide</b> <sup>[10]</sup>	38	Moderate
<b>Dimethyl sulfoxide</b> <sup>[11]</sup>	48	Quick

Ethanol and DMF have relatively high dielectric constants, which indicate that the solvents are moderately polar. Hypothetically, hydrogen bonding between the solvent and the conjugate would compete with the inter-conjugate hydrogen bonding thus disrupting the three-dimensional structure, resulting in no gelation. However, the dielectric constant of DMSO is greater than DMF (~48), yet

gelation still occurred. To explain this, it is necessary to look at the solution properties. Solubility parameters are used to predict the dissolution behaviour. Specifically the Hansen solubility parameters<sup>[12]</sup> predict solubility based on dispersion forces, dipole-dipole interactions, and hydrogen bonding. Therefore, each solvent is given three Hansen parameters;  $\delta_D$ ,  $\delta_P$  and  $\delta_H$ , respectively. The values for  $\delta_H$  show the energy from hydrogen bonds between the solvent molecules. Table 4.5 shows the values of the  $\delta_H$  Hansen parameter for the solvents used in gelation.

**Table 4.5:** Hydrogen bonding Hansen parameter ( $\delta_H$ ) of gelation solvents.<sup>[12]</sup>

Solvent	$\delta_H$
Dimethyl sulfoxide	10
Tetrahydrofuran	8
Acetone	7
Ethanol	20
Dimethylformamide	12

Notably, the  $\delta_H$  values for ethanol and DMF are higher than the other solvents, suggesting that there is more hydrogen bonding arising from these solvents, which could disrupt the structure despite the four phenylalanine peptide units. The parameter value for DMSO is close to that of DMF, however the solubility of the conjugate in DMSO was also high, thus assisting dispersion of the material in the solvent.

In conclusion, the observable data suggests that for a gel to form from the conjugates, the  $\delta_H$  parameter of the solvent must be low (i.e. the solvent should not have a high propensity to form hydrogen bonds), and that the solvent should dissolve the conjugate easily. Furthermore, at least four repeat units of peptide consisting of four evenly distributed pairs of hydrogen bonding linkages should be present to stabilise the networks.

## 4.2. Quantitative analysis of self-assembled materials

Although gelation had appeared to occur, this was determined by visible observations and so was a qualitative assessment. This was problematic as samples that appeared to be a gel, may have actually been a slow-flowing, highly viscous liquid. To this extent, three techniques were used to investigate the self-assembly behaviour; rheology, infrared spectroscopy (FTIR), and confocal microscopy. The conjugate used in all experiments was mPEO<sub>17</sub>-F<sub>4</sub>-OEt (10 mg) dissolved in a DMSO-water solution. This conjugate was chosen as it qualitatively appeared to reliably self-assemble. Throughout this Section, the analytical data collected will be compared with that of gels produced in the literature with similar materials (notably mPEO<sub>7</sub>-F<sub>4</sub>-OEt).

### 4.2.1. Rheology of self-assembled materials

Rheological studies on the self-assembled materials were carried out at least one day after self-assembly had appeared to occur. Figure 4.2 shows a plot of shear rate versus shear stress. The figure shows that the sample behaved like a non-Newtonian fluid as the slope is non-linear. This implied that the sample had some shear thickening behaviour, as there were dramatic changes in the gradient of the graph (analogous to the change in viscosity of the material).

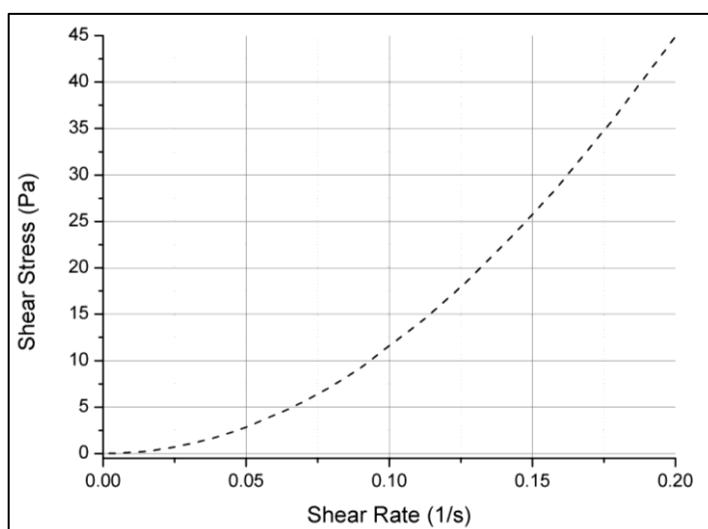


**Figure 4.2:** Rheology data for self-assembled mPEO<sub>17</sub>-F<sub>4</sub>-OEt 10 mg/ml in a 20 %v/v solution of DMSO and water.

A strain-sweep test was performed to determine the linear viscoelastic region of the samples. The strain-sweep allowed determination of the amount of strain to use in further experiments, i.e. ensuring that the sample is being observed within its linear viscoelastic region, in which stress and strain increase proportionally to each other, and are time dependent. Figures 4.3 and 4.4 show that there was no linear region for the sample.

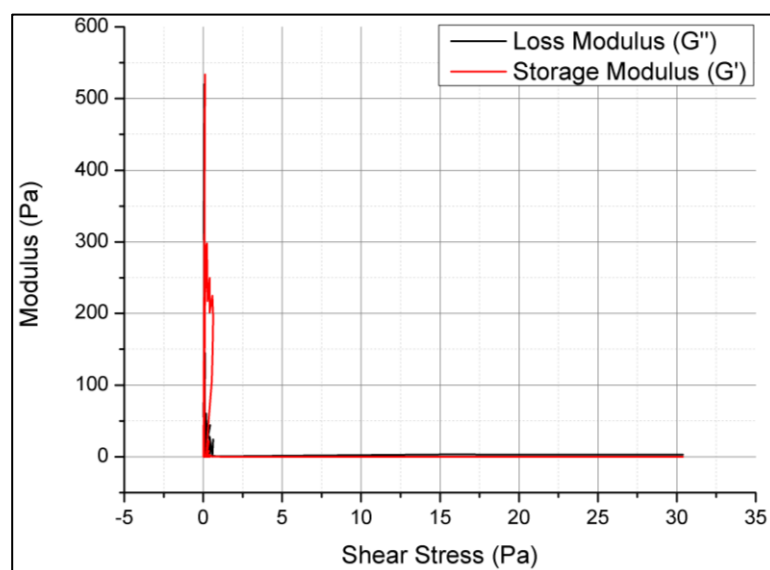


**Figure 4.3:** Strain sweep data for self-assembled mPEO<sub>17</sub>-F<sub>4</sub>-OEt 10 mg/ml in a 10 %v/v solution of DMSO and water.

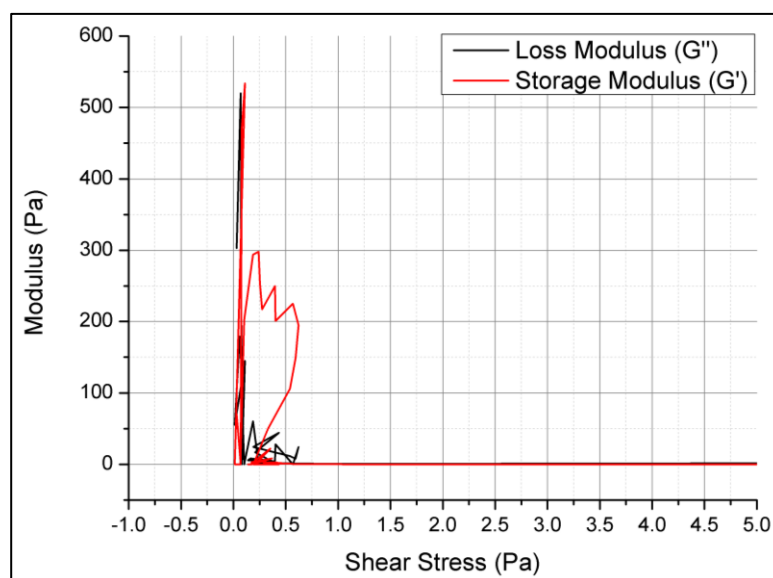


**Figure 4.4:** Magnified strain sweep data for self-assembled mPEO<sub>17</sub>-F<sub>4</sub>-OEt 10 mg/ml in a 10 %v/v solution of DMSO and water.

The graph was expected to show constant dynamic moduli in the linear viscoelastic region, until a %strain was applied, which would break down the gel. A value would then be chosen below this %strain to run frequency sweeps. It can be inferred that there was no gel-like structure when the rheology of sample was analysed, as there was no visible linear region when stress was applied. Plotting modulus versus shear stress should have shown a linear region, which dips down at a certain shear rate.

A frequency sweep test was used to further probe the nature of the material. This allows observation of the dominant components of the material, which helps to describe its behaviour. It was expected that the self-assembled material would show moduli,  $G'$  (storage modulus; material behaves as an elastic solid) and  $G''$  (loss modulus, material behaves as a liquid) that were somewhat parallel, and then deviate at some point (when the shear stress was strong enough to disrupt the structure). However, the samples did not show this behaviour at all, strongly implying that they are not gels (Figure 4.5); but perhaps instead a highly viscous, slow-flowing fluid.

The graph in Figure 4.5 shows an almost exponential  $G'$ , which suggests that the material has formed a nanostructure; indicative of gel formation. However, as no strain regions were found, coupled with the qualitative observed fragility of the gel (in the vial), it was clear that the gel had collapsed, and revert back to a solution. The exponential-like storage modulus visible in Figure 4.5 is likely attributable to frequency hardening, where the nanostructures of the collapsed material are locked together in solution, and are unable to dissociate from each other. When the frequency of the oscillations from the rheometer was increased, the “locked-in” structures formed a strong network. This theory was further reinforced when compared with the confocal microscopy images (see Section 4.2.3).

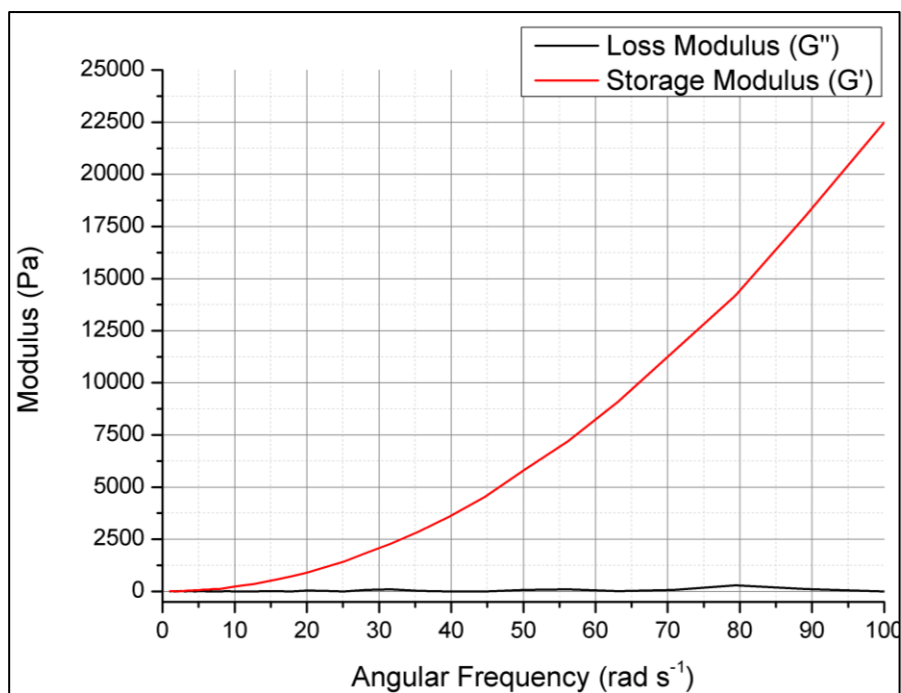


**Figure 4.5:** Frequency sweep data for self-assembled mPEO<sub>17</sub>-F<sub>4</sub>-OEt 10 mg/ml in a 10 %v/v solution of DMSO and water.

The rheology data show that the materials formed are not gel-like, as no viscoelastic behaviour was observed. However, it is possible that the “gel” collapsed on contact with the rheometer, thus changing it back to a liquid state. Nevertheless, the strain sweep showed that no viscoelastic region existed for the material, suggesting that instead of forming gels, the material self-assembles either into some kind of inhomogeneous dispersion aggregate, or into a free-flowing but highly viscous liquid. Although gels appeared not to have formed, the term gel will be continued to be used throughout this chapter, until further conclusions have been drawn. Further rheology of other conjugates tested can be found in Appendix C. Rheology data of mPEO<sub>7</sub>-F<sub>4</sub>-OEt produced via “click” chemistry are shown in Figure 4.6, and is typical of a conjugate gel<sup>[13]</sup>. It is clear to see that the modulus is approximately frequency-independent in this material, which aptly shows gel behaviour. In contrast, the rheology data of the conjugates synthesised in this project are not frequency-independent as they are not free-standing gels.

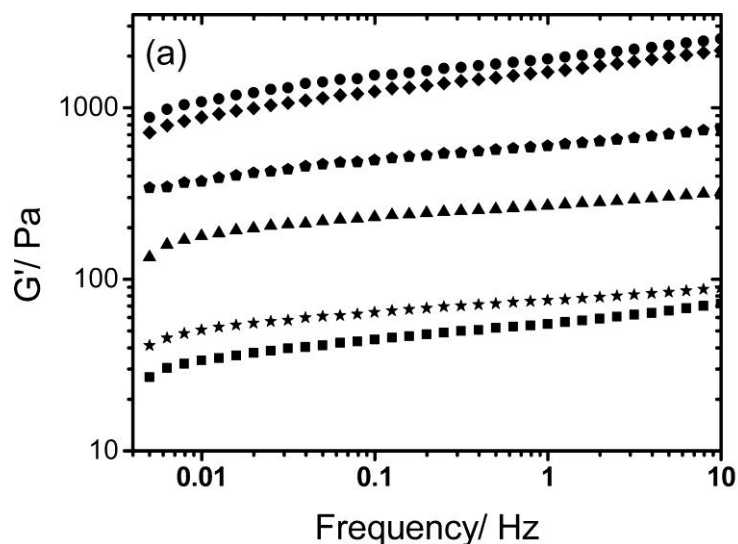


**Figure 4.6:** Frequency sweep data for different concentrations of mPEO<sub>7</sub>-F<sub>4</sub>-OEt, from the literature<sup>[13]</sup>. The conjugate concentrations were (from top to bottom) 14.4 mg ml<sup>-1</sup>, 11.0 mg ml<sup>-1</sup>, 8.7 mg ml<sup>-1</sup>, 6.3 mg ml<sup>-1</sup>, and 2.7 mg ml<sup>-1</sup>.

#### 4.2.2. FTIR spectroscopy of self-assembled materials

FTIR spectroscopy was used to investigate the change in structure as self-assembly occurred over a sustained time period (days). ATR-FTIR is a powerful technique that is able to characterise the interactions of adsorbed and absorbed water within polymeric networks<sup>[14]</sup>. By comparing the spectrum before self-assembly ( $t = 0$  hours) and after an appropriate interval ( $t = 72$  hours) it was possible to see the difference in chemical environments, reflected by the repositioning and intensity change of certain bands. ATR-FTIR gel studies, reported in the literature, have looked at the association of block co-polymers in solution. Recently, work has also been carried out on poly(*N*-isopropylacrylamide) gelation in an aqueous environment. ATR-FTIR is a power technique as it can characterise the hydrogen bonding in systems, and determine how absorbed and adsorbed water (in aqueous mixtures) interacts with the polymer gelators. However, caution is advised when interpreting the results, as the resolution of the machine was  $4\text{ cm}^{-1}$ , and many of the results fall below this level. Therefore, it is impossible to entirely attribute the change in wavenumbers to hydrogen bond interactions between the solvent and the polymer system. As a further consideration, evaporation of the solvent from the

sealed ATR-FTIR system was also possible, potentially impacting the spectra obtained.

In order to mitigate the effect of the solvent system (DMSO: water, 1: 4) a background was run with the same composition as the solvent used for self-assembly. The spectra obtained were then subtracted against this background, thus reducing the intensities of the solvent bands. Figure 4.7 shows the FTIR spectra of the conjugate at  $t = 0$  hours and  $t = 72$  hours. The data collected shows a redistribution of the solvent; there was less water and more DMSO in spectrum run at  $t = 72$  hours, which can be seen by the increase in intensity of the peaks at  $\sim 3200$  and  $3300\text{ cm}^{-1}$ , suggesting that syneresis took place, i.e. water has been expelled from the sample during self-assembly. Notably, the water band that occurs at around  $1650\text{ cm}^{-1}$  was negatively phased (appeared as a trough) in Figure 4.7, however the amide I band overlaps and is phased positively (appeared as a peak).

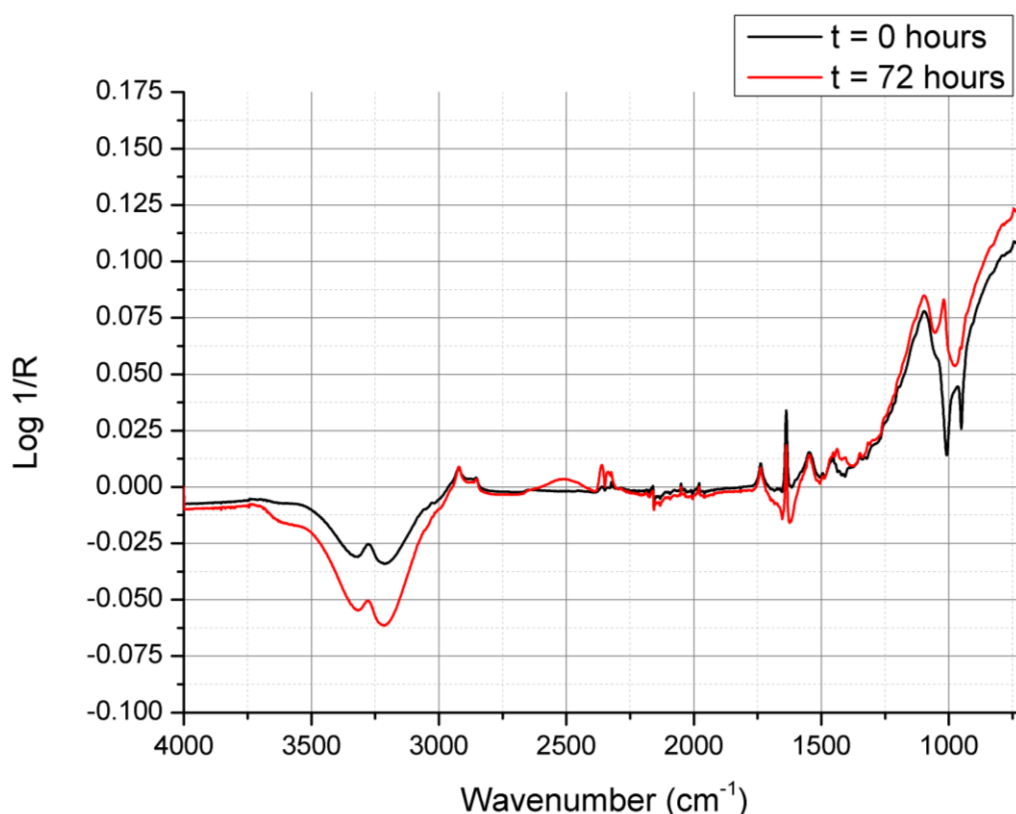


**Figure 4.7:** FTIR spectrum of mPEO<sub>17</sub>-F<sub>4</sub>-OEt on an ATR crystal in DMSO-water mixture (20 %v/v).

Focussing on the amide I region (Figure 4.8), the positively phased peak was distinctly visible. Subtracting the background solvent spectrum reduces the intensity of the water band (OH bending stretch), made it easier to distinguish the amide I band. Two points of interest were noted. Firstly, after running the spectrum of the sample after 72 hours, the peak has broadened slightly. Secondly, the position of the peak has shifted to a higher wavenumber (blue-shifted) when the sample had been run for 72 hours. This change is highlighted in the normalised data presented in Figure 4.9, and may be indicative of a change in the hydrogen bonding of the sample, suggesting a more “gelatinous” state. This is potentially reinforced by syneresis; there was less water in the sample as time progressed indicating that there were consequently fewer hydrogen bonds forming with water, and instead more intermolecular hydrogen bonds formed between conjugates. However, the shift was very small ( $\sim 1 \text{ cm}^{-1}$ ), potentially suggesting that only a small amount of “new” hydrogen bonds had formed, implying, at best, that the gel that formed was very weak (at least on the ATR crystal). One method to eliminate overlapping water signals in the amide I region, would be to use  $\text{D}_2\text{O}$ .

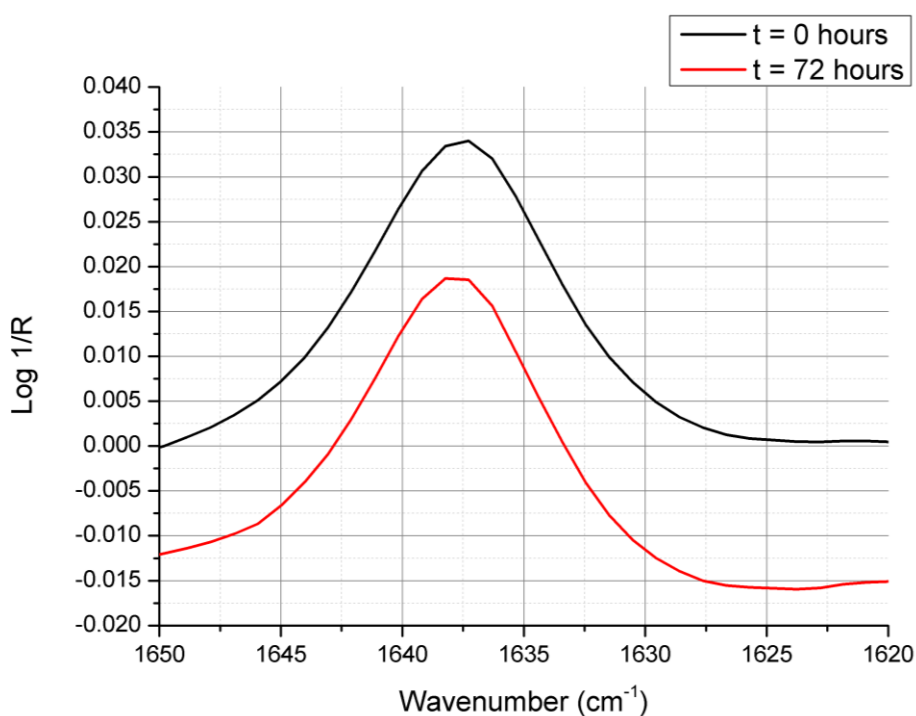


**Figure 4.8:** FTIR spectrum of  $\text{mPEO}_{17}\text{-F}_4\text{-OEt}$  on an ATR crystal in DMSO-water mixture (20 %v/v) focussing on the amide I bands.

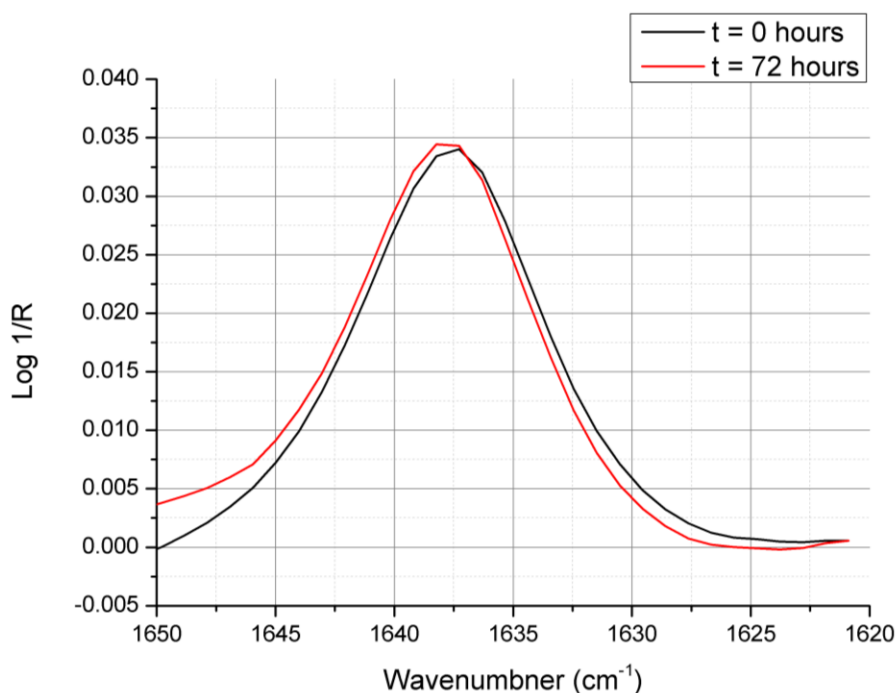


**Figure 4.9:** FTIR spectrum of mPEO<sub>17</sub>-F<sub>4</sub>-OEt on an ATR crystal in DMSO-water mixture (20 %v/v) focussing on the amide I bands (normalised).

There were also shifts noted at around 2830 cm<sup>-1</sup> and 2920 cm<sup>-1</sup>. This region is typically populated by anti-symmetrical C-H stretching bands (Figure 4.10). The small shift downfield implies that there was an attractive-repulsive interaction between non-polar CH groups. This in turn implied that there was a carbonyl shift (the main non-amide carbonyl group was the ester protecting group) again indicating the presence of “new” hydrogen bonds. As with the amide I band, the change was small (~ 2 cm<sup>-1</sup>) further emphasising that the potential gel that formed was very weak. The increase in the attractive-repulsive hydrophobic (i.e. methyl-methyl) interactions arises from the dehydration of the sample. This anti-symmetrical stretch is particularly sensitive to changes in hydrophobic interactions<sup>[15]</sup>, and so as dehydration occurs, the proximity of the hydrophobic groups increases, thus affecting the position of the band.

The final region to focus on is the amide II region (NH bending) (Figure 4.11). FTIR spectroscopy shows no change in the position of the peak after the time period. However, the intensity and width of the peak have increased after 72 hours. This suggests that some hydrogen bonding interactions have changed, however this was only by a small amount. A larger change in

hydrogen bond interactions would be accompanied by a large shift to a higher wavenumber, similar to the amide I interactions<sup>[14,15]</sup>.

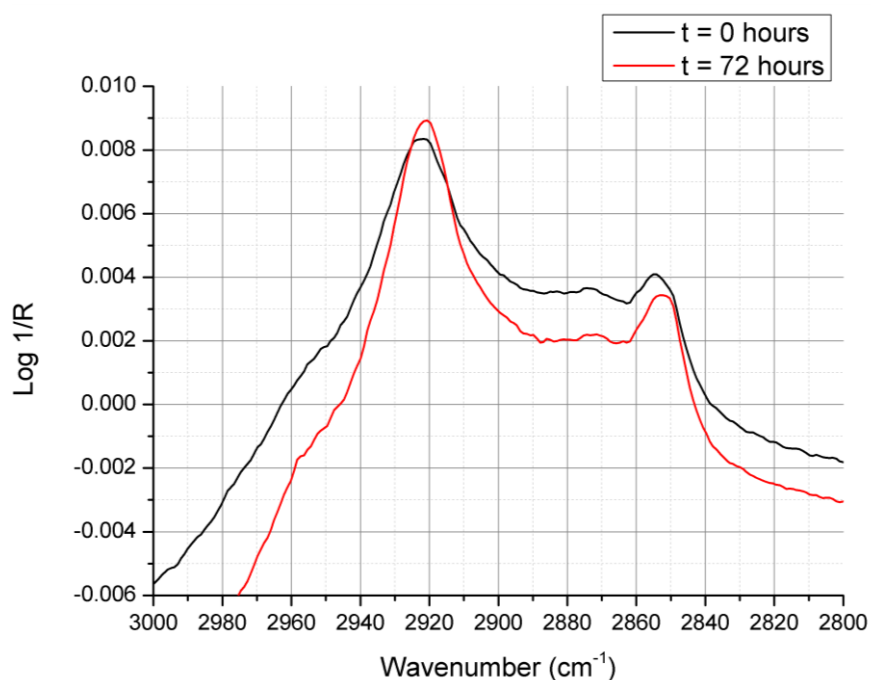


**Figure 4.10:** FTIR spectrum of mPEO<sub>17</sub>-F<sub>4</sub>-OEt on ATR crystal in DMSO-water mixture (20 %v/v) focussing on C-H bonds and carbonyl shifts.

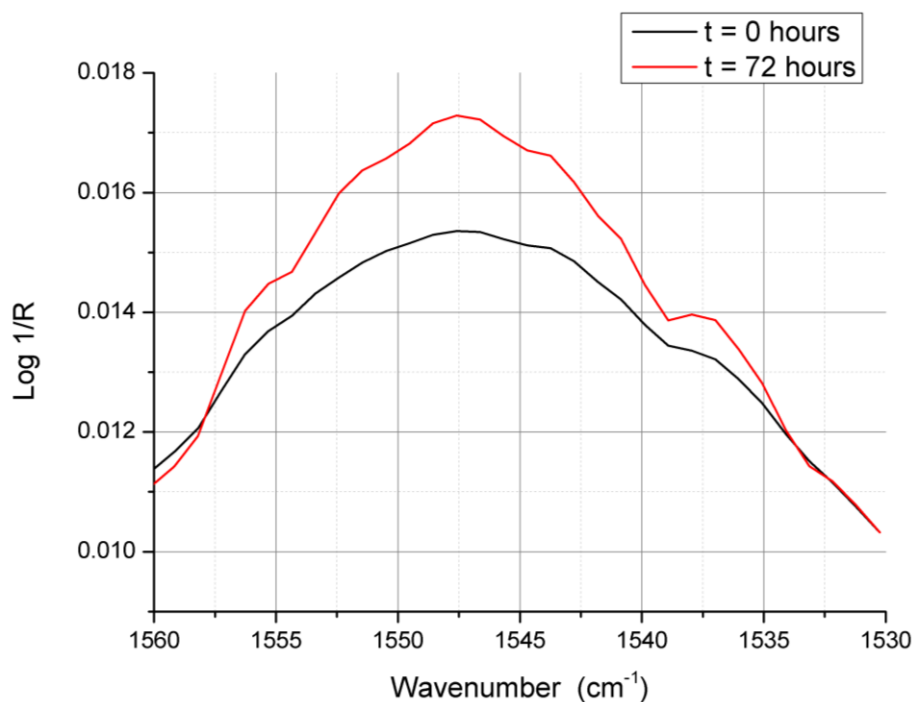


**Figure 4.11:** FTIR spectrum of mPEO<sub>17</sub>-F<sub>4</sub>-OEt on ATR crystal in DMSO-water mixture (20 %v/v) focussing on amide II region.

As shown by the data collected, the ATR-FTIR system detected changes in the hydrogen bond interactions via water interactions between the solvent and the polymer. However, as aforementioned, these changes cannot be reliably and solely attributed to self-assembly and gelation. However, the work has provided a useful foundation, and at a basic level suggests that there are some variations taking place. Running the IR experiments for a longer time period, and at higher resolution (e.g.  $<2\text{ cm}^{-1}$ ), should help to mitigate the issues experienced in these experiments.

#### 4.2.3. Confocal microscopy of self-assembled materials

Confocal microscopy is a useful optical observation technique that offers greater optical resolution than a conventional light microscope. Although, the exact mechanics are beyond the scope of this thesis, a short description of how the technique works is noted. Incident light may cause analyte molecules to fluoresce, i.e. emit a different colour of light that can be detected. If a fluorescent dye is attached to a sample, then it is possible to observe the parts of the sample with the dye molecules attached. This is the basis for fluorescence microscopy. However, the entire sample is illuminated by the excitation light, so the entire sample has the potential to fluoresce, leading to background noise. Confocal microscopy overcomes this problem by using a focal point, in the form of a pinhole. This pinhole blocks “out of focus” light (i.e. light emitted out of the plane of the sample), providing a clearer image.

The microstructure of the gel was investigated using confocal microscopy which was used to provide information about the nature of the network formed. Nile blue was used as the dye, as it fluoresces close to the near infrared region (NIR). The dye was excited at 633 nm, and light was detected between 644 and 795 nm. Using the dye reduced the possibility of autofluorescence from the sample itself<sup>[16]</sup>, which would have otherwise caused an unfocused image. Figure 4.12 shows an example of a phase-contrast microscopy image of a gel without staining; mPEO<sub>17</sub>-F<sub>4</sub>-OEt (10 mg) was dissolved in a 20 %v/v solution of DMSO and water (2 ml). By contrast, Figure 4.13, shows a confocal microscope

fluorescence image of a gel that had been incubated with Nile blue during the hydrogel production (see Section 4.1).

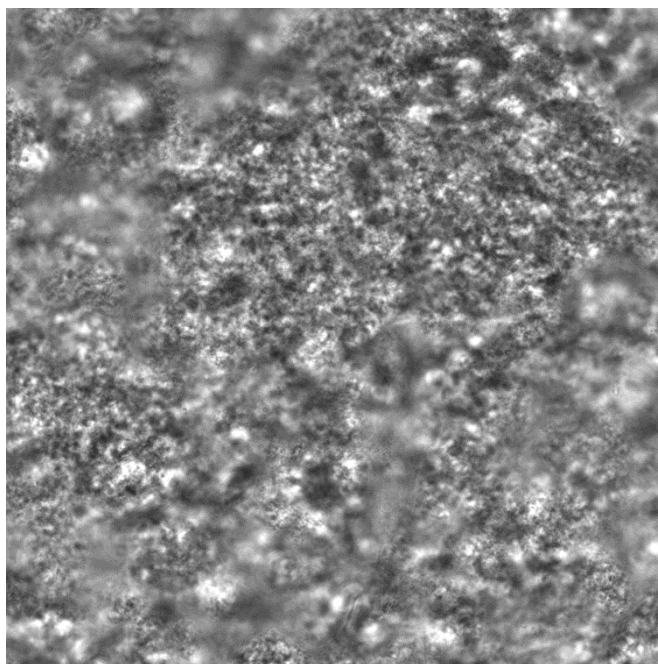


**Figure 4.12:** Confocal phase-contrast image of self-assembled mPEO<sub>17</sub>-F<sub>4</sub>-OEt.

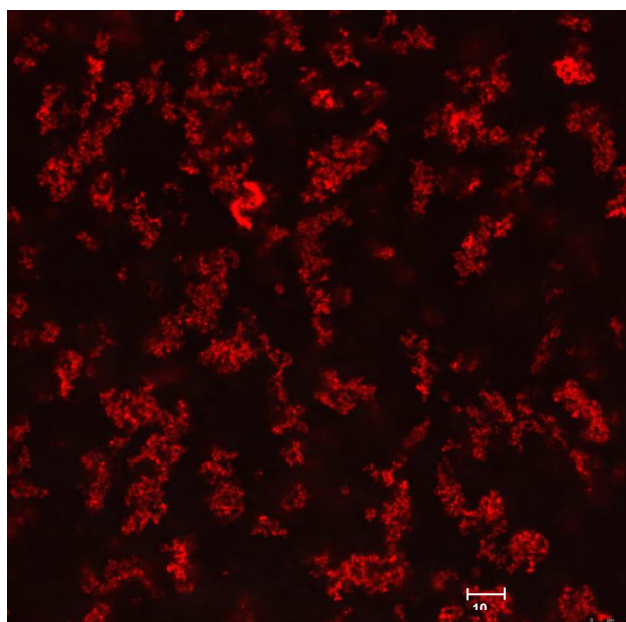


**Figure 4.13:** Confocal fluorescence image (x100 objective, immersion) of self-assembled mPEO<sub>17</sub>-F<sub>4</sub>-OEt stained with Nile Blue.

Using confocal microscopy and Nile blue dye to probe the microstructure of the self-assembled material allowed observation of the aggregated structures (Figures 4.13 and 4.14). This suggests that when self-assembly occurs in the polymer-peptide conjugates, the polymer chains cluster together as a result of the hydrogen bonding between chains (as noted in Figure 4.1). However, as shown in Figures 4.14 and Figures 4.15, the aggregation was discontinuous, as shown by regions that are not fluorescing. It can be speculated that this discontinuity was one of the reasons for the extreme fragility of the gels. The lack of fibril entanglements alongside the fact that not all of the material arranged itself into a hydrogen bond-stabilised structure, explains why self-assembly was easy to disrupt. Nile blue (structure shown in Figure 4.15) was possibly able to interact with the conjugate molecules via hydrogen bonding of the nitrogen atoms and oxygen, or through aromatic interactions, which would have lowered the number of sites per polymer chain for intermolecular hydrogen bonding.

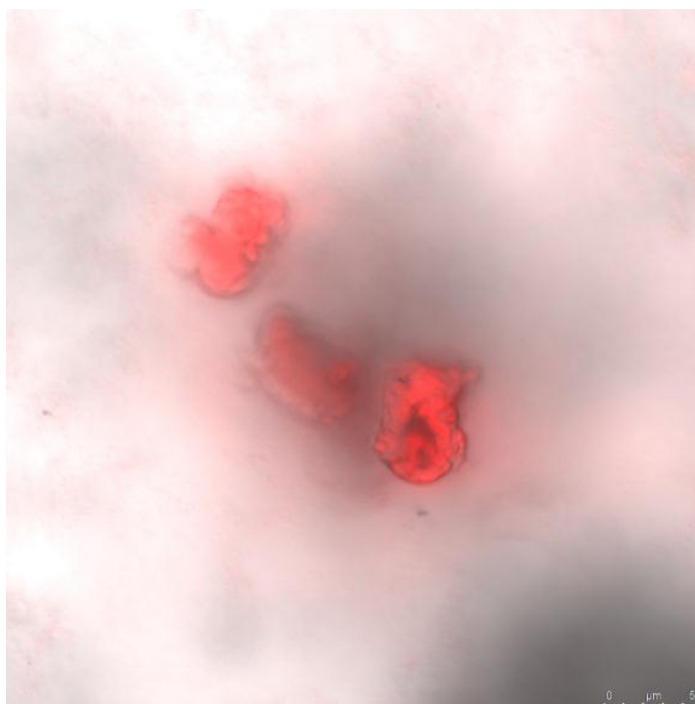


**Figure 4.14:** Confocal microscopy fluorescence and phase-contrast image (x 10 objective) of mPEO<sub>17</sub>-F<sub>4</sub>-OEt (10 mg) in 20 %v/v DMSO-water solution (2 ml).

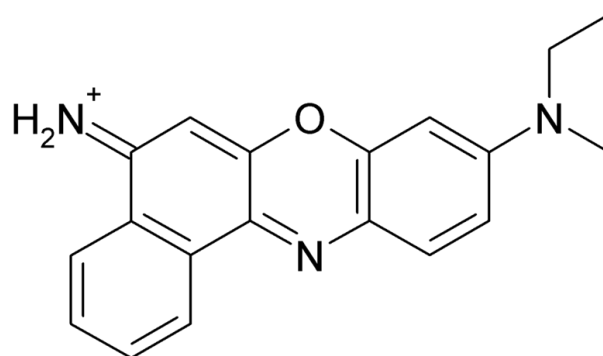


**Figure 4.15:** Structure of Nile blue.

A limitation of the images obtained was that they are an examination of a singular cross-section of the sample. However, the structures observed in the slice may not extend throughout the sample, and therefore provide only limited information on the microstructure. To this extent, a z stack, so named as it takes images along the z axis (which is in and out of the plane of the image), was carried out. This involved imaging 52 slices through the material at intervals of 2  $\mu\text{m}$ , to build a three-dimensional representation of the self-assembled conjugate (Figure 4.16). It can be seen that the material had a discontinuous structure, represented by the fluorescing regions. Conversely, the non-fluorescing regions are parts of the material where the dye molecules have not associated. This reinforces the notion that an aggregate structure was formed during self-assembly.

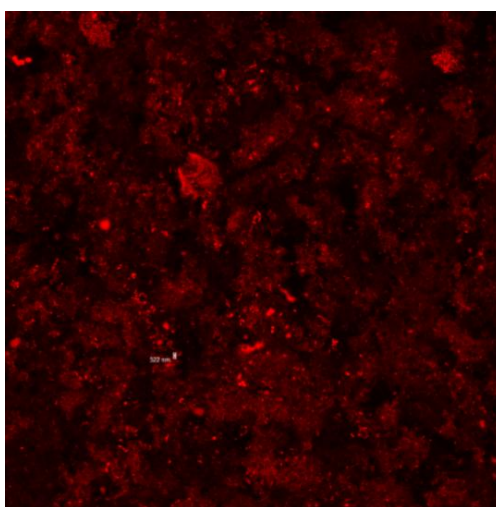


**Figure 4.16:** Confocal microscopy fluorescence z stack of mPEO<sub>17</sub>-F<sub>4</sub>-OEt (10 mg) in 20 %v/v DMSO-water solution (2 ml), stained with Nile blue.

To attain a supramolecular gel from such materials, an entangled network is required. Figure 4.17 shows a greyscale confocal image of a diphenylalanine gel assembled in a DMSO-water binary mixture. From these mixtures it is clear to see an entangled network of fibrils which physically cross-link the sample to form a gel. This is in contrast to the confocal images of extremely weak gels formed in this project, which show very little entanglement between discrete aggregated structures.

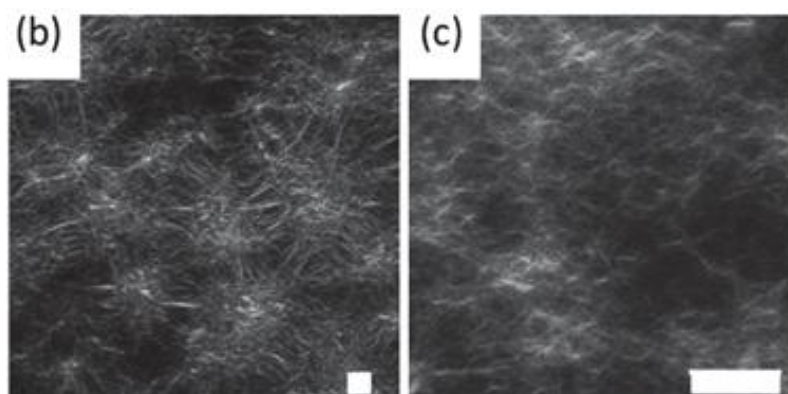


**Figure 4.17:** Confocal microscopy image of gels prepared from Fmoc-FF in DMSO (image adapted from original source).<sup>[17]</sup>

#### **4.3. The effect of temperature on self-assembly behaviour**

The primary issue with the results obtained was reliability. The reproducibility of gel formation was problematic. Initial self-assembly experiments carried out in March 2011 resulted in self-assembly after just one day. However, later experiments required more time for self-assembly to occur. Further, self-assembly seemed to vary between batches of the same material, despite the materials appearing identical when analysed by other techniques (GPC, FTIR, and NMR).

The effect of temperature on self-assembly was an important one and, it can be speculated, partially responsible for the sporadic results. The initial experiments were carried out in early spring, when the ambient temperature was cooler. Later gelation experiments were carried out in summer and autumn when the ambient temperature was raised. In order to determine if temperature was

having an effect, several experiments were carried out at ambient temperature ( $\sim 21$  °C, **Sample A**) and in an insulated cool box (2 °C, **Sample B**). After leaving the samples overnight, it was found that the neither had gelled, although the sample in the insulated box appeared to be more viscous. After a further day standing in their respective containers, **Sample B** appeared to have formed a gel, and **Sample A** appeared to have increased in viscosity. In repeated experiments, the sample in the isolated box (**Sample B**) again gelled quicker than **Sample A**. However, **Sample A** did gel eventually after five days, suggesting that increased temperature merely delays gelation. From this, it is possible to speculate why gels did not appear for certain samples; they were not left to stand for long enough for assembly to occur. The complete temperature dependence and time period for this gelation has yet to be determined and is the subject of future work.

#### 4.4. Comparison of produced self-assembled materials

Self-assembly using polymer-peptide conjugates has been carried out by our group and co-workers. Specifically, two papers focussed on producing hydrogels from mPEO<sub>7</sub>-F<sub>4</sub>-OEt<sup>[12, 17]</sup>. A comparison of the different syntheses of this material is described in Chapter 3. Figure 4.18 shows the conjugates produced using the two methods described in Chapter 3, with part (a) showing the chemical structure of the conjugate synthesised via the previous route.

Producing the conjugate via click chemistry (the conjugate shall be henceforth referred to as **A**), results in the incorporation of a triazole ring. Conversely, synthesis of the conjugate via IBCF chemistry (henceforth referred to as **B**), results only in an amide bond. This is the major structural difference between the produced conjugates, and seems to play a part in self-assembly. The linkage is also slightly different in the PEO as a repeat unit has been lost in **B**. Notably, **A**, formed gel material, and specifically a hydrogel, whereas **B** produced a gel-like material (or a viscous) liquid that had a high propensity to collapse on gentle agitation. TEM images of **A** showed the formation of long, homogenous nanotubes<sup>[13]</sup> (Figure 4.19). Unfortunately, due to extreme fragility of gels formed from **B**, and lack of available access, TEM was not performed.

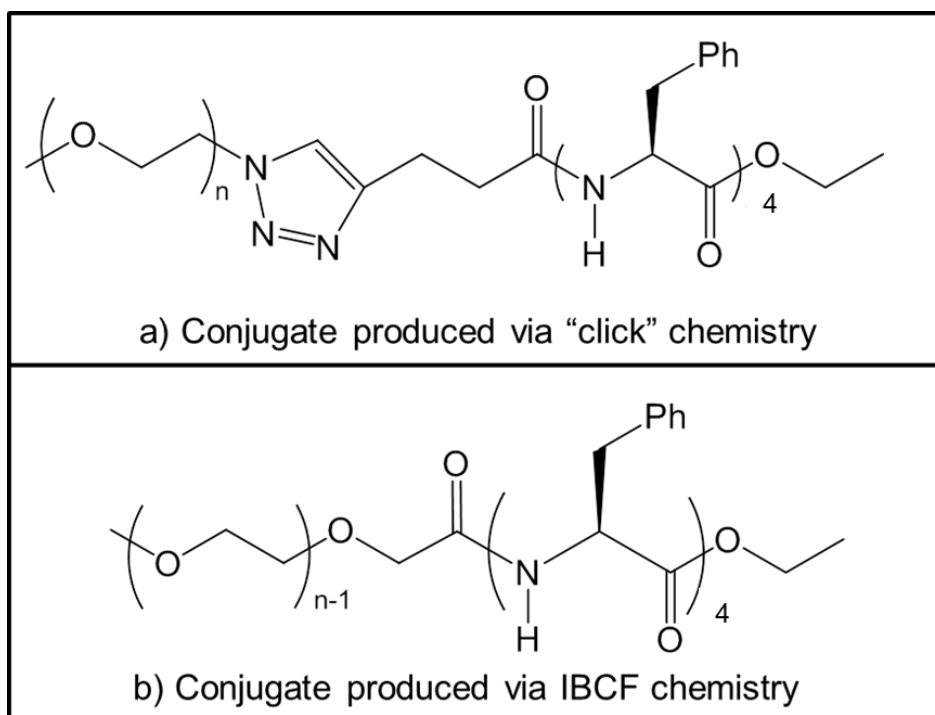


**Figure 4.18:** Structure of polymer-peptide conjugate,  $m\text{PEO}_n\text{-F}_4\text{-OEt}$ , synthesised using; a) click chemistry,<sup>[13]</sup> and b) IBCF chemistry (see Chapter 3 for full synthesis).

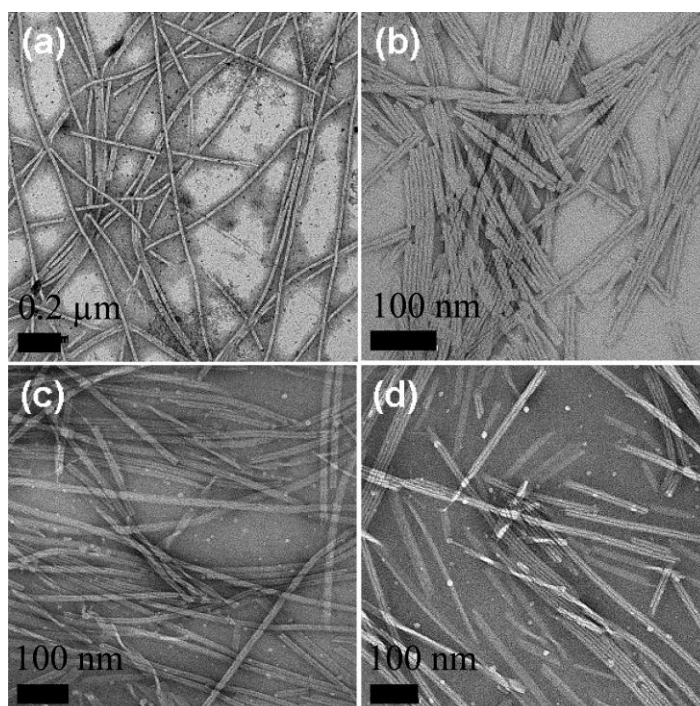


**Figure 4.19:** Transmission electron microscope image of  $m\text{PEO}_7\text{-F}_4\text{-OEt}$  showing nanotube structures synthesised via the previous route<sup>[13]</sup>.

The TEM images, coupled with the previously discussed rheology data (Figure 4.6) allow two conclusions to be drawn. Firstly, the triazole ring clearly has an effect on gel formation. The rheology data showed that the gel formed from **A** was much stronger and more stable than **B**. This is attributed to the propensity to form intermolecular hydrogen bonds between conjugates increasing, due to the additional nitrogen atoms present on the triazole ring, which can interact with the hydrogen atoms on the peptide.

The methods used for gelation differed for **A** and **B**. A gel of conjugate **A** was prepared using a solvent-exchange method, whereby the conjugate was dissolved in a THF-water co-solvent mixture. This solution was then dialysed against water to remove THF and allow hydrogel formation. Conjugate **B** was dissolved in an organic solvent, with water being added afterwards. Changing the gelation method therefore may well have affected gel formation. The modification of the protocol was a result of further work by Adams' group<sup>[18]</sup> which focussed on gel formation of diphenylalanine peptides (FF) in organic-aqueous binary solvents mixtures. Furthermore, synthesis of the conjugates via the click route has several disadvantages (see Chapter 3) making it unattractive for gel production. The new method is simpler and a more industrially-relevant than the dialysis route to gelation. However, as hydrogel formation of homologous polymer-peptide conjugates (as opposed to oligopeptide gel formation) has been previously shown to be reliable, future work should focus on the propensity of these materials for hydrogel formation, using dialysis to ensure complete removal of the organic solvent.

#### **4.5. Conclusions**

Initial self-assembly studies were carried out using PEO-phenylalanine conjugates of varying polymer chain length and peptide length. Twelve conjugates were dissolved in a variety of different solvent compositions and qualitative self-assembly behaviour was noted. It was found that at least four phenylalanine repeat units were required for any assembly to occur. This was most likely due to the number of free hydrogen bonds site available for stability, coupled with the increased hydrophobic interactions and  $\pi$ - $\pi$  stacking. The

number of environments in which the conjugates self-assembled, increased with polymer chain length. However, all of these results were based on qualitative observation, so a more quantitative analysis was undertaken.

Three analytical techniques (rheology, FTIR, and confocal microscopy) were used to probe the material in order to elucidate the microstructure and physical/chemical interactions taking place when forming a gel. The overall picture formed from these techniques is that the actual material underwent some change in hydrogen bond interactions over time (water was removed from between the polymer chains), but traditional gelation did not occur. Instead, an aggregated structure was formed that was weak, hence why the material broke down on gentle agitation.

Further work in this area should focus on improving the reliability of the system, and investigating the full extent of temperature on the propensity of the material to self-assemble. In this regard, FTIR would prove the most useful tool as it is able to track the hydrogen bond interactions between the solvent and the conjugate. The route to gelation should also be further investigated, and modified to ensure that it is both simple and industrially viable.

#### 4.6. References

1. Atkins P. and De Paula J., Atkins' Physical Chemistry. Eighth Edition ed. **2006**, Oxford: Oxford University Press.
2. Sahoo S., Kumar N., Bhattacharya C., Sagiri S. S., Jain K., Pal K., Ray S. S., and Nayak B., Organogels: Properties and Applications in drug delivery, *Designed Monomers and Polymers*, **2011**, 14: p. 95-108.
3. Sohdi A. A., Campbell D., and Topham P. D., Polymer-Peptide Conjugate Hydrogels; Towards Controlled Drug Delivery *Chiang Mai Journal of Science*, **2012**, 39(4): p. 351-372.
4. Adams D. J. and Topham P. D., Peptide Conjugate Hydrogelators, *Soft Matter*, **2010**, 6(16): p. 3707-3721.
4. Adams D. J. and Topham P. D., Peptide Conjugate Hydrogelators, *Soft Matter*, **2010**, 6(16): p. 3707-3721.
5. Ruel-Gariépy E. and Leroux J-C., In situ-forming hydrogels-review of temperature-sensitive systems, *European Journal of Pharmaceutics and Biopharmaceutics*, **2004**, 58(2–3): p. 409-426.
6. Li F., Zhu Y., You B., Zhao D., Ruan Q., Zeng Y., and Ding C., Smart Hydrogels Co-switched by Hydrogen Bonds and  $\pi$ - $\pi$  Stacking for Continuously Regulated Controlled-Release System, *Advanced Functional Materials*, **2010**, 20(4): p. 669-676.
7. Carey F. A. and Sundberg R. J., Part A: Structure and Mechanisms. Advanced Organic Chemistry. **2004**: Springer.
8. Mohsen-Nia M., Amiri H., and Jazi B., Dielectric Constants of Water, Methanol, Ethanol, Butanol and Acetone: Measurement and Computational Study, *Journal of Solution Chemistry*, **2010**, 39(5): p. 701-708.
9. Marchetti A., Preti C., Tagliazucchi M., Tassi L., and Tosi G., The *N,N*-dimethylformamide + ethane-1,2-diol solvent system. Dielectric constant, refractive index, and related properties at various temperatures, *Journal of Chemical & Engineering Data*, **1991**, 36(4): p. 365-368.
10. Dunnitt J. S. and Gasser R. P. H., Electrolyte solutions in dimethyl sulphoxide. Part 1.-Lithium chloride, *Transactions of the Faraday Society*, **1965**, 61: p. 922-927.
11. Hansem C. M., Hansen Solubility Parameters: A User's Handbook. 2nd Edition ed. **2007**, USA: Taylor & Francis Group.
12. Tzokova N., Fernyhough C. M., Topham P. D., Sandon N., Adams D. J., Butler M. F., Armes S. P., and Ryan A. J., Soft Hydrogels from

Nanotubes of Poly(ethylene oxide)-Tetraphenylalanine Conjugates Prepared by Click Chemistry, *Langmuir*, **2009**, 25(4): p. 2479-2485.

13. Sammon C., Li C., Armes S. P., and Lewis A. L., ATR-FTIR Studies of a Thermo-Responsive ABA Triblock Copolymer Gelator in Aqueous Solution, *Polymer*, **2006**, 47(17): p. 6123-6130.
14. Su Y.-L., Liu H.-Z., Guo C., and Wang J., Association Behavior of PEO-PPO-PEO Block Copolymers in Water or Organic Solvent Observed by FTIR Spectroscopy, *Molecular Simulation*, **2003**, 29(12): p. 803-808.
15. *Optical Sensor Systems in Biotechnology*, G. Rao, Editor. **2010**, Springer. p. 162.
16. Raeburn J., Pont G., Chen L., Cesbron Y., Levy R., and Adams D. J., Fmoc-diphenylalanine hydrogels: understanding the variability in reported mechanical properties, *Soft Matter*, **2012**, 8(4): p. 1168-1174.
17. Tzokova N., Fernyhough C. M., Butler M. F., Armes S. P., Ryan A. J., Topham P. D., and Adams D. J., The Effect of PEO Length on the Self-Assembly of Poly(ethylene oxide)-Tetrapeptide Conjugates Prepared by "Click" Chemistry, *Langmuir*, **2009**, 25(18): p. 11082-11089.

# **CHAPTER 5**

## **Electrospinning Novel Materials**

## 5. Electrospinning Novel Materials

Spinning new materials requires a systematic approach to ensure reliable fibre production. This chapter describes the electrospinning process of a selection of materials. Section 5.1 focuses on the initial electrospinning experiments (designed to increase familiarity with the process), using polystyrene. The following section (Section 5.2) details the investigation into the spinnability of PIM-1. Section 5.3 draws from both of the preceding sections, and summarises the fibre production of nanoparticle cages solution coupled with a hydrophobic polymer scaffolds. In Section 5.4, details regarding the spinnability of materials (polymer-peptide conjugates) produced in Chapter 3 are outlined. Finally, Section 5.5 concludes the chapter and provides a brief description of the direction for future work.

### 5.1. Electrospinning polystyrene

Polystyrene (PS) is a common and widely used aromatic polymer. There are many reports in the literature of PS fibres produced via electrospinning<sup>[1-6]</sup>. This vast array of literature, coupled with the low economic considerations and reported ease of “spinnability”, makes polystyrene a good material to use in order to understand the electrospinning process and the parameters required to successfully produce fibres. Two solvents have been investigated THF and DCM, and thus Section 5.1 is divided into two sections, encompassing these two solvents (separately).

#### 5.1.1. Electrospinning polystyrene in tetrahydrofuran

Polystyrene (500,000 Da) is soluble in a variety of solvents. Initial electrospinning experiments were adapted from work reported by Casper *et al.*<sup>[2]</sup> Preliminary electrospinning of polystyrene took place in tetrahydrofuran (THF), using a voltage of 15 kV, a tip-to-collector distance of 15 cm, and a flow rate of 1 ml hour<sup>-1</sup>, with variable concentration. Figure 5.1

shows SEM images of any deposited material formed. The concentration of polystyrene was systematically varied from 10 to 35 wt%.

At high concentrations (>25 wt%, **A1**, **A2**, and **A3**), a white fibrous material was deposited onto the collecting plate. SEM showed that the polymer had formed long, smooth fibres (Figure 5.1). The average diameter of the fibres in **A1** (35 wt%) was 6  $\mu\text{m}$ , indicating that microfibrils (diameter > 1000 nm) had been formed. As the concentration was reduced to 30 wt% (**A2**), the fibre diameter increased to 17  $\mu\text{m}$ , as expected. This widening is due to a decrease in the number of chain entanglements (as a result of the lower concentration) which help to stabilise the polymer jet during expulsion. An additional decrease in concentration (25 wt%, **A3**) resulted in narrower fibres forming, with an average diameter of 10  $\mu\text{m}$ , which was surprising as fibre diameter was expected to again increase. SEM also shows an increased number of fibres at this concentration, suggesting trade-off between fibre density and diameter, although conclusions cannot be drawn solely from this limited sample size.

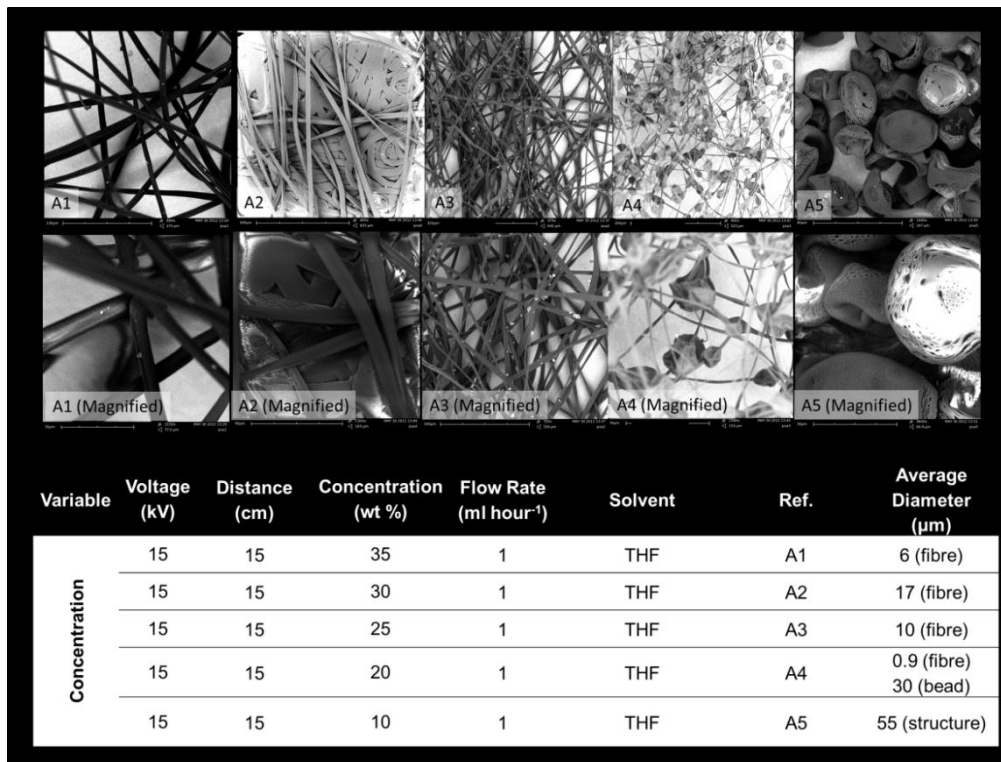


**Figure 5.1:** SEM images of polystyrene electrospun at different concentrations from tetrahydrofuran.

Moderate concentrations of polystyrene (20 wt%, **A4**) also resulted in fibre production. The average diameter of the fibres was 900 nm, indicating the nanofibres have been formed (diameter < 1000 nm). However, the SEM shows that discrete particulate structures, known as beads, formed along the fibres. These beads are the results of perturbations in the polymer jet, from deformation by surface charges and insufficient stabilisation by chain entanglements (arising from the lowered concentration). Bead diameter varied approximately from 16  $\mu\text{m}$  to 38  $\mu\text{m}$ . A final decrease in concentration (10 wt%, **A5**) resulted in non-fibrous material being deposited on the collector plate. SEM confirms that no fibre production occurred, instead the material formed small discrete polymer particles. The diameter of one of the typical structures was measured to be 55  $\mu\text{m}$ , with a circumference of 172  $\mu\text{m}$ . This concentration was too low for chain entanglements to form, thus once the induced surface charge overcame the effects of surface tension, the polymer jet was immediately perturbed and thus divided (there was no elongation of the polymer). The formation of beads and other structures is undesirable, and therefore the optimal window for spinning polystyrene in THF is at concentrations greater than 20 wt%. As these were initial tests, an investigation into what concentration would be too viscous to spin was not undertaken.

#### 5.1.2. Electrospinning polystyrene in dichloromethane

Electrospinning of polystyrene was also undertaken using dichloromethane (DCM) as a solvent. This was carried out as DCM was used in later spinning experiments, in which the solvent was “pre-set” and was not replaceable. The initial spinning parameters used was a voltage of 15 kV, a flow rate of 1 ml hour<sup>-1</sup>, and a tip-to-collector distance of 15 cm. Three concentrations (30, 25, and 20 wt%) were chosen based on the optimal window noted in the preceding section. Spinning polystyrene at the three concentrations resulted in deposition of a white fibrous material on the collecting plate. SEM (Figure 5.2) showed that at 30 wt% (**B1**), the solution formed microfibrils, with an average diameter of 11  $\mu\text{m}$ . Decreasing the concentration (25 wt%, **B2**) produced fibres with a marginal increase in average diameter (12  $\mu\text{m}$ ). This increase in

diameter was again observed when the concentration was further reduced to 20 wt% (**B3**), with the fibres possessing an average diameter of 12  $\mu\text{m}$ . In comparison to THF (**A4**), DCM solutions show no beading at 20 wt% (**A3**). As the solvent is the only parameter that has changed, it must be responsible for the lack of beading. DCM has a higher dielectric constant (i.e. how easily a material can be polarised by an induced electric field, and thus ease of atomisation) than THF (8.9<sup>[7]</sup> and 7.5<sup>[8]</sup>). Therefore, when the polymer is dissolved in DCM, there is a greater charge density, which in turn is able to overcome the surface tension, imposing higher elongation forces on thus jet, thus producing fibres with smaller diameters.

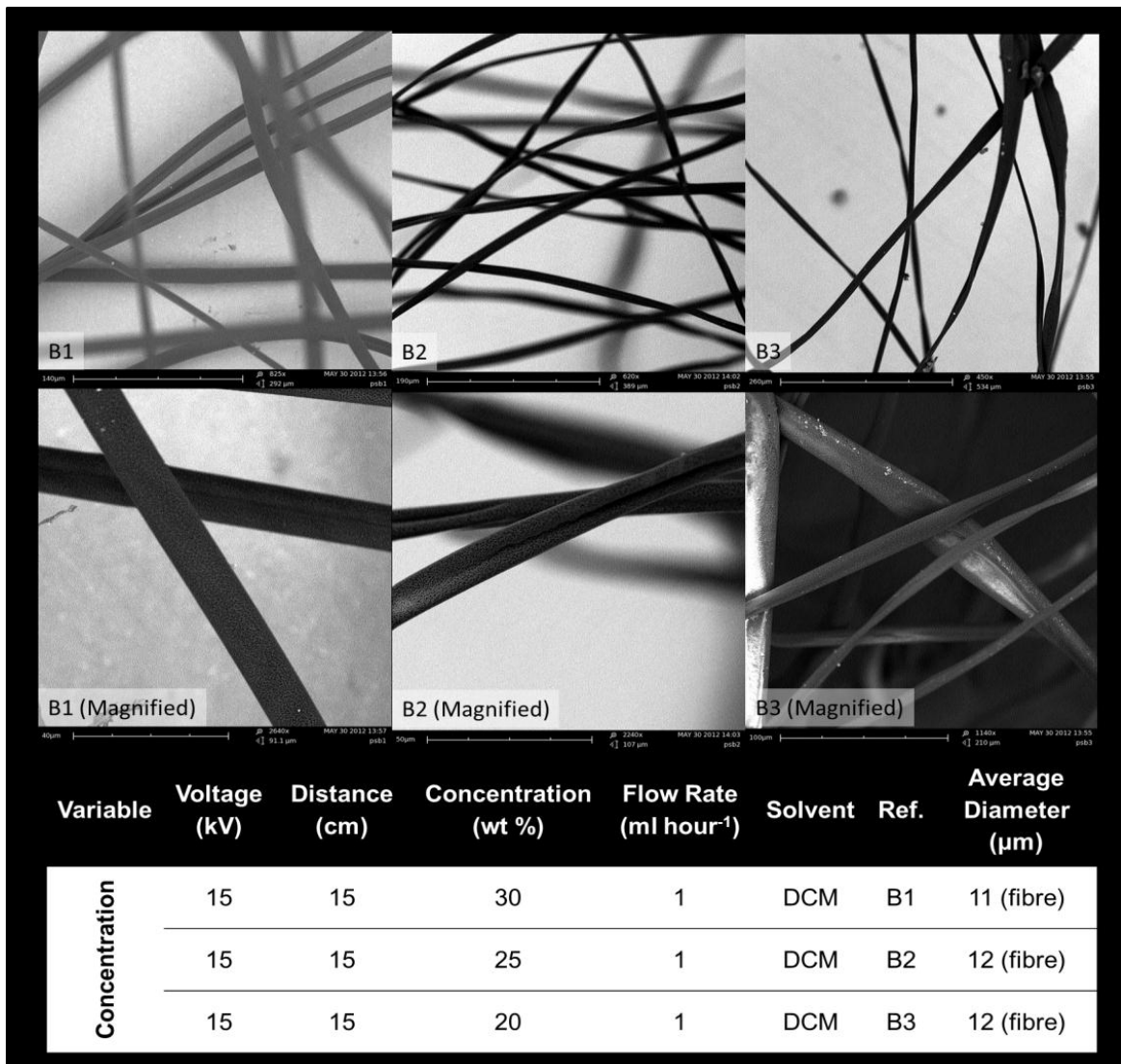


**Figure 5.2:** SEM images of polystyrene electrospun at different concentrations from dichloromethane.

Electrospinning polystyrene from DCM requires a concentration of at least 20 wt%, with smaller diameter fibres produced as the concentration increases (> 30 %). These initial experiments show the formation of both nano- and microfibrils from polystyrene. The work was useful for understanding the fundamentals of the electrospinning process. Polystyrene was also used as a scaffold with nanoparticles, and the mixture was then electrospun as discussed in Section 5.3.

## 5.2. Electrospinning polymers with intrinsic microporosity

Polymers with intrinsic microporosity (PIMs) were supplied by the University of Liverpool and used as received. The structure of the polymer received, PIM-1, is shown in Figure 5.3.

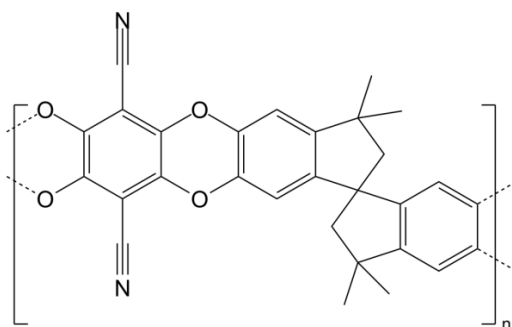


**Figure 5.3:** Structure of a polymer with intrinsic microporosity, PIM-1.

PIMs are porous materials that offer high surface areas. Microporosity has been shown to arise from rigid, spirocyclic (a bicyclic compound where the rings are joined through one atom) scaffolds, which prevent aggregation of planar components<sup>[9]</sup>. However, it is not necessary to form networks of covalent bonds in order to produce these materials. Non-networked polymers can form microporous structures because of the high rigidity, and contortion of their molecular structure, which does not allow efficient filling of space<sup>[10]</sup> when the macromolecules are packed in the solid state. The advantage of using non-networked polymers, which are soluble, is that they allow for processing using solvent-based techniques. These materials are of particular importance for gas adsorption<sup>[11]</sup>, separation (membranes)<sup>[12]</sup>, and heterogeneous

catalysis<sup>[13]</sup>. There have been no reports of fibre production of PIMs. Producing fibres of the materials would further increase the available surface area, allowing for a great range of functionality, especially with regards to gas adsorption. By producing nanofibres, this important surface area-to-volume ratio is further augmented.

Before electrospinning was attempted it was important to establish a good solvent for PIM-1 that is also suitable for the spinning process. This was critical as the polymer must be completely dissolved before spinning can take place. PIM-1 is reported to be soluble in at least three commonly known solvents; chloroform, dimethylformamide (DMF), and tetrahydrofuran (THF). Solubility tests were conducted on the polymer in THF and DMF and the results are summarised in Table 5.1. It can be seen that PIM-1 did not dissolve in DMF at all, and instead formed a suspension in all cases. Therefore, DMF alone was discounted as a possible solvent.

Although PIM-1 dissolved completely in THF (5 wt%), the viscosity of the solution was determined to be too low for electrospinning. Increasing the concentration to 10 wt% did not mitigate this problem. The solution was (qualitatively) deemed viscous enough to attempt electrospinning at 15 wt%. Further increases of solution concentration (>20 wt%) were found to be too viscous to spin.

**Table 5.1:** Qualitative solubility and viscosity observations of PIM-1.

	5 wt%	10 wt%	15 wt%	20 wt%
DMF	Suspension	Suspension	Suspension	Suspension
THF	Dissolves (insufficiently low viscosity)	Dissolves (insufficiently low viscosity)	Dissolves (viscous, but able to flow)	Dissolves (too viscous)
Composition	0.5 g in 9.5 g	1.0 g in 9.0 g	1.5 g in 8.5 g	2.0 g in 8.0 g

Initial attempts to spin a solution (15 wt%) of PIM-1 in THF did not result in fibre production, despite deposition of material onto the collecting plate. The volatility of THF in the applied electric field caused blockages of the spinning apparatus. Although, the solution viscosity was initially deemed acceptable, the effects of the solvent volatility offset this, thus it was not feasible to spin at these concentrations. Therefore, lower concentrations of PIM-1, between 5 and 15 wt%, were investigated.

Preliminary efforts using lower concentrations of PIM-1 were again hindered. THF was not deemed viable for electrospinning PIM-1. However, as THF provided the best solubility, a co-solvent system was used to mitigate its volatility. The choice of co-solvent was either chloroform or DMF and the solubility tests results are detailed in Table 5.2. A solution of 10 wt% was selected for the tests as this concentration lay between the two extremes of acceptable viscosity for spinning. In the majority of cases the resulting mixture was either insoluble or moderately viscous. A solvent composition of THF: DMF (9: 1) was found to be the optimal solvent system.

As a general note, dissolution of PIM-1 was difficult and the mixture required extensive stirring. Furthermore, the solution was incompatible with water, with the polymer solidifying on contact. Therefore, it was necessary to ensure that the dissolution conditions minimised exposure to water. PIM-1 also had a tendency to block syringes and needles after spinning.

An investigation into the effect of four parameters on the electrospinning process and the production of nanofibres was undertaken. The four parameters chosen were concentration (**C**), voltage (**D**), distance (**E**), and flow rate (**F**) and are discussed separately in the following sections.

**Table 5.2:** Solubility and viscosity observations of PIM-1 in co-solvent systems.

Solvent	100: 0	90: 10	75: 25	60: 40	50: 50	40: 60	25: 75	10: 90	0:100
<b>THF: DMF</b>	Soluble Low Viscosity	Soluble Low Viscosity	Soluble Moderate Viscosity	Partially Soluble Moderate Viscosity	Partially Soluble	Insoluble	Insoluble	Insoluble	Insoluble
<b>THF: CHCl<sub>3</sub></b>	Soluble Low Viscosity	Soluble Moderate Viscosity	Partially Soluble Low Viscosity (Precipitate)	Insoluble	Insoluble	Insoluble	Partially Soluble Low Viscosity (Precipitate)	Soluble High Viscosity Some (Precipitate)	Soluble High Viscosity
<b>CHCl<sub>3</sub>: DMF</b>	Soluble Low Viscosity	Soluble Moderate Viscosity	Soluble Moderate Viscosity	Partially Soluble High Viscosity (Precipitate)	Partially Soluble (Precipitate)	Insoluble	Insoluble	Insoluble	Insoluble

### 5.2.1. Effect of concentration on fibre formation of electrospun PIM-1

The effect of PIM-1 concentration on the formation of nanofibres was investigated. Scanning electron microscopy (SEM) was used to determine if fibre formation had been successful. Images taken with SEM at different spinning concentrations of PIM-1 are shown in Figure 5.4. Selected higher resolution images (taken at the University of Liverpool) of electrospun PIM-1 at different concentrations are shown in Figures 5.5 – 5.8.

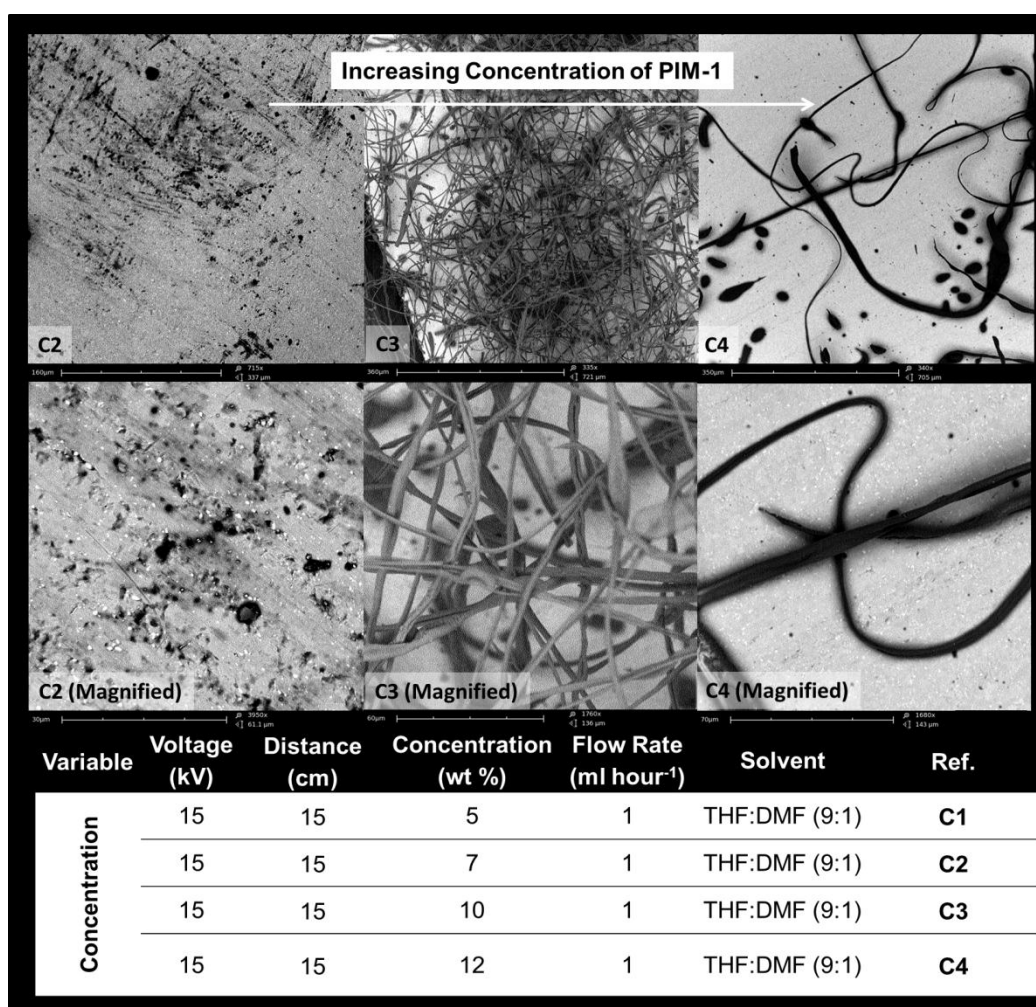


**Figure 5.4:** SEM images of PIM-1 electrospun at different concentrations.

PIM-1 was spun at 15 kV, with a tip-to-collector distance of 15 cm, and at a flow rate of 1 ml hour<sup>-1</sup>. At low concentrations (<10 wt%, **C1** and **C2**), there were no fibres observed by SEM (Figure 5.4), however there was deposition of non-fibrous material onto the collecting plate (noted at 7 wt%, **C2**). Increasing

the concentration to 10 wt% (**C3**) resulted in a thick fibrous layer forming, which was confirmed by SEM to be polymer fibres. The fibres formed were smooth and had an average diameter of 6  $\mu\text{m}$  (Figure 5.5). Strictly speaking **C3** produced microfibrils rather than nanofibrils, as the diameter was above 1  $\mu\text{m}$  (1000 nm). During this spinning experiment, thick fibrous material also emanated directly from the needle and had a consistency similar to wool. SEM (Figures 5.6) showed the “wool” had a tape-like (flat and short, rather than cylindrical) structure. A further increase in concentration (12 wt%, **C4**) also yielded polymer fibres. These fibres had a reduced diameter ( $\sim 3 \mu\text{m}$ ) (Figure 5.7), and thus were also microfibrils. Again, during this spinning experiment, polymer “wool” was produced from the aperture (Figure 5.8). The average diameter of the “wool” structures ranged between 8 and 9  $\mu\text{m}$ . At concentrations greater than 15 wt% (**C5**), no fibres were formed as the conductive solution was too viscous. Therefore, it has been established that fibre production only occurs between 10 and 15 wt% using the aforementioned parameters. This is the optimal window that was investigated for the production of thinner polymer fibres.



**Figure 5.5:** SEM images of PIM-1 (**C3**), showing microfibrils. Images courtesy of the University of Liverpool.



**Figure 5.6:** SEM images of the non-deposited “wool” from electrospinning PIM-1 (C3), showing fibre production. Images courtesy of the University of Liverpool.



**Figure 5.7:** SEM images of PIM-1 (C4), showing microfibrils. Images courtesy of the University of Liverpool.



**Figure 5.8:** SEM images of the non-deposited “wool” from electrospinning PIM-1 (**C4**), showing fibre production. Images courtesy of the University of Liverpool.

These initial results suggest that concentration is one of the dominating factors in determining fibre formation. This is due to the relationship between concentration and viscosity. At lower concentrations there are an insufficient number of entangled polymer chains that, due to Rayleigh instabilities<sup>[14]</sup>, do not lead to fibre production. As the solvent evaporates, polymer concentration increases and entanglements become more prevalent. This helps to stabilise the droplet from separation (division). However, surface charge also increases, which overcomes the surface tension of the droplet, and acts as a driving force for the division of the droplet. Insufficient chain entanglements (i.e. at low concentrations) resulted in bead formation because the polymer stream cannot be fully stabilised. This shows that the concentration must be high enough to ensure that the effects of chain entanglement are greater than the dispersive effects of the induced surface charge.

Increasing the concentration of PIM-1 introduces additional electronegative groups which generate increased repulsive forces between the molecules, thus improving elongation during Taylor cone formation, and leading to decreased fibre diameters, also reducing the amount of beading present. However, the effects of the other spinning parameters must also be considered, and are investigated in the following sections.

### 5.2.2. Effect of voltage on fibre formation of electrospun PIM-1

Changing the strength of the electric field affects the surface interactions of the solution, and thus the elongation of the fibre. If the voltage is insufficient to overcome the charge of the solution, Taylor cone formation will be inhibited and fibre formation will not occur. At extreme voltages the repulsive forces from the surface charge will cause the droplet to disperse prior to ejection. A summary of the results obtained for variable voltages are shown in Figure 5.9, at 10 wt%. This concentration was chosen because it has been demonstrated that fibre formation occurred, at 15 kV (**C3**), which provided a good starting point to modify the voltage from. The parameters from **C4** (12 wt%) were not used as only a limited amount of material was available. However, any concentration between 10 and 15 wt% would be viable, and it would be interesting to see the effect of voltage at difference concentrations within this range.

PIM-1 (10 wt%) was electrospun with a tip-to-collector distance of 15 cm, and at a flow rate of 1 ml hour<sup>-1</sup>. The electric field generated at 5 and 10 kV was too low. Although some deposition occurred at 10 kV (**D1**), SEM showed that the material was non-fibrous. Increasing the voltage to 15 kV (**C3**) resulted in fibre formation. Further increases to the voltage, to 20 kV (**D2**) and 25 kV (**D3**), did not produce any fibrous material, instead forming small discrete polymeric particles (Figure 5.9).

From the results, it can be determined that voltage plays a critical part in the formation of fibres. The effects of increased voltage (i.e. above 15 kV) show the formation of fibres is inhibited. In **D1** the electric field (10 kV) clearly did not

have enough energy to overcome the surface tension of the droplet to form a jet. Conversely, at voltages above 15 kV, the induced surface charge overcomes the surface tension of the droplets but also overcomes the stabilisation effect of chain entanglements, resulting in particle formation. Furthermore, it is possible that as high voltages were applied, the solution deformed immediately, atomising instantaneously, thus having insufficient time to form a Taylor Cone. It is therefore noted that 15 kV was determined to be in the optimal voltage range for PIM-1 material at a concentration of 10 wt%. However, increasing concentration (and therefore increasing chain entanglements) may overcome the increased propensity of the droplet to disperse at higher voltages due to a high surface charge. As discussed previously, increased concentration results in a highly viscous solution that causes needle blockage, thus hindering electrospinning. A balance between the parameters is required, and will be the subject of future work.

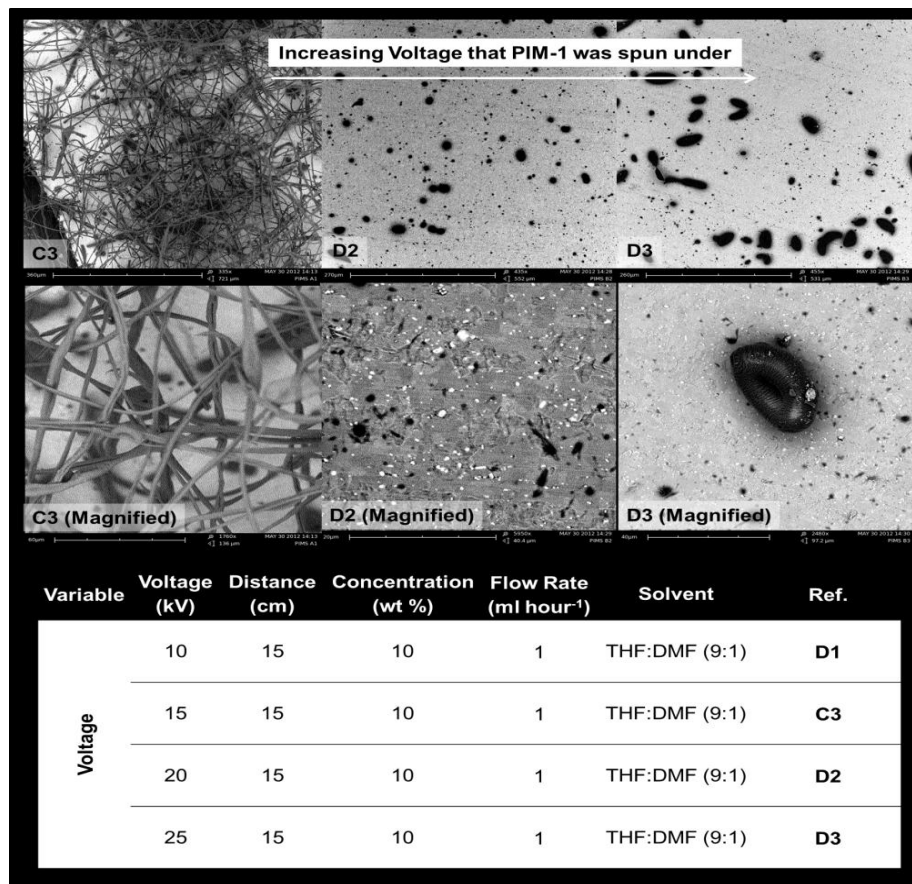


**Figure 5.9:** SEM images of PIM-1 electrospun at different voltages. D1 is not shown as there was no deposition.

### 5.2.3. Effect of tip-to-collector distance on fibre formation of electrospun PIM-1

The distance between the aperture and the collecting plate determines the amount of time the polymer spends in the electric field. This will affect the length and quality of the material produced. Figure 5.10 shows the results when the tip-to-collector distance, also termed the working distance, is varied. Distance was measured from the tip of the needle (i.e. from the aperture) to the collector plate.

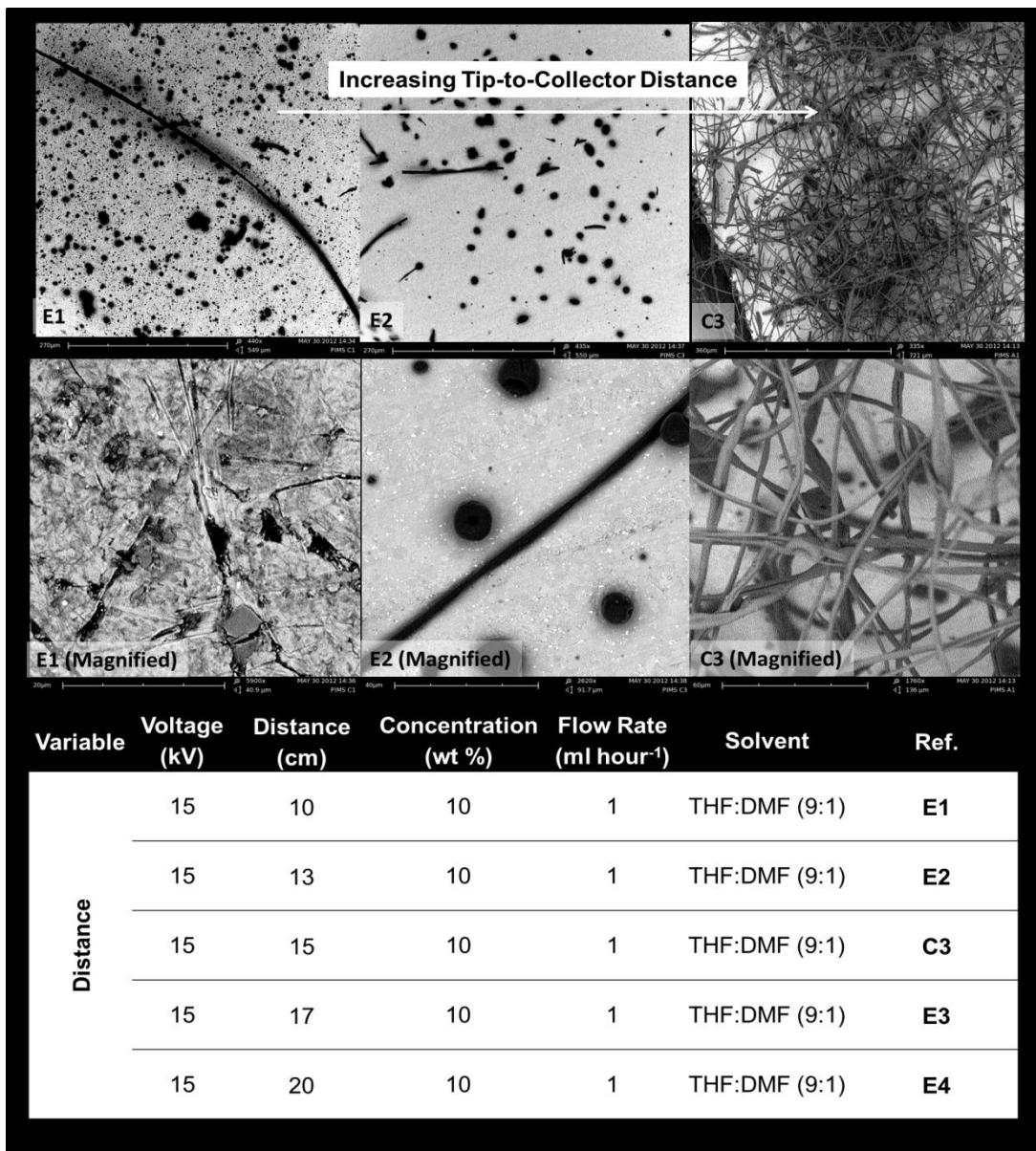


**Figure 5.10:** SEM images of PIM-1 electrospun at different tip-to-collector distances.

Electrospinning of PIM-1 (10 wt%) occurred at a voltage of 15 kV and a flow rate of 1 ml hour<sup>-1</sup>. Distances ranging between 10 and 13 cm were too short. Some deposition occurred at 10 cm (**E1**), however the material was non-fibrous. SEM showed the formation of aggregates with variable geometry ranging from spherical shapes to short worm-like structures (Figure 5.11). At a distance of 13 cm (**E2**) some fibre formation was observed, however SEM showed that the material was non-fibrous, and instead was an assortment of thin, elongated rod structures. There was also a decrease in the number of particles visible. It is speculated that these structures are the initial formation of fibrous material. The diameter of the single fibre shown in Figure 5.10 is approximately 2.8 µm. This is smaller than those reported for **C3** or **C4**, however the number of fibres is much lower and only one fibre has been measured, so conclusions cannot be drawn from these data alone. Increasing the distance further (**E3** and **E4**) resulted in no deposition forming. Therefore it is predicted that the optimal window for distance ranges between 13 and 15 cm.



**Figure 5.11:** SEM images of the deposited material from electrospinning PIM-1 (**E1**), showing aggregate deposition. Images courtesy of the University of Liverpool.

The working distance changes the flight time available to the polymer jet. It was predicted that modifying the distance would either result in the formation of thinner fibres (as the distance increases), as there is more time for a bending instability to occur, thus more time for the jet to be stretched, or to result in thicker fibres due to a reduction in the strength of the electric field. This reduction arises because the magnitude of the electric field is inversely proportional to the distance between the plates (i.e.  $E = -V/d$ ). The bending instability arises from small changes in the trajectory of the polymer jet as it is expelled from the spinneret. These perturbations generate a force due to self-repulsion of the jet as symmetry is lost. The viscoelastic nature of the polymer solution initially overcomes these forces, however the perturbation force eventually becomes larger, causing the bending instability, which in turn is stronger than the elastic component of the polymer solution, thus elongating the jet<sup>[15]</sup>.

It can be observed that tip-to-collector distance plays a somewhat important role in fibre formation. Fibres produced by varying the distance had different characteristics where increasing the pathway appeared to decrease the diameter of the fibres. Production of narrower fibres is generally beneficial (as large surface area-to-volume ratio increases their reactivity), however this is offset by the number of fibres produced, and conversely the number of discrete particles/structures produced. The general lack of fibres produced when varying the distance, is likely attributable to the local electric field being too strong or too weak, consequently making it difficult to initiate jet formation.

#### 5.2.4. Effect of flow rate on fibre formation of electrospun PIM-1

The flow rate is determined by the accuracy of the pumping system, and the viscosity of the conductive (polymer) solution. Figure 5.12 shows the results when the flow rate is varied. Electrospinning of PIM-1 (10 wt%) occurred at a voltage of 15 kV, and a distance of 15 cm. Low flow rates, such as 0.5 ml hour<sup>-1</sup> (**F1**), are too short and result in deposition that is non-fibrous. Fibres form when the flow rate is increased to 1.0 ml hour<sup>-1</sup> (**C3**) and 1.5 ml hour<sup>-1</sup> (**F2**). High

resolution SEM (Figure 5.13) shows fibres with an average diameter of 5  $\mu\text{m}$ , but also some disjointed particles (minor beading). On further increasing the flow rate to 2 ml hour<sup>-1</sup> (**F3**), a thick fibrous layer was produced. High resolution SEM revealed thinner fibres ( $\sim 4 \mu\text{m}$ ), but with a significant increase in beading (Figure 5.14).

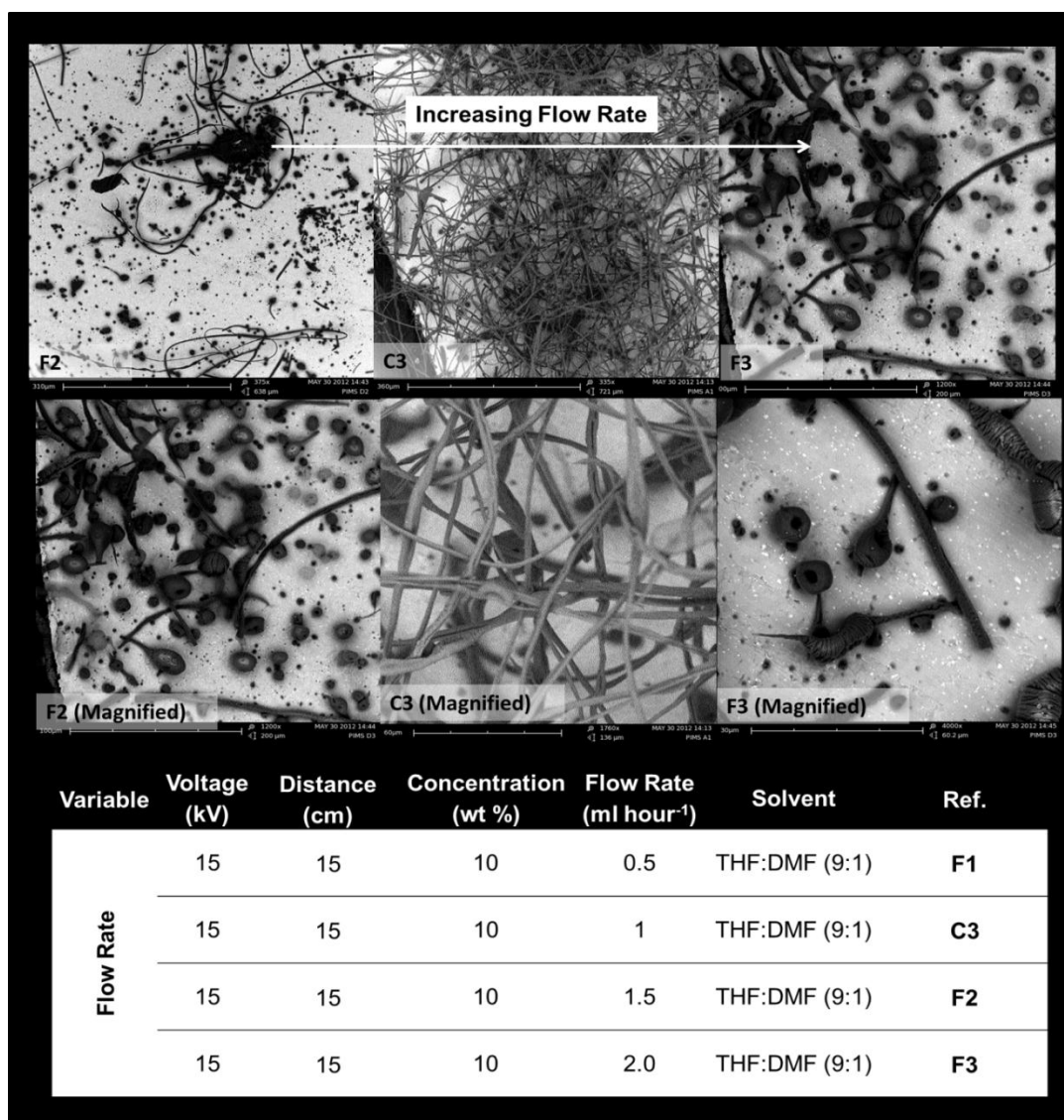


**Figure 5.12:** SEM images of PIM-1 electrospun at different flow rates.

The flow rate affects the surface tension of the solution, resulting in bead formation along the polymer jet as expulsion takes place. This is due to increased stress applied to the droplet, leading to an increase in perturbations during jet expulsion.



**Figure 5.13:** SEM images of the material from electrospinning PIM-1 (**F2**), showing fibres and beading. Images courtesy of the University of Liverpool.



**Figure 5.14:** SEM images of the material from electrospinning PIM-1 (**F3**), showing fibres and beading. Images courtesy of the University of Liverpool.

It can be concluded that the flow rate is also an important parameter in determining fibre formation. The optimal window for flow rate has been shown to be between 1 and 2 ml hour<sup>-1</sup>. Although, beading occurs at higher flow rates, this may be mitigated by using a higher concentration solution, possibly adapting the parameters from **C4** (12 wt%).

#### 5.2.5. Conclusions on the electrospinning of PIM-1

PIM-1 was a challenging material to electrospin. Issues arose from solubility and viscosity. Initial attempts to spin in a single solvent (THF) were unsuccessful due to the increased viscosity encountered when applying an electric field, owing to the volatility of the solvent. A co-solvent system was used with THF: DMF at a ratio of 9: 1 chosen as the best system. Four parameters were varied to investigate their effects on the formation of polymer fibres. A proposed optimal system was determined by SEM and is shown in Table 5.3.

**Table 5.3:** Proposed optimal system for the production of fibres of PIM-1.

Parameter	Value
Solvent	THF: DMF (9: 1)
Concentration	10 wt%
Voltage	15 kV
Tip-to-Collector Distance	15 cm
Flow Rate	1 ml hour <sup>-1</sup>

Whilst the production of “microfibres” was accomplished, nanofibre formation was not achieved. However, minor modifications of the proposed system in Table 5.3, may result in nanofibres being observed. It is important to note that the electrospinning of this material has never been reported and these preliminary steps form the foundation of future work in this area. For example, increasing flow rate (which produced thinner fibres) and increasing tip-to-collector distance may be successful. Further, achieving a balance between higher concentrations (such as those seen in **C4**) and increased

voltage, at the higher flow rates ( $> 1 \text{ ml hour}^{-1}$ ) provides a potential route for nanofibre production.

### **5.3. Electrospinning nanoparticle cages with polymer scaffolds**

Microporous nanoparticle cages have potential applications in heterogeneous catalysis, gas adsorption, and separation. As noted by Hasell *et al.* [16] particle morphology is as important as pore size with respect to application. However, nanoparticles cannot be easily drawn into fibrous materials, therefore a polymer scaffold is used. The nanoparticle cages are composed of cycloimine compounds, which have tetrahedral symmetry, with four windows that are large enough to allow entry of small molecules (e.g. gases). This increases the porosity of the cages. Electrospinning is a simple and functional approach for producing polymer nanofibres with a high surface area (and further increasing intrinsic porosity), allowing for the incorporation of nanoparticle cages into the conductive solution, and ultimately the fibre. Polystyrene (previously spun as discussed in Section 5.1) was initially used as the scaffold due to its hydrophobic nature and solubility in DCM. DCM was the dispersive solvent for the nanoparticle cages. PIM-1 (which was previously spun as discussed in Section 5.2) was also used as a scaffold, thus introducing additional microporosity into the material. The initial electrospinning experiments using these two polymers as scaffolds with the two nanoparticle cage solutions (designated as THL 294 and THL 295 due to the University of Liverpool referencing system) are detailed herein.

#### *5.3.1. Initial attempts of electrospinning nanoparticle cages using polystyrene as a scaffold*

Initial experiments spinning the polystyrene-nanoparticle cage solution used the same parameters described in Section 5.1.2 (15 kV, with a flow rate of  $1 \text{ ml hour}^{-1}$  and tip-to-collector distance of 15 cm). Polystyrene was chosen as a scaffold because it was soluble in DCM, cheap, and readily available. Furthermore, its hydrophobic nature imbues the spun material with water

tolerance, allowing for applications in a range of environments (such as outdoors). As the nanoparticles were pre-dispersed in DCM, it was necessary to adjust the amount of polystyrene used. Previously, 20 to 25 wt% solutions of polystyrene in DCM produced the best fibres. Consequently, 20 wt% was chosen as the best concentration for initial electrospinning attempts. The concentration of nanoparticles in both solutions (THL 294 and 295) was 0.5 %(w/v). As it was important to know the concentration of nanoparticles in the final solution, the concentration of the conductive solution was converted to percentage weight by volume. Thus, a 20 wt% solution of polystyrene in DCM, was calculated to be a 33 %(w/v) solution. The original nanoparticle cage solutions were made as described in the literature<sup>[16]</sup>, and differ only in the mixing temperature used; room temperature for THL 294, and -80 °C for THL 295. Spinning was performed at the same concentration (33 % w/v) for each solution, and the fibre morphology was assessed by SEM (Figures 5.15 and 5.16).



**Figure 5.15:** SEM images of initial attempts of electrospinning nanoparticle cage THL 294 with a polystyrene scaffold. Images courtesy of the University of Liverpool.



**Figure 5.16:** SEM images of initial attempts of electrospinning nanoparticle cage THL 295 with a polystyrene scaffold. Images courtesy of the University of Liverpool.

Both materials formed a white fibrous material on the collecting plate. Under SEM (Figures 5.15 and 5.16), it was confirmed that fibres had been formed, with an average diameter of approximately 5.5  $\mu\text{m}$ . Furthermore, it can be seen that there are small circular “holes” (pores) in the fibres (average diameter was less than 150 nm). These were initially assumed to be the nanoparticle cages, however it was found that the pores were attributable to effect of the spinning parameters. When polystyrene is electrospun from a volatile solvent (such as DCM), the polymer jet travels through the electric field and the solvent evaporates. Water droplets from the air condense on the surface of the fibre. As the fibre dries the droplets eventually evaporate, but leave an imprint on the surface of the material. This process is known as evaporative cooling, and also occurs in films (known as breath figures<sup>[2]</sup>), and can also be observed in **B1** and **B2**, in Figure 5.2.

Although fibres have been produced, no nanoparticle cages have been observed. However, the pores on the surface of the fibres increase the surface area, and may have also trapped the nanoparticles within the material, thus making them difficult to observe by SEM. Decreasing the humidity of the system may avoid the formation of these pores and thus allow sorption of the nanoparticle cages to the surface of the fibre.

### *5.3.2. Initial attempts of electrospinning nanoparticle cages using PIM-1 as a polymer scaffold*

PIM-1 is a hydrophobic microporous material, which was successfully spun earlier (Section 5.2). Spinning was carried out using the parameters determined before that reliably produced fibres (15 kV, with a flow rate of 1 ml hour<sup>-1</sup> and tip-to-collector distance of 15 cm). However, as the nanoparticle cages were suspended in DCM, the conductive solvent was changed to this (from a THF:DMF mixture). The designation for the electrospun polymers is PIMTHL-294 and PIMTHL-295. Spinning the polymer resulted in a yellow (the colour of PIM-1) fibrous layer forming on the collecting plate. SEM (Figure 5.17) showed that fibres had indeed been produced. Figure 5.17 also shows PIM-1 electrospun with no particles for comparison.

SEM of PIMTHL-294 showed both fibrous (with low fibre density) and particulate structures. However, the magnified image does not provide enough resolution to provide any details about morphology. Similar to the PS, no nanoparticle cages were observed. The SEM image for PIMTHL-295 again showed fibre production and particulate structures, with a notable increase in particulate density. At increased magnification, fibre morphology is visible and the microporous surface of the polymer can be observed. Again, no nanoparticle cages are discernible. Similar to PS, it is possible that cages have migrated into micropores of the polymer.

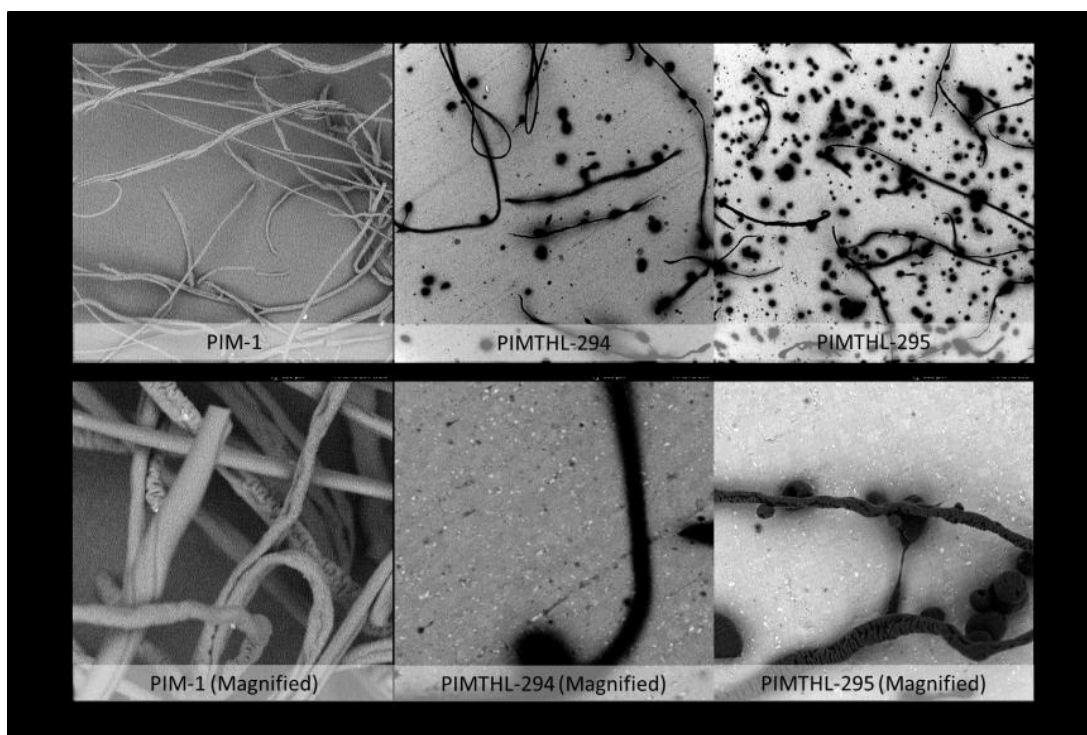


**Figure 5.17:** SEM images of initial attempts of electrospinning nanoparticle cage THL 294 and THL 295 with a PIM-1 scaffold.

#### 5.4. Electrospinning bio-hybrid materials

Bio-hybrid materials have a wide range of potential uses, including wound management, drug delivery, and tissue engineering. Producing fibres of these materials increases their surface area compared to the polymer in the bulk, thus enhancing the availability of their functionality. This section is divided into two parts: Section 5.4.1 looks at the effect of molecular weight when poly(ethylene oxide) was spun, and Section 5.4.2 focuses on the initial spinning attempts of polymer-peptide conjugates produced using the method outlined in Chapters 2 and 3.

##### 5.4.1. Determining the effect of molecular weight on fibre production of poly(ethylene oxide)

Poly(ethylene oxide) (PEO) was spun from a solution of either water or water: ethanol. Spinning parameters were varied in order to initiate fibre

production. A second set of experiments was carried out to investigate how changing molecular weight affects fibre production. The results from spinning PEO with molecular weights of 300,000 Da, 100,000 Da, 8,000 Da, and 4,000 Da are described herein.

#### *5.4.1.1. Electrospinning poly(ethylene oxide), molecular weight 300,000 Da*

Electrospinning PEO with a molecular weight of 300,000 Da (henceforth referred to as PEO<sub>6820</sub> to show the degree of polymerisation) was carried out from a 15 wt% conductive solution. PEO<sub>6820</sub> was chosen as an example of a high molecular weight system. The solvent chosen for all experiments was water or a binary system of water and ethanol. PEO was soluble in all mixtures and complete dissolution was attained by overnight stirring.

##### ***5.4.1.1.1. Effect of solvent composition on electrospinning poly(ethylene oxide)<sub>6820</sub>***

Electrospinning PEO with a molecular weight of 300,000 Da was carried out with specific parameters (15 wt%, at a voltage of 15 kV, a flow rate of 1 ml hour<sup>-1</sup>, and a tip-to-collector distance of 15 cm). Complete dissolution of PEO<sub>6820</sub> was more difficult than all other PEO. As before, four parameters were varied in order to manufacture fibres. Figure 5.18, shows the effect on fibre production by varying the solvent composition. At all solvent compositions investigated, fibrous material was deposited onto the collecting plate. SEM confirmed that the material was comprised of fibres.

At higher concentrations of ethanol (>50 %v/v, **G1-G4**), the number of fibres produced decreased as the concentration of ethanol decreased. Furthermore, fibre diameter varies significantly, ranging from 600 nm (**G1**) to 1500 nm (**G4**). It can be also seen that polymeric particles have been formed at 60 %v/v (**G4**) and 70 %v/v (**G5**).

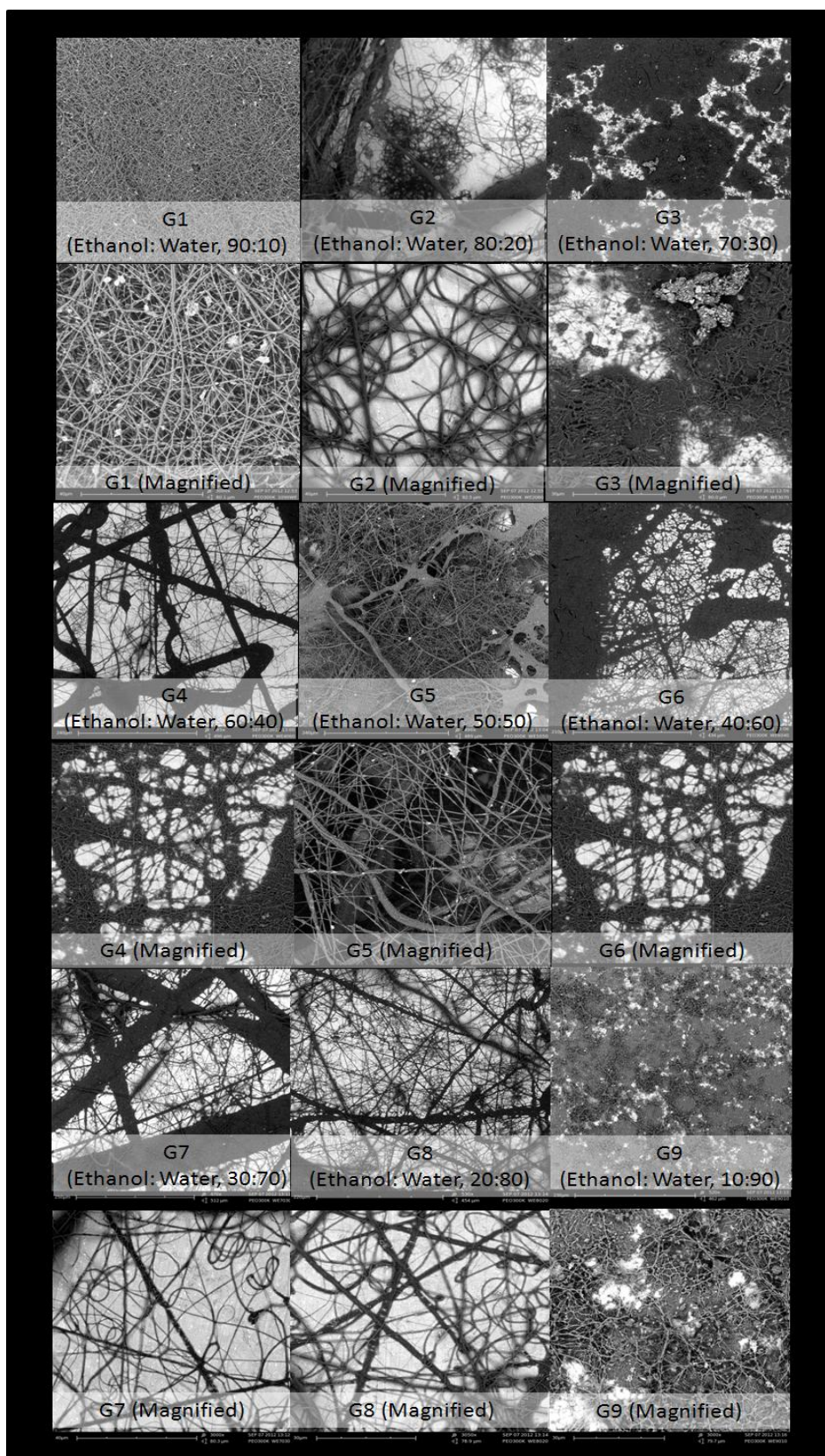


**Figure 5.18:** The effect of solvent composition on fibre production of PEO<sub>2275</sub>. (Spinning Conditions: voltage 15 kV, distance 15 cm, flow rate 1 ml hour<sup>-1</sup>, concentration 15 wt%).

Reducing the ratio of ethanol to water to 50 %v/v (**G5**), resulted in thicker fibres (average diameter was approximately 1.4  $\mu\text{m}$ ) being formed, however fewer discrete polymeric structure were visible. The fibres are observed to have more uniform character. Further reducing the concentration of ethanol (<50 v/v%, **G6-G9**) resulted in fibre production, however the fibre density was decreased. Fibre diameter was comparable to those at higher concentrations of ethanol. Notably, at a very low concentration of ethanol (10% v/v, **G9**), polymer beads were present. This is the only concentration at which beads formed, and was unexpected as the properties of the solution (and, critically, the dielectric constant) should be dominated by the increased concentration of water, making it easier to induce an electric field. It is predicted that the concentration of PEO<sub>6820</sub> was too low in this experiment.

#### **5.4.1.1.2. Effect of voltage on electrospinning poly(ethylene oxide)<sub>6820</sub>**

PEO<sub>6820</sub> was spun from water (15 wt%) at a flow rate of 1 ml hour<sup>-1</sup>, and a tip-to-collector distance of 15 cm. At very low voltages (5kV, **H1**), fibres were not observed by SEM (Figure 5.19). The polymer formed sheet like structures at this voltage. However, increasing the voltage to 10 kV (**H2**) resulted in fibre production, with an average fibre diameter of approximately 300 nm. SEM showed a non-uniform distribution of fibres, with aggregation of the fibres into more densely packed networks. This can be seen in the darker regions of the SEM (Figure 5.24, **H2**). At this voltage (10 kV), the electric field is strong enough to cause atomisation and to induce surface charges. Increasing the voltage to 15 kV (**H3**) also resulted in fibre production. The average diameter of the fibres was similar to **H2**, approximately 350 nm. Although, the diameter has increased slightly, the fibres are more uniform (generally long and thin), and there is no aggregation.

At higher voltages (> 15 kV, **H4** and **H5**), fibres were again produced, however discrete structures can also be observed. At this point, the strength of the electric field was high, causing atomisation to occur instantly and causing the droplet to immediately develop into a polymer jet. However, during flight, the

strong electric field will perturb the jet, thus causing minor imperfections. These imperfections result in the formed structures observed in **H4** and **H5**.

In short, it can be deduced that the optimal voltage for spinning PEO<sub>6820</sub> lays around 15 kV.

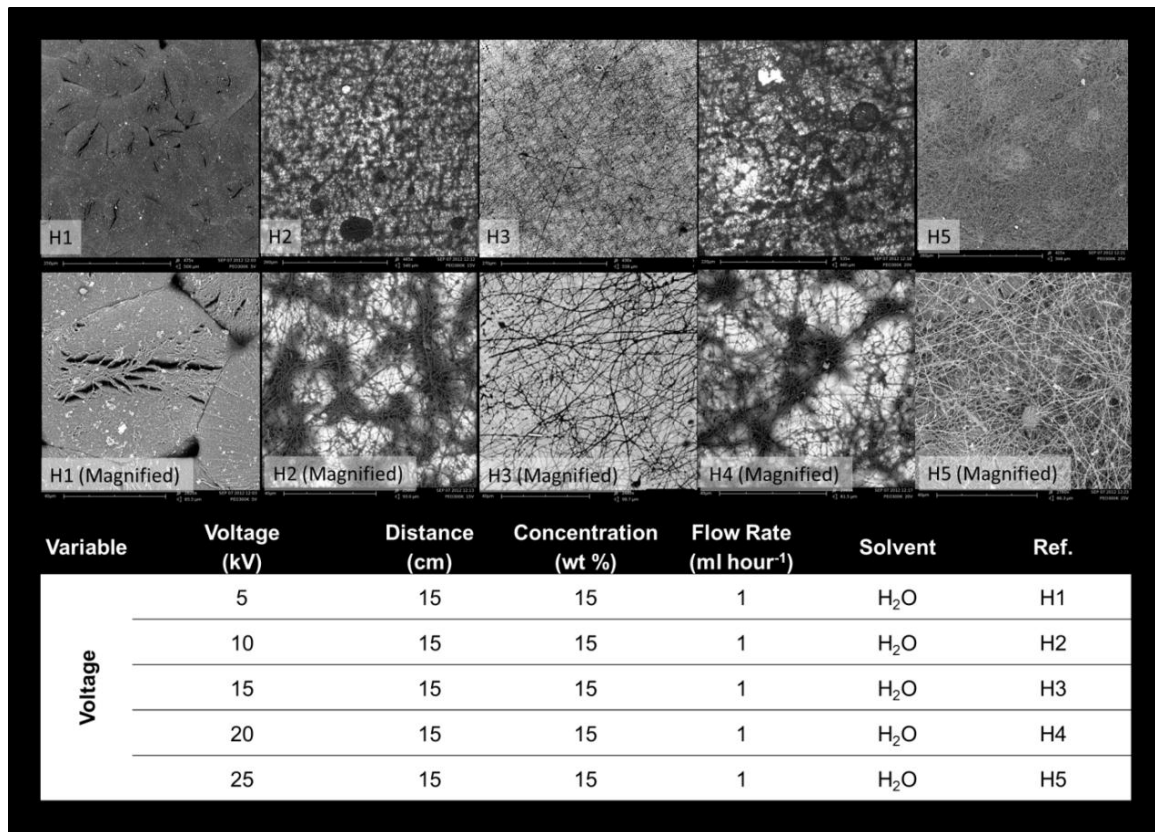


**Figure 5.19:** The effect of voltage on fibre production of PEO<sub>6820</sub>.

#### **5.4.1.1.3. Effect of distance on electrospinning poly(ethylene oxide)<sub>6820</sub>**

PEO<sub>6820</sub> was spun from water (15 wt%) at a flow rate of 1 ml hour<sup>-1</sup>, and a voltage of 15 kV. At short tip-to-collector distances (11 cm, **J1**), SEM showed (Figure 5.20) that the deposition comprised of many micro and nanostructures, but that no fibre production occurred.

However, when the distance was increased, fibres were produced in all instances (**J2-J4**). At a distance of 13 cm (**J2**), nanofibres were produced (with an average diameter of 780 nm), although, a few discrete structures were also

observed. Increasing the working distance above 15 cm resulted in thinner fibres being produced with an average diameter of 620 nm (17 cm, **J3**) and 320 nm (19 cm, **J4**), the latter comparable to **H3**. The increased distance increases the time that the polymer jet spends in the electric field, thus allowing more time for elongation.

In summary, the optimal window for producing fibres when varying working distance was shown to be greater than 15 cm for spinning PEO<sub>6820</sub>, and that the working distance can be varied above this limit to control the fibre diameter.

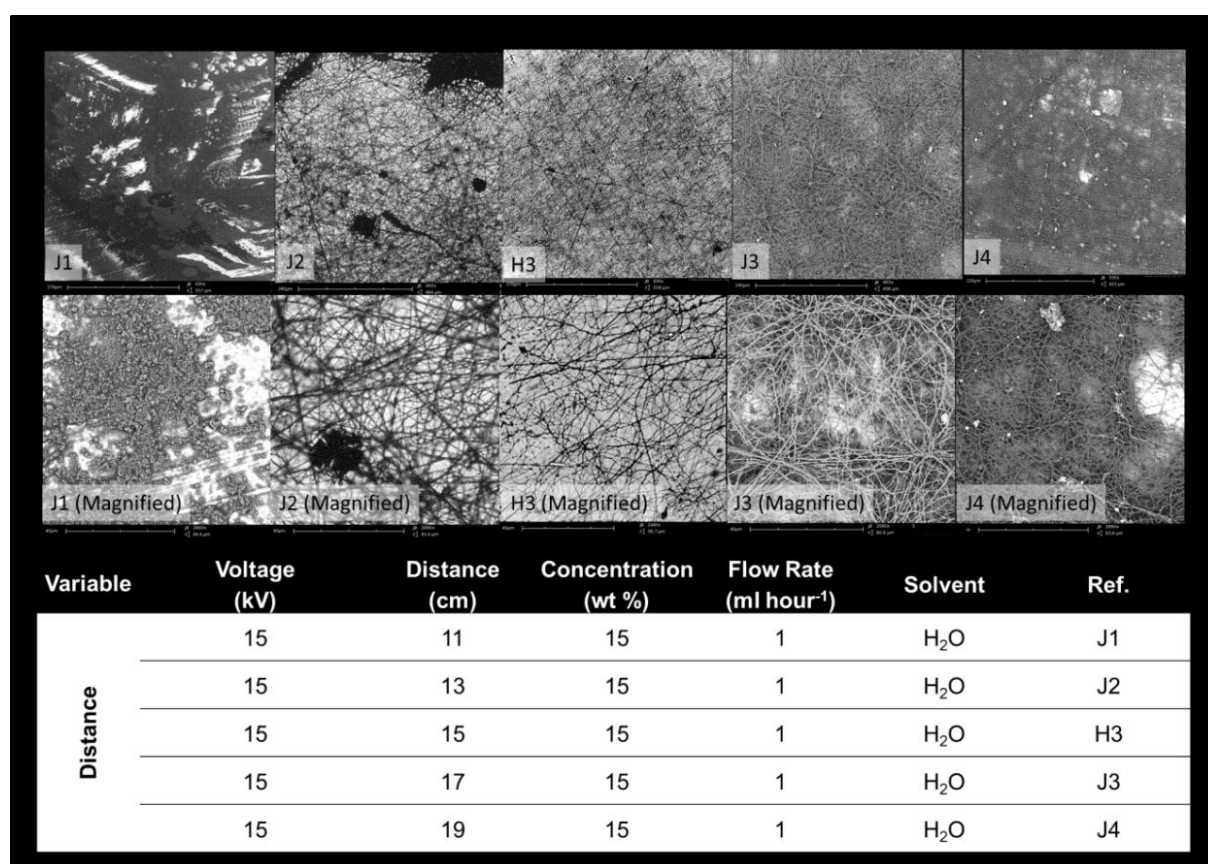


**Figure 5.20:** The effect of distance on fibre production of PEO<sub>6820</sub>.

#### **5.4.1.1.4. Effect of flow rate on electrospinning poly(ethylene oxide)<sub>6820</sub>**

PEO<sub>6820</sub> was spun from water (15 wt%) at a voltage of 15 kV and a tip-to-collector distance of 15 cm. At a low flow rate (0.5 ml hour<sup>-1</sup>, **K1**), fibrous material was deposited on to the collecting plate. SEM (Figure 5.21) showed

that the material had indeed formed fibres, with an average fibre diameter of approximately 630 nm; therefore nanofibres had been produced. However, SEM also showed some interconnected polymer structures. Fibre morphology was generally consistent (long, thin fibres), and the number of fibres produced was high, however the additional polymer structures are undesirable. Increasing the flow rate ( $> 1.0 \text{ ml hour}^{-1}$ , **K2-K4**) did not result in any fibres forming. SEM showed that the material formed a monolayer (**K2**), with discrete structures appearing to be interspersed throughout as the flow rate was further increased (**K3** and **K4**).

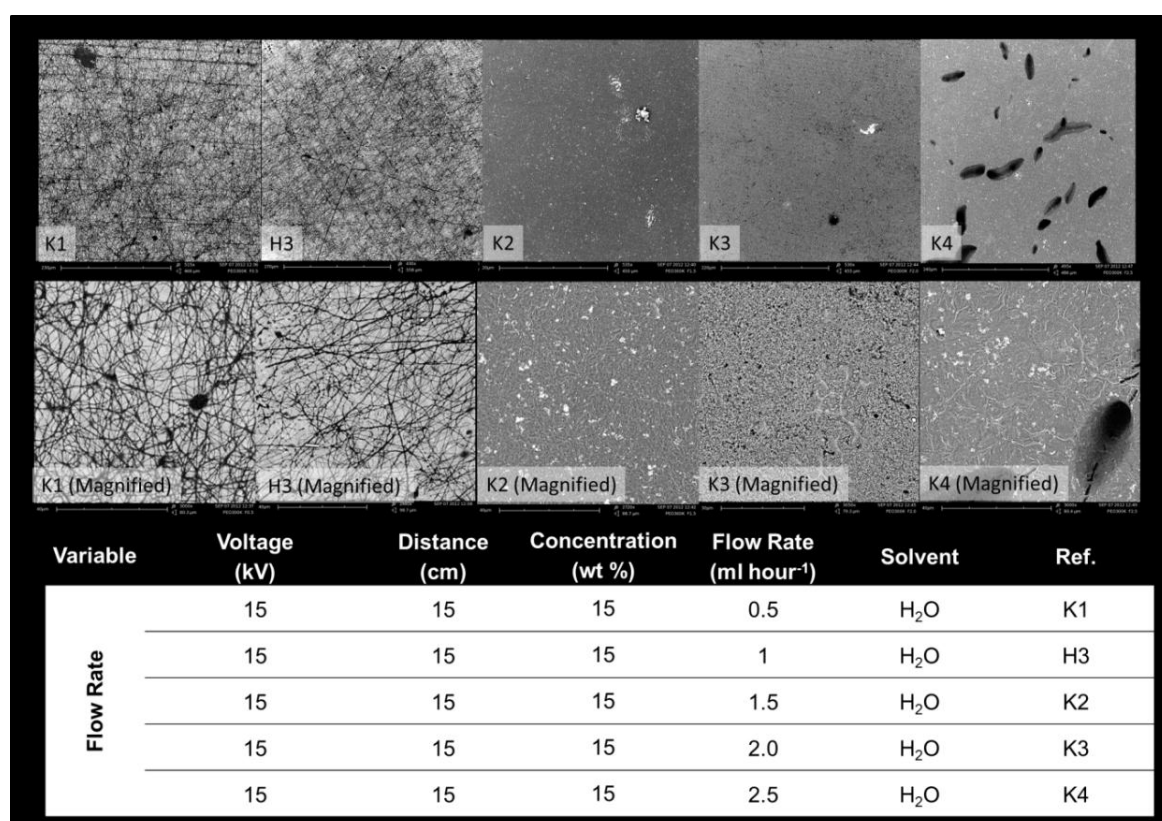


**Figure 5.21:** The effect of flow rate on fibre production of PEO<sub>6820</sub>.

When the flow rate is increased above  $1.0 \text{ ml hour}^{-1}$ , it augments the tension that the polymer droplet experiences, which leads to dispersal of the droplet, thus inhibiting fibre formation. The optimal window for flow rate is therefore determined to be somewhere between  $0.5$  and  $1.5 \text{ ml hour}^{-1}$ , with  $1.0 \text{ ml hour}^{-1}$  shown to produce optimum fibres.

#### 5.4.1.2. *Electrospinning poly(ethylene oxide), molecular weight 100,000 Da*

Electrospinning PEO with a molecular weight of 100,000 Da (henceforth referred to as PEO<sub>2275</sub>) was carried out from a 15 wt% conductive solution. The solvent chosen for all experiments was water as it was shown during spinning of PEO<sub>6820</sub> (see Section 5.4.1.1) that fibres were reliably produced in solutions where water was the dominant solvent. Electrospinning PEO<sub>2275</sub> in various binary solvent systems was carried out and reaffirmed this conclusion (see Appendix D1).

As before, three parameters (voltage, distance, and flow rate) were varied and any fibre production was noted. PEO<sub>2275</sub> was chosen as an example of a medium molecular weight system. The results for these experiments are summarised in Appendix D1. In contrast to PEO<sub>6820</sub>, fibres were only produced in one experiment (in water only). The spinning parameters for this experiment (**L8**) were a voltage of 15 kV, a working distance of 15 cm, and a flow rate of 1 ml hour<sup>-1</sup>.

#### 5.4.1.3. *Electrospinning poly(ethylene oxide), molecular weight 8,000 Da*

Electrospinning PEO with a molecular weight of 8,000 Da (henceforth referred to as PEO<sub>182</sub>) was carried out from a 45 wt% conductive solution. The change in concentration was due to qualitative observations of solution viscosity. At 15 wt%, the solution was determined to have an insufficiently low viscosity to be viable for electrospinning. Increasing the concentration by a factor of three resulted in a solution with an acceptable viscosity for electrospinning. This viscosity change was necessary because of the low molecular weight PEO<sub>182</sub>. The solvent chosen for all experiments was water (based on experiments spinning from various binary systems of water and ethanol (see Appendix D1) Varying the three spinning parameters (voltage, distance, and flow rate) did not result in the formation of fibres, instead discrete particulate polymer structures were formed. The results of these experiments can be found in Appendix D2.

#### 5.4.1.4. *Electrospinning poly(ethylene oxide), molecular weight 4,000 Da*

Electrospinning PEO with a molecular weight of 4,000 Da (henceforth referred to as PEO<sub>91</sub>) was also carried out from at 45 wt% conductive solution. As with PEO<sub>182</sub>, the increase in concentration compared to the higher molecular weight PEO was due to qualitative observations of solution viscosity. The solvent chosen for all experiments was water. Similar to PEO<sub>182</sub>, no fibres were produced during spinning. Polymer layers were the dominant structures observed by SEM (see Appendix D3 for full results at all parameters).

#### 5.4.1.5. *The effect of different molecular weight PEO on fibre production*

From the electrospinning experiments undertaken, it is reasonable to assert that molecular weight is an important parameter in determining fibre production. With the exception of the concentration, which was changed for aforementioned viscosity reasons, spinning different molecular weight PEO with the same spinning parameters did not always result in fibres. This is clearly illustrated in Figure 5.22.

Figure 5.22 generally shows that there is a threshold molecular weight that the polymer must be above in order to attain nanofibres. Although spinning PEO<sub>2275</sub> (average  $M_n$  100,000 Da, **L8**) did result in fibres, and had a higher fibre density than PEO<sub>6820</sub> (average  $M_n$  300,000 Da, **H3**), the average diameter of **L8** was approximately 700 nm. In contrast, the average fibre diameter of the larger molecular weight PEO, **H3**, was approximately 350 nm, which is more beneficial in terms of surface area-to-volume ratio. Conversely, decreasing the molecular weight to 8000 Da, (**R3**) did not result in fibres. Instead, the material formed discrete polymeric aggregates. Finally, at the lowest molecular weight spun (4000 Da, **V3**), no aggregated structures were observed; instead a continuous polymer layer was produced.

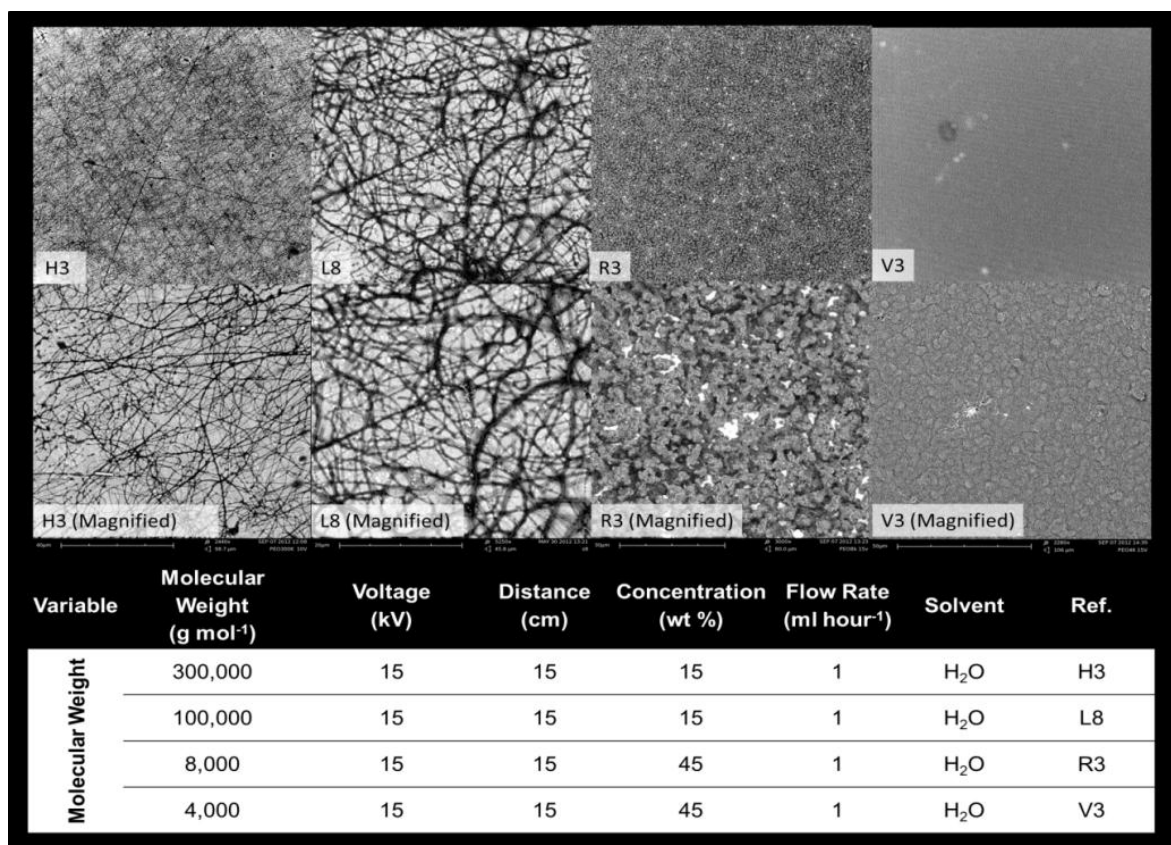


**Figure 5.22:** SEM showing the structures produced when electrospinning different molecular weight PEOs using the same spinning parameters.

#### 5.4.2. Electrospinning polymer-peptide conjugates

Only two conjugates were deemed viable for spinning (using qualitative viscosity and solubility observations). These were the higher molecular weight conjugates; mPEO<sub>12</sub>-F<sub>4</sub> and mPEO<sub>17</sub>-F<sub>4</sub>. Although, the chosen conjugates had a relatively high molecular weight in their homologous families, they are actually very low molecular weight materials (~1200 Da to 1400 Da) compared to materials typically used in electrospinning.

These materials have never been spun, therefore it was necessary to establish the optimal conditions required for spinning. Four solvent systems were investigated. The results of solvent testing on mPEO<sub>17</sub>-F<sub>4</sub>-OEt are shown in Table 5.4. Hexafluoroisopropanol (HFIP) was tested as it was shown to be compatible with the peptides<sup>[17]</sup>, and is also known to disrupt hydrogen bonds,

thus facilitating easy dissolution of the conjugate. THF and chloroform were both good solvents for the conjugate. However, the dielectric constant of these three solvents is low, making it harder to induce surface charges onto the polymer droplet. DMF was also used as it had a much higher dielectric constant than the other materials ( $\sim 38$ )<sup>[18]</sup> and was compatible with the conjugate. From Table 5.4, the 40 and 50 wt% polymer solutions in HFIP and the 30 and 40 wt% polymer solutions in chloroform (qualitatively) showed the best viscosity for electrospinning.

Although, the 60 wt% polymer solution in THF showed acceptable viscosity, the volatility of THF (as described earlier in Section 5.2) makes it less attractive for spinning. The materials are not commercially available and have to be synthesised in house via multiple step procedures (see Chapter 3), therefore spinning at lower concentrations was preferable. However, the viscosity of the conjugate in DMF was also moderate at 60 wt%. Although using the smallest concentration of conjugate was desirable, spinning in HFIP and chloroform would be difficult due to the low dielectric constants, however, DMF is difficult to atomise. A co-solvent system between THF and DMF, in a ratio of 3: 2 was selected (based on additional solubility tests).

mPEO<sub>12</sub>-F<sub>4</sub>-OEt and mPEO<sub>17</sub>-F<sub>4</sub>-OEt were spun from a binary solvent system of THF and DMF (3: 2) at a voltage of 15 kV, a working distance of 15 cm, and a flow rate of 1 ml hour<sup>-1</sup>. The voltage and distance were selected due to prior success spinning at these parameters, albeit using different polymers. SEM images of mPEO<sub>12</sub>-F<sub>4</sub>-OEt (Figure 5.23) show no fibre production. At relatively low concentrations of polymer (**Y1** and **Y2**, 55 and 60 wt%), a polymer layer was formed on the collecting plate. SEM showed a continuous polymer structure. However, increasing the concentration to 65 wt% (**Y3**), led to more discrete polymer structures forming, suggesting that the concentration was high enough for some physical interactions to occur.

**Table 5.4:** Qualitative solubility and viscosity observations of mPEO<sub>17</sub>-F<sub>4</sub>-OEt in various solvent systems.

Weight Percent	Comments			
	HFIP	CHCl <sub>3</sub>	THF	DMF
90 %	Insoluble	Insoluble	Partially Soluble High Viscosity	Soluble High Viscosity
80 %	Insoluble	Insoluble	Partially Soluble High Viscosity	Soluble High Viscosity
70 %	Insoluble	Partially Soluble High Viscosity	Partially Soluble Moderate Viscosity	Soluble Moderate Viscosity
60 %	Partially Soluble High Viscosity	Partially Soluble High Viscosity	Soluble Moderate Viscosity	Soluble Moderate Viscosity
50 %	Soluble Moderate Viscosity	Soluble High Viscosity	Soluble Low Viscosity	Soluble Low Viscosity
40 %	Soluble Moderate Viscosity	Soluble Moderate Viscosity	Soluble Very Low Viscosity	Soluble Low Viscosity
30 %	Soluble Low Viscosity	Soluble Moderate Viscosity	Soluble Very Low Viscosity	Soluble Low Viscosity
20 %	Soluble Low Viscosity	Soluble Low Viscosity	Soluble Very Low Viscosity	Soluble Very Low Viscosity
10 %	Soluble Very Low Viscosity	Soluble Low Viscosity	Soluble Very Low Viscosity	Soluble Very Low Viscosity

Figure 5.24 shows the SEM images of electrospun mPEO<sub>17</sub>-F<sub>4</sub>-OEt. At all polymer concentrations no fibres were formed, instead large, discrete polymer structures were produced (**Z1** and **Z2**, 55 and 60 wt%). Increasing the concentration to 65 wt% (**Z3**) caused short, needle-like structures to form, which may be a precursor to fibre-like structures. The density of the rods was much higher than any of the discrete structures produced in **Y3**, **Z1**, and **Z2**, and provides an interesting springboard for future work.

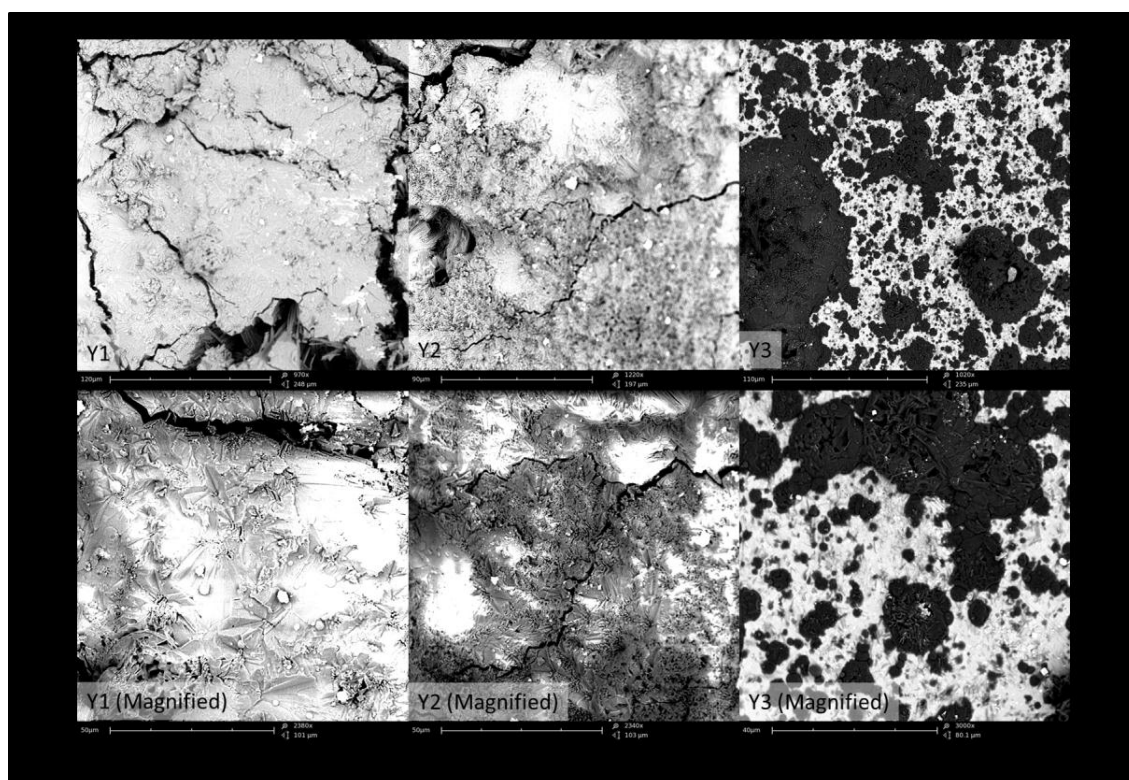


**Figure 5.23:** The effect of spinning mPEO<sub>12</sub>-F<sub>4</sub>-OEt in THF: DMF (3: 2) at different concentrations (**Y1**, 55 wt%, **Y2**, 60 wt%, and **Y3**, 65 wt%).

Initial experiments showed that raising the conjugate concentration (mPEO<sub>17</sub>-F<sub>4</sub>-OEt) above 65 wt% greatly increased viscosity of the conductive solution, which blocked the delivery system (this is also partially attributable to the volatility of THF). Furthermore, due to time constraints and limited availability of the conjugate material, experiments in which the other parameters were varied, were not undertaken. However, it is predicted that increasing the voltage and working distance of a 65 wt% (**Z3**) solution of mPEO<sub>17</sub>-F<sub>4</sub>-OEt in the same solvent conditions may produce fibre-like structures. For

mPEO<sub>12</sub>-F<sub>4</sub>-OEt, a further increase in concentration is more viable than mPEO<sub>17</sub>-F<sub>4</sub>-OEt, due to the reduced molecular weight of the conjugate, although based on the SEM image, **Z3** is most likely to give fibres. As discrete structures had begun to form at 65 wt%, increasing the concentration to between and 70 and 75 wt% would provide the best window for fibre production. Further (slight) increases in the voltage and working distance would likely also aid fibre production.

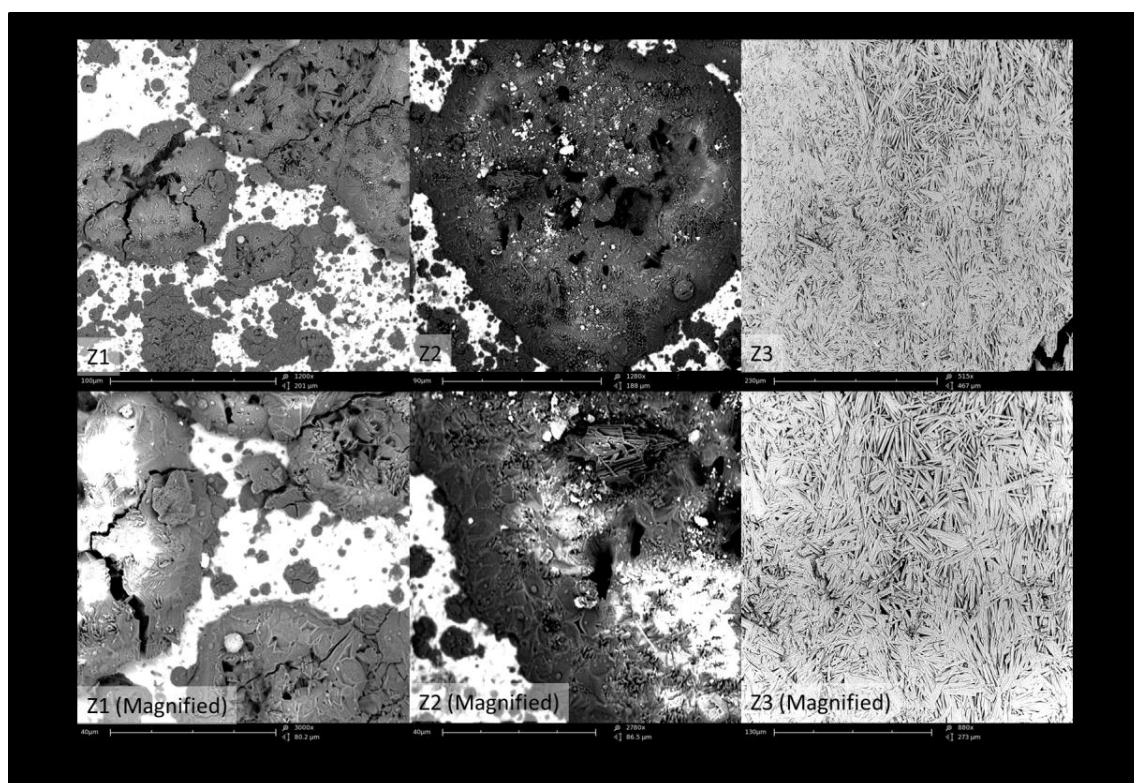


**Figure 5.24:** The effect of spinning mPEO<sub>17</sub>-F<sub>4</sub>-OEt in THF: DMF (3: 2) at different concentrations (**Z1**, 55 wt%, **Z2** 60 wt%, and **Z3** 65 wt%).

In summary, mPEO<sub>12</sub>-F<sub>4</sub>-OEt and mPEO<sub>17</sub>-F<sub>4</sub>-OEt were spun from THF: DMF (3: 2) but did not result in any fibre production. mPEO<sub>17</sub>-F<sub>4</sub>-OEt showed the most promising structures, when spun at 65 wt%. Further work in this area will focus on investigating the concentration range for fibre production and then optimising spinning parameters within this window.

## **5.5. Electrospinning conclusions**

Electrospinning an array of novel materials to produce micro- and nanofibres required optimisation of at least six distinct spinning parameters; voltage, working distance, flow rate, concentration, solvent of the conductive solution, and molecular weight of the polymer. For each material spun, there was an optimal window for the parameters, between which fibres were produced. Each system had to be tailored individually depending on the polymers and solvents used.

Although spinning large materials, such as the higher molecular weight PS and PIM-1, did result in the production of fibres, electrospinning lower molecular weight materials, such as the polymer-peptide conjugates and PEO, generally resulted in the production of discrete polymeric structures or polymer sheets. Future work in this area should focus on improving the conjugate spinning systems, or on investigating electrospinning of higher molecular weight conjugates. Further work should also be carried out on spinning the nanoparticle cage solutions with a hydrophobic polymer, and evidencing retained nanoparticles using SEM.

## 5.6. References

1. Baker S. C., Atkin N., Gunning P. A., Granville N., Wilson K., Wilson D., and Southgate J., Characterisation of Electrospun Polystyrene Scaffolds for Three-Dimensional *in vitro* Biological Studies, *Biomaterials*, **2006**, 27(16): p. 3136-3146.
2. Casper C. L., Stephens J. S., Tassi N. G., Chase D. B., and Rabolt J. F., Controlling Surface Morphology of Electrospun Polystyrene Fibers: Effect of Humidity and Molecular Weight in the Electrospinning Process, *Macromolecules*, **2003**, 37(2): p. 573-578.
3. Wannatong L., Sirivat A., and Supaphol P., Effects of Solvents on Electrospun Polymeric Fibers: Preliminary Study on Polystyrene, *Polymer International*, **2004**, 53(11): p. 1851-1859.
4. Asran A. S., Seydewitz V., and Michler G. H., Micromechanical Properties and Ductile Behavior of Electrospun Polystyrene Nanofibers, *Journal of Applied Polymer Science*, **2012**, 125(3): p. 1663-1673.
5. Wang C., Hsu C.-H., and Lin J.-H., Scaling Laws in Electrospinning of Polystyrene Solutions, *Macromolecules*, **2006**, 39(22): p. 7662-7672.
6. Eda G., Liu J., and Shivkumar S., Solvent Effects on Jet Evolution During Electrospinning of Semi-Dilute Polystyrene Solutions, *European Polymer Journal*, **2007**, 43(4): p. 1154-1167.
7. Sigma-Aldrich, Dichloromethane, **2012** [cited July 2012, 2012]; Available from: <http://www.sigmaaldrich.com/chemistry/solvents/dichloromethane-center.html>.
8. Sigma-Aldrich, Tetrahydrofuran, **2012** [cited July 2012, 2012]; Available from: <http://www.sigmaaldrich.com/chemistry/solvents/tetrahydrofuran-center.html>.
9. Fritsch D., Bengtson G., Carta M., and McKeown N. B., Synthesis and Gas Permeation Properties of Spirobischromane-Based Polymers of Intrinsic Microporosity, *Macromolecular Chemistry and Physics*, **2011**, 212(11): p. 1137-1146.
10. Budd P. M., Ghanem B. S., Makhseed S., McKeown N. B., Msayib K. J., and Tattershall C. E., Polymers of intrinsic microporosity (PIMs): robust,

solution-processable, organic nanoporous materials, *Chemical Communications*, **2004**(2): p. 230-231.

11. Budd P. M., McKeown N. B., Ghanem B. S., Msayib K. J., Fritsch D., Starannikova L., Belov N., Sanfirova O., Yampolskii Y., and Shantarovich V., Gas permeation parameters and other physicochemical properties of a polymer of intrinsic microporosity: Polybenzodioxane PIM-1, *Journal of Membrane Science*, **2008**, 325(2): p. 851-860.
12. Budd P. M., Elabas E. S., Ghanem B. S., Makhseed S., McKeown N. B., Msayib K. J., Tattershall C. E., and Wang D., Solution-Processed, Organophilic Membrane Derived from a Polymer of Intrinsic Microporosity, *Advanced Materials*, **2004**, 16(5): p. 456-459.
13. McKeown N. B. and Budd P. M., Polymers of intrinsic microporosity (PIMs): organic materials for membrane separations, heterogeneous catalysis and hydrogen storage, *Chemical Society Reviews*, **2006**, 35(8): p. 675-683.
14. Shenoy S. L., Bates W. D., Frisch H. L., and Wnek G. E., Role of chain entanglements on fiber formation during electrospinning of polymer solutions: good solvent, non-specific polymer-polymer interaction limit, *Polymer*, **2005**, 46(10): p. 3372-3384.
15. Stranger J., Tucker N., and Staiger M., Electrospinning Process and Apparatus, in *Electrospinning*. **2005**, Smithers Rapra: Shrewsbury. p. 10-17.
16. Hasell T., Chong S. Y., Jelfs K. E., Adams D. J., and Cooper A. I., Porous Organic Cage Nanocrystals by Solution Mixing, *Journal of the American Chemical Society*, **2011**, 134(1): p. 588-598.
17. Singh G., Bittner A. M., Loscher S., Malinowski N., and Kern K., Electrospinning of Diphenylalanine Nanotubes, *Advanced Materials*, **2008**, 20(12): p. 2332-2336.
18. Marchetti A., Preti C., Tagliazucchi M., Tassi L., and Tosi G., The *N,N'*-dimethylformamide + ethane-1,2-diol solvent system. Dielectric constant, refractive index, and related properties at various temperatures, *Journal of Chemical & Engineering Data*, **1991**, 36(4): p. 365-368.

# **CHAPTER 6**

## **Conclusions and Future Work**

## 6. Conclusions and Future Work

This final chapter summarises the results of the work undertaken in this project (Section 6.1) and describes the future work for each part of the project (Section 6.2).

### 6.1. Conclusions

#### 6.1.1. Innovative synthesis of polymer-peptide conjugates

Polymer-peptide conjugates were produced from a reaction between carboxylic acid-functionalised monomethoxy-poly(ethylene oxide) and phenylalanine oligopeptides. The reaction scheme proceeded by a convergent route, with each individual component synthesised in high yield. Phenylalanine oligopeptides were prepared using a Boc-protected strategy and isobutylchloroformate (IBCF) coupling, whilst monomethoxy-poly(ethylene oxide) was modified via Jones Oxidation.

Due to its high compatibility with the oligopeptide and its facile purification method, IBCF coupling was used to join the polymer and peptides components together to form a conjugate via amide bond formation. Two additional methods were investigated (DCC and PyBOP) for coupling, however neither matched the efficiency and yield of IBCF.

Twelve well-defined polymer-peptide conjugates were produced using IBCF coupling. The yields for the conjugates were initially high, however as oligopeptide length increased (i.e. from F<sub>1</sub> to F<sub>4</sub>) they fell to moderate levels. Additionally, as the polymer chain length increased (from mPEO<sub>7</sub> to mPEO<sub>17</sub>), a further reduction in the yield was noted. Table 6.1 shows the highest yields obtained for the conjugated produced in this manner.

**Table 6.1:** Summary of percentage yields of polymer-peptide conjugates produced using IBCF coupling chemistry.

	<b>F<sub>1</sub></b>	<b>F<sub>2</sub></b>	<b>F<sub>3</sub></b>	<b>F<sub>4</sub></b>
<b>mPEO<sub>7</sub></b>	85	91	80	77
<b>mPEO<sub>12</sub></b>	79	90	72	90
<b>mPEO<sub>17</sub></b>	73	70	67	51

Direct amidation was the primary route used to produce conjugates. An alternative synthetic route, esterification, was also studied. Esterification reduced the number of reaction steps required to produce conjugates, potentially raising yields, and bypassing the use of chromium. This was carried out by deprotecting the carboxyl terminus of the Boc-protected amino acid, then directly coupling it to mPEO via its hydroxyl group. This eliminated the need for modification of the polymer prior to coupling. Lithium hydroxide was used as the deprotecting agent. Deprotection was quick, however the yields of the isolated deprotected peptides were only moderate. A further deprotection method was investigated using BBTO, although yields were poor.

Two esterification techniques were investigated for conjugate synthesis. Fischer esterification was used but did not result in conjugate formation, likely due to the presence of the strong acid interacting with the Boc protecting group. The second method used was Steglich esterification, which was based on DCC coupling chemistry used previously in an initial attempt to couple the oligopeptides together. This protocol was more tolerant to the reagents and conjugate synthesis ensued. The yields for the reactions were moderate (~60 %) and fell as oligopeptide length increased. In comparison to IBCF coupling, this method was lower yielding, although it avoided the use of chromium.

### 6.1.2. Self-assembly behaviour of bio-hybrid materials

The propensity of the bio-hybrid materials produced in Chapter 3 to self-assemble into gels was investigated. Qualitative observations showed that gel-like structures were formed, only when four phenylalanine oligopeptide were incorporated into the conjugate. It was concluded that only when four peptide units were present, would there be sufficient potential intermolecular hydrogen bonding to form a stable three-dimension networked structure; a gel.

Quantitative analysis was also performed, with mPEO<sub>17</sub>-F<sub>4</sub>-OEt in a DMSO-water binary solvent system selected as the model conjugate. Rheology showed that the properties of the structure formed were not gel-like, but instead behaved as a Newtonian fluid. However, ATR-FTIR analysis showed that there was a change in the hydrogen bonding environments in the self-assembly system, with water being expelled from between the conjugates over several days, thus allowing increased hydrogen bond interactions between conjugate chains. Finally, confocal microscopy showed aggregate-like structures, as opposed to an entangled network of fibrils, reinforcing that the conjugate had not formed a gel. The difficulty in repeating the gelation experiments suggested that temperature was a critical factor in determining self-assembly, and should be monitored carefully in the route to self-assembly.

### 6.1.3. Electrospinning novel materials

Electrospinning was used to produce fibres from an array of materials. Initially, to become familiar with the electrospinning process, polystyrene was spun from tetrahydrofuran (THF) and dichloromethane (DCM). Microfibres (fibre diameter > 1000 nm) were produced (observed by SEM) in both cases, and the effect of varying the polymer concentration in the solution was investigated. Decreasing the concentration of polymer in the solution resulted in larger fibre diameters, with beading becoming more prevalent at the lower concentrations. The effect of the solvent also played a part in fibre production and was linked to fibre diameter. Fibres spun from DCM, which has a higher dielectric constant (8.9), showed no beading at a chosen concentration (20 wt%). However, beading was

visible when spinning at the same concentration from THF, which has a dielectric constant of 7.5.

Polymers with intrinsic microporosity (PIMs) were electrospun to produce fibres with greater surface areas, and, hence, increase the effective porosity of the material. Initial attempts to spin the polymer, PIM-1, were unsuccessful due to poor solvent choice. However, a binary solvent mixture of THF: DMF was used, and fibres were successfully produced from a 10 wt % solution. Four electrospinning parameters (concentration, voltage, distance, and flow rate) were varied to establish their effect on fibre production. The optimal spinning parameters for PIM-1 were then determined.

Nanoparticle cages suspended in DCM were also spun in order to increase fibre microporosity and adsorption properties. However, a scaffold polymer was required for spinning. Two hydrophobic polymers were chosen, polystyrene and PIM-1. When spinning the nanoparticles with polystyrene, fibrous material was visible on the collecting plate, however SEM showed only the polymer fibres; no cages were visible. Further, “pores” on the surface of the fibres were visible, arising from the effect of evaporative cooling

The effect of molecular weight on fibre production was investigated. Four different molecular weight PEO were spun under identical conditions (with the exception of concentration, due to its effect on viscosity). Fibres were formed at higher molecular weights only (approximately  $M_n$  300,000 and 100,000  $\text{g mol}^{-1}$ ), with discrete structures forming at the lower molecular weights.

The bio-hybrid materials produced in Chapter 3 were electrospun. Several solvents tests were carried out to determine the best solvent system for spinning, taking into account solution viscosity and volatility. A binary solvent mixture of THF: DMF was chosen. Although the conjugates were successfully spun, no fibres were observed. However, mPEO<sub>17</sub>-F<sub>4</sub>-OEt did show the formation of needle-like structures, which may be a precursor to fibres.

## 6.2. Future Work

### 6.2.1. Future direction of the synthesis of polymer-peptide conjugates

Although the synthesis of phenylalanine oligopeptides was fast and high yielding, increasing the peptide length, further resulting in a growing incompatibility with the solvent, will begin to impact yields. Future work in this area will be to investigate peptides longer than four repeat units. Furthermore, the amino acid used to produce the oligopeptide and ultimately the conjugate is another area of investigation. For example, phenylalanine and tyrosine differ only in that the latter has a hydroxyl group, making it hydrophilic, which would affect the properties of the final conjugate. Finally, whilst a solution phase approach has been used to produce short chain peptides, employing a solid phase approach may be more suitable for longer length peptides.

Production of polymer-peptide conjugates was carried out using IBCF coupling (amidation) chemistry. However, this involves both peptide and polymer modification prior to coupling. The initial esterification attempts described in Chapter 3 allow for the production of conjugates by modifying (by deprotection) the peptide only. This also eliminates the need for chromium-based oxidation, thus drastically reducing potential toxicity in the final materials and the synthetic process employed. Future work should focus on optimising the system for esterification. Furthermore, producing conjugates (Boc-F<sub>x</sub>-PEO<sub>y</sub>) in this manner, allows for easy production of triblocks (and more) by simple deprotection of the N-terminus using TFA. Thus, it will be possible to produce multiple-block conjugates, with additional polymer or peptide units depending on the desired functionality.

### 6.2.2. Future directions of the self-assembly behaviour of bio-hybrid materials

Developing a reliable route to gelation for the bio-hybrid materials produced is critical. The effect of temperature on the time scale for self-assembly for these materials is an important parameter that directly affects the reliability. Further work should also focus on exploring the complete changes in the ATR-FTIR

spectrum. An *in situ* gelation experiment on the ATR crystal would provide useful kinetic data for self-assembly.

Stability remains an issue with the material, therefore changing the amino acid will affect the strength of the self-assembled material. Tyrosine is structurally similar to phenylalanine, but has an added hydroxyl group on the phenyl ring, making it more hydrophilic and thus giving the conjugate a greater propensity to form hydrogen bonds. Furthermore, investigating the effect of increased peptide unit length (for example F<sub>5</sub>-F<sub>8</sub>) should further reinforce gel stability.

### 6.2.3. Future directions of electrospinning novel materials

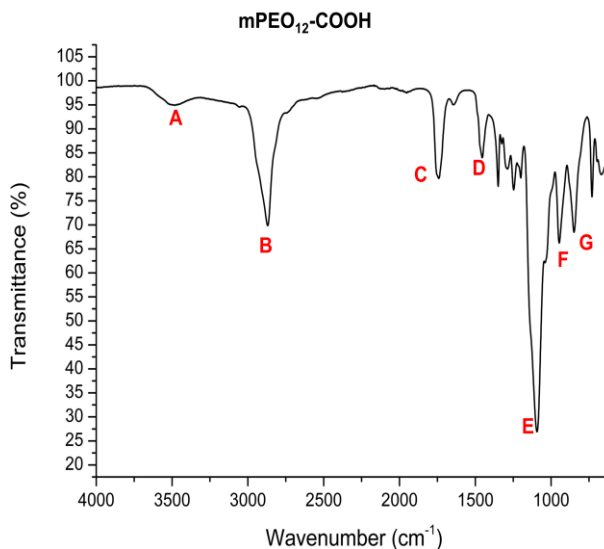
Although electrospinning polymer-peptide conjugates was successful, no fibres were produced. As aforementioned, SEM showed that mPEO<sub>17</sub>-F<sub>4</sub>-OEt produced needle-like structures when spun at high concentration. These structures are most likely precursor to fibres. Therefore, further work should focus on producing fibres with the conjugate, and then optimising the other spinning parameters, thus controlling fibre density and diameter.

The nanoparticle cage solutions were spun using hydrophobic polymer scaffolds, either PIM-1 or polystyrene. In both instances, although fibres were produced, no nanoparticles were observed by SEM. Due to the effects of the solvent, “breath holes” also formed on the fibres that may have incorporated the cages. As this was the result of solvent, future work in this area should emphasise spinning from alternative solvents, and ensuring incorporation of the nanoparticles. Nanofibres formed from PIM-1 (and also these nanoparticle cage nanofibres) should receive attention for their use in gas adsorption.

# Appendices

## Appendix A: Band Assignment of IR Spectra

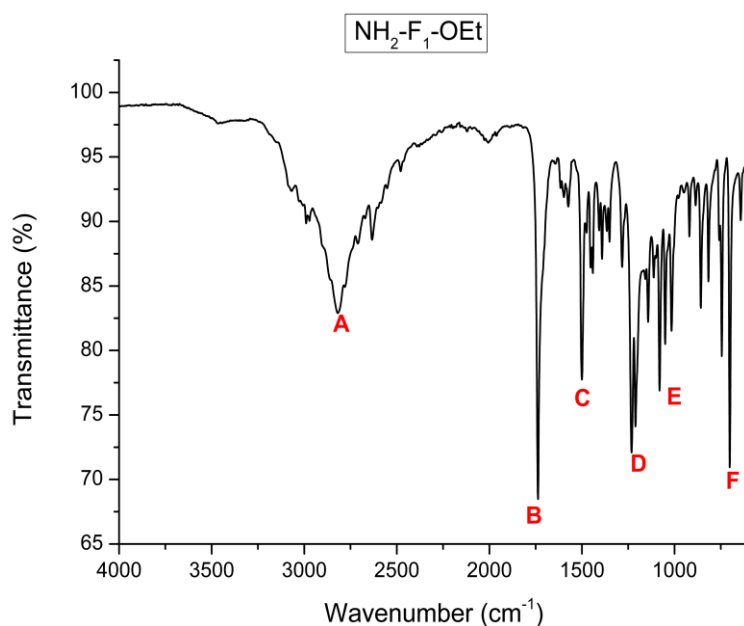
### Appendix 1.1: IR spectrum and band assignment of mPEO<sub>12</sub>-COOH



Original image from Figure 3.14.

mPEO <sub>12</sub> -COOH			
Peak Label	Wavenumber (cm <sup>-1</sup> )	Intensity	Bond
A	3509	Broad Medium	H Bonded OH
B	2869	Broad Medium	CH <sub>2</sub> and CH <sub>3</sub> (-C-H stretching) or CH <sub>3</sub> -O
C	1741	Medium	Saturated Carboxylic Acid -C=O-OH
D	1455	Medium	CH <sub>3</sub> and CH <sub>2</sub> -C-H deformations
E	1093	Strong	Ether -C-O stretching
F	947	Medium	CH <sub>2</sub> rocking and CO stretching
G	849	Medium	CH <sub>2</sub> and CO stretching/rocking

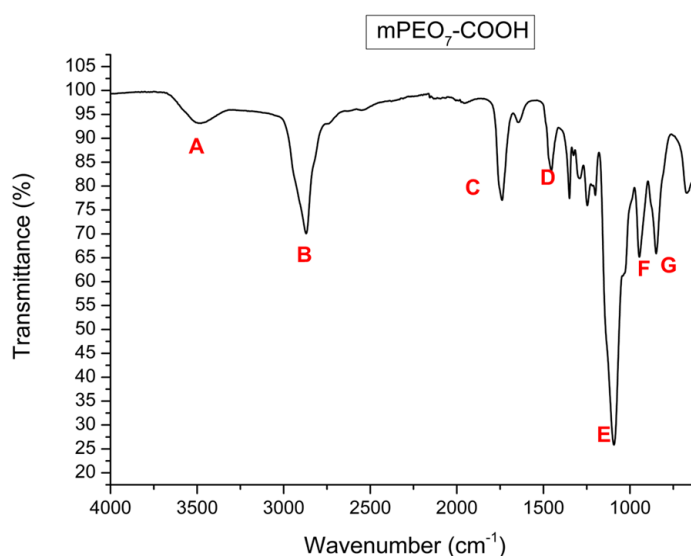
**Appendix 1.2: IR spectrum and band assignment of NH<sub>2</sub>-F<sub>1</sub>-OEt**



**Original image from Figure 3.21.**

NH <sub>2</sub> -F <sub>1</sub> -OEt			
Peak Label	Wavenumber (cm <sup>-1</sup> )	Intensity	Bond
A	2819	Broad Strong	-CH <sub>3</sub> and -CH <sub>2</sub> stretching
B	1737	Strong	Saturated ester -CO-O-
C	1500	Medium	-NH <sub>3</sub> and aromatic ring
D	1210	Strong	Ester C-O stretching
E	1080	Medium	Ester and Ether -C-O stretching
F	702	Strong	Monosubstituted Aromatic

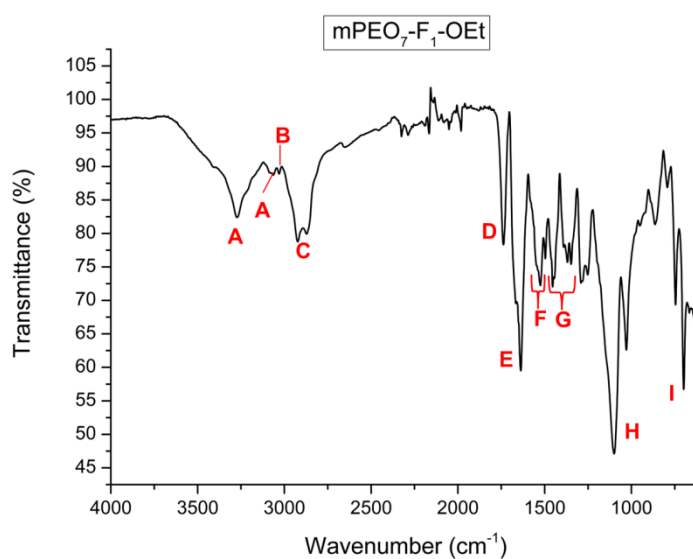
### Appendix 1.3: IR spectrum and band assignment of mPEO<sub>7</sub>-COOH



Original image from Figure 3.22.

mPEO <sub>7</sub> -COOH			
Peak Label	Wavenumber (cm <sup>-1</sup> )	Intensity	Bond
A	3476	Broad Medium	H Bonded OH
B	2870	Broad Medium	CH <sub>2</sub> and CH <sub>3</sub> (-C-H stretching) or CH <sub>3</sub> -O
C	1739	Medium	Saturated Carboxylic Acid -C=O-OH
D	1454	Medium	CH <sub>3</sub> and CH <sub>2</sub> -C-H deformations
E	1092	Strong	Ether -C-O stretching
F	946	Medium	CH <sub>2</sub> rocking and CO stretching
G	849	Medium	CH <sub>2</sub> and CO stretching/rocking

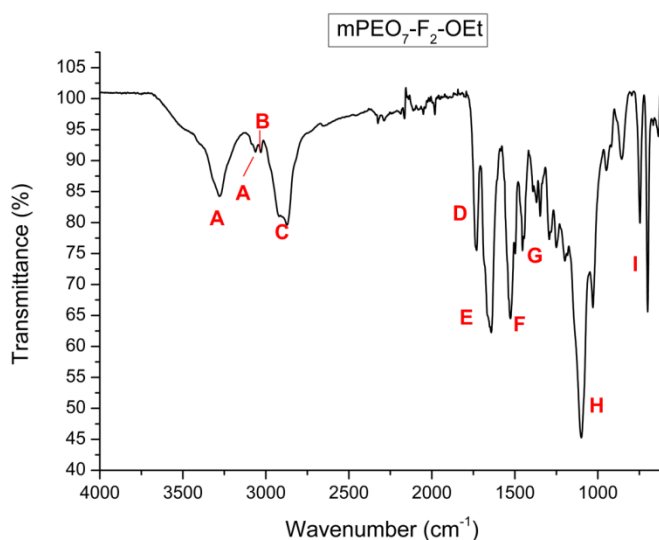
## Appendix 1.4: IR spectrum and band assignment of mPEO<sub>7</sub>-F<sub>1</sub>-OEt



Original Image from Figure 3.23.

mPEO <sub>7</sub> -F <sub>1</sub> -OEt			
Peak Label	Wavenumber (cm <sup>-1</sup> )	Intensity	Bond
A	3277	Broad Medium	Secondary Amide (N-H stretching) Lowered by H Bond
B	3050	Weak	Aryl-H
C	2925 and 2871	Medium	CH <sub>2</sub> and CH <sub>3</sub> (-C-H stretching)
D	1742	Medium	Saturated Ester -C=O-O
E	1666 and 1637	Strong	Secondary Amide stretching C=O and N-H bending
F	1550-1496	Medium	Aromatic And N-H bending
G	1454	Medium	CH <sub>3</sub> and CH <sub>2</sub> -C-H deformations
H	1100 and 1030	Strong	Ester and Ether -C-O stretching
I	746 and 699	Strong	Monosubstitued Aromatic

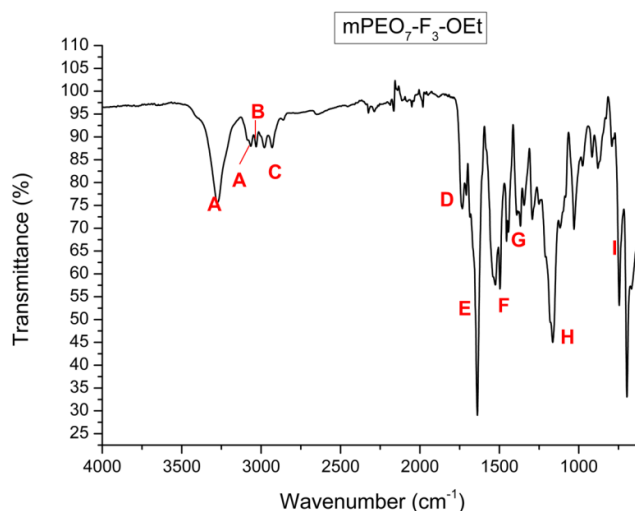
## Appendix 1.5: IR spectrum and band assignment of mPEO<sub>7</sub>-F<sub>2</sub>-OEt



Original image from Figure 3.27.

mPEO <sub>7</sub> -F <sub>2</sub> -OEt			
Peak Label	Wavenumber (cm <sup>-1</sup> )	Intensity	Bond
A	3281	Broad Medium	Secondary Amide (N-H stretching) Lowered by H Bond
B	3045	Weak	Aryl-H
C	2919 and 2872	Medium	CH <sub>2</sub> and CH <sub>3</sub> (-C-H stretching)
D	1730	Medium	Saturated Ester -C=O-O
E	1642	Strong	Secondary Amide stretching C=O and N-H bending
F	1526-1497	Medium	Aromatic And N-H bending
G	1454	Medium	CH <sub>3</sub> and CH <sub>2</sub> -C-H deformations
H	1100 and 1030	Strong	Ester and Ether -C-O stretching
I	746 and 699	Strong	Monosubstituted Aromatic

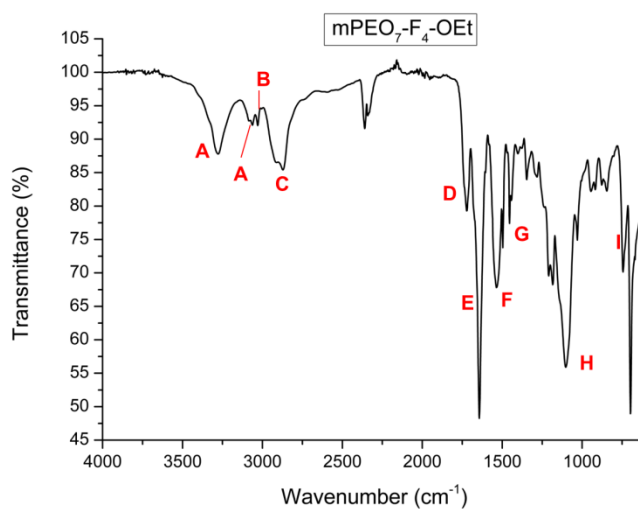
## Appendix 1.6: IR spectrum and band assignment of mPEO<sub>7</sub>-F<sub>3</sub>-OEt



Original Image from Figure 3.32.

mPEO <sub>7</sub> -F <sub>3</sub> -OEt			
Peak Label	Wavenumber (cm <sup>-1</sup> )	Intensity	Bond
A	3278	Broad Medium	Secondary Amide (N-H stretching) Lowered by H Bond
B	3033	Weak	Aryl-H
C	2938 and 2928	Medium	CH <sub>2</sub> and CH <sub>3</sub> (-C-H stretching)
D	1725	Medium	Saturated Ester -C=O-O
E	1638	Strong	Secondary Amide stretching C=O and N-H bending
F	1526-1497	Medium	Aromatic And N-H bending
G	1454	Medium	CH <sub>3</sub> and CH <sub>2</sub> -C-H deformations
H	1134 and 1030	Strong	Ester and Ether -C-O stretching
I	745 and 697	Strong	Monosubstituted Aromatic

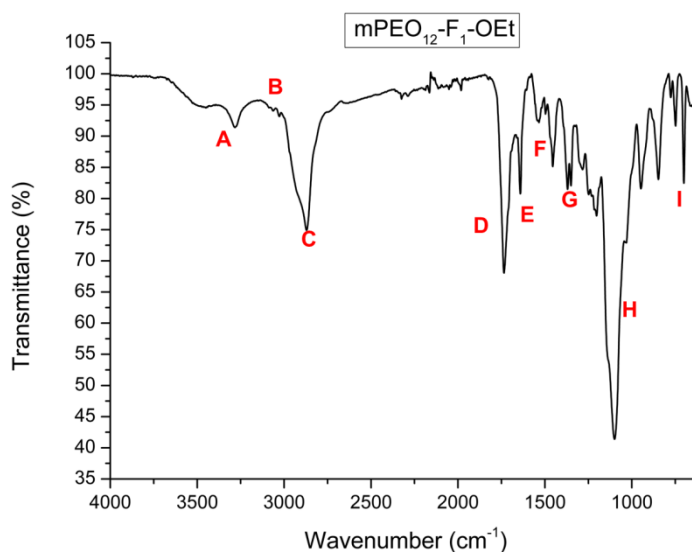
## Appendix 1.7: IR spectrum and band assignment of mPEO<sub>7</sub>-F<sub>4</sub>-OEt



Original Image from Figure 3.38.

mPEO <sub>7</sub> -F <sub>4</sub> -OEt			
Peak Label	Wavenumber (cm <sup>-1</sup> )	Intensity	Bond
A	3277	Broad Medium	Secondary Amide (N-H stretching) Lowered by H Bond
B	3029	Weak	Aryl-H
C	2931 and 2871	Medium	CH <sub>2</sub> and CH <sub>3</sub> (-C-H stretching)
D	1721	Medium	Saturated Ester -C=O-O
E	1635	Strong	Secondary Amide stretching C=O and N-H bending
F	1536-1496	Medium	Aromatic And N-H bending
G	1454	Medium	CH <sub>3</sub> and CH <sub>2</sub> -C-H deformations
H	1102 and 1030	Strong	Ester and Ether -C-O stretching
I	744 and 697	Strong	Monosubstitued Aromatic

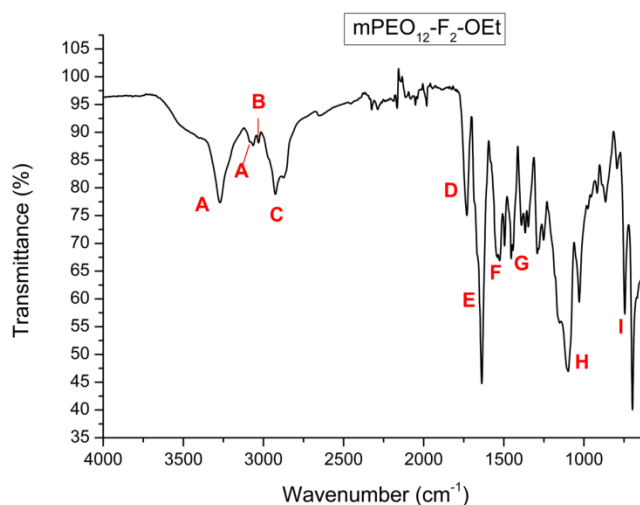
### Appendix 1.8: IR spectrum and band assignment of mPEO<sub>12</sub>-F<sub>1</sub>-OEt



Original Image from Figure 3.42.

mPEO <sub>12</sub> -F <sub>1</sub> -OEt			
Peak Label	Wavenumber (cm <sup>-1</sup> )	Intensity	Bond
A	3282	Broad Weak	Secondary Amide (N-H stretching) Lowered by H Bond
B	3035-2871	Weak	Aryl-H and CH <sub>2</sub> and CH <sub>3</sub> (-C-H stretching)
C	1735	Medium	Saturated Ester -C=O-O
D	1641	Medium	Secondary Amide stretching C=O and N-H bending
E	1541-1496	Weak	Aromatic And N-H bending
F	1454	Medium	CH <sub>3</sub> and CH <sub>2</sub> -C-H deformations
G	1102 and 1030	Strong	Ester and Ether -C-O stretching
H	743 and 697	Medium	Monosubstituted Aromatic

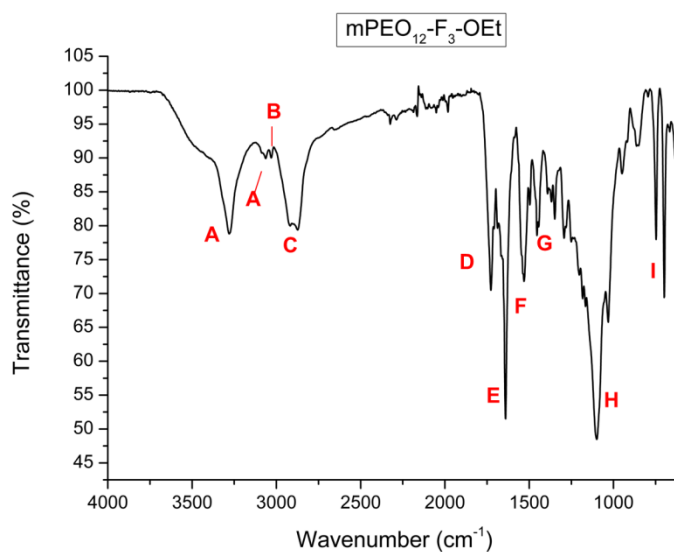
## Appendix 1.9: IR spectrum and band assignment of mPEO<sub>12</sub>-F<sub>2</sub>-OEt



Original Image from Figure 3.46.

mPEO <sub>12</sub> -F <sub>2</sub> -OEt			
Peak Label	Wavenumber (cm <sup>-1</sup> )	Intensity	Bond
A	3270	Broad Medium	Secondary Amide (N-H stretching) Lowered by H Bond
B	3027	Weak	Aryl-H
C	2920 and 2877	Medium	CH <sub>2</sub> and CH <sub>3</sub> (-C-H stretching)
D	1738	Medium	Saturated Ester -C=O-O
E	1636	Strong	Secondary Amide stretching C=O and N-H bending
F	1536-1495	Medium	Aromatic And N-H bending
G	1454	Medium	CH <sub>3</sub> and CH <sub>2</sub> -C-H deformations
H	1098 and 1030	Strong	Ester and Ether -C-O stretching
I	745 and 697	Strong	Monosubstituted Aromatic

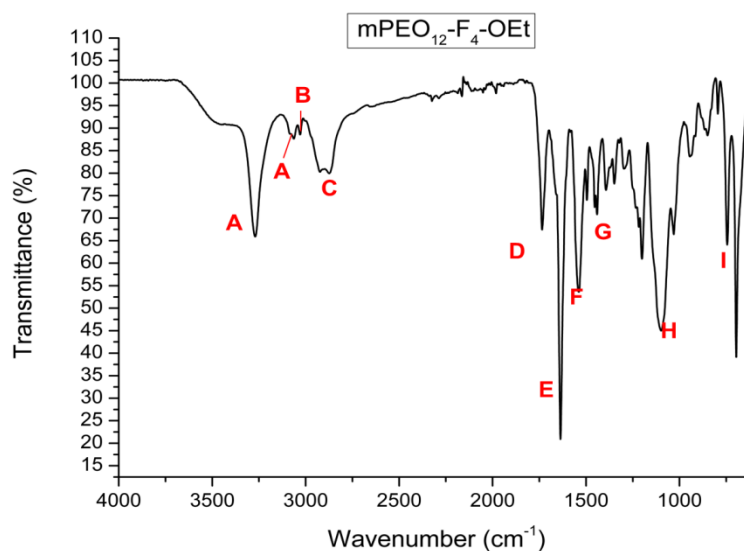
### Appendix 1.10: IR spectrum and band assignment of mPEO<sub>12</sub>-F<sub>3</sub>-OEt



Original Image from Figure 3.51.

mPEO <sub>12</sub> -F <sub>3</sub> -OEt			
Peak Label	Wavenumber (cm <sup>-1</sup> )	Intensity	Bond
A	3280	Broad Medium	Secondary Amide (N-H stretching) Lowered by H Bond
B	3034	Weak	Aryl-H
C	2920 and 2877	Medium	CH <sub>2</sub> and CH <sub>3</sub> (-C-H stretching)
D	1727	Medium	Saturated Ester -C=O-O
E	1640	Strong	Secondary Amide stretching C=O and N-H bending
F	1536-1495	Medium	Aromatic And N-H bending
G	1454	Medium	CH <sub>3</sub> and CH <sub>2</sub> -C-H deformations
H	1099 and 1030	Strong	Ester and Ether -C-O stretching
I	747 and 698	Strong	Monosubstitued Aromatic

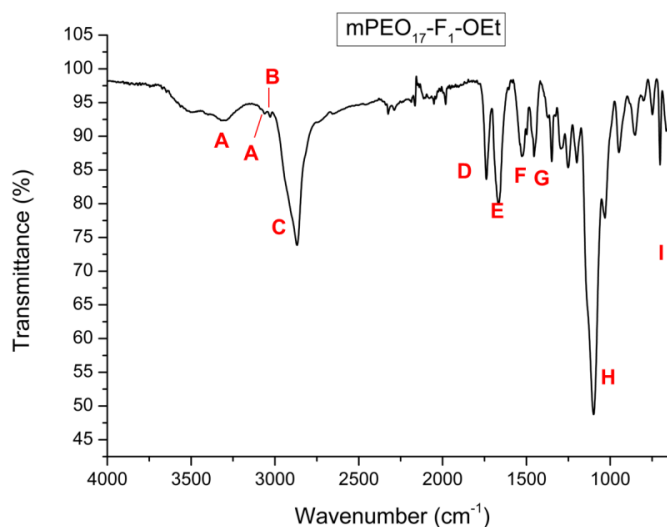
## Appendix 1.11: IR spectrum and band assignment of mPEO<sub>12</sub>-F<sub>4</sub>-OEt



Original image from Figure 3.55.

mPEO <sub>12</sub> -F <sub>4</sub> -OEt			
Peak Label	Wavenumber (cm <sup>-1</sup> )	Intensity	Bond
A	3270	Broad Medium	Secondary Amide (N-H stretching) Lowered by H Bond
B	3015	Weak	Aryl-H
C	2928 and 2877	Medium	CH <sub>2</sub> and CH <sub>3</sub> (-C-H stretching)
D	1732	Medium	Saturated Ester -C=O-O
E	1637	Strong	Secondary Amide stretching C=O and N-H bending
F	1544-1495	Medium	Aromatic And N-H bending
G	1454	Medium	CH <sub>3</sub> and CH <sub>2</sub> -C-H deformations
H	1098 and 1030	Medium	Ester and Ether -C-O stretching
I	745 and 697	Strong	Monosubstitued Aromatic

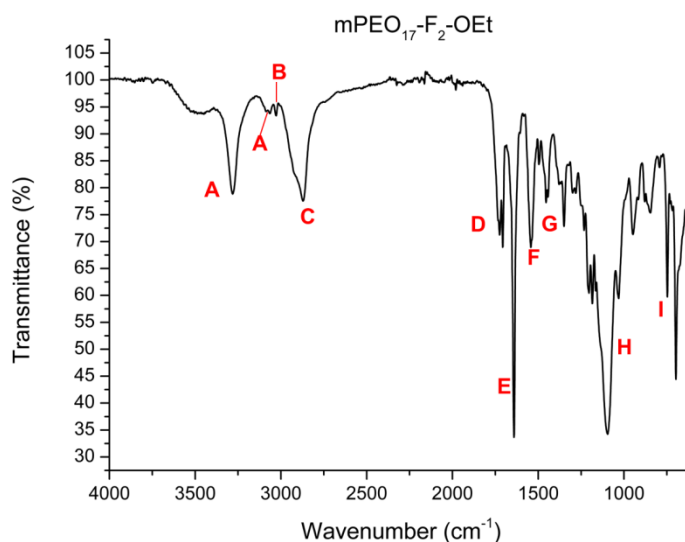
## Appendix 1.12: IR spectrum and band assignment of mPEO<sub>17</sub>-F<sub>1</sub>-OEt



Original image from Figure 3.59.

mPEO <sub>17</sub> -F <sub>1</sub> -OEt			
Peak Label	Wavenumber (cm <sup>-1</sup> )	Intensity	Bond
A	3320	Broad Weak	Secondary Amide (N-H stretching) Lowered by H Bond
B	3045	Weak	Aryl-H
C	2928 and 2867	Broad Medium	CH <sub>2</sub> and CH <sub>3</sub> (-C-H stretching)
D	1739	Medium	Saturated Ester -C=O-O
E	1664	Medium	Secondary Amide stretching C=O and N-H bending
F	1538-1495	Medium	Aromatic And N-H bending
G	1454	Medium	CH <sub>3</sub> and CH <sub>2</sub> -C-H deformations
H	1099 and 1031	Strong	Ester and Ether -C-O stretching
I	703 and 631	Strong	Monosubstitued Aromatic

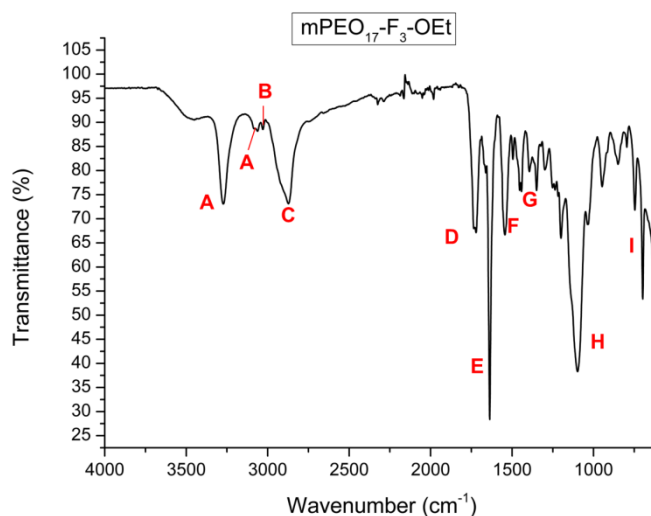
### Appendix 1.13: IR spectrum and band assignment of mPEO<sub>17</sub>-F<sub>2</sub>-OEt



Original image from Figure 3.63.

mPEO <sub>17</sub> -F <sub>2</sub> -OEt			
Peak Label	Wavenumber (cm <sup>-1</sup> )	Intensity	Bond
A	3281	Broad Medium	Secondary Amide (N-H stretching) Lowered by H Bond
B	3043	Weak	Aryl-H
C	2873	Broad Medium	CH <sub>2</sub> and CH <sub>3</sub> (-C-H stretching)
D	1724	Medium	Saturated Ester -C=O-O
E	1642	Strong	Secondary Amide stretching C=O and N-H bending
F	1543-1493	Medium	Aromatic And N-H bending
G	1454	Medium	CH <sub>3</sub> and CH <sub>2</sub> -C-H deformations
H	1095 and 1037	Strong	Ester and Ether -C-O stretching
I	747 and 696	Strong	Monosubstitued Aromatic

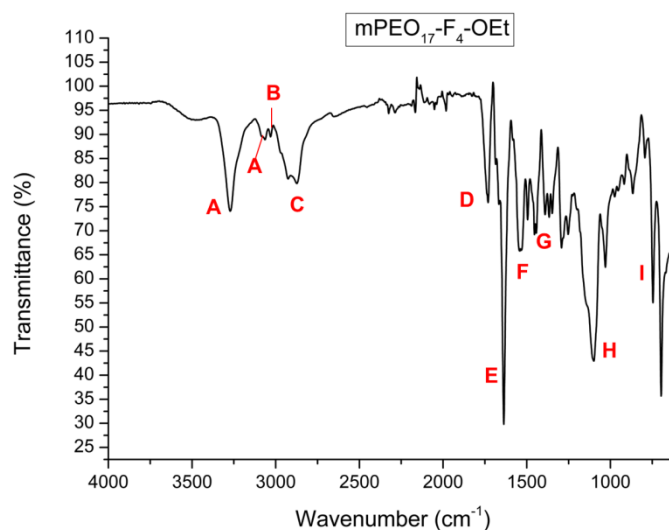
### Appendix 1.14: IR spectrum and band assignment of mPEO<sub>17</sub>-F<sub>3</sub>-OEt



Original image from Figure 3.67.

mPEO <sub>17</sub> -F <sub>3</sub> -OEt			
Peak Label	Wavenumber (cm <sup>-1</sup> )	Intensity	Bond
A	3272	Broad Medium	Secondary Amide (N-H stretching) Lowered by H Bond
B	3031	Weak	Aryl-H
C	2872	Broad Medium	CH <sub>2</sub> and CH <sub>3</sub> (-C-H stretching)
D	1735	Medium	Saturated Ester -C=O
E	1637	Strong	Secondary Amide stretching C=O and N-H bending
F	1544-1493	Medium	Aromatic And N-H bending
G	1454	Medium	CH <sub>3</sub> and CH <sub>2</sub> -C-H deformations
H	1098 and 1037	Strong	Ester and Ether -C-O stretching
I	746 and 698	Strong	Monosubstituted Aromatic

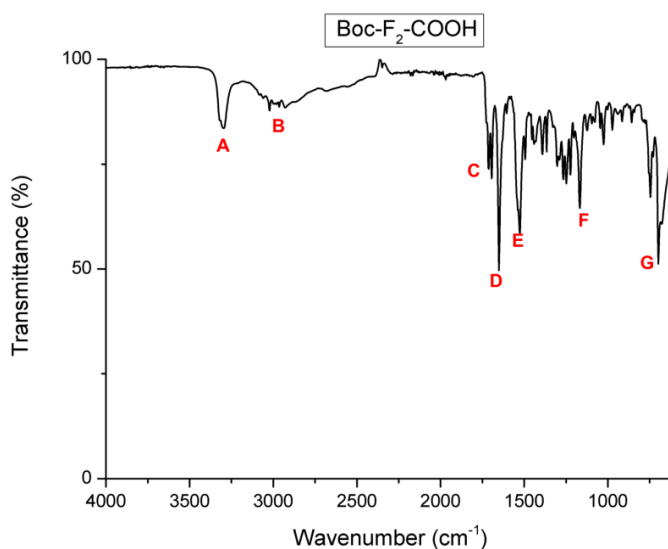
### Appendix 1.15: IR spectrum and band assignment of mPEO<sub>17</sub>-F<sub>4</sub>-OEt



Original image from Figure 3.71.

mPEO <sub>17</sub> -F <sub>4</sub> -OEt			
Peak Label	Wavenumber (cm <sup>-1</sup> )	Intensity	Bond
A	3278	Broad Medium	Secondary Amide (N-H stretching) Lowered by H Bond
B	3045	Weak	Aryl-H
C	2877	Broad Medium	CH <sub>2</sub> and CH <sub>3</sub> (-C-H stretching)
D	1735	Medium	Saturated Ester -C=O-O
E	1637	Strong	Secondary Amide stretching C=O and N-H bending
F	1544-1493	Medium	Aromatic And N-H bending
G	1454	Medium	CH <sub>3</sub> and CH <sub>2</sub> -C-H deformations
H	1099 and 1030	Strong	Ester and Ether -C-O stretching
I	746 and 697	Strong	Monosubstitued Aromatic

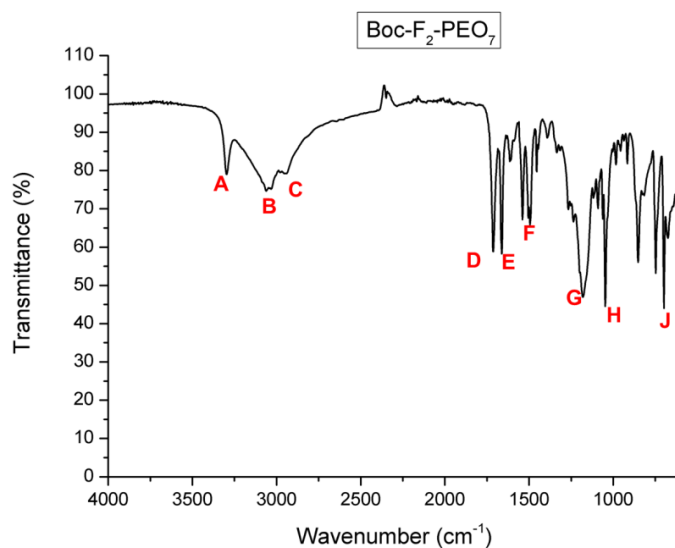
## Appendix 1.15: IR spectrum and band assignment of Boc-F<sub>2</sub>-COOH



Original image from Figure 3.75.

Boc-F <sub>2</sub> -PEO <sub>7</sub>			
Peak Label	Wavenumber (cm <sup>-1</sup> )	Intensity	Bond
A	3345	Broad Medium	Secondary Amide (N-H stretching) Lowered by H Bond
B	2917 and 2874	Weak	CH <sub>2</sub> and CH <sub>3</sub> (-C-H stretching)
C	1734	Medium	Saturated Ester -C=O-O
D	1639	Medium	Secondary Amide stretching C=O
E	1540-1497	Medium	Aromatic And N-H bending
F	1120	Strong	Ester -C-O stretching
G	748 and 699	Strong	Monosubstituted Aromatic

**Appendix 1.16: IR spectrum and band assignment of Boc-F<sub>2</sub>-PEO<sub>7</sub>**



**Original Image from Figure 3.83.**

Boc-F <sub>2</sub> -PEO <sub>7</sub>			
Peak Label	Wavenumber (cm <sup>-1</sup> )	Intensity	Bond
A	3310	Broad Medium	Secondary Amide (N-H stretching) Lowered by H Bond
B	3060	Weak	Aryl-H
C	2919 and 2872	Medium	CH <sub>2</sub> and CH <sub>3</sub> (-C-H stretching)
D	1728	Medium	Saturated Ester -C=O-O
E	1660	Medium	Secondary Amide stretching C=O and N-H bending
F	1540-1497	Medium	Aromatic And N-H bending
G	1454	Medium	CH <sub>3</sub> and CH <sub>2</sub> -C-H deformations
H	1048	Strong	Ester and Ether -C-O stretching
I	748 and 699	Strong	Monosubstituted Aromatic

## Appendix B: Gelation behaviour of polymer-peptide conjugates

**Appendix B1:** Qualitative observations of gel formation of mPEO<sub>7</sub>-F<sub>1</sub>-OEt. The percentage shows the proportion of organic solvent in the mixture with water.

mPEO <sub>7</sub> -F <sub>1</sub> -OEt	Gels at Room Temperature				Gels at 60 °C			
Solvents	5 %	10 %	20 %	40 %	5 %	10 %	20 %	40 %
DMSO	x	x	x	x	x	x	x	x
THF	x	x	x	x	x	x	x	x
Acetone	x	x	x	x	x	x	x	x
Ethanol	x	x	x	x	x	x	x	x
DMF	x	x	x	x	x	x	x	x
5 mg/ml								
mPEO <sub>7</sub> -F <sub>1</sub> -OEt	Gels at Room Temperature				Gels at 60 °C			
Solvents	5 %	10 %	20 %	40 %	5 %	10 %	20 %	40 %
DMSO	x	x	x	x	x	x	x	x
THF	x	x	x	x	x	x	x	x
Acetone	x	x	x	x	x	x	x	x
Ethanol	x	x	x	x	x	x	x	x
DMF	x	x	x	x	x	x	x	x
10 mg/ml								

*N.B.* **x** represents no gel forming (or an unstable gel), **y** represents a stable gel forming, and **p** denotes “partial” self-assembly behaviour.

**Appendix B2:** Qualitative observations of gel formation of mPEO<sub>7</sub>-F<sub>2</sub>-OEt. The percentage shows the proportion of organic solvent in the mixture with water.

mPEO <sub>7</sub> -F <sub>2</sub> -OEt	Gels at Room Temperature				Gels at 60 °C			
Solvents	5 %	10 %	20 %	40 %	5 %	10 %	20 %	40 %
DMSO	x	x	x	x	x	x	x	x
THF	x	x	x	x	x	x	x	x
Acetone	x	x	x	x	x	x	x	x
Ethanol	x	x	x	x	x	x	x	x
DMF	x	x	x	x	x	x	x	x
5 mg/ml								
mPEO <sub>7</sub> -F <sub>2</sub> -OEt	Gels at Room Temperature				Gels at 60 °C			
Solvents	5 %	10 %	20 %	40 %	5 %	10 %	20 %	40 %
DMSO	x	x	x	x	x	x	x	x
THF	x	x	x	x	x	x	x	x
Acetone	x	x	x	x	x	x	x	x
Ethanol	x	x	x	x	x	x	x	x
DMF	x	x	x	x	x	x	x	x
10 mg/ml								

*N.B. x represents no gel forming (or an unstable gel), y represents a stable gel forming, and p denotes “partial” self-assembly behaviour.*

**Appendix B3:** Qualitative observations of gel formation of mPEO<sub>7</sub>-F<sub>3</sub>-OEt. The percentage shows the proportion of organic solvent in the mixture with water.

mPEO <sub>7</sub> -F <sub>3</sub> -OEt	Gels at Room Temperature				Gels at 60 °C			
Solvents	5 %	10 %	20 %	40 %	5 %	10 %	20 %	40 %
DMSO	x	x	x	x	x	x	x	x
THF	x	x	x	x	x	x	x	x
Acetone	x	x	x	x	x	x	x	x
Ethanol	x	x	x	x	x	x	x	x
DMF	x	x	x	x	x	x	x	x
5 mg/ml								
mPEO <sub>7</sub> -F <sub>3</sub> -OEt	Gels at Room Temperature				Gels at 60 °C			
Solvents	5 %	10 %	20 %	40 %	5 %	10 %	20 %	40 %
DMSO	x	x	x	x	x	x	x	x
THF	x	x	x	x	x	x	x	x
Acetone	x	x	x	x	x	x	x	x
Ethanol	x	x	x	x	x	x	x	x
DMF	x	x	x	x	x	x	x	x
10 mg/ml								

*N.B. x represents no gel forming (or an unstable gel), y represents a stable gel forming, and p denotes “partial” self-assembly behaviour.*

**Appendix B4:** Qualitative observations of gel formation of mPEO<sub>7</sub>-F<sub>4</sub>-OEt. The percentage shows the proportion of organic solvent in the mixture with water.

mPEO <sub>7</sub> -F <sub>4</sub> -OEt	Gels at Room Temperature				Gels at 60 °C			
Solvents	5 %	10 %	20 %	40 %	5 %	10 %	20 %	40 %
DMSO	x	x	x	y	x	x	y (very weak)	y
THF	x	x	x	y	x	x	y (very weak)	y
Acetone	x	x	x	x	x	x	x	x
Ethanol	x	x	x	x	x	x	x	x
DMF	x	x	x	x	x	x	x	x
5 mg/ml								
mPEO <sub>7</sub> -F <sub>4</sub> -OEt	Gels at Room Temperature				Gels at 60 °C			
Solvents	5 %	10 %	20 %	40 %	5 %	10 %	20 %	40 %
DMSO	x	x	y	y	x	x	y (very weak)	y
THF	x	x	x	y	x	x	y (very weak)	y
Acetone	x	x	x	x	x	x	x	x
Ethanol	x	x	x	x	x	x	x	x
DMF	x	x	x	x	x	x	x	x
10 mg/ml								

*N.B. x represents no gel forming (or an unstable gel), and y represents a stable gel forming.*

**Appendix B5:** Qualitative observations of gel formation of mPEO<sub>12</sub>-F<sub>1</sub>-OEt. The percentage shows the proportion of organic solvent in the mixture with water.

mPEO <sub>12</sub> -F <sub>1</sub> -OEt	Gels at Room Temperature				Gels at 60 °C			
Solvents	5 %	10 %	20 %	40 %	5 %	10 %	20 %	40 %
DMSO	x	x	x	x	x	x	x	x
THF	x	x	x	x	x	x	x	x
Acetone	x	x	x	x	x	x	x	x
Ethanol	x	x	x	x	x	x	x	x
DMF	x	x	x	x	x	x	x	x
5 mg/ml								
mPEO <sub>12</sub> -F <sub>1</sub> -OEt	Gels at Room Temperature				Gels at 60 °C			
Solvents	5 %	10 %	20 %	40 %	5 %	10 %	20 %	40 %
DMSO	x	x	x	x	x	x	x	x
THF	x	x	x	x	x	x	x	x
Acetone	x	x	x	x	x	x	x	x
Ethanol	x	x	x	x	x	x	x	x
DMF	x	x	x	x	x	x	x	x
10 mg/ml								

*N.B. x represents no gel forming (or an unstable gel), y represents a stable gel forming, and p denotes “partial” self-assembly behaviour.*

**Appendix B6:** Qualitative observations of gel formation of mPEO<sub>12</sub>-F<sub>2</sub>-OEt. The percentage shows the proportion of organic solvent in the mixture with water.

mPEO <sub>12</sub> -F <sub>2</sub> -OEt	Gels at Room Temperature				Gels at 60 °C			
Solvents	5 %	10 %	20 %	40 %	5 %	10 %	20 %	40 %
DMSO	x	x	x	x	x	x	x	x
THF	x	x	x	x	x	x	x	x
Acetone	x	x	x	x	x	x	x	x
Ethanol	x	x	x	x	x	x	x	x
DMF	x	x	x	x	x	x	x	x
5 mg/ml								
mPEO <sub>12</sub> -F <sub>2</sub> -OEt	Gels at Room Temperature				Gels at 60 °C			
Solvents	5 %	10 %	20 %	40 %	5 %	10 %	20 %	40 %
DMSO	x	x	x	x	x	x	x	x
THF	x	x	x	x	x	x	x	x
Acetone	x	x	x	x	x	x	x	x
Ethanol	x	x	x	x	x	x	x	x
DMF	x	x	x	x	x	x	x	x
10 mg/ml								

*N.B. x represents no gel forming (or an unstable gel), y represents a stable gel forming, and p denotes “partial” self-assembly behaviour.*

**Appendix B7:** Qualitative observations of gel formation of mPEO<sub>12</sub>-F<sub>3</sub>-OEt. The percentage shows the proportion of organic solvent in the mixture with water.

mPEO <sub>12</sub> -F <sub>3</sub> -OEt	Gels at Room Temperature				Gels at 60 °C			
Solvents	5 %	10 %	20 %	40 %	5 %	10 %	20 %	40 %
DMSO	x	x	x	x	x	x	x	x
THF	x	x	x	x	x	x	x	x
Acetone	x	x	x	x	x	x	x	x
Ethanol	x	x	x	x	x	x	x	x
DMF	x	x	x	x	x	x	x	x
5 mg/ml								
mPEO <sub>12</sub> -F <sub>3</sub> -OEt	Gels at Room Temperature				Gels at 60 °C			
Solvents	5 %	10 %	20 %	40 %	5 %	10 %	20 %	40 %
DMSO	x	x	x	x	x	x	x	x
THF	x	x	x	x	x	x	x	x
Acetone	x	x	x	x	x	x	x	x
Ethanol	x	x	x	x	x	x	x	x
DMF	x	x	x	x	x	x	x	x
10 mg/ml								

*N.B. x represents no gel forming (or an unstable gel), y represents a stable gel forming, and p denotes “partial” self-assembly behaviour.*

**Appendix B8:** Qualitative observation of gel formation of mPEO<sub>12</sub>-F<sub>4</sub>-OEt. The percentage shows the amount of organic solvent used in a mixture with water.

mPEO <sub>12</sub> -F <sub>4</sub> -OEt	Gels at Room Temperature				Gels at 60 °C			
Solvents	5 %	10 %	20 %	40 %	5 %	10 %	20 %	40 %
DMSO	x	x	x	p	x	x	x	y (weak)
THF	x	x	x	x	x	x	x	y
Acetone	x	x	x	x	x	y (weak)	y (weak)	x
Ethanol	x	x	x	x	x	x	x	x
DMF	x	x	x	x	x	x	x	x
5 mg/ml								
mPEO <sub>12</sub> -F <sub>4</sub> -OEt	Gels at Room Temperature				Gels at 60 °C			
Solvents	5 %	10 %	20 %	40 %	5 %	10 %	20 %	40 %
DMSO	x	x	x	p	x	x	x	y
THF	p	x	x	x	y	y	y	y
Acetone	x	y	y	x	p	y	y	y
Ethanol	x	x	x	x	x	x	x	y
DMF	x	x	x	x	x	x	x	x
10 mg/ml								

*N.B. x represents no gel forming (or an unstable gel), y represents a stable gel forming, and p denotes “partial” self-assembly behaviour.*

**Appendix B9:** Qualitative observations of gel formation of mPEO<sub>17</sub>-F<sub>1</sub>-OEt. The percentage shows the proportion of organic solvent in the mixture with water.

mPEO <sub>17</sub> -F <sub>1</sub> -OEt	Gels at Room Temperature				Gels at 60 °C			
Solvents	5 %	10 %	20 %	40 %	5 %	10 %	20 %	40 %
DMSO	x	x	x	x	x	x	x	x
THF	x	x	x	x	x	x	x	x
Acetone	x	x	x	x	x	x	x	x
Ethanol	x	x	x	x	x	x	x	x
DMF	x	x	x	x	x	x	x	x
5 mg/ml								
mPEO <sub>17</sub> -F <sub>1</sub> -OEt	Gels at Room Temperature				Gels at 60 °C			
Solvents	5 %	10 %	20 %	40 %	5 %	10 %	20 %	40 %
DMSO	x	x	x	x	x	x	x	x
THF	x	x	x	x	x	x	x	x
Acetone	x	x	x	x	x	x	x	x
Ethanol	x	x	x	x	x	x	x	x
DMF	x	x	x	x	x	x	x	x
10 mg/ml								

*N.B.* **x** represents no gel forming (or an unstable gel), **y** represents a stable gel forming, and **p** denotes “partial” self-assembly behaviour.

**Appendix B10:** Qualitative observations of gel formation of mPEO<sub>17</sub>-F<sub>2</sub>-OEt. The percentage shows the proportion of organic solvent in the mixture with water.

mPEO <sub>17</sub> -F <sub>2</sub> -OEt	Gels at Room Temperature				Gels at 60 °C			
Solvents	5 %	10 %	20 %	40 %	5 %	10 %	20 %	40 %
DMSO	x	x	x	x	x	x	x	x
THF	x	x	x	x	x	x	x	x
Acetone	x	x	x	x	x	x	x	x
Ethanol	x	x	x	x	x	x	x	x
DMF	x	x	x	x	x	x	x	x
5 mg/ml								
mPEO <sub>17</sub> -F <sub>2</sub> -OEt	Gels at Room Temperature				Gels at 60 °C			
Solvents	5 %	10 %	20 %	40 %	5 %	10 %	20 %	40 %
DMSO	x	x	x	x	x	x	x	x
THF	x	x	x	x	x	x	x	x
Acetone	x	x	x	x	x	x	x	x
Ethanol	x	x	x	x	x	x	x	x
DMF	x	x	x	x	x	x	x	x
10 mg/ml								

*N.B.* **x** represents no gel forming (or an unstable gel), **y** represents a stable gel forming, and **p** denotes “partial” self-assembly behaviour.

**Appendix B11:** Qualitative observations of gel formation of mPEO<sub>17</sub>-F<sub>3</sub>-OEt. The percentage shows the proportion of organic solvent in the mixture with water.

mPEO <sub>17</sub> -F <sub>3</sub> -OEt	Gels at Room Temperature				Gels at 60 °C			
Solvents	5 %	10 %	20 %	40 %	5 %	10 %	20 %	40 %
DMSO	x	x	x	x	x	x	x	x
THF	x	x	x	x	x	x	x	x
Acetone	x	x	x	x	x	x	x	x
Ethanol	x	x	x	x	x	x	x	x
DMF	x	x	x	x	x	x	x	x
5 mg/ml								
mPEO <sub>17</sub> -F <sub>3</sub> -OEt	Gels at Room Temperature				Gels at 60 °C			
Solvents	5 %	10 %	20 %	40 %	5 %	10 %	20 %	40 %
DMSO	x	x	x	x	x	x	x	x
THF	x	x	x	x	x	x	x	x
Acetone	x	x	x	x	x	x	x	x
Ethanol	x	x	x	x	x	x	x	x
DMF	x	x	x	x	x	x	x	x
10 mg/ml								

*N.B.* **x** represents no gel forming (or an unstable gel), **y** represents a stable gel forming, and **p** denotes “partial” self-assembly behaviour.

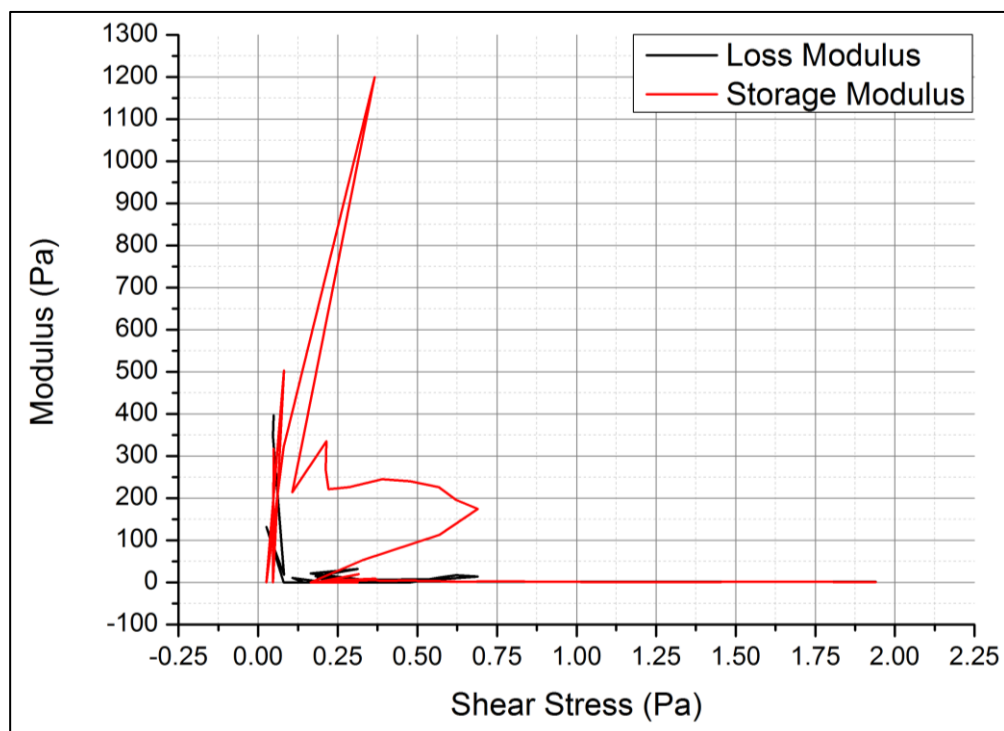
**Appendix B12:** Qualitative observations of gel formation of mPEO<sub>17</sub>-F<sub>4</sub>-OEt. The percentage shows the amount of organic solvent used in a mixture with water.

mPEO <sub>17</sub> -F <sub>4</sub> -OEt	Gels at Room Temperature				Gels at 60 °C			
Solvents	5 %	10 %	20 %	40 %	5 %	10 %	20 %	40 %
DMSO	p	y	y	x	y	y	y	y
THF	x	x	x	x	x	x	y	y
Acetone	x	p	p	x	x	y	y	y
Ethanol	x	x	x	x	x	x	x	x
DMF	x	x	x	x	x	x	x	x
5 mg/ml								
mPEO <sub>17</sub> -F <sub>4</sub> -OEt	Gels at Room Temperature				Gels at 60 °C			
Solvents	5 %	10 %	20 %	40 %	5 %	10 %	20 %	40 %
DMSO	p	y	y	y	y	y	y	y
THF	x	x	p	y	y	y	y	y
Acetone	x	x	x	y	p	y	y	y
Ethanol	x	x	x	x	x	x	x	x
DMF	x	x	x	x	x	x	x	x
10 mg/ml								

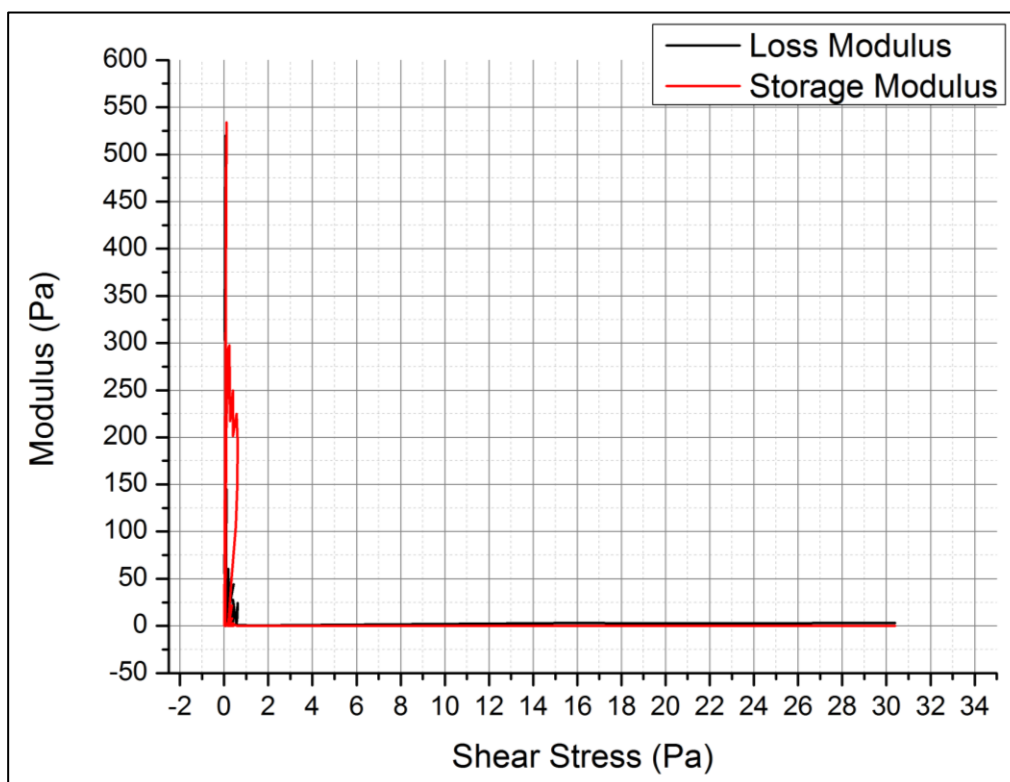
*N.B. x represents no gel forming (or an unstable gel), y represents a stable gel forming, and p denotes “partial” self-assembly behaviour.*

## Appendix C: Rheology of mPEO<sub>17</sub>-F<sub>4</sub>-OEt Gels

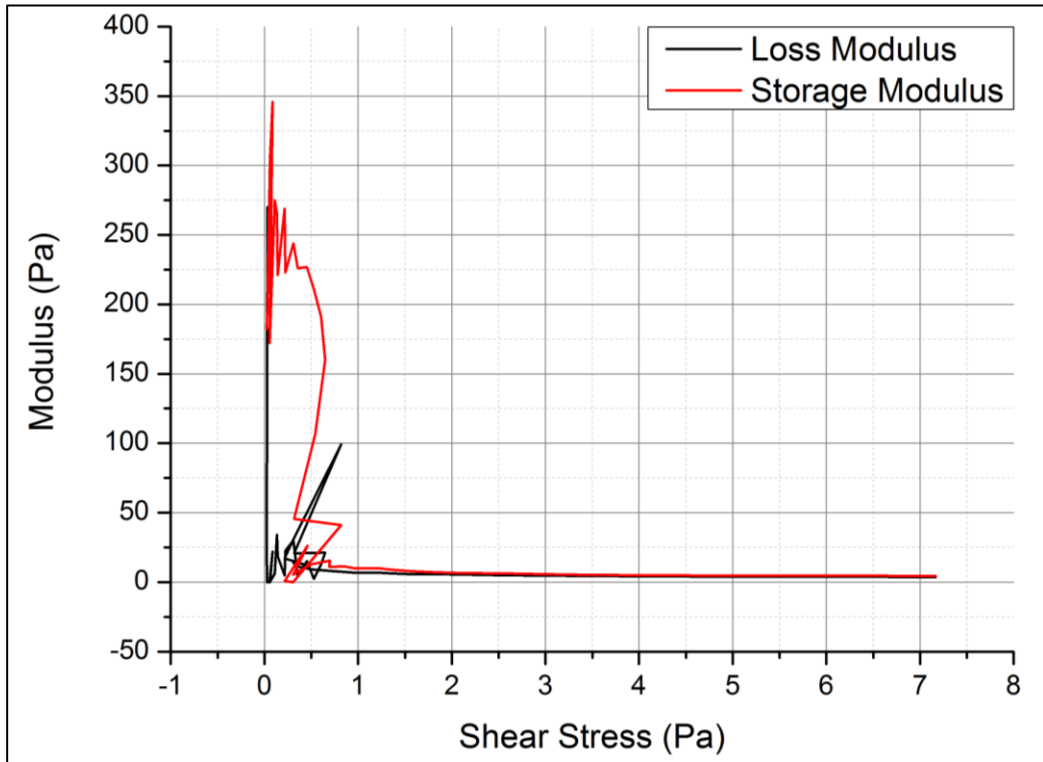
Appendix C1: Strain-sweep data for 10 %v/v, DMSO: water (2 ml).



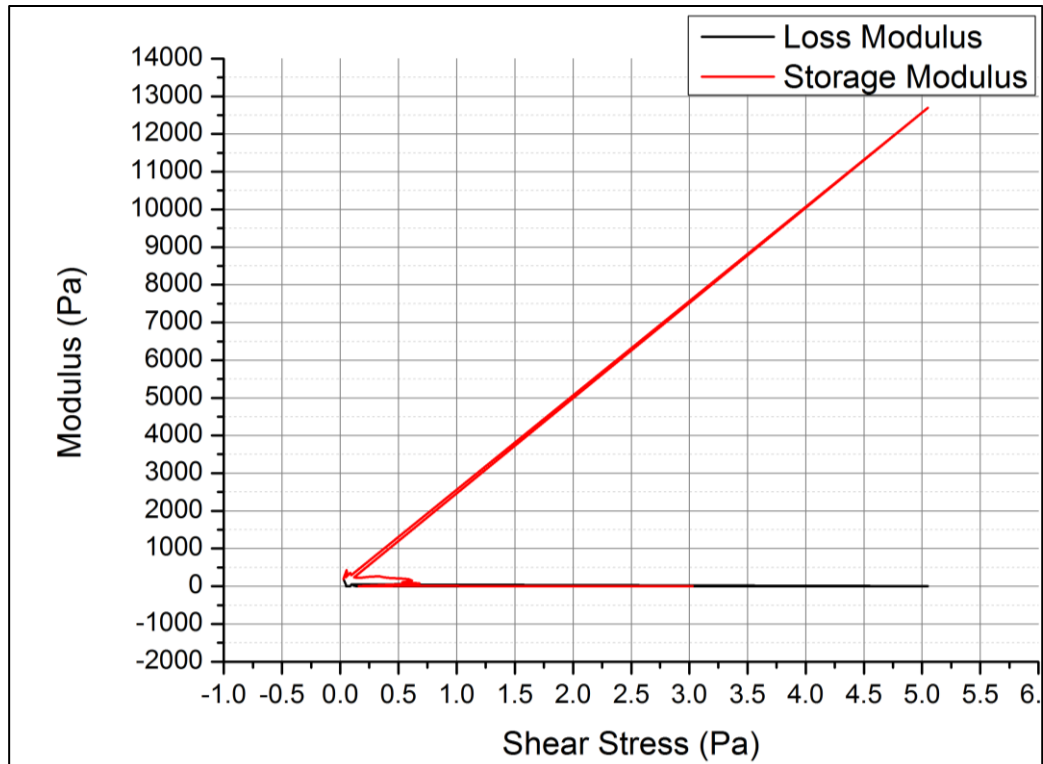
Appendix C2: Strain-sweep data for 10 %v/v, DMSO: water (2 ml) Sample 2.



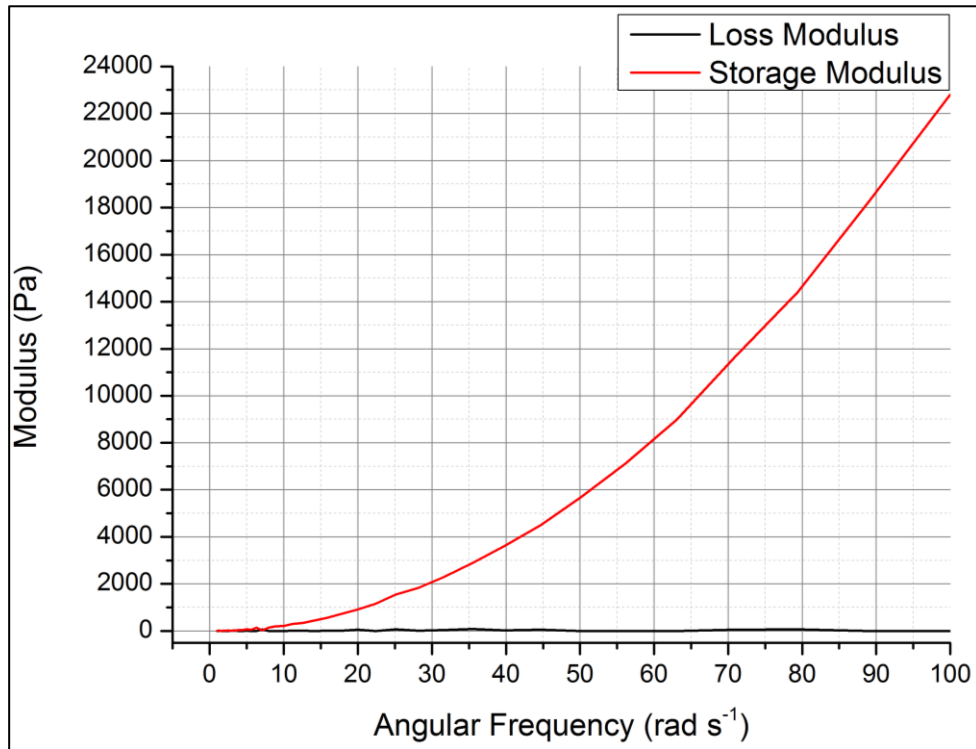
**Appendix C3:** Strain-sweep data for 20 %v/v, DMSO: water (2 ml).



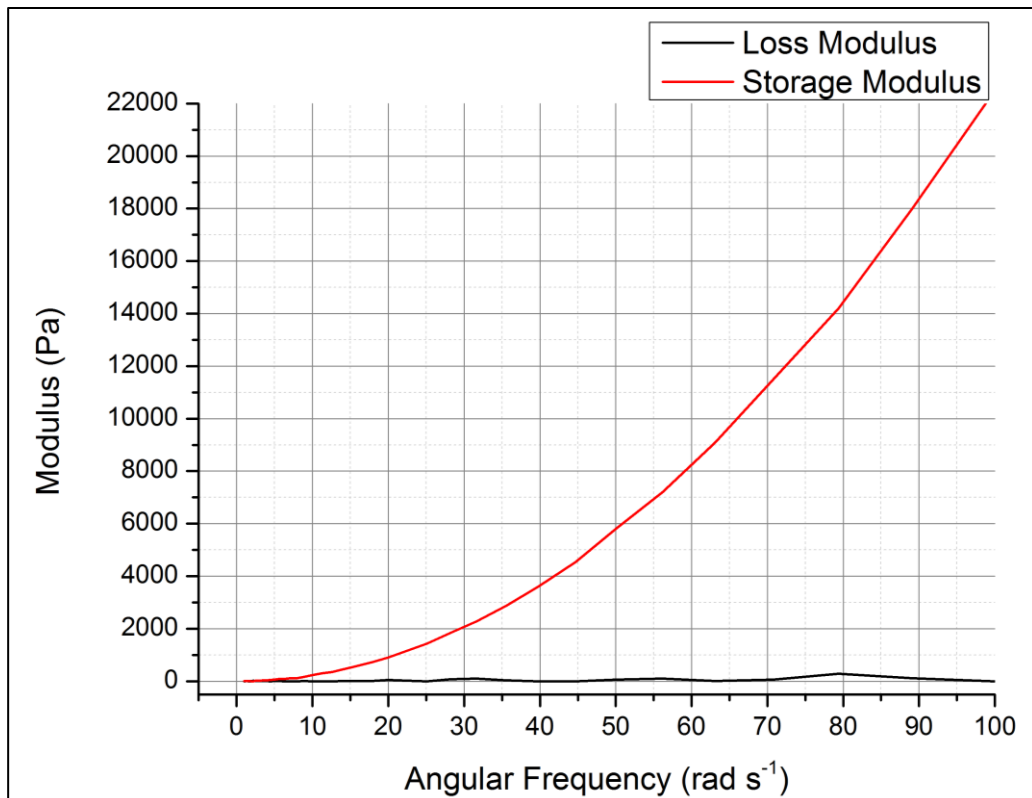
**Appendix C4:** Strain-sweep data for 20 %v/v, DMSO: water (2 ml) Sample 2.



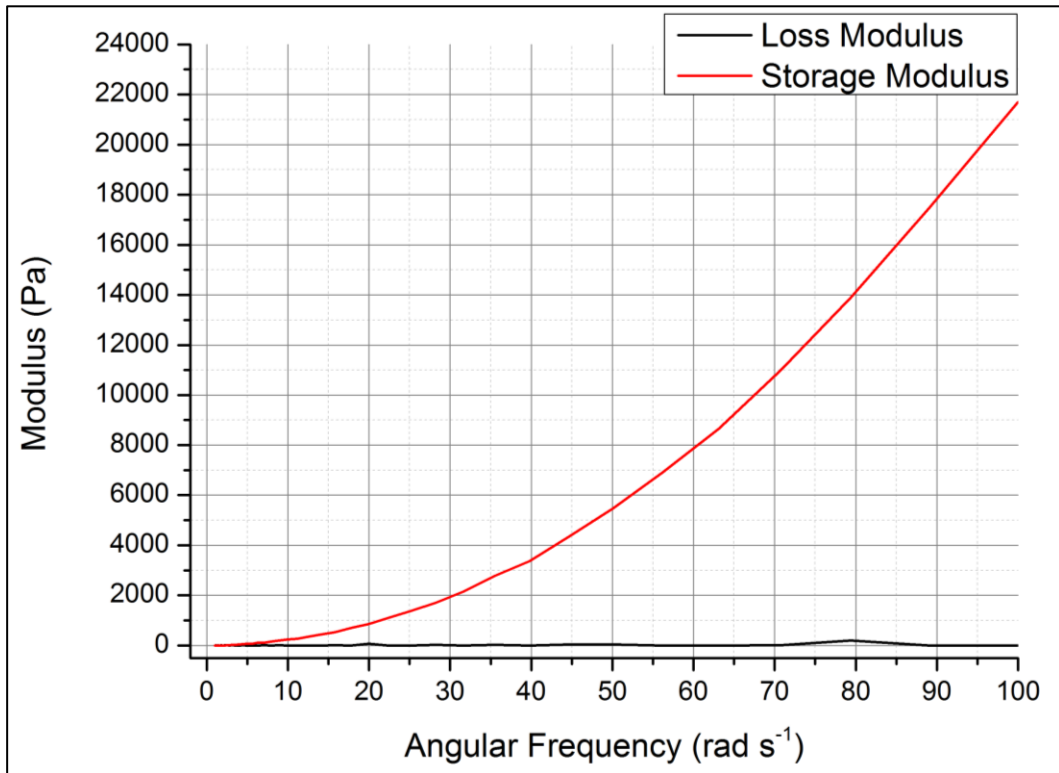
**Appendix C5:** Frequency-sweep data for 10 %v/v, DMSO: water (2 ml).



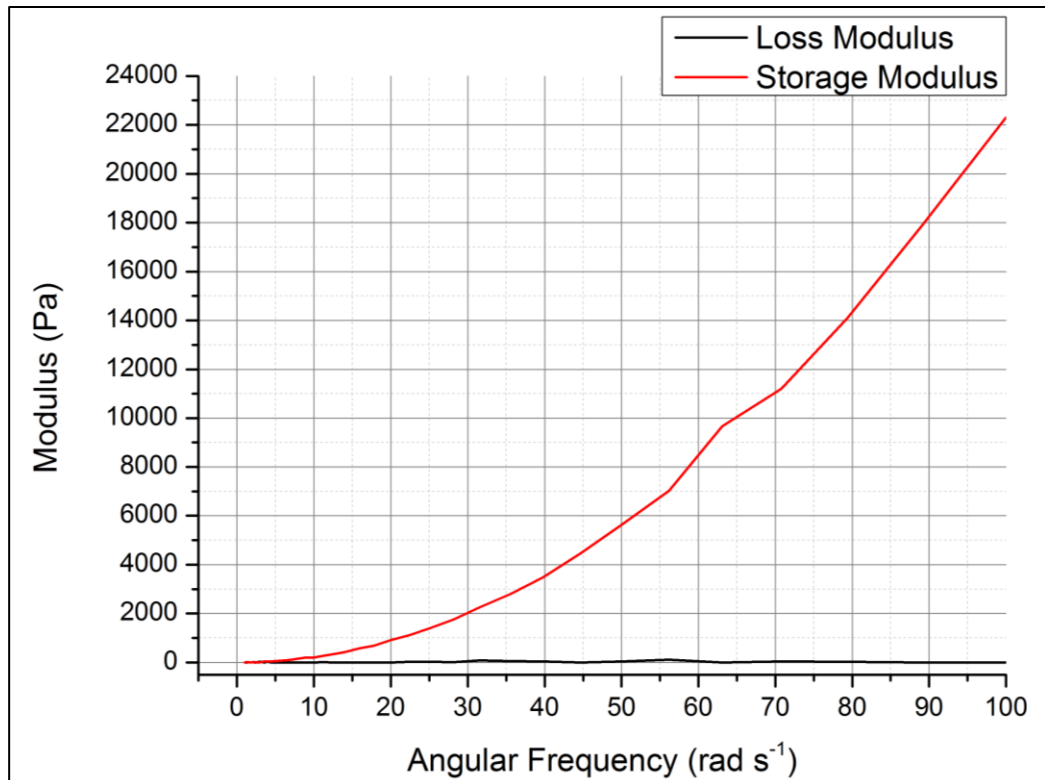
**Appendix C6:** Frequency-sweep data for 10 %v/v, DMSO: water (2 ml), Sample 2.



**Appendix C7:** Frequency-sweep data for 10 %v/v, DMSO: water (2 ml).



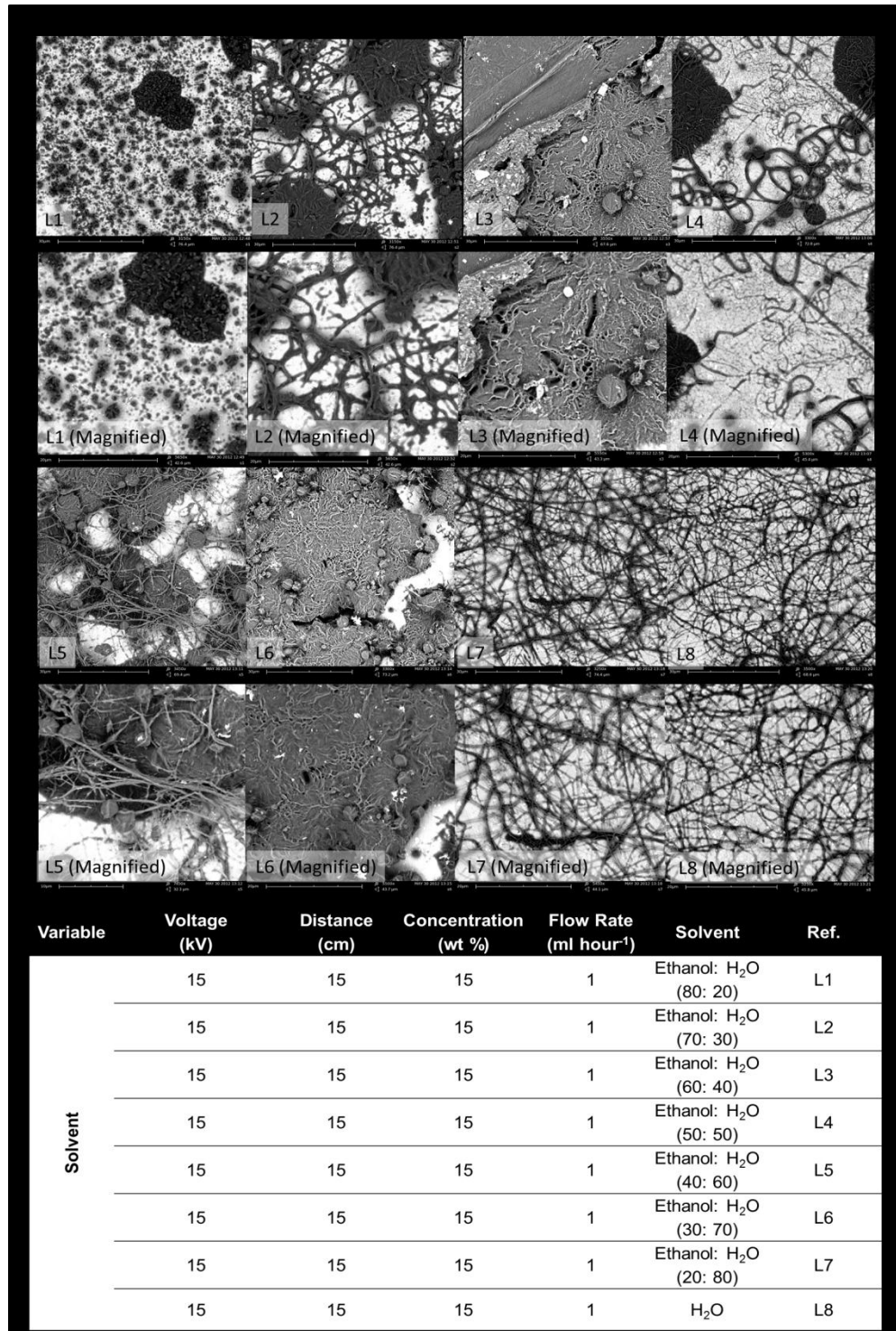
**Appendix C8:** Frequency-sweep data for 10 %v/v, DMSO: water (2 ml), Sample 2.



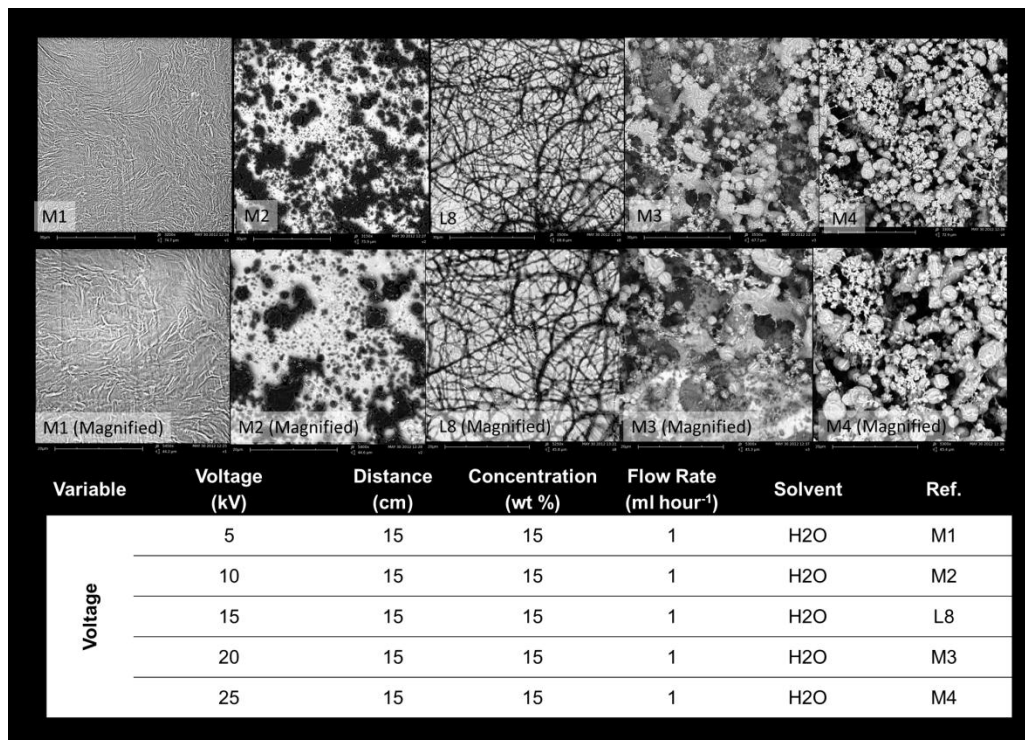
## Appendix D: Electrospinning different molecular weight PEO

### Appendix D1: Electrospinning PEO<sub>2275</sub>

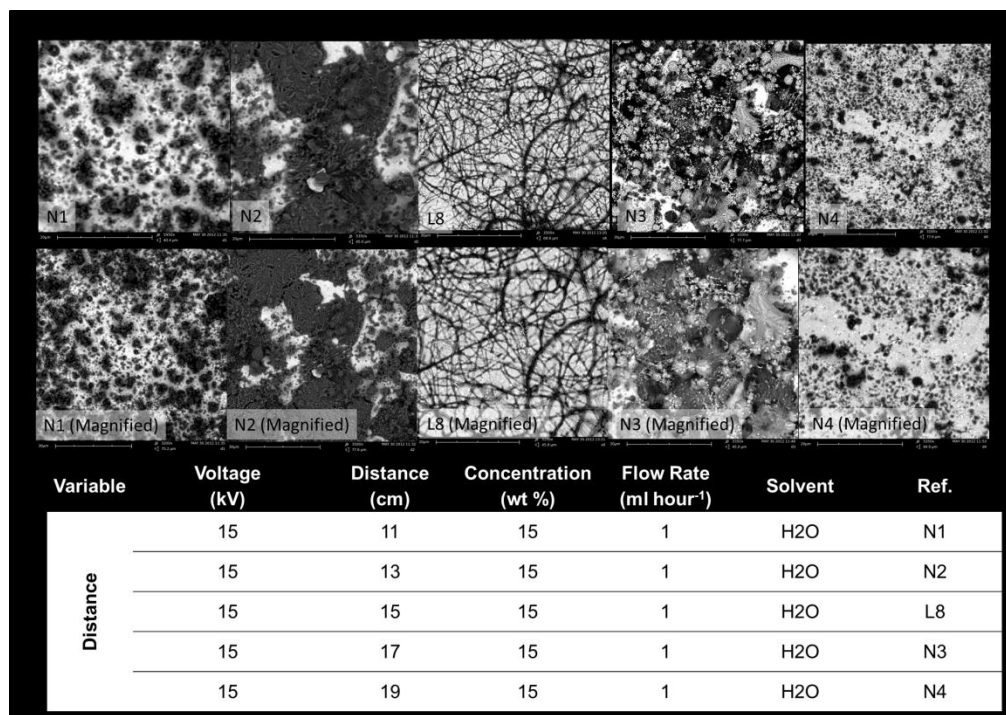
**Appendix D1.1:** The effect of solvent composition on the fibre production of PEO<sub>2275</sub>.



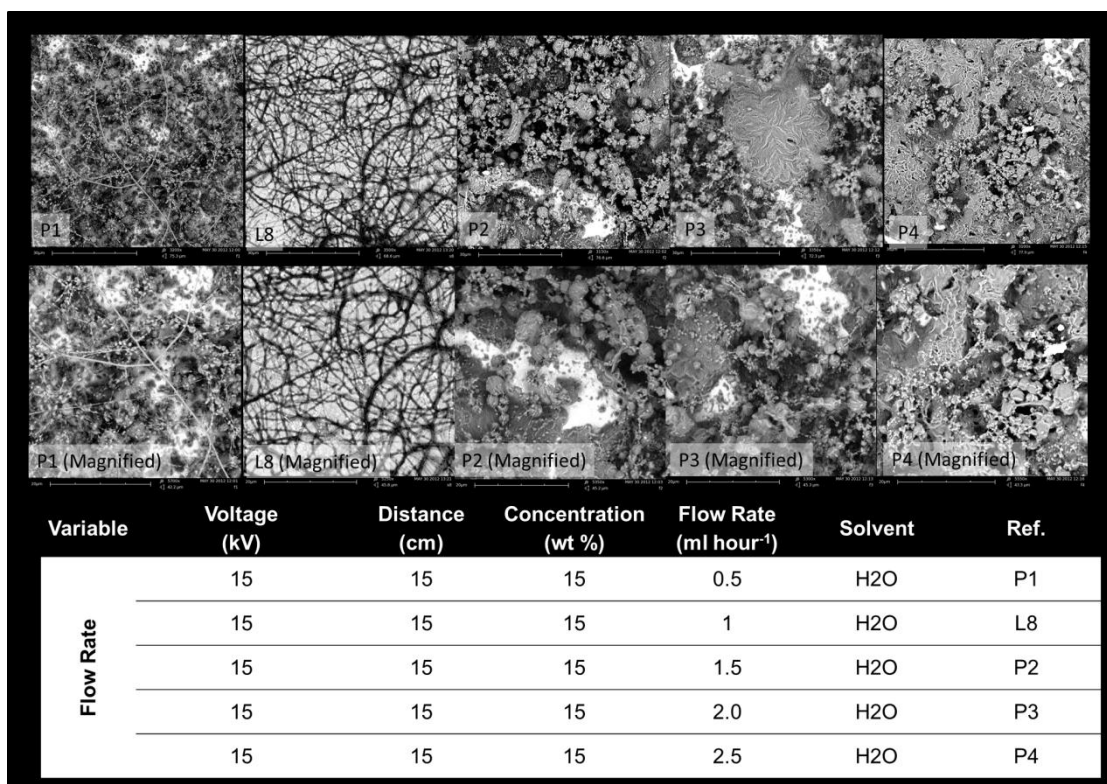
**Appendix D1.2:** The effect of voltage on the fibre production of PEO<sub>2275</sub>.



**Appendix D1.3:** The effect of working distance on the fibre production of PEO<sub>2275</sub>.

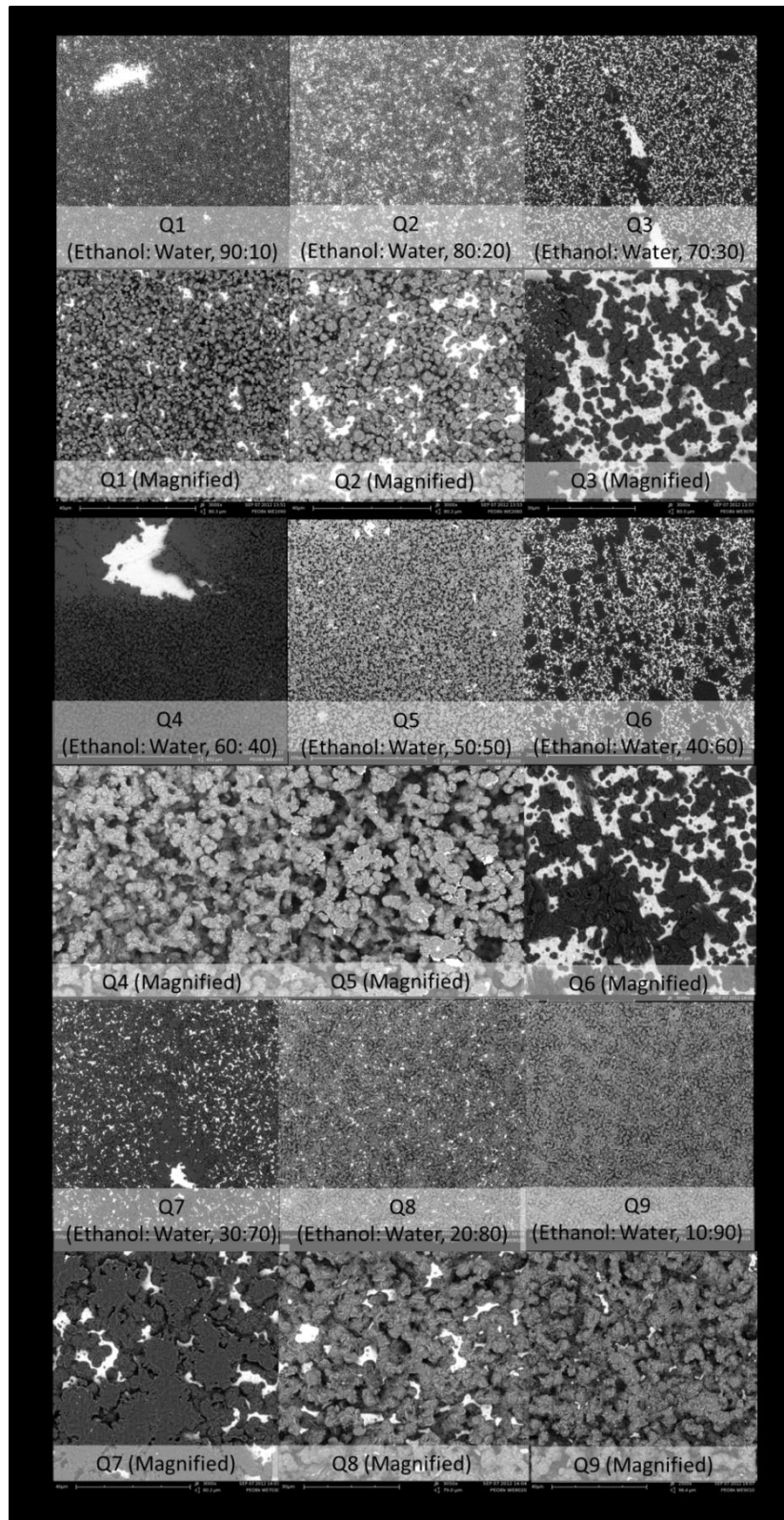


**Appendix D1.4:** The effect of flow rate on the fibre production of PEO<sub>2275</sub>.

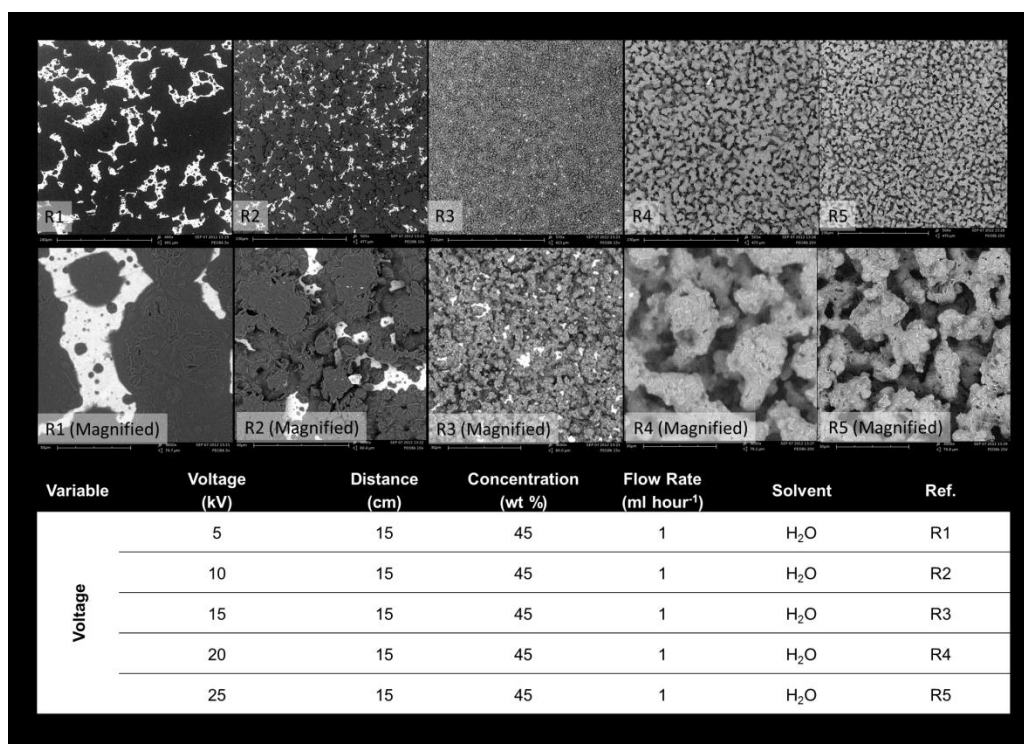


## Appendix D2: Electrospinning PEO<sub>182</sub>

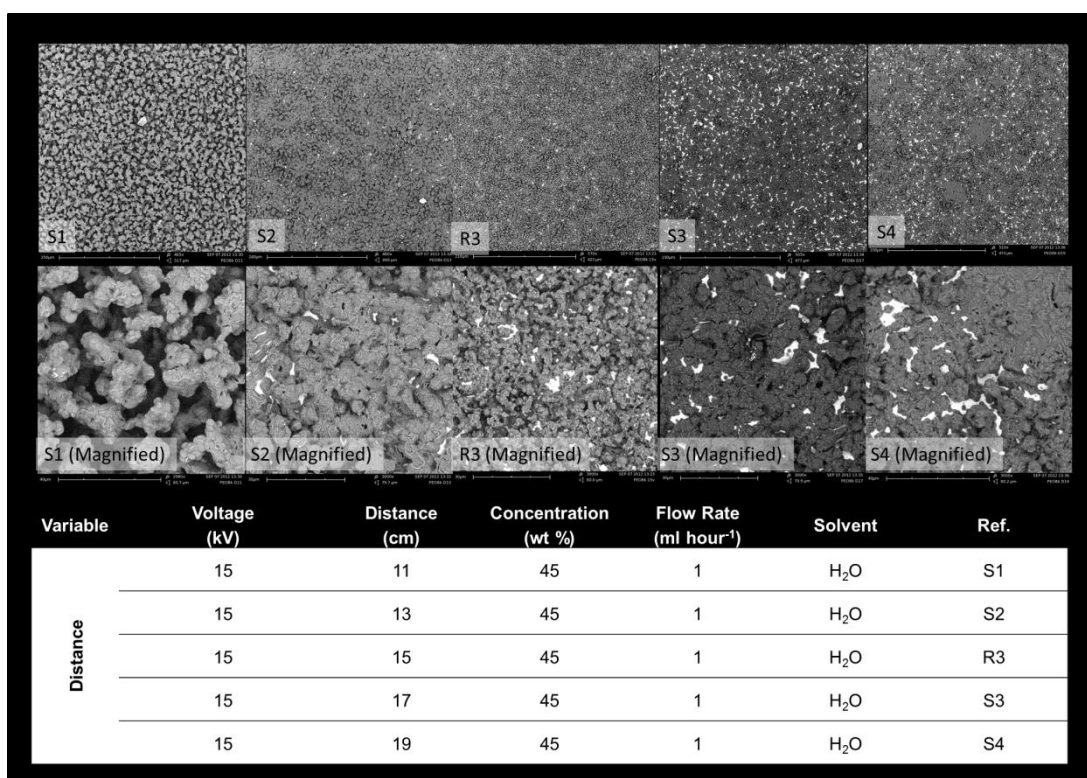
### Appendix D2.1: The effect of solvent composition on the fibre production of PEO<sub>182</sub>.



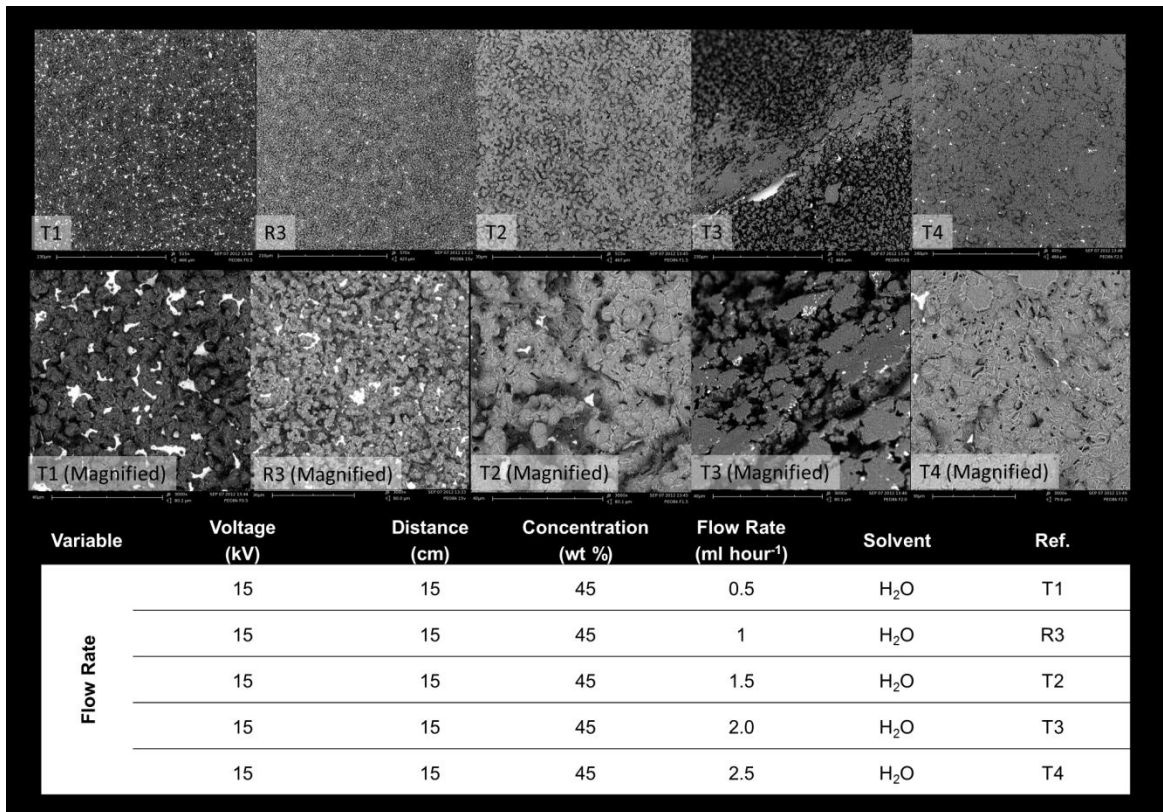
**Appendix D2.2:** The effect of voltage on the fibre production of PEO<sub>182</sub>.



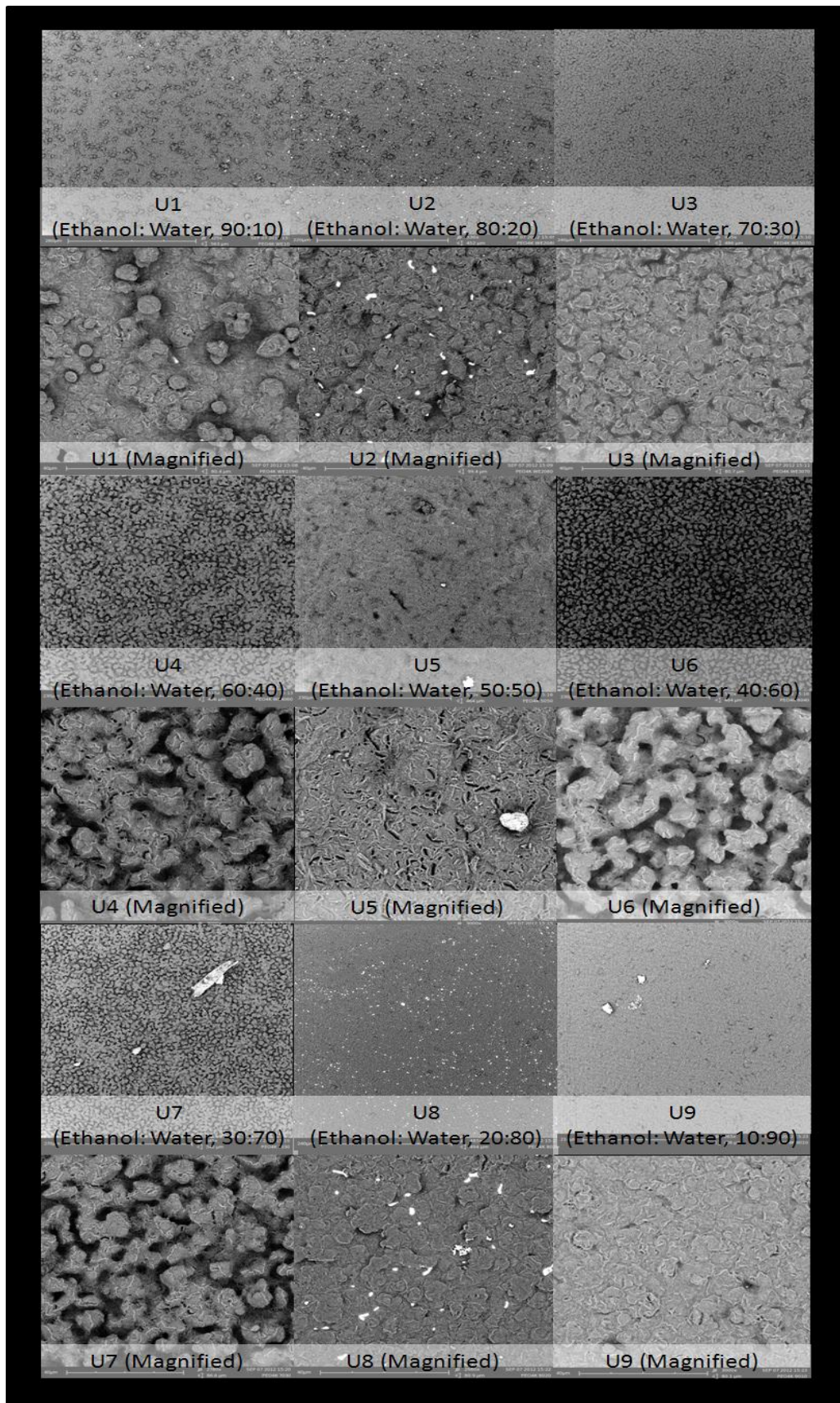
**Appendix D2.3:** The effect of working distance on the fibre production of PEO<sub>182</sub>.



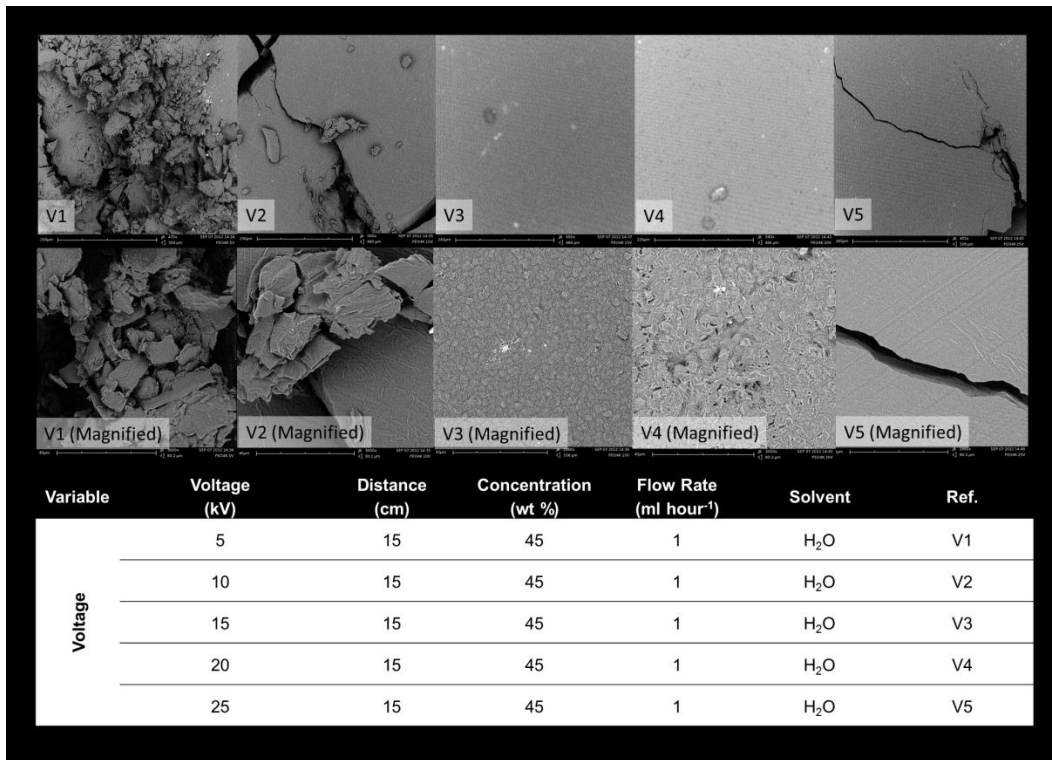
**Appendix D2.4:** The effect of flow rate on the fibre production of PEO<sub>182</sub>.



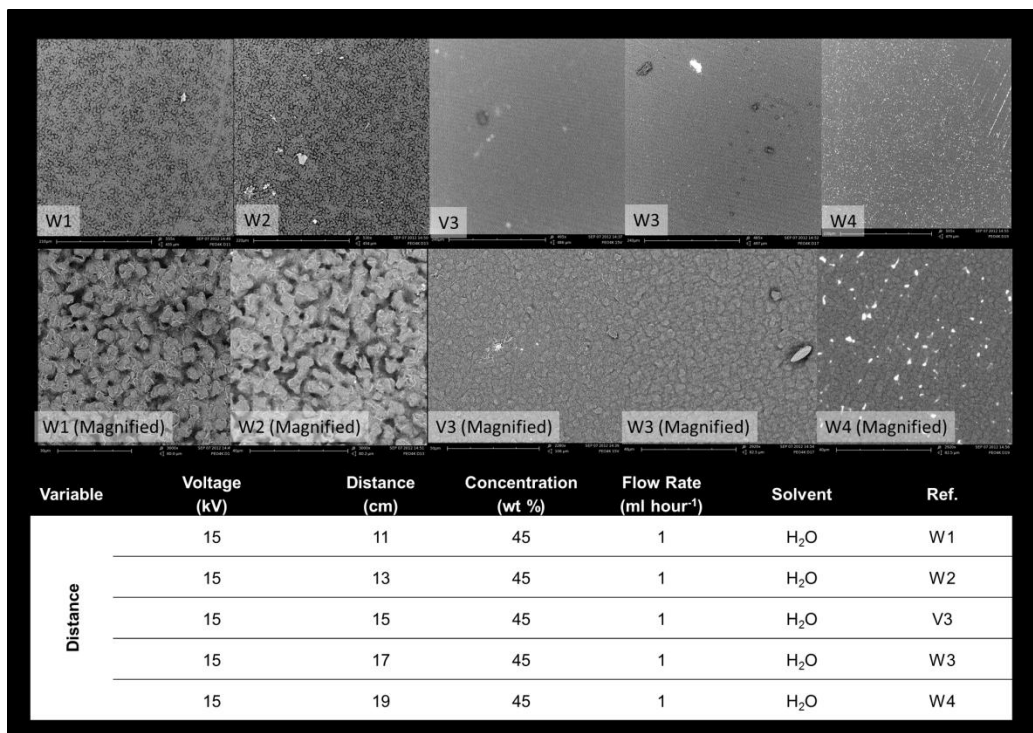
**Appendix D3.1:** The effect of solvent composition on the fibre production of PEO<sub>91</sub>.



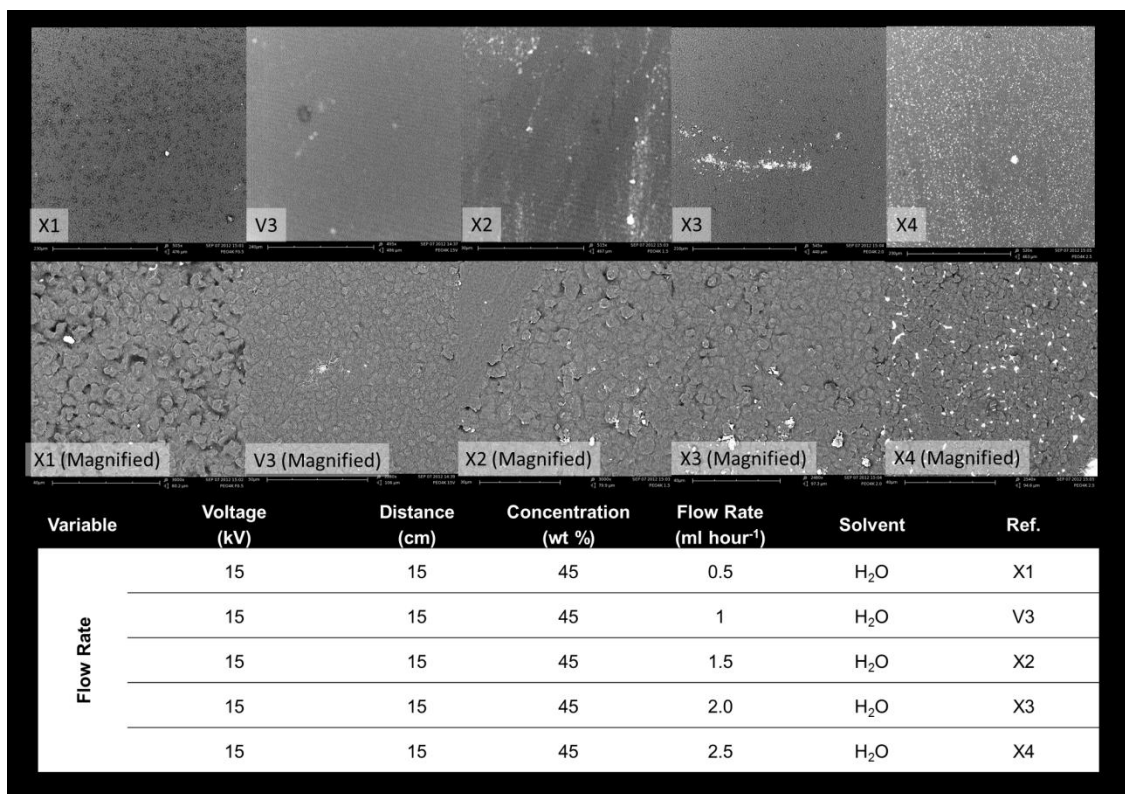
**Appendix D3.2: The effect of voltage on the fibre production of PEO<sub>91</sub>.**



**Appendix D3.3: The effect of working distance on the fibre production of PEO<sub>91</sub>.**



**Appendix D3.4: The effect of flow rate on the fibre production of PEO<sub>91</sub>.**



## List of Publications from this work

- 1) Sohdi, A. A., D. Campbell, et al. (2012). "Polymer-Peptide Conjugate Hydrogels; Towards Controlled Drug Delivery " Chiang Mai Journal of Science 39(4): 351-372.
- 2) Sohdi A. A., Perry M. C., Khaleghi M. R., Adams D. J., and Topham P. D., Facile synthesis of polymer-peptide conjugates via direct amino acid coupling chemistry, *In Preparation*.